DATA-DRIVEN METHODS FOR ANALYZING BALLISTOCARDIOGRAMS IN LONGITUDINAL CARDIOVASCULAR MONITORING

A Dissertation

Presented to

the Faculty of the Graduate School

At the University of Missouri-Columbia

In Partial Fulfillment

of the Requirements for the Degree

Doctor of Philosophy

by

MOEIN ENAYATI

Dr. Marjorie Skubic, Dissertation Supervisor

Dr. James Keller, Dissertation Co-Advisor

December 2019

The undersigned, appointed by the dean of the Graduate School, have examined the Dissertation entitled

DATA-DRIVEN METHODS FOR ANALYZING BALLISTOCARDIOGRAMS IN LONGITUDINAL CARDIOVASCULAR MONITORING

presented by Moein Enayati,

a candidate for the degree of Doctor of Philosophy, and hereby certify that, in their opinion, it is worthy of acceptance.

Professor Marjorie Skubic

Professor James Keller

Professor Mihail Popescu

Professor Laurel Despins

Dedicated with love and appreciation to

my parents, wife, son,

and everyone who supported me in this journey with their ideas.

THANK YOU!

ACKNOWLEDGMENTS

Writing this dissertation was a rich experience and an exceptional opportunity to develop both professionally and personally. For that, I owe a great deal of gratitude to many people for their encouragement and advice throughout the process of researching and writing, whom I like to mention a few in particular.

I would like to thank my advisors Dr. Marjorie Skubic and Dr. James Keller for providing the opportunity to pursue what has become one of the most challenging, enlightening, and rewarding endeavors I have ever undertaken. Your support, guidance, patience, and encouragement over the past years have pushed me to accomplish more than I ever thought possible. You have helped me navigate through the uncertainty of academic research. I am forever grateful for what have learned from your wisdom.

My special thanks to Dr. Mihail Popescu for his valuable suggestions during these past years, who provided numerous research opportunities for me and countless insights about the current research topics. I also appreciate Dr. Marilyn Rantz and Dr. Laurel Despins from the school of nursing, who kindly supported me in exploring the clinical aspects of the phenomena and design and performing appropriate and clinically acceptable data collections.

Finally, thanks to all the students, friends, and teachers who have shared their thoughts and ideas along the way. My special thanks to Nasibeh Zanjirani Farahani and my colleagues Bo-Yu Su, Shawn Fernandes, and Ruhan Yi whose help and suggestions had always encouraged me in going further. I'm glad to have spent time together here at Mizzou.

TABLE OF CONTENTS

LIST OF FIGURES

LIST OF TABLES

ABSTRACT

Cardiovascular disease (CVD) is the leading cause of death in the US; about 48% of American adults have one or more types of CVD. The importance of continuous monitoring of the older population, for early detection of changes in health conditions, has been shown in the literature, as the key to a successful clinical intervention. We have been investigating environmentally-embedded in-home networks of non-invasive sensing modalities. This dissertation concentrates on the signal processing techniques required for the robust extraction of morphological features from the ballistocardiographs (BCG), and machine learning approaches to utilize these features in non-invasive monitoring of cardiovascular conditions.

At first, enhancements in the time domain detection of the cardiac cycle are addressed due to its importance in the estimation of heart rate variability (HRV) and sleep stages. The proposed enhancements in the energy-based algorithm for BCG beat detection have shown at least 50% improvement in the root mean square error (RMSE) of the beat to beat heart rate estimations compared to the reference estimations from the electrocardiogram (ECG) R to R intervals. These results are still subject to some errors, primarily due to the contamination of noise and motion artifacts caused by floor vibration, unconstrained subject movements, or even the respiratory activities. Aging, diseases, breathing, and sleep disorders can also affect the quality of estimation as they slightly modify the morphology of the BCG waveform.

Wavelet-based and the empirical mode decomposition (EMD) techniques were then applied to remove the noise components of the signal. Both the original and the enhanced implementations of the energy algorithm were then applied to the output of each denoising method, to compute an average heart rate for each epoch of 30 seconds. A detailed analysis of these estimations is provided for each combination of datasets and denoising techniques. In overall, the Daubechies wavelet decomposition and the ensemble empirical mode decomposition (EEMD) were shown to provide

the best results. While the estimations provided by the original energy algorithm have errors in the range of 16 beats per minute, combining the enhanced energy algorithm and the denoising techniques reduces the average error to about 4 beats per minute.

Most of our BCG instruments have more than one data channel including the 3 axes of the accelerometer or the 4 transducers of the hydraulic bed sensor. Even after denoising the BCG signals from different channels, the waveforms acquired from each channel may have a different level of signal quality (SQ) mostly due to their distance from the body's center of mass or their direction. Multiple channel selection schemas have been studied in the current dissertation, to provide a general guideline on choosing the best signal among all available ones. The results of these automatic channel selections can match the manual selections by 78%, which is much higher than the 30%-50% acquired from the previous DC level approach.

After denoising the signal and providing a robust estimation for the fiducial points of the BCG waveform, a morphological BCG template is created using the ensemble averaging. Abnormal and normal variations of these templates were studied under different conditions. For example, the amplitude of the J-peak is shown to decrease from the baseline by 7.4% during exhalation while it increases by 5.2% during inhalation. These morphological features of the BCG waveform are also investigated for the cuff-less estimation of the relative change in the blood pressure on 48 subjects. Among different morphological features, the summation of the amplitude of the two sides of the J-peak (IJ+JK) shows a mean correlation above 94% to the reference changes in the systolic blood pressure.

All the methods and algorithms discussed in this manuscript have been evaluated against multiple datasets collected simultaneously from the ballistocardiography device and the reference signals such as ECG. We have recruited a total of 62+51+75+50 volunteers in 4 different IRB approved studies, both in the lab and hospital settings, for periods of as long as eight hours of continuous data collection.

1. INTRODUCTION

1.1. Motivation

According to the American Heart Association [1], cardiovascular disease (CVD) was the underlying cause of death for nearly 836,546 adults in the US, between 2013 to 2016. About 48% of American adults have one or more types of CVD, which covers about 89.3% of males and 91.8% of females of 80 years or older. In the US, Coronary heart disease is the leading cause of death related to cardiovascular disease, followed by stroke, heart failure, and high blood pressure. About 80.0% of males and 85.6% of females of 75 years or older suffer from high blood pressure. With the goal of meeting the desire of the older adults to remain in their home setting while controlling healthcare costs, we have been investigating, and refining health alerts produced by environmentally-embedded in-home sensor networks designed to detect early signs of health change and functional decline in older adults, the keys to successful intervention.

Home-based intelligent monitoring systems have the potential to detect health problems based on relative changes in normal life activities over an extended period [2]. Longitudinal in-home vital signs measurement gives clinicians the ability to track long-term trends in patients' health conditions. This information can be used to direct therapeutic decisions or determine the need for a follow-up visit [3]. Unobtrusive in-home systems could especially benefit older adults and subjects of reduced mobility [4]. When our sensor network detects these changes, the system automatically sends appropriate alerts to the caregivers to allow early intervention (Figure 1.1). Thus, by helping older adults remain healthier, active, and in control of their chronic illnesses with early detection of changes in health status and early intervention by health care providers, millions can remain independent as they age, avoiding or reducing debilitating and costly hospital stays and, for many, avoiding or delaying the move to a nursing home.

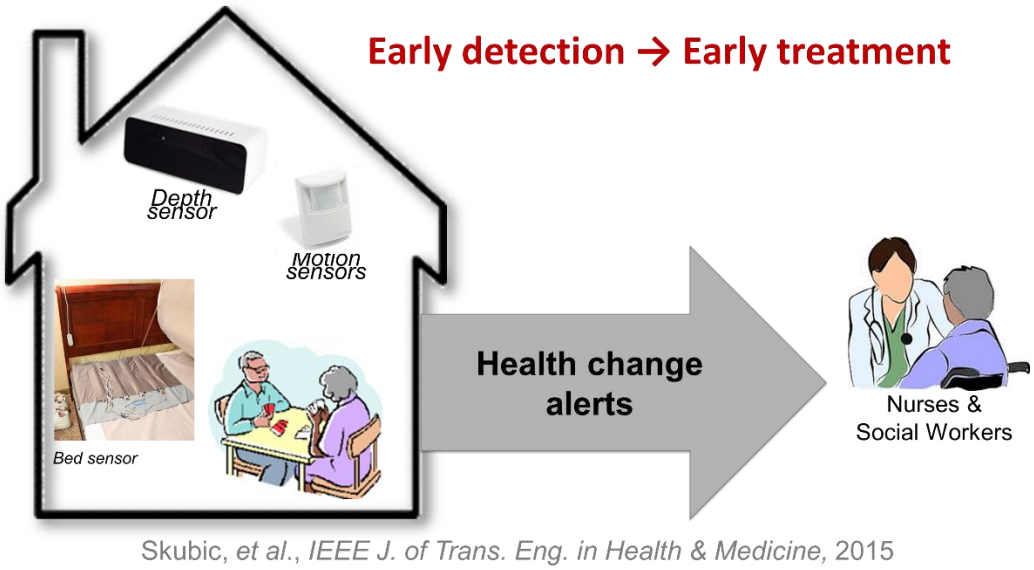

Figure 1.1. Environmentally-embedded in-home sensor networks for early detection of health change and functional decline in older adults.

Ballistocardiography (BCG) is a non-invasive technique of monitoring cardiovascular parameters which captures the cyclic motion of the human body caused by the movement of heart and blood flow inside the arteries during each heartbeat. It has been shown to be very valuable, particularly for long-term evaluation of myocardial strength [2]. The effect of CVD on the morphological variations in the BCG waveform have been studied previously, and BCG has been demonstrated as a potential cardiovascular diagnostic tool [3]. A 20-year BCG follow-up of 211 subjects by Starr and an 18-month clinical BCG measurement by Mandelbaum et al. on 100 patients recovering from heart attack show the prognostic value of BCG in monitoring cardiac function. BCG signals can be captured using the low-cost sensors that are embedded in a bed or chair, with the advantage of not needing the presence of medical staff [6].

Ballistocardiography offers advantages over the ECG measurement, as (i) direct body contact is not required and (ii) the signal is not limited to the cardiac function but also reflects the status of the more extensive cardiovascular system. These advantages provide intriguing possibilities of continuous passive monitoring of the cardiovascular system without requiring

anything from the patient. Presently, though, a crucial issue limits the utilization of BCG over ECG. Over the years, ECG measurements and their interpretations have been standardized, so that, given a specific lead placement, abnormalities in the ECG waveform bear particular clinical meaning. Conversely, to date, standardized methods to interpret the BCG signal obtained from different sensing devices are not available; thus, hindering the use of BCG as a clinical diagnostic and monitoring instrument. The lack of knowledge of how the physiological BCG waveform should look with different sensing systems makes it extremely challenging to identify and characterize instances when changes in the BCG waveform are indicative of pathological conditions.

A variety of systems can be used to capture BCG signals, including beds [7, 8], chairs [9], and weighing scales [10]. Bed-based sensors, in particular, have the potential advantage of long term BCG acquisition throughout the night [3]. Our hydraulic bed sensor targets the longitudinal and noninvasive monitoring of vital signs including, but not limited to, the heart rate, respiratory rate, sleep posture, sleep stage, blood pressure, and other cardiac conditions [11-13]. While these systems provide a high degree of freedom for the subjects [6], they are highly susceptible to motion artifacts [3]. The coincidence of BCG bandwidth (0.5-10 Hz) with several sources of motion, including respiratory fluctuation of the chest, body postural change, or limb movements, is the leading cause [14]. According to [15], even in the controlled longitudinal experiments with BCG, only 29% of the head-foot waveforms (in men) are considered normal, and the rest have different levels of noise. Inaccurate estimation of cardiac parameters from the artifact-contaminated BCG records could negatively affect the quality of future studies. This emphasizes the need for methods to deal with motion artifacts and to choose the best possible channel, before any feature extractions and health analysis.

Furthermore, most of the existing machine learning studies in the field of ballistocardiography are based on features engineered using the expert domain knowledge, which requires an intensive, time consuming and manual process of design and experiment with the hope

of learning some general properties throughout the entire population. Developing such a generalizable set of features requires a large population of all different ages and disorders as the training set. It has been reported that the cardiovascular parameters and in specific the ones potentially accessible via ballistocardiography vary a lot among subjects of different age and health condition. This implies the necessity of exploring newer and more generalizable feature extraction methods, and also the application of modern techniques to transfer the knowledge gained and developed through other sensing modalities, to infer vital information from BCG. Mathematical and data-driven models could help in providing causal relationships between the health conditions and the anticipated variations in the ballistocardiographic parameters.

In a long-term view, this research will investigate the state-of-the-art techniques to provide data-driven models for accurate extraction of reliable and understandable ballistocardiography features using the template waveforms acquired from real subjects in their typical day and night activities at their home or assisted living facilities. Better non-invasive monitoring predictors for different vital signs, including the change in blood pressure, restlessness, and sleep conditions will help the family members and the nursing staff to provide better care for this growing population.

1.2.Primary Goals

The primary objectives of this research include:

- Better understanding of the physiology of ballistocardiography through:
  - Studying the literature on the origin of ballistocardiography.
  - Understanding the potential parameters that affect the BCG waveform.
  - Comparing the properties of different ballistocardiography devices.
- Collecting a comprehensive set of data:
  - Controlled and in-lab data collections for exploring new concepts.
  - Overnight data collections in home or hospital settings with manual annotations.

- Exploring the non-BCG components of the acquired signal
    - Sleep posture classification by means of the DC level of the four hydraulic bed transducers.
- Designing more robust algorithms to detect cardiac function:
    - Incorporating physiology-based enhancements in time domain heartbeat detection.
    - Evaluating the effect of noise on this algorithm and the appropriate compensations.
    - Selecting a channel to increase the accuracy and reduce the computational time.
- Preprocessing the signals acquired from the hydraulic bed sensor for the longitudinal and non-invasive measurement of cardiovascular parameters:
    - Reduction, detection, and cancellation of the noise and motion artifacts.
    - Selecting the channel with the highest signal quality index.
    - Identifying the potentially less affected and highly consistent segments of the signal, regarding the motion artifacts, sleep posture, and hemodynamics such as sleep stages, from a longitudinal perspective.
- Creating waveform templates and extracting morphological features used to track different health parameters:
    - Studying the normal systemic variations of the BCG waveforms during respiratory cycles or as a result of aging.

      Estimating the change in blood pressure by monitoring the morphological variations of the BCG waveform.

1.3.Proposed Research Tasks

The following table shows the work plan presented in the research proposal, with updates on what has been completed in the final dissertation. The significant part of the new work is related to different motion artifact detection and denoising techniques. I also tried different channel selection schemas. Therefore, I introduced the signal quality index (SQI), SNR, and two other methods for channel selection, and compared them against the Oracle approach. I also have studied the effect of these improvement techniques on the accuracy of sleep stage classification. Although the results were not different from the previous case, I provided in Chapter 9 a detailed description on the implementation and some discussion on the possible reasons.

Table 1. The proposed research tasks with the corresponding chapter in this dissertation

Description	Previous Progress	Current Progress	Chapter Number
Fundamentals of ballistocardiography ●Physiology ●Instrumentations(Classic, Modern) ●Classes(D-V-A)	100%	100%	Ch2 Ch3
Different approaches to create morphological templates ●Alignment ●Normalization ●Averaging (Mean, Median) ●Dynamic Time Warping	100%	100%	Ch7
Already published work	100%	100%	Ch5
Energy algorithm to estimate heart rate from ballistocardiographs			
Time domain features and NN for sleep posture detection			Ch4
Feasibility study on morphological features to estimate the relative change of blood pressure			Ch8
Time and frequency domain features for sleep stage detection			BHI19
Age related variations in the morphology of BCG			EMBEC17
Respiratory related variations in the morphology of BCG			BHI17
Related data collections	100%	100%	Ch3.4
HRV and Blood pressure / 60 young subjects / 10 + 3 + <7 minutes			Ch5
Blood pressure / 50 young-old subj / 10 minutes			Ch8
Sleep posture / 60 young subjects / 1 + 1 + 1 minutes			Ch4
SleepLab data / 75 patients / 7-8 hours			BHI19
Different Mattresses / 2 Subjects / 3 x (5 x 10) minutes			Ch7.3
Chair sensor / 45 older subjects / 10 minutes			Ch3.4
Distortions in ballistocardiographs ●Motion artifacts ●Respiratory variations ●System (Instrumentation/Mattress)	100%	100%	Ch7.3
Motion artifact detection and reduction	90%	100%	Ch6
Time-frequency features for motion artifact detection	100%	100%	Ch6.4
EMD & Wavelets for motion artifact reduction	60%	100%	Ch6.3
Morphological variations caused by respiratory cycle	100%	100%	Ch7.3.2
●Cause(RSA/HRV) ●Effects(Energy, Blood Pressure) ●Compensation			Ch5.2.1
Improved energy algorithm for beat detection	90%	100%	Ch5.2
Re-implement selected literature on beat detection	40%	*	channel selection
Improved sleep stage classification using ●Improved HRV features ●Improved respiratory features ●Reduced motion artifacts	70%	100%	Ch10.1
Cuff-less monitoring of relative blood pressure variations ●Improved energy algorithm ●Reduced noise and artifact ●Respiratory effect	80%	100%	Ch8

1.4. Dissertation Organization

Chapter 2 provides an in-depth review of the main physiological functionalities of the cardiovascular system and standard approaches to evaluate them. It reviews the historical evolution of ballistocardiography, including a list of the most extensive studies in the field, physiological formulation of BCG, the classical instrumentations, and their sample waveforms. The standardization process to group all classical devices into four general categories, as well as a list of recent and modern instrumentation, is included in this chapter.

Chapter 3 will specifically focus on the ballistocardiography devices that have been developed in our lab. I have been using two different BCG sensors, including the hydraulic bed sensor and the accelerometer-based suspended bed, as a replica for Isaac Starr's sensor. We also have tried recliner chair for respiratory and heart rate monitoring. The detailed specification of each sensor as well as a sample signal recording from each one is provided. This chapter also provides the required information about the IRB approved data collections that are being used in this dissertation. Our datasets always contain synchronized ECG signal as a reference, while depending on the case many other simultaneously recorded signals are also available.

Chapter 4 reports the application of machine learning techniques on estimating the sleep posture from the hydraulic bed sensor. Sleep posture introduces variations in the signals acquired by the hydraulic bed sensor, including the differences in the DC bias. It is also considered as a potential source of variations in the morphology of BCG waveforms, due to the change in the heart's orientation. Meanwhile, different postures may introduce different breathing and sleep qualities, thus extracting the sleep posture will provide benefits for different applications. By extracting some statistics from the amplitude of the four transducers, a feed-forward artificial neural network was trained and tested against manually annotated data. The data collection was designed explicitly for this purpose and consists of data on four different sleeping postures from 60 subjects in the lab. The initial idea was to utilize the variation in the shape of BCG signals as an indicator

for the direction of BCG variations. But finally, the direction of the chest rib cage seemed to have the highest impact on the hydraulic bed sensor signals than the variations in the BCG morphology. I have also realized some other possible improvements in the processing and analysis techniques that the rest of the dissertation will focus on, as schematically presented in Figure 1.2.

Chapter 5 focuses on time-domain detection of a heartbeat from the BCG as the surrogate approach for the beat to beat estimation of heart rate and therefore the critical step in the noninvasive analysis of heart rate variability and sleep stages. Our previously published energy algorithm is studied using different datasets with different levels of noise contamination and age-related BCG abnormality. Multiple improvements are proposed and tested to enhance the quality of the beat detection. The beat to beat estimations of the resulted enhanced energy algorithm are evaluated against the ECG R-peak estimations as the ground truth and have shown at least 50% improvement in the accuracy of the beat to beat heart rate estimation.

Chapter 6 deals specifically with the motion artifact contamination of the ballistocardiograms and its effect on lowering the accuracy of our algorithms to estimate the beat-to-beat heart rates and consecutively the heart rate variability (HRV), sleep stage classification and perhaps any features being extracted from the BCG sensors. This chapter first shows the application of two general noise reduction techniques, namely the wavelet decomposition and the empirical mode decomposition (EMD), and some of their variants. It is followed by introducing a machine learning method based on time and frequency domain features to detect, localize, and discard the remaining artifact affected parts of the signal. The last section of this chapter investigates different approaches for channel selection and evaluates them against the manual channel selection; hereafter called the oracle. The overall accuracy improves by about 70% compared to the conventional approach.

Having prepared a clean BCG signal from the best channel and an enhanced beat detection algorithm, Chapter 7 describes how to create a morphological BCG template through segmentation and ensemble averaging. Some normalization and alignment techniques are proposed in order to

create a more reliable template and monitor their variations during different physiological events. The typical morphology of the BCG waveform is shown to be altered due to some systematic variations in the cardiovascular system, such as age or respiration. This chapter also contains the utilization of morphological templates to characterize our BCG devices.

In Chapter 8, our non-invasive approach to estimate the relative change in systolic blood pressure based on the variation of morphological parameters is discussed. In the previous chapters, I have provided details on denoising, selection, segmentation, and template creation from the BCG signals, and described different parameters one might consider in designing the proper features from the BCG. In Chapter 8, I have provided the results of some new features to estimate the change in blood pressure that have not yet been published. I have also described how the inflation of the reference blood pressure cuff affects the BCG waveforms and the morphological features.

In Chapter 9, I have investigated some new ideas to improve the accuracy of sleep stage classification. Supported by the results that I have reported in the previous chapters on different approaches to improve the accuracy of beat to beat heart rate estimation from the BCG signals, I focused on the enhancement of the HRV features in sleep stage classification. First, using the channel selection techniques, I pick the best transducer and then using the enhanced energy algorithm I better defined the individual BCG cycles. On top of them, I tried two new classification algorithms compared to our previously published paper. Results of these experiments do not show any improvement in the classification accuracy, which has been discussed at the end of the chapter.

Although each chapter has its own dedicated results and conclusion section, Chapter 10 also provides an overview and summary of the work as a whole, the major contributions, and my suggested ideas for future work. Finally, detailed description of the codes and information about the organization of datasets are provided in Appendices A and B.

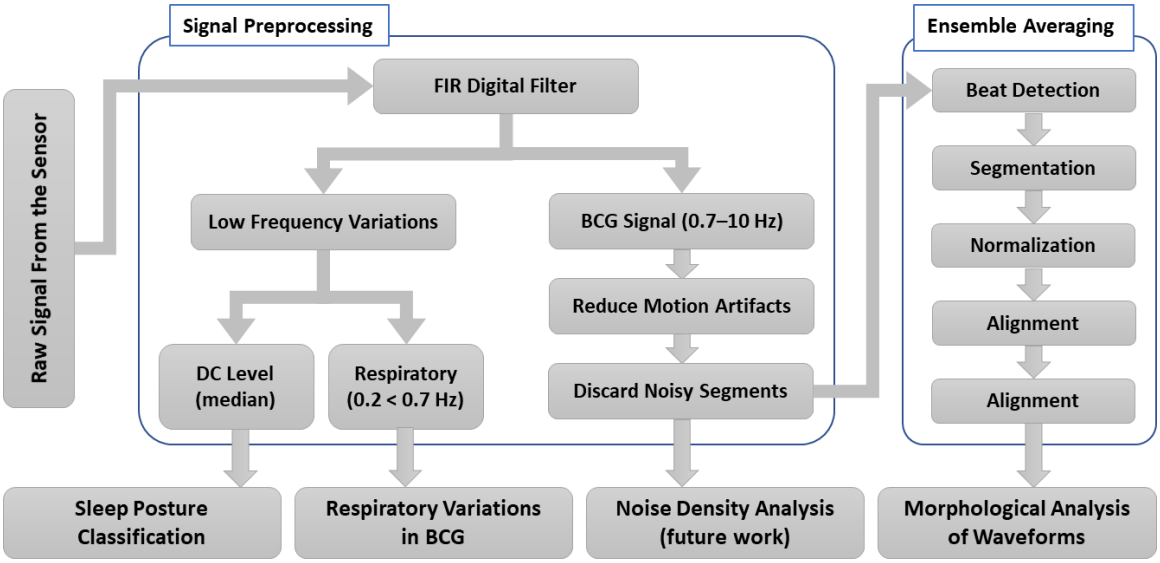

Figure 1.2. Proposed steps required in morphological analysis of waveforms, starting from the raw BCG signal to the creation of waveform templates.

1.5. Contributions

- Development of an enhanced algorithm for accurate beat detection in BCG
  - Fast, time domain, and robust against small motion artifacts.
- Investigation of different approaches to evaluate and improve the quality of the BCG signal
  - Application of noise reduction techniques to minimize the effect of artifacts.
  - Designing a machine learning approach to detect and discard noisy segments.
  - Introducing the use of different signal quality indices to select the best channel.
- Sleep posture classification from the four hydraulic bed sensors
  - Identifies consistent portions of sleep over multiple nights, which results in more consistent morphological templates in longitudinal studies.
- Template-based analysis of the morphology of BCG waveforms
  - Designing the procedure to create physiologically, reliable BCG templates.

- Studying the variation of these templates during the respiratory cycle, or due to the change in cardiovascular parameters such as the change in blood pressure or aging.

- Preparation of the most extensive annotated datasets using the hydraulic bed sensor
  - I was engaged in 4 IRB approved data collections with more than 570 hours of BCG signal synchronized with other reference signals including but not limited to ECG and PPG.

1.6. Publications

This work has resulted in the following 12 publications, wherein all of them, I was engaged with both the data collection and developing the algorithms. My main contribution in these papers is mostly about the signal segmentation, creation of the templates and machine learning approaches in the analysis of morphological features with a focus on the potential impact of motion artifacts and age and respiratory variations of the measurements.

(1) **Enayati, M.**, Skubic, M., Zanjirani Farahani, N., 2019. Motion Artifact Detection in Ballistocardiograms using Machine Learning Techniques. *IEEE International Conference on Biomedical and Health Informatics* May. 19-22, 2019, Chicago, Illinois, USA.

(2) Yi, R., **Enayati, M.**, Keller, J.M., Popescu, M., Skubic, M., 2019. Non-Invasive In-Home Sleep Stage Classification Using A Ballistocardiography Bed Sensor. *IEEE International Conference on Biomedical and Health Informatics* May. 19-22, 2019, Chicago, Illinois, USA.

(3) Ullal, A., Su, B.Y., **Enayati, M.**, Skubic, M., Despins, L., Popescu, M., Keller, J., 2019. Non-Invasive Monitoring of Vital Signs for Older Adults Using Recliner Chairs. *IEEE Journal of Biomedical and Health Informatics. (Under review)*

(4) Guidoboni, G., Sala, L., **Enayati, M.**, Sacco, R., Szopos, M., Keller, J., Popescu, M., Despins, L., Huxley, V., Skubic, M., 2018. Cardiovascular function and ballistocardiogram: a relationship interpreted via mathematical modeling. *IEEE Transactions on Biomedical Engineering*.

(5) Su, B.Y., **Enayati, M.**, Ho, K.C., Skubic, M., Despins, L., Keller, J.M., Popescu, M., Guidoboni, G., and Rantz, M., 2018. Monitoring the Relative Blood Pressure Using a Hydraulic Bed Sensor System. *IEEE Trans. on Biomedical Engineering*.

(6) **Enayati, M.**, Skubic, M., Keller, J.M., Popescu, M. and Farahani, N.Z., 2018, July. Sleep Posture Classification Using Bed Sensor Data and Neural Networks. In *2018 40th Annual*

International Conference of the IEEE Engineering in Medicine and Biology Society (EMBC) (pp. 461-465). IEEE.

(7) **Enayati, M.**, B.-Y. Su, L. Despins, and M. Skubic (2017). Investigating the Interaction between Ballistocardiogram and Cardiac Age. *European Medical and Biological Engineering Conference EMBEC*.

(8) **Enayati, M.**, B. Y. Su, L. Despins, M. Skubic, J. M. Keller, and M. Popescu (2017). Investigating the Interaction between Ballistocardiogram and Respiratory Phases. 2017 *IEEE International Conference on Biomedical and Health Informatics* Feb. 16-19, 2017, Orlando, Florida, USA.

(9) Skubic, M., Su, B.Y., **Enayati, M.**, Zare., A., Jiao, C., Lyons, P. and H., K.C. (2016). Multimedia Investigation of BCG and SCG Signals. *CIC, BCG-SCG Workshop*, Vancouver, B.C., Canada.

(10) Lydon, K., Su, B.Y., Rosales, L., **Enayati, M.**, Ho, K.C., Rantz, M., and Skubic, M., 2015, August. Robust heartbeat detection from in-home ballistocardiogram signals of older adults using a bed sensor. In *Engineering in Medicine and Biology Society (EMBC), 2015 37th Annual International Conference of the IEEE* (pp. 7175-7179).

(11) **Enayati, M**., Banerjee, T., Popescu, M., Skubic, M., and Rantz, M., 2014, August. A novel web-based depth video rewind approach toward fall preventive interventions in hospitals. In *Engineering in Medicine and Biology Society (EMBC), 2014 36th Annual International Conf. of the IEEE* (pp. 4511-4514). IEEE.

(12) Banerjee, T., **Enayati, M**., Keller, J.M., Skubic, M., Popescu, M., and Rantz, M., 2014, August. Monitoring patients in hospital beds using unobtrusive depth sensors. In *Engineering in Medicine and Biology Society (EMBC), 2014 36th Annual International Conference of the IEEE* (pp. 5904-5907). IEEE.

2. BACKGROUND ON BALLISTOCARDIOGRAPHY

2.1.Definition

Ballistocardiography is the technique to visualize the slight movements imparted to the human body's center of mass caused by the cyclic displacement of the heart and flow of blood in the vessels after each cardiac contraction [16]. Heart activity can be described as a cyclic repetition of two mechanical phases: The systolic or ejection phase when the blood in the heart chambers being pumped out via the heart contraction, and the diastolic phase wherein the heart is resting and being filled by the blood. Figure 2.2 represents the internal and external anatomy and circulation of the heart. The heart contraction in the systolic phase results in the movement of the heart and causes a change in the distribution of blood through the body. This movement is being captured and visualized through a technique named Ballistocardiography [17].

J.W. Gordon [18] was the first who published his observations of the oscillations in the needle of the old mechanical weight scales, synchronous to the heartbeat of the person (Figure 2.1.b). He used the ordinary (by that time) sphygmography device (Figure 2.1.a) to derive this motion, which is caused by heart pushing the blood upward into the aorta. The blood then flows downward to the lower body, after hitting the aortic arch. These action and reaction forces cause cyclic variations in measurements of the weighing scale [16].

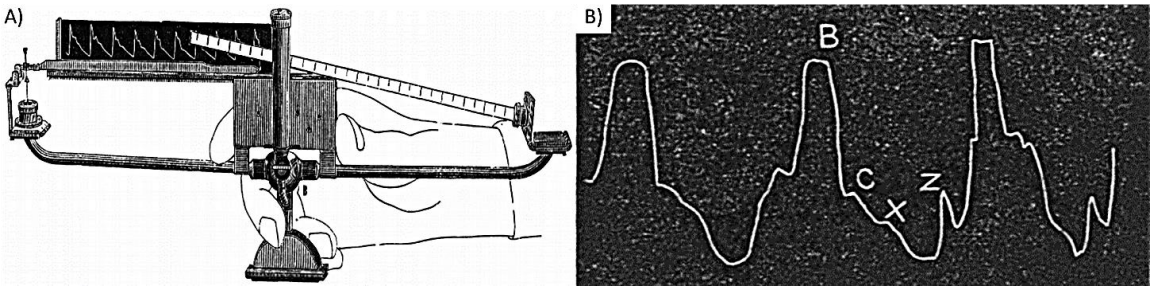

Figure 2.1. Keyt simple sphygmograph with the calibrated tube from [19](A), and an example reading(B).

One of the first BCG measurements in the controlled environment was recorded by Henderson [20] (1905) using a "swinging table" and a set of levers, followed by the seismograph bed used by [21], and [22] who suspended an aluminum chair from steel springs. However, it took until 1961 when Starr and Wood [16] developed the first mature description for ballistocardiography and its measurement. By 1954 there were at least 300 papers on ballistocardiography in medical literature throughout the world [23].

The prognostic value of ballistocardiograms was reported by Starr in [24] after five years of follow up studies on 221 hospital patients (or until death). Starr determined relationships between longevity and BCG and proposed recommendations for doctors to utilize the BCG recordings in their evaluations. Table 2.1 lists the most significant studies on variations and the diagnostic and prognostic potential of ballistocardiography.

Table 2.1. Review of the most extensive ballistocardiography studies.

Reference	**Duration**	**Num. of Subjects**	**Study**
Starr and Wood [16]	20 years	211 healthy subjects	Physiological age of the heart
Alametsä and Viik [25]	12 years	1 healthy subject	BCG Alterations on EMFi
Lynn and Wolf [26]	7 years	134 patients	Prognosis ischemic disease
Erina [27]	1 time	428 patients	Diagnosis of arteriosclerosis
Scarborough, et al. [28]	1 time	369 normal subjects	Normal vs. Borderline BCG
Abrams and Edger [29]	1 time	319 young soldiers	Normal variations of BCG
Brotmacher [30]	1 time	200 subjects	Normal vs. Abnormal BCG
Jones [31]	12 days	157 patients	Arteriosclerotic heart disease
Henderson [32]	5 times	124 normal subjects	Smoking and heart disease
Moser, et al. [33]	1 time	100 patients	Myocardial Infarction
Mandelbaum and Mandelbaum [34]	1 time	100 normal subjects	Coronary artery disease
Pordy, et al. [35]	2 times	80 normal subjects	Normal vs. Abnormal BCG
Brown Jr, et al. [36]	1 time	50 patients	Symptoms of Angina Pectoris

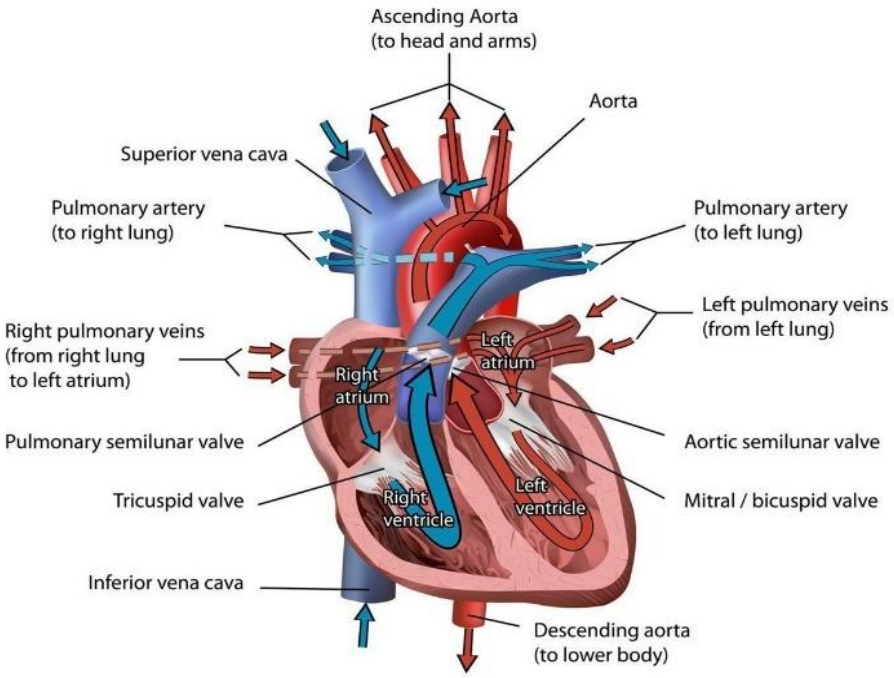

Figure 2.2. Internal and external anatomy and circulation of the heart. The heart consists of four chambers. The upper heart is the atria (two atrial chambers), and the lower part is the ventricles (two ventricular chambers). The muscle composing walls of the heart are called the myocardium. The veins of the body terminate in two great vessels that empty into the right atrium: the superior vena cava (from the upper body) and the inferior vena cava (from the lower body). Blood exits the heart through the pulmonary artery (which takes unoxygenated blood to the lungs from the right ventricle) and through the aorta (which distributes oxygenated blood to the body from the left ventricle). Oxygenated blood from the lungs enters the left atrium from the pulmonary vein. The pulmonary artery is the only artery that carries unoxygenated blood, and the pulmonary vein is the only vein that carries oxygenated blood.

2.2.Physiological Formulation

According to the first report of the committee on ballistocardiographic terminology [37], regardless of the type of the measurement device, the ballistocardiogram consists of two general categories of systolic and diastolic waves. The systolic waves are named H, I, J, and K followed by the diastolic waves of L, M, and N. The presystolic G wave also sometimes appears in the BCG recordings. A brief description of each peak is provided here:

- **The H wave** is the first headward deflection of the BCG that begins near the ECG R peak.
- **The I wave** appears early in the systole, in the footward direction.
- **The J wave** is the largest headward wave of the BCG, which occurs later in the systole.
- **The K wave** is the next footward ballistic wave to appear near the end of systole and may extend into the early diastole.
- **The L and N waves** are the smaller headward waves in the diastole with a footward wave in between them named the **M wave**.

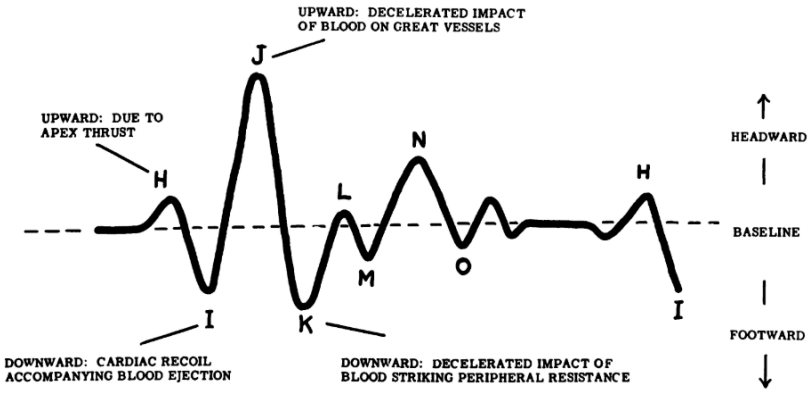

Figure 2.3. Example of a standard ballistocardiogram signal with its main waves. Picture from [36]

Starr proposed the application of Newtonian physics to the problem of heart disease, as a quantitative way of looking at the old physiological conception of cardiac weakness. Using a

cadaver Starr tied large tubes in the aorta and pulmonary artery. He injected water or blood into the great vessels against normal counter pressures, using large syringes, and used his arms' muscles for the myocardium. He then injected a normal stroke volume in the regular ejection time to simulate the systole [38]. In another study, Starr used standard weights of 115 lbs. to make a mechanical impulse to calibrate his BCG bed. The response recordings obtained by automatic application of the mechanical impact maker to the head of the cadaver [39].

When a subject lies on the table, he is not conscious of its motion, but the records obtained are characteristic and reproducible. Multiple forces have been identified by [40] as the source of this motion, including the recoil caused by pumping blood out of the heart, or when the blood reaches the aortic arch and the curve of the pulmonary artery. Also, the accelerated blood that moves footward after the arch of aorta produces a small recoil impact. Reproducing the waveform from these forces is not completely possible, due to the variations in the physical properties of the body. These recoil vibrations mainly affect the descending waves, while having a much smaller effect on the ascending waves; hence, more reliable features can be extracted from the ascending waves.

2.3. Instruments

2.3.1. Classical instruments

Multiple groups have investigated instrumentation for accurate BCG measurements. For instance, Bixby and Henderson [41] used a light beam system, a photokymograph and an old electrocardiograph with a photographic recording camera, to measure the ballistocardiographic movement of the body. Starr first tried and later abandoned the freely swinging table (ultra-low frequency)[16], and instead proposed measuring only the longitudinal motion by a sturdy steel spring, which was able to cancel the respiratory movements. This device, as shown in Figure 2.4, is a thin panel braced and mounted on a frame with a total weight of 50 pounds. They have designed

a mechanism of flexible wall-mounted joints to prevent the lateral motion of the table. An adjustable spring mounted on the rigid holding structure, which is screwed to the floor. This spring holds one end of a small mirror and its other end is mounted on the apparatus frame. Thus, small stretches of the spring will cause slight movements in the mirror. A very similar apparatus was designed and commercialized by Japanese company Nihon Kohden in 1952. This device was using the body's recoil caused by the ejection of blood from the ventricles and thus was able to measure the blood passing through the heart and the forces of cardiac contraction [6, 42]. Figure 2.4 shows some examples of these classical BCG instruments.

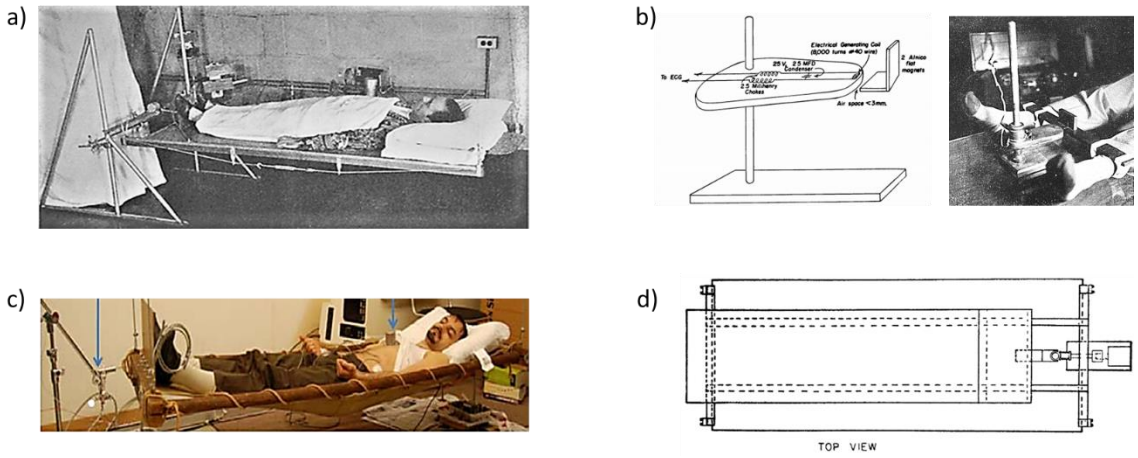

Figure 2.4. Examples of the classical BCG instrument: (a) Starr's one-directional high frequency, floating BCG board and its mirror-based ECG camera [39]*. (b) Dock's electromagnetic BCG device*[34]*. (c) Original Ultra-low frequency BCG suspended bed created by Burger and Noordergraaf* [43] *picture from* [44, 45]*. (d) Nickerson's (low frequency) BCG table* [46].

2.3.2. Four major types of BCG instruments

Despite having a common source, each device shows a slightly different "template" for the same subject [6]. Due to the design differences between these devices, each one might have a different natural frequency response, which primarily results in different dampening and filtering of the actual signal. The Committee on Ballistocardiographic Nomenclature defined four essential

types of ballistocardiography devices, including the high-frequency, low-frequency, ultra-low frequency, and the direct-body [47] ballistocardiographs.

The high-frequency ballistocardiograph (HF-BCG) also known as Starr-type is a table, bed, or platform holding the body, weighing from 1 to 1/10 of an adult body weight, with a footboard to improve the coupling. **Starr**'s ballistocardiograph was made of a thin ply panel mounted on a spruce frame without any vertical or lateral movements [39] [46], while **Dock** designed an electromagnetic ballistocardiograph with a light bar of wood, and a magnet mounted to it to move against a coil embedded in the bed frame [34, 48-50].

This type has 7 standard waves, where the H wave is the peak near the beginning of the systolic ejection and expulsion of blood into the aorta, followed by the I wave in early systole which reflects the rapid acceleration of blood in the descending and abdominal aorta, pulmonary trunk and carotid arteries [51]. The J wave is the most significant upward wave, which immediately comes after the I wave in the late systole. It comes after the acceleration of blood in the descending and abdominal aorta, and the deceleration of blood in the ascending aorta. The last wave in the systolic phase is the foot-ward K wave. It is usually followed by two smaller headward waves of L and N in the diastole. The footward wave between them is called the M wave. The tiny footward wave right before the H wave in the presystolic (pre-ejection) phase, is called the G wave. The I–J amplitude reflects the force of contraction of the left ventricle, and the I–J interval reflects its contractility [51].

The low-frequency ballistocardiograph (LH-BCG), also known as Nickerson-type, is very similar to the HF-BCG with a critically damped platform using a deadweight equal to the weight of the subject. **Nickerson** used a wooden table to capture ballistocardiogram. These devices generate the same number of waves (G, H, I, J, and K) as in the HF-BCG, but with a time delay. This device is sensitive to the respiration, so most of the data was acquired when the subject was holding his breath, with special care to avoid an inadvertent Valsalva maneuver.

Ultra-low frequency ballistocardiograph (UF-BCG) is a suspended platform (hammock) weighing 1/6 to 1/60 of the body weight with minimal vertical or flexural vibrations. The UF-BCG usually have fewer sinusoidal waves, with a tiny K wave, all come earlier in time than the HF_BCG waves. The best results usually appear after suspending the respiration as the respiratory movements are much higher than the BCG in the amplitude.

Direct-body ballistocardiograph (DB-BCG) is to capture the motions of a single part of the body and does not need the subject to lie on any suspended or special platform, but rather to recline on a rigid surface with different transducers used to measure the body part motions. The waveforms are similar in form to the ones from the HF-BCG with a time delay. Here again, the respiratory activity affects the recordings unless the subjects hold their breath.

Figure 2.5 shows the templates acquired from multiple apparatuses, including the Ultra-low frequency [18],[20]. High-frequency apparatuses ($\omega_0 = 10Hz - 15Hz$) are better at reflecting the forces while the ultra-low frequency devices ($\omega_0 < 1Hz$) are better in displacement measurement [45]. Despite having a common source, each device shows a slightly different "template" for the same subject [6].

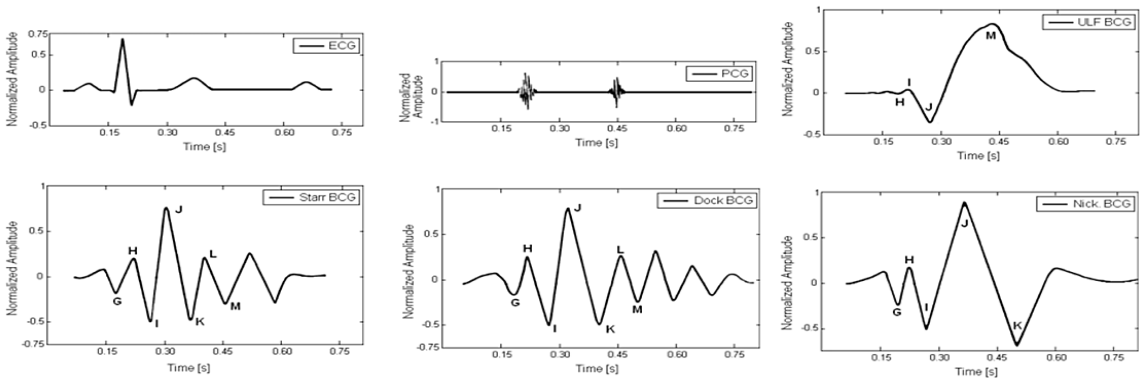

Figure 2.5. Illustration of one cardiac cycle template from multiple sensing modalities. The top row has the ECG, PCG (Phonocardiogram), followed by four different measurements of BCG: Ultralow Frequency[18], Starr's HF BCG bed [39], Dock's electromagnetic HF BCG device[34], and Nickerson's LF BCG table [46]. Variations in the BCG templates are due to the mechanical aspects of the apparatus.

2.3.3. Modern instruments

Ballistocardiography could not be used for clinical purposes because of the unrefined nature of the previous BCG acquisition devices with their limited technology, and the sizeable inter-subject variability of the waveforms without proper interpretation [52, 53]. More recently, the technological and manufacturing advancement in the MEMS technology opens new doors to develop different efficient and affordable non-invasive sensor modalities to capture ballistocardiography in standard home settings by embedding them in commonly used objects (e.g., weight scales, bed, chair).

Bed-based transducers are the most widely used BCG devices which cover different modalities including the charge-sensitive [54], piezoelectric mats [55] and electromechanical films [56, 57] that are developed after the recent advancements in the MEMS technology. A new ElectroMechanical Film (EMFi) with a cellular charge-sensitive polypropylene structure can generate an electric charge proportional to the amount of pressure applied to the film [56, 57]. This structure makes the EMFi sensitive enough to capture dynamic forces exerted to the surface, including the electromechanical activities of the heart [57].

Load cells are also shown to be capable of capturing the small ballistic movement of the center of mass and have been placed under the mattress [58], and under the bed legs [59-61]. Etemadi, et al. [62] recorded the forces applied to the strain gauges of a modified home bathroom scale. These forces are due to the heartbeat, respiration, and body movements. They have also embedded the ECG and PPG sensors to the scale surface and its hand holder (Omron HBF-500 [63], InnerScan BC-534, Tanita[14]).

Accelerometers are capable of capturing tiny motions in the bed frame or mattress caused by the respiration and heartbeat. They have been used for the measurement of respiration rate, heart rate, heart rate variability, and stroke volume [64, 65]. Accelerometers are also used to measure the ballistocardiographic movements of the bed or the seismocardiogram on the chest [66-68].

Fiber optics are placed between a pair of microendes, and any movement of the subject causes displacement between them and changes the light intensity[69]. Pressure based transducers including the pneumatic strips[70],[58, 71] that measures heartbeat through a thin, air-sealed cushion placed under or on top of the bed mattress, or the water-based transducers to be placed under the pillow used by [72]. The MU hydraulic bed sensor contains four water-based pressure transducers placed under the mattress and shown to be capable of capturing restlessness, respiration, and heart rate.

Figure 2.6. Examples of modern BCG sensors for in-home applications. a) Emfit sensor [73], b) Beddit sleep monitor[74], c)MU's hydraulic bed sensor [75], d) Murata contactless bed sensor[65], e) Modified bathroom scale (Omron HBF-500) [63], f) Load cells (MNC-50L, CAS, Co. Ltd., Korea)[59]

Each of these sensors has its own advantages and disadvantages. For example, the very popular electromechanical film (EMFi) sensors are more expensive, while the very inexpensive accelerometers tend to capture fewer morphological details. The load cells provide valuable measurement about the displacement of the center of mass but are harder to install, while the more accessible bathroom scales could capture short periods of time while the subject stays still on the scale. Table 2.2 provides a list of recent innovations for in-home measurement of ballistocardiography and their pros and cons.

Table 2.2. Comparing the pros. and cons. of different BCG sensors.

	Pros	**Cons**
Weighing scale	Exact Y direction Possibility to connect other sensors	Motion Artifact Short time Not for all health conditions
Under Mattress	Contact-less Longtime overnight	Motion artifact
Bed Frame	Contact-less Overnight	Motion artifact No detailed morphology
Under Pillow	No mattress-effects Focused on the head area	Motion artifact Biased toward the head flow
Chair	Possibility to use during the working day or resting time	Motion artifact Complexity in install Not clear waveform

3. MU BCG INSTRUMENTS AND DATA COLLECTIONS

A variety of systems are currently being used for research purposes in our lab and for different data collections, including the hydraulic bed sensor, suspended bed, and the chair sensor. Our hydraulic bed sensor targets the longitudinal and noninvasive monitoring of vital signs including, but not limited to, the heart rate, respiratory rate, sleep posture, sleep stage, blood pressure, and other cardiac conditions [11-13]. The suspended bed is a replica of the original ultra-low frequency suspended bed that is used by Isaac Starr, and we use it mainly as a reference to validate our efforts in modeling the BCG. We also have been working on extending our BCG sensors coverage to even outside the bed. Therefore, we designed an accelerometer-based chair sensor and studied its capabilities in monitoring the heart rate and respiratory rate. Although I am not using the data from the chair sensor in this dissertation, it is included for completeness.

3.1. The hydraulic bed sensor

Our hydraulic bed sensor, as the primary source of data collection for this work, initially was designed to capture heart rate and respiratory rate, while the person lays on the bed, mostly during the night [75]. It is composed of a set of four water tubes each fitted with a pressure sensor to be placed under the bed mattress for the purpose of non-invasive ballistocardiography measurement. The four-channel signal contains a DC bias (the weight of the body lying on the bed) in its raw format. Figure 3.1 represents a sample configuration of four hydraulic bed transducers on a regular bed and underneath its mattress, and the filtered ballistocardiography signals acquired from the four transducers. It also shows the synchronously captured ECG signal as a reference for the electrical activity of the heart. The best arrangement for the transducers has been previously studied, and we used the same recommendation in all data collected for this research. DC values of the four channels are believed to be correlated to the placement of the person on the bed [76].

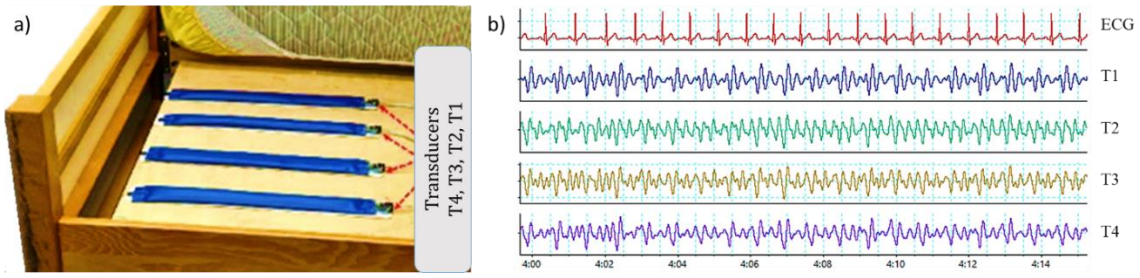

Figure 3.1. MU's hydraulic bed transducers and example of their BCG signals: (a) T1 through T4 are the four transducers longitudinally placed underneath the mattress close to the headboard of the bed with pressure sensors under the torso area. (b) 15 seconds synchronized ECG signal and the corresponding 4 BCG channels from the transducers.

3.2. The chair sensor

Considering the increase in the median age of the general population, which has resulted in the increased risk of cardiovascular ailments [77], and the quality of the independent life of the elderly, in-home monitoring the vital signs have become essentially important. A recliner chair could potentially be used as a target for data collection, as it is often used by older adults, even for sleeping at night, for those with breathing difficulty, neck and back problems, or other pain. In [78], a sensor system is proposed for recliner chairs, which measures heart rate and respiratory rate of the person sitting on it. The system uses two accelerometers placed strategically to capture these vital signs noninvasively and without direct contact with the body, while at the same time, being hidden from view.

Several different chair sensors have been used in the literature mostly to capture activities [79-81], such as posture, sedentary activities, and behavior assessment, sometimes with costly sensors [82]. In an effort to measure the BCG signals from the chair, Junnila, et al. [83] has placed electromechanical film (EMFi) sensors on the seat and backrest of the chair, and Baek, et al. [84] placed polyvinylidene fluoride films (PVDF) on the seat to measure the change of pressure. In addition, the pressure mats and the FSRs in [82, 85] are placed on the surface of the seat and the backrest of the chair, which change the look and feel of the chair. Our system, in contrast, is

designed primarily to be an inexpensive and easy-to-mount sensor, which is entirely out of sight after installation on the recliner chairs. Our target population in this chapter is older adults.

Figure 3.2. MU's accelerometer-based chair sensor for vital sign monitoring (a) Accelerometer placed under the seat cushion of the recliner chair. (b) Accelerometer placed on the side of the seat cushion, hidden between the seat cushion and the arm of the chair. The accelerometers are not visible during normal operation and require no contact with the occupant to function. (c,d) Two chair positions were tested in the study: Upright (left) and Reclined (right). For ground truth reference, a chest band and a finger pulse transducer were worn by each study participant.

Besides finding the placement on the chair which potentially contains the highest amplitude in the captured acceleration, we were constrained to place the sensors in the locations on the chair that are hidden from view, which will not cause any discomfort and also would not need any modifications of the chair. While no studies have been done on the morphology of the waveforms,

the experiment on 45 older subjects (with an average age of 78 years) published in [78] shows high accuracy in estimation of heart rate and respiratory rate.

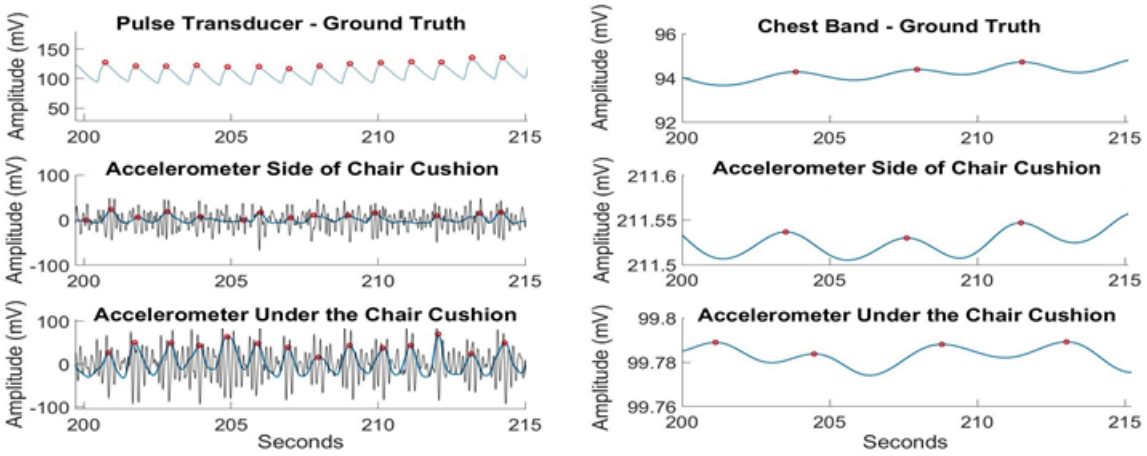

Figure 3.3. Example of BCG signals obtained from the chair accelerometers (a). Overlaid on the BCG signal is the output of our Energy algorithm, (b) Respiration signals obtained from the chair accelerometers.

3.3. The suspended bed

Our suspended bed is a replica of the suspended ballistocardiography bed originally designed by Burger, et al. [43] according to the details provided by Ngai, et al. [45]. This ultra-low frequency ballistocardiograph device is made of a lightweight foldable aluminum frame approximately 207 cm by 78 cm fixed on top of two lateral wood frames. The frame is suspended at four points from the ceiling with 3 m long steel cable of approximately 2.5 mm in diameter such that the cables are parallel to each other. One accelerometer (Kionix EVAL-KXR94-2283 [86]) with 3 active axes of 1000mV/g sensitivity, was placed on the wood frame and four short hydraulic transducers positioned underneath the torso area. I studied different soft and rigid materials (thin plastic cot, wood board, thin air mattress) on top or under the transducers to improve the quality of the BCG waveforms. The total weight of the bed and all extra materials were always kept at less than 8 Kg.

To verify that our suspended bed is inconsistent with the true concept, we followed the recommendations provided by Tavakolian [44], where he tested a very similar design for the

suspended bed and verified the device is an ultra-low frequency device according to the definition. I have also made a secondary visual comparison between the accelerometer signals and the templates from the book by Starr ad Noordergraaf [87] and showed similar patterns between our templates and the ones reported in that book.

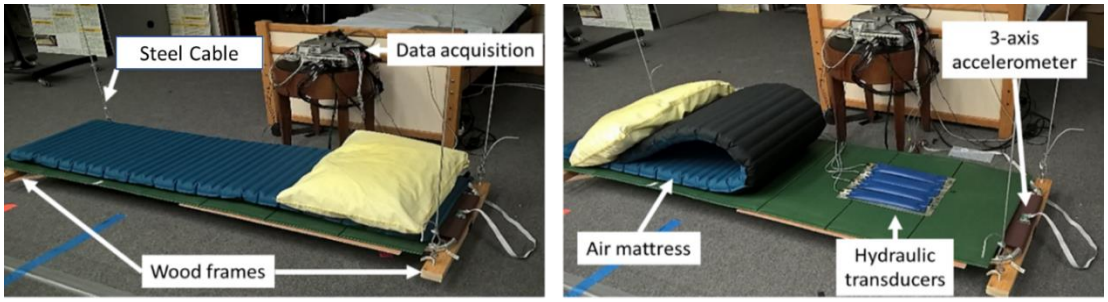

Figure 3.4. MU's suspended bed with cod, wood board, thin pad, transducers, and air mattress.

To our knowledge, this is the most reliable and accessible approach to measure the true acceleration ballistocardiography, as any movement of the body would be measured directly by the accelerometers on its frame. Figure 3.5 shows example synchronous recordings from 3 axes of the accelerometer on the suspended bed, 4 transducers of the hydraulic sensor placed on the suspended bed, and the electrocardiography signal from the person who laid still on the bed. Clear accelerometer signals acquired from this method, are used as ground truth reference for our mathematical model of the BCG presented in a future chapter.

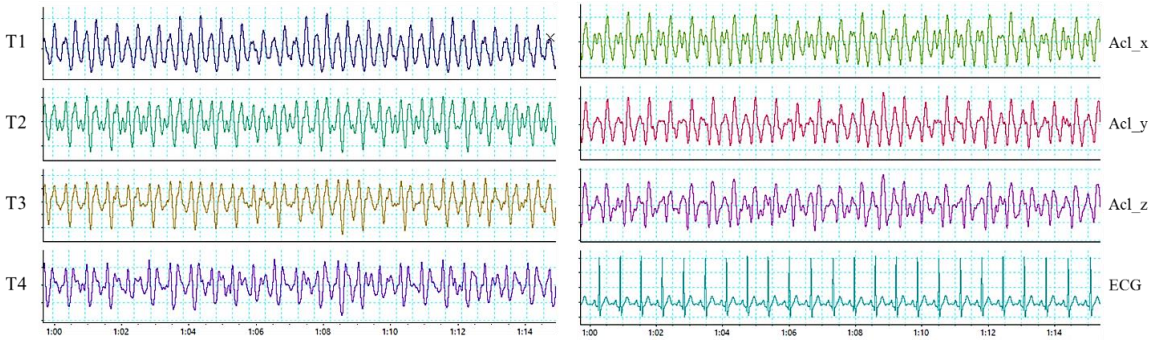

Figure 3.5. Example synchronous signals captured on our suspended bed: (Left) BCG signals from four hydraulic transducers, (Right) signals from the accelerometer along with ground truth ECG.

The very same accelerometers have also been tested to collect Seismocardiographic (SCG) signals. In general, ECG provides information about the electrical activity of the heart and BCG captures the movement of the center of mass of the entire body, while SCG measures the movement in the heart if located in the right place on the chest. By proper filtering of the SCG, we can get information about the open and closure of the heart valves, also known as “lub” and “dub”. For normal healthy subjects, the heart sound consists of two well-defined components, S1(the lub) and S2 (the dub). S1 corresponds to the systolic period and is a good indicator of the heart contraction and begins with the mitral valve closure. The second heart sound (S2) is the indicator of the diastolic period where the heart relaxes, usually starting by the closure of the aortic valve.

As suggested by [88], the accelerometer is placed on the sternum and held in place using the 3M Tegaderm adhesive patches, with its y-axis in the head-toe direction and the x-axis point in the left-right direction with respect to the subject. Preprocessing of the SCG signal to extract the heart sounds has been made through a bandpass filter with 20–250 Hz cut-off frequencies. Figure 3.6 shows an example data collected synchronously from the electrocardiogram (ECG), the 3-axis accelerometer on the chest (SCG), the phonocardiogram reconstructed by filtering the SCG, and also one channel ballistocardiogram (BCG).

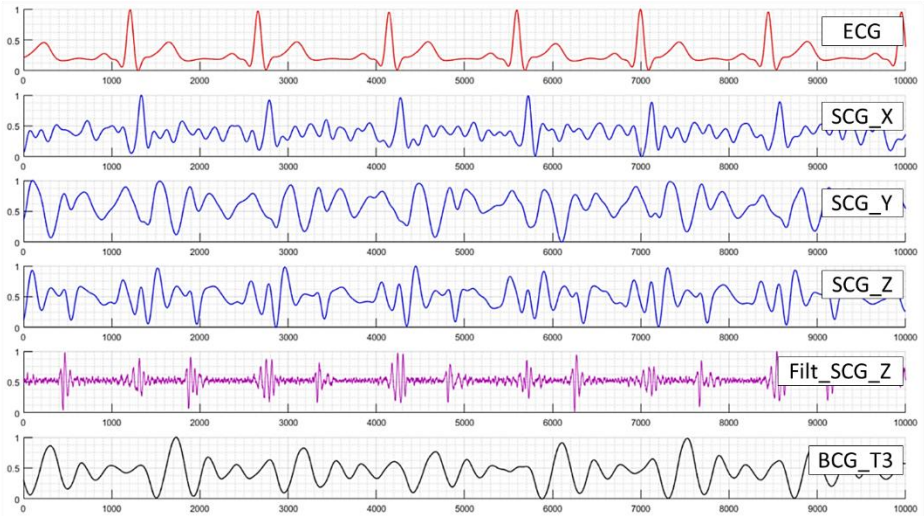

Figure 3.6. Example of data collected synchronously from the ECG, SCG, and BCG. Three accelerometer axes and one BCG transducer are shown.

All these sensors are capturing the same phenomena, which is directly or indirectly related to the flow of blood in the body and displacement of the center of mass. They are so sensitive to even small movements that usually their signals are subject to motion artifacts. A detailed discussion on the sources of motion artifacts and their effect on the quality of vital sign measurements is provided in a future chapter of this dissertation, followed by multiple methods to reduce, detect and discard these artifacts from the BCG.

3.4. Datasets

I have collected some small datasets with our research team members as subjects, as an initial proof-of-concept. I also have designed or have been involved in multiple IRB approved studies to collect ballistocardiography data from volunteers of different age and health conditions. For most of these datasets, we tried to have a complete set of sensors as the reference for the analysis, including the ECG, PPG, pulse, and respiratory band. We have used an ADInstrument's PowerLab 16/35, with the latest version of LabChart, to create separate files per subject per study. The PSG data from the hospital sleep lab was received in the ".EDF" format for the wearable sensors, and the normal."DB3" files related to the bed sensor. All files have been exported to MATLAB files for any future analysis, as described in the appendix.

3.4.1. Data collections

Table 3.1 provides statistics about the three most extensive datasets that we collected specially to validate our hypotheses on the ballistocardiographs collected from the hydraulic bed sensor. Multiple targets have been addressed by these datasets, including the estimation of heart rate variability (HRV), detection of sleeping posture on the bed, evaluating the change in blood pressure caused by exercise in young, healthy subjects as well as older residents of Tiger Place.

Table 3.1. Overview of the datasets collected for this study.

IRB #	Initial Purpose	Condition	Duration	Subjects	Age	Gender	Health	Setting
2002586	HRV	Supine Rest	10 min	62	18-50	15F/47M	Healthy	Lab setting
	Sleep Posture	Four postures	5 min	62				
	Blood Pressure	Supine Rest	3 min	62				
	Blood Pressure	After Exercise	7-11 min	62				
2006391	Blood Pressure	Supine Rest	10 min	50	19-95	34F/15M	Mix	TigerPlace
2008526	Sleep Stages	Over night	1 night	56	31-86	27F/49M	Mix	Boone H

3.4.2. Reference sensors and annotations

In most of the data collections, we tried to use multiple reference sensors to expand the future possibilities to use them. All data were collected synchronously using the PowerLab data acquisition system from the sensors listed in Table 3.2. In the hospital settings where the reference signals came from the clinical devices, hydraulic bed signals were manually synchronized to the rest of the signals using a physical marker that nurses provide on both data right before the beginning of the data collection. For that reason, the nurses were asked to push three times on one of the ECG leads that are connected to the patients, so that three distinct noisy regions with high amplitudes appear on both the PSG recordings and the bed sensor signals. Then we manually aligned these markers to provide synchronized PSG and BCG signals for all subjects.

Table 3.2. List of sensors that have been used in my data collections*, along with the bed sensor. Except from the sleep lab data, other datasets were collected using the AD Instruments LabChart.*

Sensor name		**Placement**	**Num channels**
ECG	Electrocardiogram	3 leads on the chest	1
PPG	Photoplethysmogram	Right index fingertip	1
PEFS	Piezo-Electric Finger Sensor	Right ring fingertip	1
Respiratory Band		Around the chest	1
Blood pressure cuff		Left arm	Store separately
BCG	Ballistocardiogram	Under the mattress	8
Accelerometer		Edge of the mattress	3
Smartphone		Edge of the mattress	Store separately

3.4.3. Health status questioners

To have accurate health information at the time of data collection, some short-term health-related questions were provided in the questionnaire form, as listed below. This information was used firstly as a criterion during the recruitment, and secondly as a future reference for comparing the between-group variations. Table 3.3 provides an example of these questionnaire forms which older subjects were asked to fill. We used different questionnaires for each study based on the requirements of each as described in the corresponding IRB project protocol.

Table 3.3. Health status questionnaire to provide information about the volunteers.

Age:	**Gender:**	**Height:**	**Weight:**	**Date Time:**
Have you ever been diagnosed with any of the following in the past six months?				

Yes	No	Have you drunk Coffee, Tea, or Alcohol in the past 6 hours?
Yes	No	Heart problems (such as heart surgery, heart attack, irregular heartbeat, CHF)?
Yes	No	Lung problems (COPD or emphysema)?
Yes	No	Do you use the pacemaker?
Yes	No	Do you ever have chest or heart pain?
Yes	No	Do you lose your balance because of dizziness / do you ever lose consciousness?
Yes	No	Are you currently taking medication for high blood pressure or heart condition?
Yes	No	Heart problems (such as heart surgery, heart attack, irregular heartbeat, CHF)?
Yes	No	Lung problems (COPD or emphysema)?
Yes	No	Do you ever have chest or heart pain?
Yes	No	Do you lose your balance because of dizziness, or do you ever lose consciousness?
Yes	No	Are you currently taking medication for high blood pressure or a heart condition?
Yes	No	Do you have any other physical condition that would need physician approval before starting an exercise program?
Yes	No	Has your physician ever told you that you have bone, joint, or back problems that can be made worse by physical activity?

4. SLEEP POSTURE CLASSIFICATION

4.1. Background

With the recent advances in health care, the average lifespan of older adults is increasing. This increases the necessity of better and more accessible monitoring tools specialized for the needs and conditions of this population. One significant aspect of elderly life is a large amount of time they spend in bed. Adults usually spend one quarter to one-third of their daily life in bed [89] while the elderly usually stay in bed more than that. If their sleeping posture and movements are measured and evaluated quantitatively over a period of time, not only can nurses assist them better, but also the automatic health monitoring systems can be used to detect health issues.

There is a two-way relationship between health and sleep posture. Some sleep disorders may appear due to the decline or changes in health condition. For example, Leung, et al. [90] reported that for patients with Congestive Heart Failure (CHF), the amount of time spent in the right lateral position is significantly more than the amount of time spent in the left lateral position. My proposed classification technique can help them in reducing the discomfort caused by the enlarged apical heartbeat or further hemodynamic or autonomic compromise. Meanwhile, about 20~40% of the elderly population are suffering from sleep apnea and hypopnea syndrome (SAHS), and more than half of the patients remain undiagnosed [91]. By modification of sleep position and preventing supine sleep, Jackson, et al. [92] reported improvement of sleep-disordered breathing for positional Obstructive Sleep Apnea (OSA) patients.

In sleep studies, neurophysiological signals and polysomnography (PSG) are used due to their accuracy [93]. Sleep studies are usually expensive, and the patients are asked to stay overnight in hospitals. In-home sleep monitoring systems would help researchers to analyze sleep conditions in a natural setting such as the patient's own home. Long-term care facilities may also take

advantage of sleep-related information on the treatment plans for their residents. As a result, we see an increase in demand for low cost and efficient monitoring systems for the elderly [94].

In polysomnography, different devices such as accelerometers, gyroscopes, and magnetometers are being placed on the chest, wrist, or feet of the subject. Although these sensors can accurately measure the thoracic respiration, heartbeat, as well as body posture, they all need to be worn during sleep, making an inconvenient sleep experience for the subjects. Noninvasive methods such as camera-based techniques are the common approach of monitoring in-bed postures. As an example, the use of 3D depth scans of the body is explored in [95]. The main issues with the camera-based approaches are privacy concerns and limitations in obtaining images at night.

The majority of recent noninvasive methods for in-bed posture recognition use high-density pressure mats to identify the structure of the whole body. A dense grid of 42×192 pressure sensors was used in [96], with sampling rate at 1 frame every 3 seconds, to classify the supine, prone, left and right postures. While, a total of 6144 square sensors within a region of 33×73 inches were utilized by Sun, et al. [97], for their limb clustering algorithm. Conductive textile sheet [98] and static charge sensitive bed [89] are also being used for posture detection.

Although most of these methods reported high recognition accuracy, usually hundreds of pressure sensors are required in a mat for a complete data acquisition. Recent approaches are seen to decrease the number of sensing elements. In [99], 48 conductive sensors were placed between the mattress and the bedsheet. They reported 80.76% accuracy for their classification task. Hsia, et al. [100] uses 16 long-narrow force-sensing resistor (FSR) sensors. Additionally, Viriyavit, et al. [101] had only four sensors, i.e., two piezoelectric and pressure sensors are used for data acquisition. They reported 89.9% accuracy for three postures, i.e., back, left, and right, with 5-fold cross-validation and on 120 hours of data collected from one subject.

On the other hand, different classification algorithms have been applied by researchers for the estimation of in-bed sleep postures, including Bayesian classification [100], K-nearest

neighbors [96], and SVM [102]. An accuracy of 98% is reported by Boughorbel, et al. [96] through the application of KNN and SVM. Hierarchical inference model with the binary SVM classification also tested by Liu and Ostadabbas [102], where they reported high accuracy of 91% after applying PCA. Despite the ease of application, Neural Networks have been used only in a handful of papers. For example, Seo, et al. [89] used neural networks to estimate pose and motion, to assist the patients using their Intelligent Bed Robot System (IBRS).

The focus of the current chapter is on the evaluation of different parameter settings for the application of neural networks in sleep posture detection using the data acquired from an in-home setting of only four hydraulic bed sensors. Section 4.2 of this chapter presents a brief overview of the system and the data collected for the experiments. Data preprocessing and feature extraction, and the classification method will be described in Section 4.3. In Section 4.4, I have discussed different parameters in the classification method, and the experiments and their results. Finally, 4.5 provides a brief summary of the work, along with avenues for future investigation.

4.2. Sensor and data

In this study, I am using the MU hydraulic bed sensor designed for capturing ballistocardiogram (BCG) signals [75]. It is composed of a set of four water tubes, each fitted with a pressure sensor (Figure 4.1) which are placed under the bed mattress for the purpose of non-invasive heart motion measurement. The four-channel signal is sampled at 100 Hz and in its raw format, it contains a DC bias (the weight of the body lying on the bed). I simply ran a moving average to remove the high-frequency part of the signal and keep the DC bias. Variations in the DC values of the four channels are known to be correlated to the location of the person on the bed.

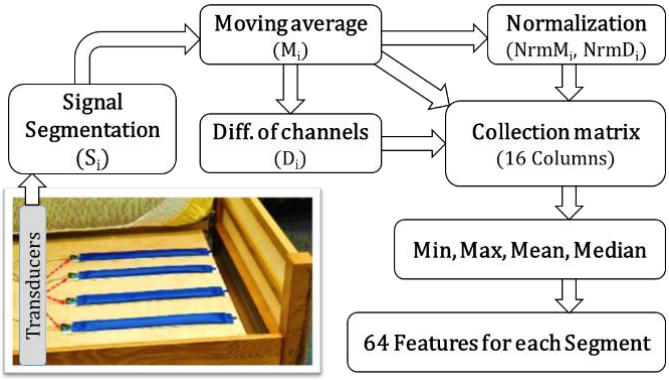

Figure 4.1. The workflow of bed-data preparation for the classification task, from the transducers to the feature extraction. Our bed sensor consists of four hydraulic transducers placed underneath the bed mattress.

A total of 58 young, healthy subjects were recruited and asked to lie still on each of the main postures for one minute. The exact definition of supine, prone, left lateral, and right lateral, was somewhat subjective and left for the subjects' interpretation (Figure 4.2).

The data collection procedure was approved by the University of Missouri Institutional Review Board (MUIRB). A separate file containing four data channels has been created for each subject and per posture. In order to create the dataset, all channels were divided into multiple segments of equal length. Features extracted from each segment are used for signal segmentation, as described in algorithm I.

The algorithm I Signal segmentation

Goal: Segmentation of data acquired from one subject on a specific posture.

Requires: Ti, Signal acquired from each transducer for the entire length.

ST, Segmentation length. Could be 5, 10, 15, or 20 seconds.

```
1:function signal_segmentation(T1, T2, T3, T4)
2:    ST = 15*Fs;                          % Segment length in Seconds
3:    for i=1:4 do
4:        Si = reshape( Ti, len(Ti)/ST, ST);  % Cut the signal
5:    end
6:End
```

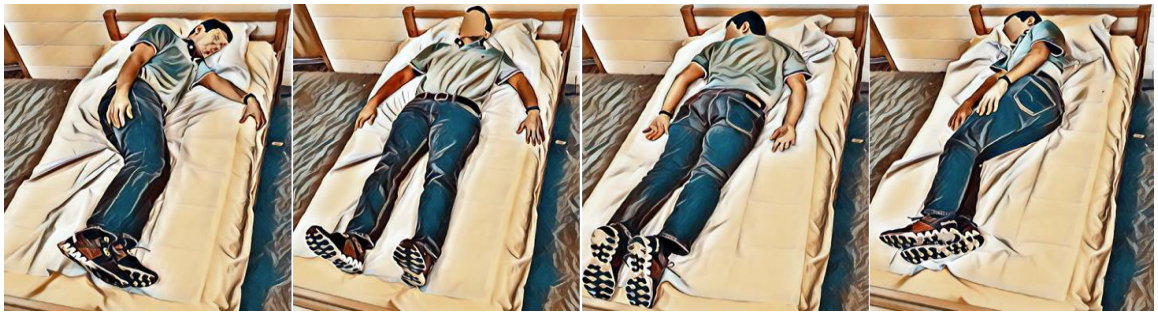

Figure 4.2. 58 volunteers were asked to lay still on each posture for one minute. The exact definition of Supine, Prone, Left Lateral, and Right Lateral, was somewhat subjective and left for the subjects' interpretation.

4.3. Method

4.3.1. Feature extraction

Authors of [103], [93] reported the use of a set of statistical features including mean, standard deviation, minimum and maximum of sensor values and also the kurtosis of the frame values. They reported high accuracy rates for using statistical features, especially being applied to a limited number of sensors. Consequently, I also based my classification on a set of simple statistical features, as described in algorithm II. All channels were divided into equal-length segments S_i. The length of segments varies between configurations (e.g., 1,…,5 seconds). Then a set of 16 simple statistical features were extracted from each signal, in the following manner. A moving average M_i is computed for each channel, resembling the DC value of that channel over time. Then, the difference between the adjacent channels was computed as $D_i = M_i - M_{i+1}$. We then normalized both computed vectors of M_i and D_i, using formulas 1 and 2 where we subtract the mean value in order to center the data and then divide by the global range of that segment:

$$NrmM_i = \frac{M_i - mean(M_{1\ldots4})}{\max(M_{1\ldots4}) - \min(M_{1\ldots4})} \quad (1)$$

$$NrmD_i = \frac{D_i - mean(D_{1\ldots4})}{\max(D_{1\ldots4}) - \min(D_{1\ldots4})} \quad (2)$$

Finally, we put all these 16 vectors in the form of a columnar matrix. By applying four functions of Min, Max, Mean, and Median on the columns of this matrix, we made our feature set of size 64 (=16x4).

Algorithm II Feature extraction

Goal: Extracting features from one signal segment in the time

Requires: **Si,** Signal acquired from each of the four transducers

```
1:function feature_extraction(S1, S2, S3, S4)
2:    W = 5*Fs;                  % Window size in Seconds
3:    for i=1:4 do M(i) = moving_mean(S(i), W);          % DC bias
4:    for i=1:4 do D(i)  = M(i)-M(i+1);                  % Diff. channels
5:    for i=1:4 do NrmM(i) = (M(i)-mean(M(:)))/range(M(:));
6:                 NrmD(i)  = (D(i) - mean(D(:))) /range(D(:));
7:    Matrix   = [M(:,:), D(:,:), NrmM(:,:), NrmD(:,:)];   % Collection
8:    Features = [min(Matrix), max(Matrix),              % Statistical func.
9:                mean(Matrix), median(Matrix)];
10:end
```

With a total of 64 features per sample point, for 58 subjects and over 4 sleeping postures, I ran multiple experiments to investigate the best configuration settings. I applied Matlab's PCA function called *pcares*, to sort the features in the original domain. Moreover, then we selected the first 4 or first 16 features for classification tasks. For the principal component analysis (PCA), we compared the set of best 16 features to the set of best 4 features.

PCA is one of the most widespread methods in data analysis. It consists of applying orthogonal transformations to variables that are assumed to be possibly correlated, in order to make them linearly uncorrelated, aiming to preserve the most variations between the data variables and avoid redundancy. Hence the first principal component is the one that accounts for the most data variability, while the second account for less variance, and is orthogonal to the previous one, etc. The resulting uncorrelated variables form then an orthogonal basis set.

4.3.2. Classification Procedure

The classification process was performed using a feedforward neural network. I explored some parameters of the neural network itself, including the number of hidden layers and the number of nodes per layer, the activation function of each layer, and the amount of regularization. I used MATLAB's implementation for the neural network as an easy to use API, which provides the ability to manually set all these parameters (Figure 4.3).

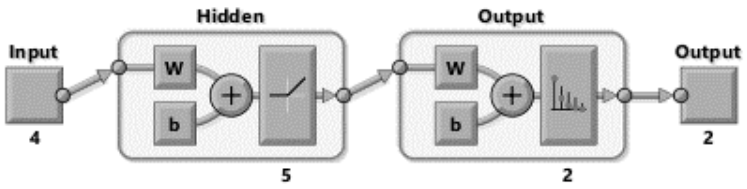

Figure 4.3. An example neural network with one layer of 5 nodes. For input, it uses 4 features after PCA, and generated 2-class labels as output.

For the number of hidden layers, both 1 and 2 layers were used. I then changed the number of nodes per layer, to be either 5, 10, 20, or 30 neurons to change the complexity of the model. Also, for the activation function, the hyperbolic tangent sigmoid function (*tansig*) was used, which is a faster implementation of tanh function. I also used the Positive linear function (*poslin*), which is MATLAB's implementation of the rectified linear unit (ReLu), as described in Figure 4.4.

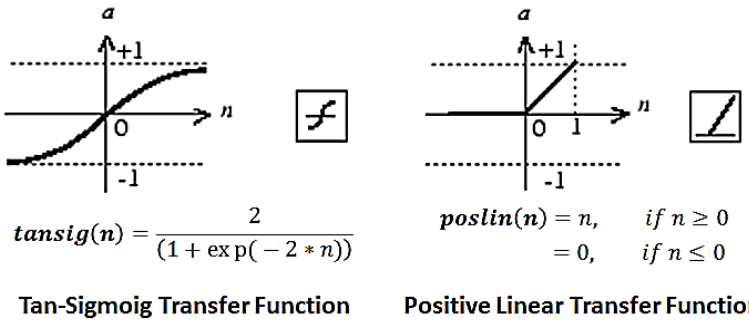

Figure 4.4. Schematic definition and formulation of the two transfer functions that I compared.

Regularization was another parameter to explore, which addresses the over-fitting problem in training the neural networks. In over-fitting, the network "memorizes" the training examples,

instead of learning a general pattern. Having very few training samples, or too many free parameters (weights of the network) without using regularization may cause overfitting. I tried three values of 0, 0.1, and 0.5 for the regularization.

Another gap in the literature was related to the validation of the classification accuracy. Despite some papers which did not mention their validation approach, most of the researchers in this field used a k-Fold CV, and there are few papers in which the Leave-One-Subject-Out (LOSO) validation was used [98]. Based on the typical assumption of having independent and identically distributed (i.i.d) dataset, many machine learning researchers use the k-Fold CV to evaluate their classification tasks. In each fold of the k-Fold CV, $1/k$ of all sample points will be selected randomly and tested against the rest of the samples. However, in human activity recognition, we do not always have i.i.d dataset. In fact, Safonov, et al. [104] reported having a non-negligible grouping of data points by subjects. In contrast, in LOSO, samples of one subject are tested against the model being trained by all samples from other subjects together, as described by algorithm III.

Algorithm III LOSO Cross-Validation (CV)

Goal: Leave-One-Subject-Out Cross-Validation
Requires: N, Number of subjects
Fn, Set of 64 feature extracted from subject *n*.
fTrain, the function used to train the neural network
fTest, the function used to test the neural network

```
1:function LOSO_CrossVal([F1, F2, …, F58])
2:    net = feedforward(hiddenSizes, ActivationFn, Regularization);
3:    for i=1:58 do
4:        test_FeatureSet = Fi;                % Test Features, current user
5:        train_FeatureSet = F - Fi;           % All other samples to train
6:        net = train(net, train_FeatureSet)   % Train the network
7:        acc(i) = test(net, test_FeaturesSet) % Test the network
8:  end
9:% Evaluate the overall(mean) accuracy
10:end
```

I used both of these cross-validation methods to make sure my proposed system is capable of classifying, not just random test samples from all subjects combined (as defined in the 10-Fold

cross-validation), but also it is able to learn a general pattern from part of the population and use it for classification of a new unseen subject (claimed in LOSO).

4.4.Experiments and results

In the current work, each classification process consists of setting multiple parameters started by defining the length of signal segments, followed by the number of features selected after PCA, setting the number of hidden nodes, activation function and the amount of regularization for neural network, and finally ended by deciding the type of cross-validation method to evaluate that specific classification task accuracy. Selecting a subset of posture data helps us to explore different class label problems such as classification of "Lateral vs. Non-Lateral", or "Supine vs. Prone".

We used four values for the segmentation length (5,10,15, and 20 seconds), three values for the number of features selected after PCA (4, 16, 64 features), three values for the regularization (0, 0.1, and 0.5), two different activation functions (tansig, poslin), and eight configurations for the number of layers and neurons in the neural network (one layer of 5,10,20 or 30 nodes, or two layers by adding 5 nodes to the second layer). We applied all these configurations on 6 posture-based problem settings (e.g., Supine vs. Non-Supine which are reported in the second column of Table 2.1) and evaluated the classification accuracy using two cross-validation methods (10-Fold and LOSO). Since we had 58 subjects, for LOCO CV, the data from 57 subjects were used for training and was tested against the data from the remaining one subject. This procedure repeated for 58 times always leaving samples of a new subject out for testing.

In total, we ran the entire classification process, for 6912 number of different configurations, which often takes weeks for training and cross-validation. To speed up this work, the computation was performed on the high-performance computing infrastructure provided by Research Computing Support Services at the University of Missouri.

This study gave us a good idea of what postures the neural network is capable of classifying better and what would be the best setting for each classification problem. We report comparisons between the results of 10-Fold CV versus the LOSO, which shows how well a trained network can classify records from unseen subjects in Table 4.1.The best results were produced with 5 second segmentation time, 16 features, more neurons in the first layer, and no regularization.

Table 4.1. Accuracy of posture classification changes with combination of parameters.

Classification Problem		Splitting Time (S.)				Num. Features			Regularization			Num. Hidden Layer Nodes							
		5	10	15	20	4	16	64	0	0.1	0.5	5	10	20	30	10_5	20_5	30_5	5_5
k-Fold	L vs. NL	91	90	89	87	85	91	93	94	94	92	84	88	91	92	90	92	92	85
	LL vs. RL	95	93	93	92	92	94	95	78	76	63	92	93	93	94	93	94	95	92
	S vs. NS	84	81	79	76	75	80	84	83	82	78	74	79	82	83	80	83	84	75
	S vs. P	86	82	80	76	77	81	85	78	77	68	75	80	83	84	81	83	84	77
	S vs. P vs. L	77	77	73	70	66	75	81	92	91	85	67	73	78	80	74	78	80	67
	S vs. P vs. LL vs. RL	76	70	73	70	65	75	79	82	81	77	65	71	76	78	72	75	78	65
	k-Fold total	85	82	81	78	77	83	85	84	83	77	76	80	84	85	81	84	85	77
Leave One Subject Out	L vs. NL	87	87	86	86	83	88	88	89	89	89	83	86	88	88	87	88	88	83
	LL vs. RL	89	89	89	89	89	90	88	70	70	61	89	89	89	89	89	89	89	89
	S vs. NS	71	72	72	72	71	73	72	72	72	72	71	73	73	73	72	72	72	70
	S vs. P	72	73	72	72	72	73	72	68	69	64	72	73	73	73	73	72	72	70
	S vs. P vs. L	67	68	67	66	63	69	69	88	88	84	63	67	69	69	66	68	69	63
	S vs. P vs. LL vs. RL	67	66	68	67	62	69	70	72	72	72	63	67	69	70	66	69	70	62
	LOSO Total	76	75	76	74	73	77	75	76	76	73	73	75	77	77	75	76	76	73

*Postures including Lateral(L), Non-Lateral(NL), Left Lateral(LL), Right Lateral(RL), Prone(P), Supine(S), Non-Supine(NS). Values shown in percentage.

Table 4.2 shows the average and maximum values of 576 separate runs of the entire procedure from feature extraction to cross-validation. The values are computed by aggregating (Avg. or Max) all available data, to illustrate the average accuracy and ultimate potential of each posture setting (the Max column). The max accuracy columns are related to the single configurations which have the highest cross-validation accuracy among all possible configurations. LOSO tends to have lower average accuracy in comparison to the k-Fold because of the higher number of unseen patterns introduced by the left-out subject. For k-Fold, the maximum accuracy

was always above 99%, which means there was at least one configuration setting, which ended up in 99% correct classification of the target. For LOSO, the best value was 93%, which is again less than the results for the k-Fold.

Table 4.2. The average vs the best accuracies for posture classification*, for all possible configurations separated by the posture problem.*

Classification problem	**Avg. Accuracy**		**Max Accuracy**	
	kfold	***LOSO***	***kfold***	***LOSO***
L vs. NL	89%	86%	99%	92%
LL vs. RL	93%	89%	100%	93%
S vs. NS	80%	72%	99%	79%
S vs. P	81%	72%	100%	80%
S vs. P vs. L	74%	67%	99%	76%
S vs. P vs. LL vs. RL	72%	67%	100%	75%
Grand Total (Avg. or Max)	81%	75%	100%	93%

* Lateral(L), Non-Lateral (NL), Left Lateral (LL), Right Lateral (RL), Prone (P), Supine (S)

According to this table, left lateral and right lateral postures were the easiest to classify, probably due to the fact that the rib cage wall moves in opposite directions for these two postures. This possibly introduces differences in the acquired waveforms of the four transducers. The second highest accuracy is related to the classification of lateral from non-lateral postures. Again, the same reasoning is applicable, as the rib cage moves horizontally in the lateral posture while this movement is mostly vertical for the supine and prone postures. By combining left and right laterals together (Lateral) and supine and prone together (Non-Lateral), we achieved as high as 99% accuracy for k-Fold CV and up to 92% accuracy with LOSO. These values are related to the best configuration settings that we explored in this paper and are reported in Table 4.3.

Table 4.3 contains some other examples of the best performing configurations, which lead to high classification rates. Best results usually came from either 0 or 0.1 regularization values. Sixteen features after PCA worked as well as all 64 features in a 10-Fold CV and worked a little better than all 64 features for the LOSO method.

Table 4.3. Sample parameter settings for posture classification *that lead to configurations with higher accuracy rates. Classification accuracies shown in this table are in percentage (%).*

	Transfer Fun.	**tansig**	**tansig**	**tansig**	**tansig**	**poslin**	**poslin**	**poslin**	**poslin**
Configuration	Splitting Time	5	5	5	15	15	20	15	10
	Num. Features	64	64	64	16	16	16	16	4
	Hidden Sizes	20	30	10_5	30	5	30_5	5_5	30
	Regularization	0.1	0	0	0.1	0.1	0.1	0.5	0.5
k-Fold	L vs. NL	96	99	96	92	90	90	88	87
	LL vs. RL	100	99	98	95	93	93	93	90
	S vs. NS	97	98	96	82	77	77	75	76
	S vs. P	97	100	94	79	78	71	78	77
	S vs. P vs. L	93	99	89	77	72	66	64	66
	S_P_LL_RL	92	100	89	80	72	74	59	62
	k-Fold max	100	100	98	95	93	93	93	90
Leave One Subject Out	L vs. NL	86	86	88	91	88	87	86	86
	LL vs. RL	88	89	90	91	90	90	92	88
	S vs. NS	70	70	71	73	77	72	74	76
	S vs. P	68	69	72	72	74	73	73	76
	S vs. P vs. L	66	63	66	71	71	67	62	64
	S_P_LL_RL	67	65	69	75	70	72	54	60
	LOSO max	88	89	90	91	90	90	92	88

*Postures including Lateral(L), Non-Lateral (NL), Left Lateral (LL), Right Lateral (RL), Prone(P), Supine(S), Non-Supine (NS).

Table 4.4. Sample confusion matrix for 10-fold cross-validation *on four-posture classification problem, for one specific configuration setting. Values in percentage.*

Target Postures	**Recognized Posture**			
	Supine	**Prone**	**Left Lat.**	**Right Lat.**
Supine	87.2	1.3	4	7.5
Prone	0.6	98.1	1.3	0
Left Lat.	4.3	1.8	92.8	1.1
Right Lat.	9	0	1.8	89.2

The lowest performance was obtained for the classification of all four major postures, separately, by the maximum rate of 75% using LOSO. It is noticeable that even for this problem,

there is at least one configuration setting which achieves 100% accuracy for k-Fold cross-validation, so it is essential to consider this big difference while comparing results in different methodologies. Table 4.4 shows the confusion matrix for just one of these configurations, made over four-posture classification and averaged over 10-Fold cross-validation.

4.5. Discussion and future work

In this chapter, I discussed a low cost and easy to use in-home device for sleep posture classification that could be used to find correlations between sleep patterns and health conditions such as sleep apnea or CHF. Inconvenient wearable devices or expensive dense pressure mats are usually being used in classifying sleep postures in hospitals. Here, I proposed a new application for our hydraulic bed sensor, which is already installed in many elderly homes and care facilities for longitudinal heart rate and respiration monitoring [75]. I investigated a variety of different parameter settings to find the potentials and limitations of the bed sensor for posture classification using neural networks.

The MU bed sensor with four hydraulic pressure transducers was placed underneath the mattress to maintain sleeping comfort. We collected one-minute data on each posture of supine, prone, left lateral and right lateral, from 58 subjects. Different configuration settings for feature extraction and neural network were explored, and overall performance and some of the best performing configurations were reported.

Our results confirm that in case we use the 10-Fold cross-validation, it is possible to achieve the 100% accuracy for most of posture classification problems. Meanwhile, as it was expected, the accuracy achieved by applying the LOSO CV is, on average less than the 10-Fold CV for the same setting (Table 4.2). This reduced accuracy is due to the fact that in the 10-Fold CV, the dataset is assumed to be independent and identically distributed (i.i.d), which is not always correct [104].

In general, the highest classification rates were usually related to separating the two lateral postures (left and right) from each other (Table 4.3). I believe this is because the rib cage moves in the opposite horizontal directions in these two postures. Classification of lateral versus non-lateral posture was ordered the second. This can also be correlated to the orthogonal direction of chest movement in these postures.

In the future, we will use these best configuration settings to initialize the neural networks for posture classification in homes and care facilities. Noninvasive posture classification in real home environments would give us opportunities firstly to study the sleep patterns of the residents and correlations to the health conditions, and secondly to improve our estimations of restlessness. It also will open potentials for posture-based segmentation for more accurate estimations of vital signs, as they might be correlated to posture.

5. ROBUST HEART RATE ESTIMATION FROM BCG

5.1. Background

Unobtrusive and continuous monitoring of vital signs such as heart rate has broad applications at homes and hospitals and has gained increased interest due to the revival of ballistocardiography. Research has shown that important information can be derived from data collected using BCG sensing technology. Contact-free and non-invasive measurement of respiratory rate, heart rate, sleep stages, sleep postures, and blood pressure are among the possible applications of the ballistocardiography devices, such as our hydraulic bed sensor [105, 106].

Non-invasive assessment of heartbeats in the time domain, among all others, has specific importance because it is being used as a prerequisite for most of the other estimations. BCG reflects the mechanical vibrations of the body caused by cardiac activity [107]. Time-domain detection of cardiac cycles provides information to estimate the beat-to-beat heart rate variation, which is also known as the heart rate variability (HRV) [76]. Segmentation of BCG signals according to the cardiac cycle, makes it possible to estimate and monitor some of the essential mechanical properties of the cardiovascular system, including the blood pressure, cardiac output, and stroke volume.

However, many "automatic/voluntary" and "involuntary" movements of the human body can affect the measurements acquired by the ballistocardiography devices. Respiratory movement of the rib cage wall causes cyclic variations in the DC level of BCG signals, consistently correlated to the respiratory rate. Standard high pass filters cannot completely separate this respiratory variation from the BCG signals. On the other hand, respiration has some systemic/internal effects on cardiac activity, which naturally affect the BCG waveforms. In this chapter, some of these effects are described, and solutions are provided for better separation of respiratory variations from the signal.

Multiple sensor systems are currently being used for non-invasive pulse rate monitoring, including a video camera, an ultrasonic device, mattress-based sensor, infrared diode, and pillow-based sensor [11]. The detection of heartbeats in the BCG signal can aid in tracking these parameters noninvasively. Wearable sensors are also emerging for tracking cardiac health. Important cardiac parameters to track include heart rate, heart rate variability, and irregular heartbeats or arrhythmias. Robust methods are needed to address the noisy environments, especially for in-home settings.

Accurate detection of BCG cycles is a crucial step in morphological analysis of BCG and is the first step in many feature extraction techniques. We have previously published a paper on the estimation of heart rate in the time domain, using the energy of the ballistocardiograms [11], which will be called "the original energy algorithm". The signal of each transducer was modeled as follows:

$$Signal(t) = Resp(t) + BCG(t) + Noise(t)$$

where t is the time stamp, $Signal(t)$ is the acquired signal from one sensor, $Resp(t)$ is the respiration component, $BCG(t)$ is the true ballistocardiography content and $Noise(t)$ represents the additive noise at each time. I used a 6^{th} order Butterworth bandpass filter with cutoff frequencies at 0.7 Hz to 10 Hz, to filter out the high-frequency noise and the low-frequency respiration.

By definition, the ballistocardiographic signal follows a specific pattern during each cardiac cycle, including some standard waveforms as shown previously in Figure 2.3. As described there, the largest headward variation in the BCG waveform is called the J-peak and is the primary reference for different BCG measurements. The J-peak is also an excellent candidate to distinguish individual BCG beats and estimate the heart rate in the time domain. There are already multiple sophisticated algorithms to estimate the location of the J-peak using machine learning techniques [58, 105].

In our previous paper [11], we utilized the short-time (0.3-Second) energy of the signal instead of the amplitude of the J-peak, to detect the cardiac cycles. The short-time energy function is defined in the formula:

$$\varepsilon_i = \sum_{n=0}^{N-1} x_i(n)^2$$

MATLAB's movsum function with a window of 0.3 seconds has been utilized for the estimation of the energy of the signal. A simple moving average function then removes useless high-frequency variations to provide a nice and smooth energy waveform. As shown in Figure 5.1, peaks of the energy function occur once in every cardiac cycle, especially in healthy subjects.

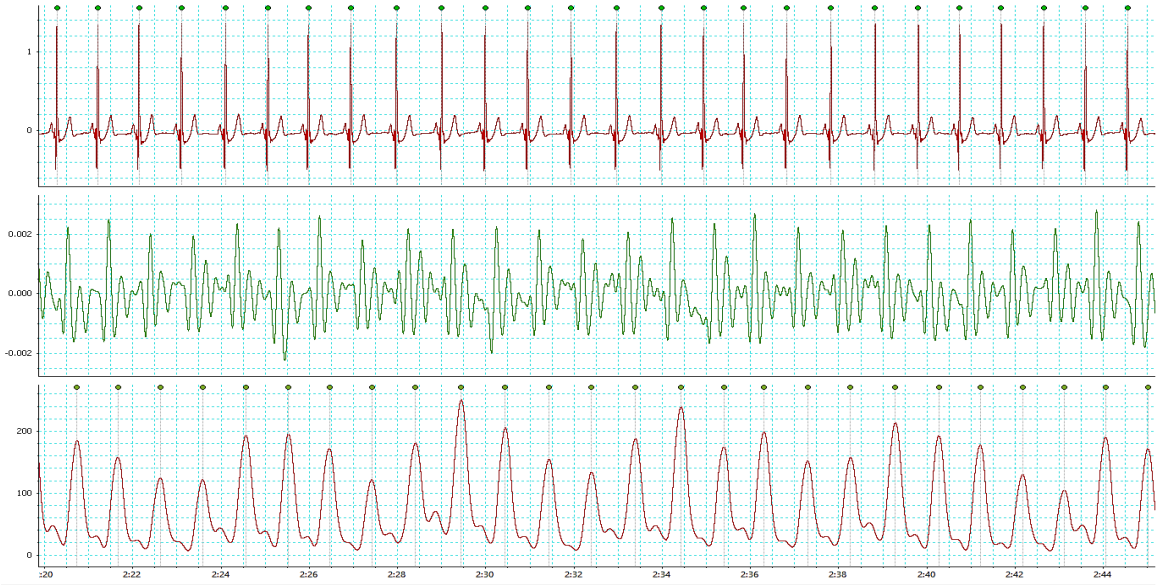

Figure 5.1. Original energy on clean BCG matches the ECG cycles. ECG signal and its peaks(top), filtered BCG signal(middle), the energy waveform computed from the BCG, and its peaks (bottom).

Despite the simplicity of the implementation, the original energy algorithm is known to have a relatively large amount of noise in the beat-to-beat estimation of the heart rate, without extra smoothing. This, in fact, is due to the high possibility of misses in the peak detection approach. This usually causes an extra peak being detected in a single cycle which itself makes one sub-cycle

of inaccurately short (increased heart rate estimation). Similarly, missing peaks due to the lowered signal energy, the estimated beat to beat heart rate will be much lower than it should be. Off course, by averaging all these values, the good approximation will be provided for the average heart rate.

There are multiple conditions which can affect the accuracy of heart rate estimations and more specifically, the ability to estimate beat to beat intervals. Among them is the remaining effect of respiratory variation in the amplitude of the BCG signal. The conventional digital filtering cannot completely separate and discard the respiratory variations of the baseline (DC) from the BCG signals. This is partly due to the non-stationary nature of the BCG and the respiratory signals, which makes the frequency of the two signals vary over time. Moreover, there are some systemic/internal relations between the activity of these two systems, inside the body, which causes more powerful cardiac activities during the inhale. These natural variations appear in the amplitude of the BCG, during the respiratory cycle [108] and therefore affect the amplitude of the energy waveforms and make it harder to detect the peak of the energy in some cases, as shown in Figure 5.2.

Figure 5.2. Energy algorithm might not work properly even on regular BCG beats.

A very similar condition appears when processing the BCG signals of older subjects, with less prominent J-peaks, as demonstrated in Figure 5.3. In such cases, the energy algorithm is

vulnerable to miss detections of the cardiac beats, as the variation of the peaks and therefore, the energy of the waveforms are not easily distinguishable.

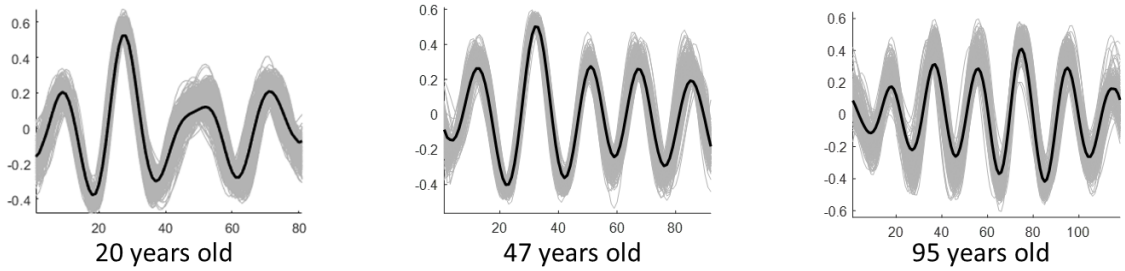

Figure 5.3. Example of loss of significant J-peak during the process of aging. Usually, a prominent J-peak in young subjects is easily distinguishable, while in older subjects, especially with prior cardiac disease, the j-Peak is just slightly different from the rest of the peaks.

5.2. Enhancing the beat detection accuracy

According to my observations in multiple data collections, I found many cases that the original energy algorithm misses the location of the cardiac cycle. Here, I will describe some of these cases and provide step by step enhancement on the energy algorithm.

5.2.1. Better separation from respiration

One critical source of these problems is due to the nonstationary nature of both BCG and respiratory signals, as they overlap in the frequency domain. The conventional choice of cutoff frequencies for the bandpass filtering (0.7-10 Hz) is designed based on the average minimum and maximum heart rate in the entire population. These are not always the best possible choices for every individual. Incomplete cancellation of the respiratory variations from the BCG signal will cause some J-peaks being damped by respiratory DC and hard to separate from the rest of the waves. A two-step personalization of these parameters for each individual by means of an approximate heart rate and respiratory rate was helpful to refine the filtering properties.

The personalization process is based on the time-domain or frequency-domain estimation of the heart rate and respiratory rate. I have used Welch's power spectral density estimator, with a window size of 120 seconds and 30 seconds overlap. To estimate the best values for the lower cut-off frequency, I focused on the range of 1 Hz to 5 Hz to find the point of the maximum power. This should be an important BCG frequency for that subject, so we want to keep that frequency content. Then I found the corresponding trough right before that peak as an approximate location for the lower frequency cut-off. The higher cut-off frequency is kept on 5Hz, as shown in Figure 5.4.

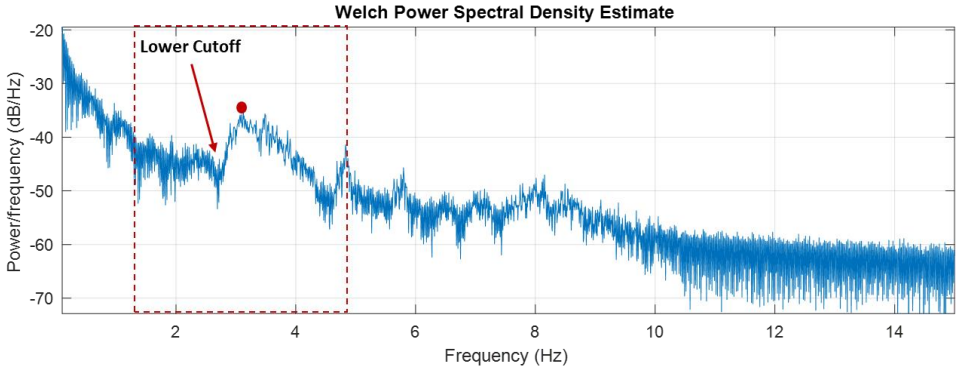

Figure 5.4. Zoomed version of the Welch power spectral density on raw BCG signal. The highlighted region in red is used to refine the lower cutoff frequency of the bandpass filter.

5.2.2. Baseline deviation of the signal

Deviation of the BCG mean from the baseline (the local DC bias, long-term median) is also the source of some problems, as the absolute value from the baseline is being used in the process of computing the energy. If for any reason, such as respiration, the local mean of the BCG shifts to higher amplitudes, then the computed energy would artificially show higher values. Conversely, if the local mean of BCG goes below the baseline, the corresponding energy wave would have an amplitude lower than the actual. Both of these artifacts may cause difficulties in the detection of the neighboring peaks.

To resolve this issue, I have computed and adjusted the local baseline using the lower and upper BCG envelopes. I have used MATLAB's envelope function to fit upper and lower polynomials to every 10 consecutive peaks. The point by point difference between the upper and lower peaks is considered as the optimal baseline. Figure 5.5 shows on top a sample BCG signal with almost three respiratory cycles and multiple BCG beats superimposed on them. It also shows the upper and lower envelopes created using MATLAB's envelope function. The point by point average of the upper and lower BCG envelopes shows a pattern similar to the respiratory variations from the respiratory band and also from the transducers.

The lower plot in Figure 5.5 shows the flattened BCG signal by subtracting the point by point mean of the upper and lower envelopes from the original waveform. As presented here, the result is clean and stable and does not have the normal variations remaining from the incomplete filtering of the respiratory signal.

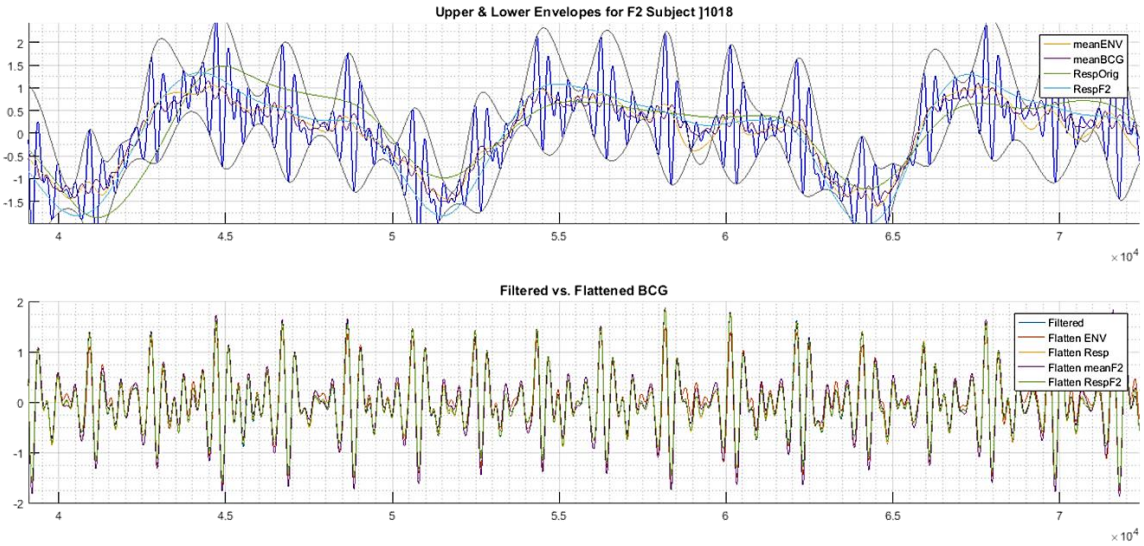

Figure 5.5. The 1st energy enhancement by resolving the deviation from the mean by averaging the upper and lower envelops.

5.2.3. BCG amplitude normalization using respiration

As described in [109], heart activity varies during different respiratory phases. Otis, et al. [110] studied the respiratory-related changes of the cardiac output, employing BCG, and reported a decrease in stroke volume during inhalation. Starr and Friedland [111] also studied the genesis of the respiratory variations in the ballistocardiograms. During inspiration, the filling, and so the output of the right heart increases immediately, but the left heart's output does not increase until an interval of several seconds has elapsed [111].

The output of the right heart reduces on expiration, which is followed by an interval of reduction in the left heart's output [111]. The change in the right heart's output during the respiratory cycle is larger than that of the left. This causes more blood being pumped out of the heart and therefore a higher amplitude in the BCG waveform, during the inhale. Although it might not be precisely linear, my experiments also show a clear correlation between the respiratory depth and the amplitude of the J-peak.

The energy algorithm suffers from the high variation of the J-peaks during the respiration. The peak detection will miss some of the real J-peaks assuming them as being the low amplitude noise, and will incorrectly detect some other peaks as J-peak due to their extended amplitude. To solve this issue, I divided the amplitude of the BCG signal by the amplitude of the respiratory signal, so that it cancels part of the respiratory-related variations of the J-peak. The resulting J-peaks and their energy waves have more stable amplitude among the neighboring cycles. The preliminary results illustrated in Figure 5.6 show a great improvement by normalizing the amplitude of the peaks of the energy algorithm.

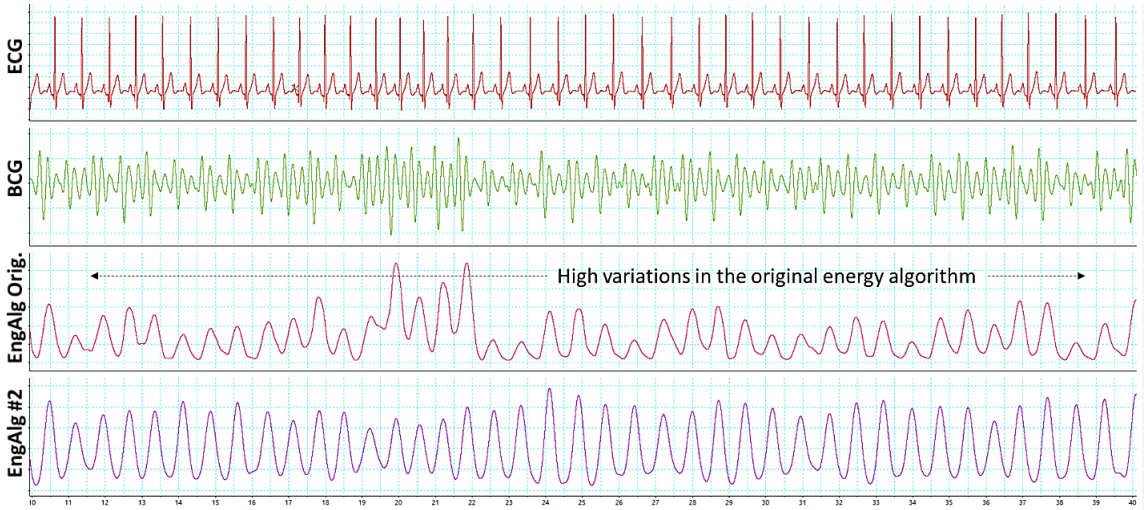

Figure 5.6. The 2nd enhancement of energy peaks by normalizing the energy waveform and a lowpass filter. The peak detection algorithms work much better on this second derivation of the energy algorithm.

5.2.4. Less significant J-peaks, within one cardiac cycle

In some cases, especially for older adults, the J-peak is not anymore that much different from the rest of the waves and is hard to separate from the rest of the peaks during one cardiac cycle. I decided to use other properties of the J-peak on top of its high amplitude. There is one other parameter that is significantly different between the J-peak and the rest of the peaks, and that is the slope of the J-peak. As reported by Starr and Friedland [111], J-peak is caused by the movement of the center of mass of the body, right after the heart pumps the blood into the aorta. After that, the blood flow would slow down, and the rest of the peaks would not be as sharp as the J-peak. Here I have focused on the cases where the amplitude of multiple peaks are almost the same; thus, the normal energy function cannot highlight the beats correctly.

To resolve this issue, I used the fact that the slope of the J-peak should also be larger than the rest of the peaks. Therefore, in the 3rd improvement of the energy algorithm, I first computed the first derivative the of the BCG signal, and then computed its energy function and also applied the respiratory correction (like in step 2). An example waveform is shown in Figure 5.7, with the

ECG signal, the BCG signal where both of the original and the second implementation of the energy algorithm fail to detect the BCG beats due to the low variation in the amplitude of the BCG peaks.

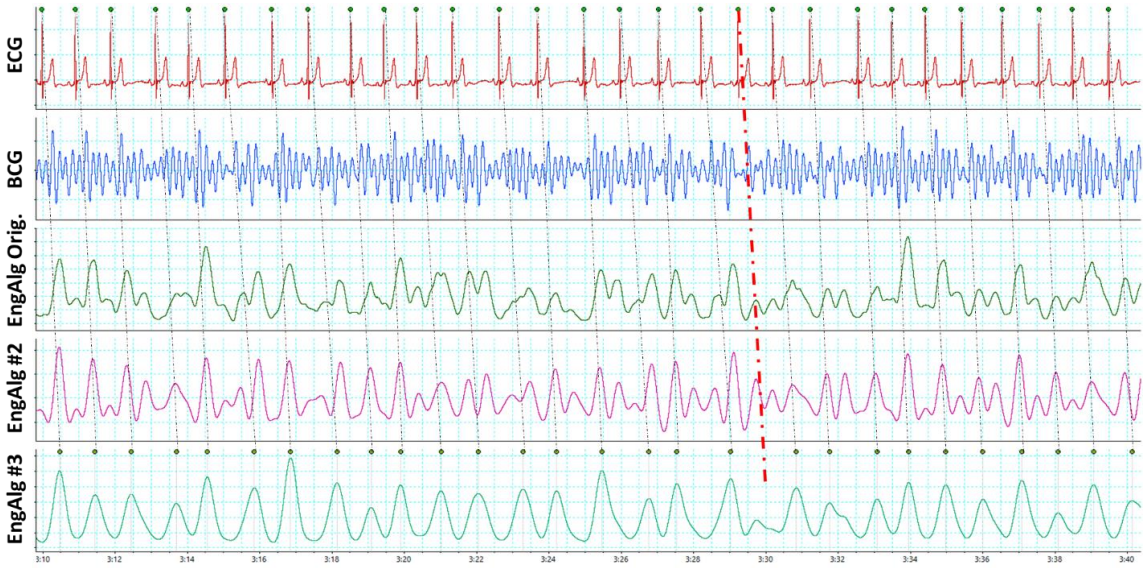

Figure 5.7. The 3rd enhancement of energy waveform using the first derivative of BCGhas less variability of the peak amplitudes in each cycle. Both the original energy algorithm and my first extension for it could not detect much of the beats, while the 3rd approach which uses the 1st derivative of the signal to construct the energy, shows much more clear peaks a just misses one beat in 30 seconds, due to a lower amplitude.

5.2.5. Guided J-peak detection

Accurate localization of the J-peak in BCG waveforms plays an important role in some applications, such as extracting the J-peak features. Despite the common thought about the timing of the energy waveform with respect to the BCG J-peak, my experiments show the BCG J-peaks do not necessarily coincide with the peak of the energy algorithm. Even in the case of a clean BCG signal from a young, healthy subject, as shown in Figure 5.1, the peak of the energy waveform, mostly (not always) appears on the JK edge of the waveform. I have tried different filtering parameters, but the variability is still obvious. This is important if we try to use the peaks of the energy waveform, as the fiducial point in the cardiac cycle.

In order to specifically finding the location of every individual J-peak, I proposed the utilization of energy peaks as a guide for J-peak localization. The enhanced version of the energy algorithm is capable of finding some fiducial points in every individual heart cycle. The idea is to search in between every two consecutive peaks of the energy waveform and find the best match for the J-peak. By definition, the J-peak is the most prominent variation in the amplitude of the BCG waveform. This usually interpreted as the peak with the highest amplitude, which is highly inaccurate on different devices. Here instead, I use the peak with the largest slope, to define the J-peak, which will handle part of the issues with the age-related deformations of the BCG waveforms

One other consideration is regarding the cases where two neighboring peaks of the BCG have very similar properties. This makes it very difficult even for human investigators, to confidently annotate one of the two beats as the true J-peak. I have decided to always choose the first peak as the J-peak, for the sake of consistency. I have demonstrated in Figure 5.8 the peaks of the original energy waveform (red crosses), the peaks of the enhanced energy waveform (red dots), and the detected location of the J-peaks (green dots), as described above.

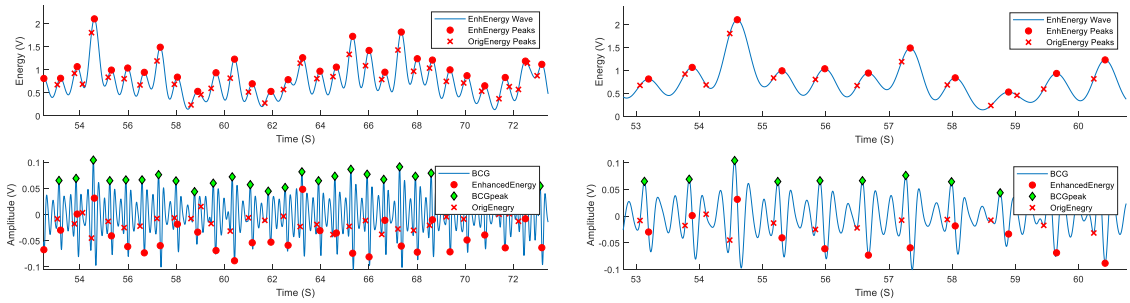

Figure 5.8. Refining the J-peak locations using the energy peaks as reference. The figure shows even the peaks of the enhanced energy wave do not perfectly alight the J-peaks. Bottom: Sample BCG signal recorded from a young, healthy subject, and the locations of J-peaks. Top: Corresponding Energy waveform and its peak locations. Right: is the zoomed version of the same signals.

5.3. Evaluation and Results

5.3.1. Evaluation approach

The best reference to evaluate any algorithm on cardiac cycle detection is the use of the ECG R-peaks. ECG, as the electrical activator of the heart, has been studied very well and multiple algorithms are currently available for automatic detection of the ECG R-peaks. I have re-implemented the famous Pan-Tompkins [112] algorithm in MATLAB, and have used it on short ECG recordings, in the range of 2-20 minutes. For longer recordings, such as 7-8 hours of overnight data received from the sleep lab, I ended up using the AD Instrument's LabChart software. This software has multiple algorithms for R-peak detection, and I used the Bazett as the default setting.

Pan-Tompkins [112] is a real-time algorithm to find the QRS complexes in the ECG signals through the analysis of the amplitude, slope, and width of the peaks. An embedded adaptive thresholding and filtering technique reduces the false alarms and improves the sensitivity of the detections. On the other hand, considering the correlation between the QT interval and RR interval, many algorithms tried to provide more advanced approaches to detect the QRST complexes. LabChart has implemented the Bazett's [113] approach, which used the correlation between the measured QT interval and the square root of the RR interval. Interested readers are encouraged to find more details about these algorithms in [112-114].

After finding the reference ECG R-peaks, the continuous beat-to-beat heart rate could be computed using the time interval between the neighboring R-peaks (RR interval), as depicted in the following formula:

$$for\ jth\ cardiac\ cycle; \quad HR_j = \frac{60 * Fs}{RRI_j}$$

Where Fs is the sampling rate in Hz, and RRI is the interval between the two R-peaks, and HR is the beat to beat heart rate estimated in beats per minutes (bpm).

Bland-Altman plot is used to analyze the agreement between two measurements. In the standard process, the average of two readings is used as the x-axis and their difference to be used for the y-axis of the resulting point in the plot (s).

$$S(x_i, y_i) = [\frac{1}{2}(S1_i + S2_i),\ S1_i - S2_i]$$

Where S1 and S2 are the two series to be compared, and x and y are the locations of the resulting point. As a common approach, in case of existence, the ground truth measurement could be used on the x-axis instead of the average of the two. As we usually have the reference HR from the ECG signal, I have used them on x-axis. An example Bland-Altman is plotted in Figure 5.9 beside the correlation plot, for the beat to beat HR values that were estimated from the pulse figure sensor compared to the ECG R-peaks.

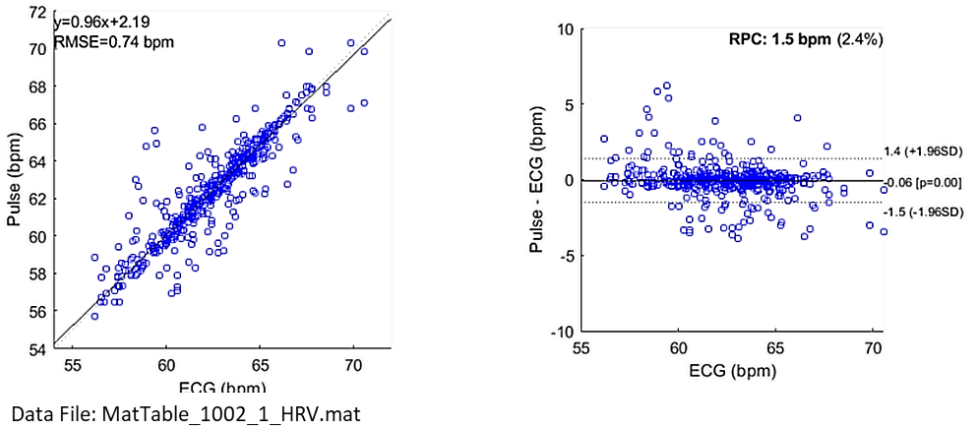

Figure 5.9. Bland-Altman plot of beat to beat HR estimations using the pulse sensor vs. the ECG based method. Even the wearable pulse sensor has some estimation errors.

To use the standard Bland-Altman technique for the beat to beat evaluation of the heart rate estimates, there should be an estimate for every cardiac cycle. In other words, the method would not work if the energy algorithm misses some of the peaks or incorrectly detects more peaks. Unfortunately, Due to the physiological delay between BCG and ECG, the R-peak timings would not be of great help, by themselves. In order to provide a simple way to align the heart rate estimations from the two approaches, I decided to use interpolation to synthetically add the missing

values in between the existing ones, and also discard the extra points in one cycle. To do so, I have used MATLAB's interp1 function to interpolate both time series into a common time stamp, with a sample rate of 2Hz. This will ensure the coverage of most of the detections as well as promising distances to the actual detected points.

Also, to assess the quality of average heart rate estimation, I have used two approaches. In the first one, an average heart rate is being computed for every epoch of 30 seconds. This approach uses the timings of the actual detected fiducial points and computed heart rate utilizing the peak to peak intervals. In the second approach, the moving median function with the 30-second sliding window was applied to the interpolated heart rate estimations, to provide a smoother estimation for each time series.

The following functions will be used to assess the accuracy of the beat detections. The first one looks at the overall estimation of the average heart rate for the entire 10-minute of data. The second method compares the inter-beat intervals to see how well the j-peaks were detected.

1. Root mean square difference (RMSD) between the estimations from ECG and BCG:

$$RMSD = \sqrt{\sum_{i=1}^{N} (HR_{ECG} - HR_{BCG})^2}$$

2. Reproducibility Coefficient (RPC) measured upon the creation of the Bland-Altman plot:

$$RPC = 1.96 * STD$$

5.3.2. Results

For a detailed analysis of agreement between our estimated heart rate compared to the reference values from the ECG RR interval, I have created a Bland-Altman plot for the four transducers on each file. As shown in Figure 5.10 for a random healthy subject, the accuracy of beat detection relies a lot on the channel selection. For example, in this figure, channel 4 (right,

bottom row) has a nice linear correlation to the ECG estimates, and therefore have very small RMSE (1.1 bpm) and a small reproducibility coefficient (18 bpm), while both RMSE and RPC values are much higher on the other channels.

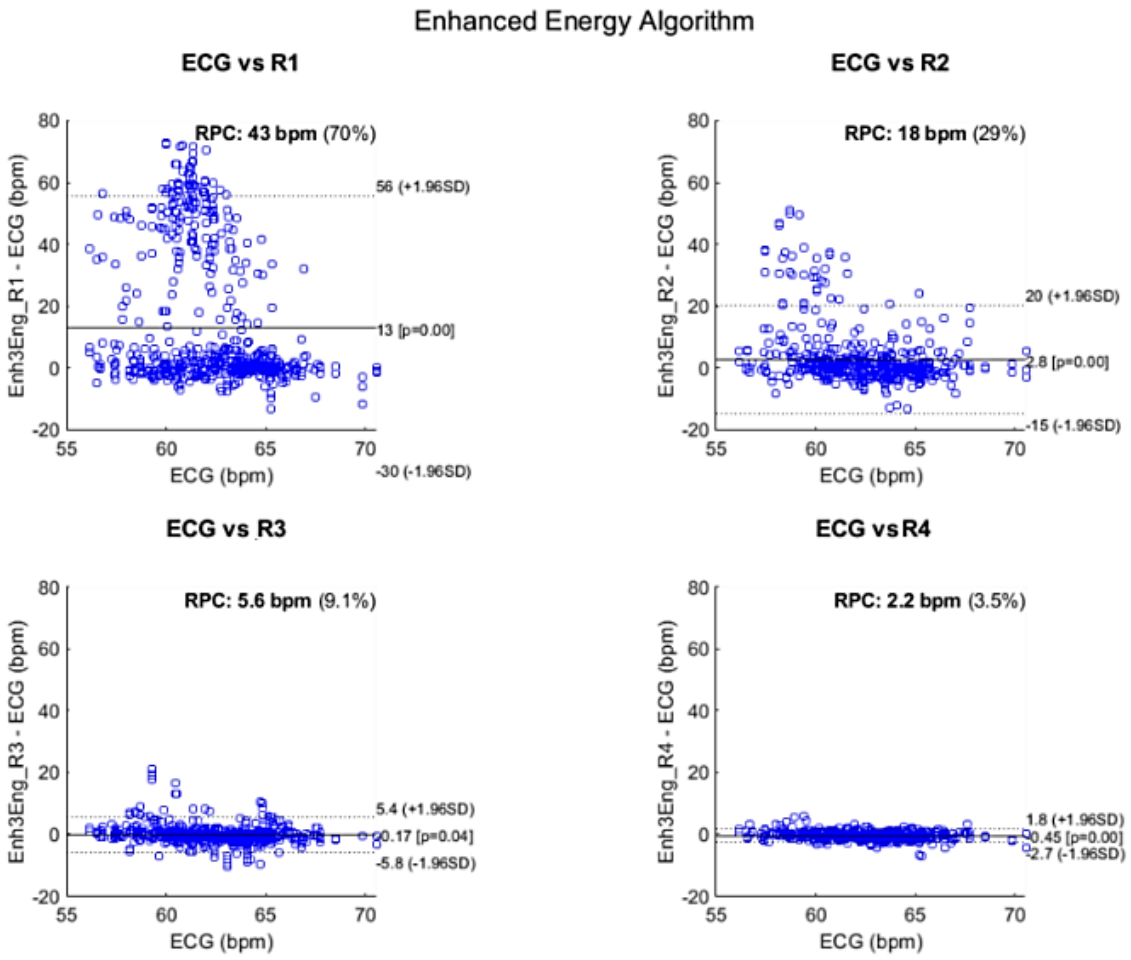

Figure 5.10. Bland-Altman plot for the HR estimates using the enhanced energy algorithm on four transducers using Data from a sample young, healthy subject from the HRV dataset. Although good agreements available in transcoders 3 and 4, the other two transducers show a large deviation from the reference values. These results encourage me to focus more on enhancing the quality of the BCG signal.

As I am working on a large data set consisting of hundreds of files (subjects × trials), Bland-Altman plotting for every individual is not reasonable, especially due to the large difference between these datasets with respect to the signal quality caused by motion or due to the age. Instead,

I have computed the RMSE and also the RPC values and aggregated them over all subjects to provide group by group overall statistics. The results of this section mainly obtained from the three databases which synchronous ECG recordings, namely the followings:

1. **HRV**: 60 young, healthy subjects in the supine position,
2. **POS**: 60 young subjects with 4 different sleep postures,
3. **TP**: 50 mostly older residents and workers of TigerPlace.

First, I have computed the average RMSE over all subjects of each dataset, for the estimations acquired by applying both the original and the enhanced energy algorithms on the bed sensor. As provided in Table 5.1., the newly proposed enhancements of the energy algorithm improved the accuracy of beat to beat estimations both in the mean and standard deviation of the error in every single dataset, by a factor of 2-3 times.

Table 5.1. Evaluation of beat detection algorithms before denoising or channel selection. *Even before applying any denoising or channel selection, the enhanced energy algorithm outperforms the original one by a factor of 2-3 according to the RMSE.*

RMSE (bpm)	**All Subjects**		**HRV**		**Pos**		**TP**	
	Mean	**STD**	**Mean**	**STD**	**Mean**	**STD**	**Mean**	**STD**
Original alg.	16	11.1	15.4	10.6	17.2	9.4	16.9	13.9
Enhanced alg.	7	5	5.7	4.9	8.3	4.5	6.9	5.5

Note that these values are acquired from the raw signal before any noise reduction or cancellation. Therefore, the dataset that contains four change of postures has the highest amount of error caused by the motion artifacts. For older subjects (TP), in addition to the age-related deformations that appeared in the BCG waveforms, the reference ECG and PPG signals were also noisy at times. This causes an incorrect ground truth reference and consequently out of range RMSE values. As depicted in Figure 5.11, the finger pulse sensor for at least three subjects shows a high RMSE value, and in one case, BCG estimation is also off. I checked those instances carefully. For

one subject the finger sensor looked very irregular, and for the others, the ECG was so noisy, perhaps due to a loose sensor-skin connection. Thus in a few cases with high noise contamination in the ECG signal, I have used the PPG peaks to estimate the reference beat to beat heart rate. This is partially due to the different structure of the skin in older subjects, which causes some noise artifacts in PPG or ECG.

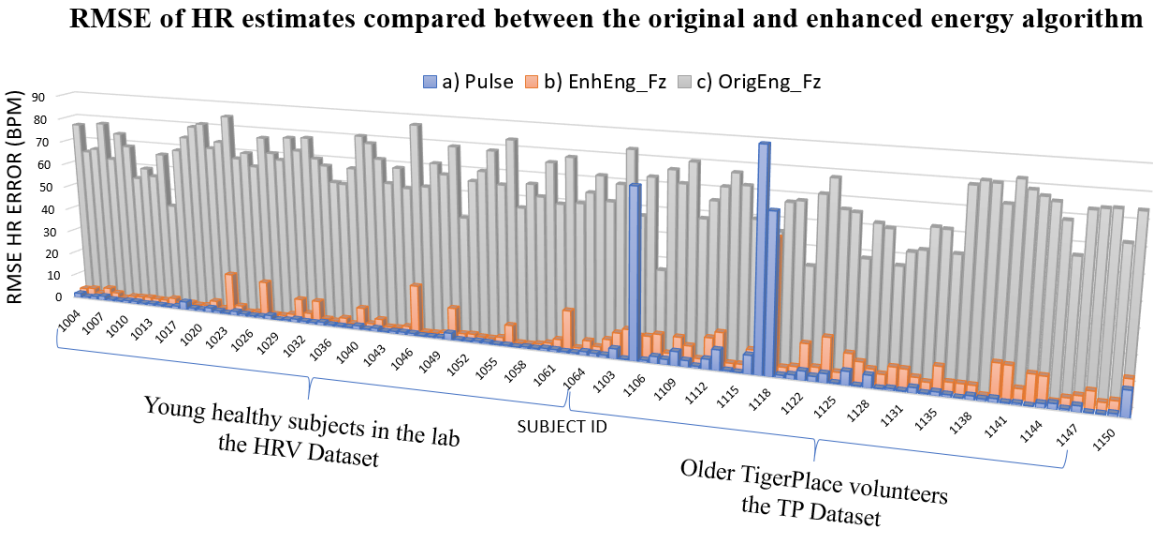

Figure 5.11. Beat to beat RMSE of the original vs. the enhanced energy algorithm shows a huge improvement on the beat to beat estimations. The original energy algorithm (gray) has a high RMSE on all subjects, while the error on the enhanced energy (orange) is comparable to the pulse sensor (blue). There are a few subjects in which the enhanced energy estimate is not as good; those subjects also have low accuracy by means of the pulse sensor, which perhaps is due to their movements, and the body-sensor coupling.

5.4.Discussion and future work

Even after applying all these steps, there still exists the chance of having delays between the J-peaks being detected from each of the four transducers. This is mainly due to the difference in the morphology of BCG waveforms captured from the four transducers, as shown in Figure 5.12.

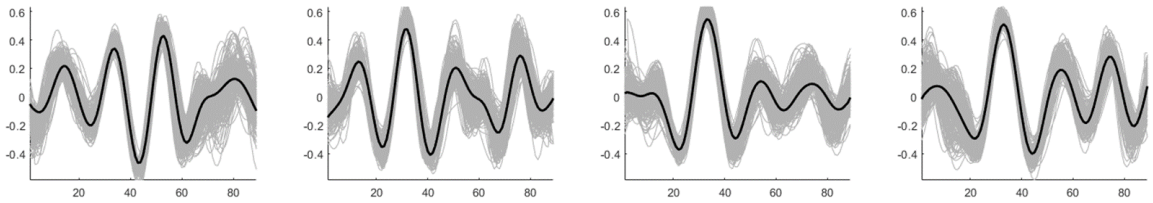

Figure 5.12. Example of different templates created from the 4 transducers from the hydraulic bed sensor on a random healthy subject. Templates show slightly different waveform morphology, which causes a miss-alignment between the detections of different transducers.

Although a persistent miss-alignment between the J-peaks in different transducers is transparent for the estimation of heart rate, it might be an inconsistent and random detection due to a small variation in the amplitude. Therefore, in future work, one can combine the information of all four transducers together to improve the detection on the others. As presented in Figure 5.13, the idea is to use the average J-peak location from three of the transducers to find a reasonable window for the appearance of the J-peak on the other transducers. This process should be done in short sliding windows (0.5 Sec.), to reduce the change of covering multiple cardiac cycles.

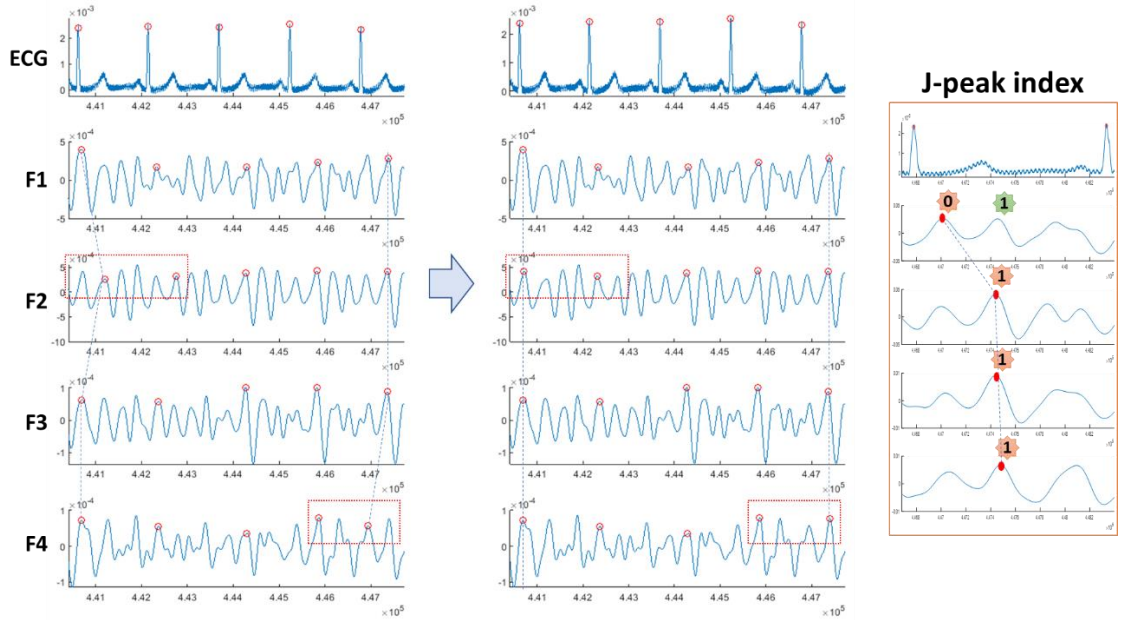

Figure 5.13. J-peaks of four transducers may not align as their morphologies differ. Figure on the left represents a real example of the miss alignments in the BCG peaks detected from the four transducers. The right side of the figure shows how the proposed alignment could make corrections on the individual traducer.

As the final experiment, I used the enhanced energy algorithm on the overnight BCG data recorded at the sleep lab from their normal patients. While not perfect, we tried to align these BCG signals to their corresponding EDF files from the sleep lab, which contains an ECG recording as well. I have imported these ECG signal of 20 subjects to LabChart and analyzed them to extract the ECG R-peaks. In Figure 5.14 I have superimposed the reference HR from the PSG on the estimations that I have acquired from the for transducers of our sensors using the enhanced energy algorithm. While there is a general agreement between these measurements, for most of the time there is at least one transducer whose estimations are off and mostly above the ground truth.

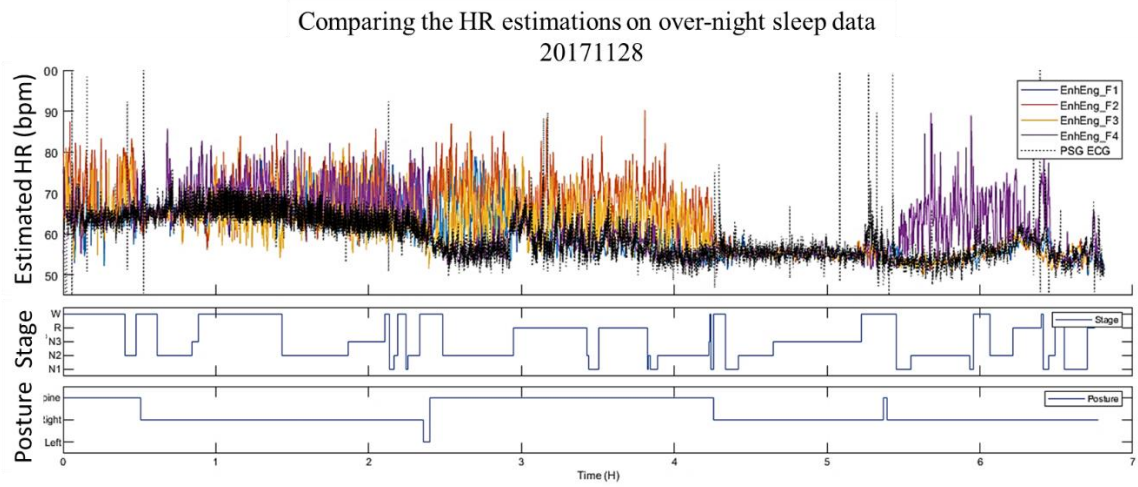

Figure 5.14. Evaluation of the enhanced energy algorithm on a 7-hour sleep lab data shows some periods of high accuracy and some periods or low accuracy for different transducers. The black dots are the HR estimations from the ECG R-peaks, and the colored lines are the estimations from the four transducers. Although, each sensor has some periods of high error, for the most of times there is at least one transducer with very low deviation from the reference.

For comparison, I have also plotted the sleep annotations regarding sleep posture and sleep cycles. Supine posture seems to coincide with the appearance of yellow and red lines, which are the errors related to the two transducers in the middle of the bed (F2 and F3). There is a much smaller error for these two transducers, while the subject is on their side. The exact source of this problem requires more investigations on the configuration of the bed and sensors. One possible

cause could be the different type of activity during those two periods, such as wake and REM, or the possibility of blockage of the transducers on that specific configuration.

Now that I made some significant improvements in the quality of the beat to beat heart rate estimation, I will use the average heart rate of epochs to evaluate the quality of different algorithms, in the rest of this dissertation.

6. HANDLING DISTORTION AND VARIATION IN BCG

As will be discussed in a future chapter, BCG waveforms are subject to variations due to different circumstances including the age and respiration. In general distortions are deformations of BCG signal caused by non-systemic (ambient) sources, such as the relative vibration of the sensor and the subject which causes sudden spikes in the signal, or the stable relocation of the subject which causes a constant change in the direction, distance and the quality of decoupling of the sensor and the body respectively. Some normal systemic variations are also expected in the acquired BCG, due to the change in the health conditions or even during the regular internal cycles of the body, which will be discussed later.

Not all of these variations are reflecting a change in the mechanical activities and properties of the person's body but rather might be related to the random variations in the sensing environment. These variations are less likely to be helpful in early detection of health conditions; thus, they need to be detected and treated so that they will not affect the analysis. Three categories of such artifacts in the ballistocardiography have been recognized including (1) the motion artifacts either caused by the body movements or from the ambient noise, (2) the variable coupling of body and the sensor including the contact area, distance to the sensor and the body direction, and (3) the normal parasympathetic variations of the hemodynamics such as heart rate variability (HRV) and the respiratory sinus arrhythmia (RSA).

Similarly, as described by Alihanka, et al. [54], when interpreting the data, the patient's change of position during the sleep must be taken into consideration. In supine position or when the subject is sleeping on the right side, the BCG amplitude is about the same, but if the subject is sleeping for example on their left side, the apex beat of the heart may be recorded with an amplitude about two times the usual BCG amplitude. This happens when the region of the thorax (where the apex beat of the heart is strong), comes in close contact with the mattress (e.g., on the left side).

In this chapter, I first define different sources of motion artifacts and their effect on biosignals such as ECG, PPG, and BCG. Various approaches for artifact detection, reduction and removal have been provided with a brief theoretical background for each. An intensive review of the existing literature in Section 6.2 will provide enough evidence on the lack of advanced motion detection and removal techniques for BCG. In Section 6.3, multiple motion reduction techniques will be used to eliminate the noise from the BCG signal, and Section 6.4 provides different techniques to evaluate the signals and detect the motion artifacts. Finally, Section 6.5 explores the utilization of these techniques to choose the best channel among the four transducers.

6.1.Background

Ballistocardiography was initially used to study cardiac mechanics and obtain diagnostic information about the cardiac contractility [39, 115, 116]. It provides a nice visual representation of the mechanical activities of the heart and the cardiovascular system. Therefore, the visually perceptible variations in the morphology of the BCG waveforms, have always been of interest for many researchers. There is a general agreement between researchers that regardless of the type of BCG device, the IJ amplitude declines by age [117]. Trends in IJ amplitude or derived functions such as stroke volume have been found by investigators in several laboratories.

Abramson [22] was the first who tried formulating the relation between the BCG curves and the cardiac output. He showed that the BCG amplitude relates to the force of the heart and the way it ejects the blood [23]. However, it is not very clear how the BCG amplitude and stroke volume and the body size are related to each other. Taylor and Walker [117] provided evidence that shows Nickerson's low-frequency device gave a relatively large correlation coefficient between the body's surface area and the cardiac output.

BCG has shown the ability to detect cardiac changes in the early stages of the disease before symptoms manifest [6, 118]. While there is not yet a clear and precise explanation on the effect of change in hemodynamics to the ballistocardiography waveform, studies have shown that ballistocardiography can provide fundamental information about the occurrence of myocardial ischemia [119], or the ischaemic heart disease (I.H.D.) [120]. Starr, et al. [39] reported the potential variations of the BCG morphology related to the weakness of one side of the heart. Starr and Wood [16] also showed that the BCG amplitudes of those patients who developed heart disease were on average, initially only 25 percent of those who did not. In other words, small IJ amplitude significantly increases the chance of developing some form of cardiac abnormality in the future (after 5 to 20 years).

Many studies have explored the morphological variations of the ballistocardiography as an effect of age or physical activity. Rosenblatt [121] reported a decrease in the amplitude of ballistocardiograms for people of age 50 or more in comparison with a younger population, which reportedly is due to the condition of the cardiovascular system (e.g., healthy versus a diseased heart) [6, 51, 118]. Healthy subjects have strong contractility to generate large waveforms, whereas smaller waveforms come after weak contractility [122]. Thus, BCG can more accurately predict the heart’s age than the person's chronological age [6]. Twenty years ballistocardiography follow up on 211 healthy subjects (174 men, 37 women), by Starr and Wood [16] showed the amplitude of the BCG waveform diminishes with age.

Besides the "normal" effect of aging, the percentage of abnormal BCG waveforms increases. This is while the ordinary clinical tests do not diagnose any health problems [23]. The abnormality in BCG contour could appear in the form of deviations from the normal template, small noises, and notches of normal waves, reduction or absence of normal waves, and the presence of abnormal waves. The diseased heart appears to lose the fine coordination of the normal contraction. Most elderly patients with coronary heart disease or congestive heart failure have abnormal BCG

recordings. Changes in the conditions of the disease usually clearly change the BCG waveforms, for example, the small BCG amplitude in the in patients with congestive heart failure, often improves as the patient responds to therapy.

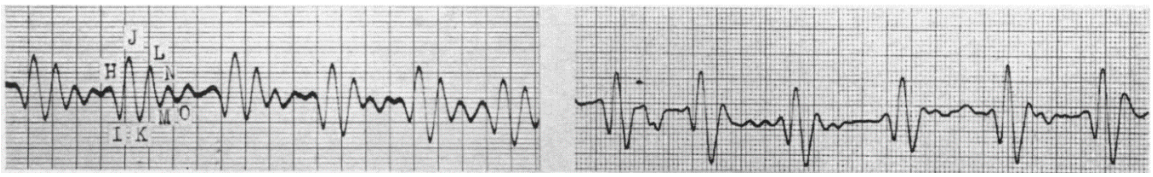

Figure 6.1. BCG obtained from a young, healthy woman after twenty two months. The right-hand tracing, which is the later one, show some decrease in the size of the diastolic complexes, but no change in the systolic ones. (image from [30])

The Ballistocardiogram waveform tends to vary during the respiratory cycle and shows more abnormal complexes at expiration while approaching normal patterns at full inspiration [23]. This can be described as an example of **Starling's law of the heart** [23], in which the best contraction of a weakening heart appears at a time during the respiratory cycle in which it is best filled. As a result, there are many cases in which only the inspiration phase contains normal BCG complexes. Indeed, for patients in declining health, the percentage of abnormal BCG waveforms can be used as a guide to evaluate the severity of myocardial impairment. Starr and Wood [16] realized that women have smaller BCG amplitudes than men, not because they are smaller in size, but because they are women and their heart’s contraction applies smaller force to the blood.

The morphology of the ballistocardiograms can be changed due to a change in the hemodynamics, or as a result of the external sources of motion. These motions usually appear due to the ambient noise, limb movement or the movement of the person on the bed while changing the sleep posture can affect the quality of the readings.

A variety of systems are used to capture BCG signals, including beds [7, 8], chairs [9], and weighing scales [10]. Bed-based sensors, in particular, have the potential advantage of long term

BCG acquisition throughout the night [3]. Our hydraulic bed sensor targets the longitudinal monitoring of vital signs such as heart rate, sleep posture, blood pressure, and other cardiac conditions, noninvasively [11-13]. Collecting BCG signals while the subject is in the supine position, provides an ideal platform for non-invasive estimation of blood pressure. With the subject mostly flat in a similar position on the bed, body part elevations will not contribute to blood pressure change. Thus, blood pressure changes in this position are related to some physiological variations.

While these systems provide a high degree of freedom for the subjects [6], they are highly susceptible to motion artifacts [3], as represented in Figure 6.2. The coincidence of BCG bandwidth (0.5-10 Hz) with several sources of motion, including respiratory fluctuation of the chest, body postural change, or limb movements, is the leading cause [14]. According to [15], even in the controlled setting of longitudinal experiments with BCG, only 29% of the head-foot waveforms (in men) are considered normal, and the rest have different levels of noise. Inaccurate estimation of cardiac parameters from the artifact-contaminated BCG records could negatively affect the quality of future studies. This emphasizes the need for methods that are robust against motion artifacts.

The necessity of having accurate and reliable sensor information on the clinical status of the patients during the anesthesia have been discussed by Takla, et al. [123]. Motion artifacts are the primary source of distortion in achieving the desired features. To overcome the potential issue that motion artifacts can impose on the quality of biosignals in general, different techniques have been designed and developed both for detection and also the removal of motion artifacts especially from ECG signals ([124-130]). Hamilton, et al. [125] removed motion artifacts from the Holter ECG signals and designed and improved methods to remove coarse cardiopulmonary resuscitation (CPR) artifacts from the ECG signal. Ambient light interface and finger motion artifacts can corrupt these characteristic features of the pulse oximeters. Lee, et al. [131] was able to design a filter to reject pulse oximetry artifacts, caused by the ambient light and the finger motions.

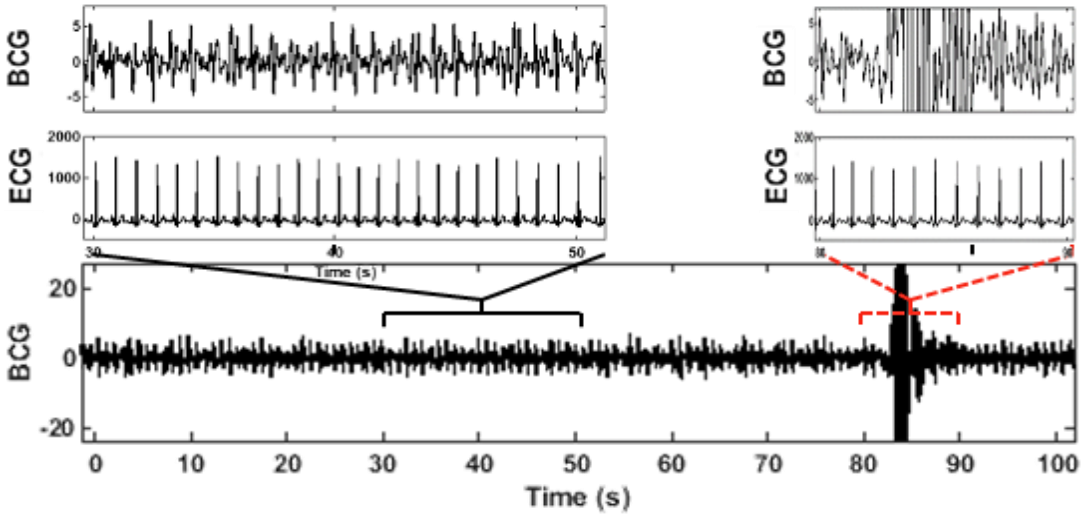

Figure 6.2. Example effect of motion artifact in BCG signal compared to the corresponding ECG signal.

From a technical point of view, a few general approaches are getting more attention among the researchers, including the wavelet-based denoising ([128, 132, 133]), Adaptive Filters ([125-127, 134-138]), and Empirical Mode Decomposition ([129, 139, 140]). Some case base solutions in the frequency space ([131, 141-143]) along with some feature space ([144, 145]) data analysis have also been introduced in the literature. Working in the feature space is usually highly dependent on an accurate beat detection, which itself is a challenge in the case of BCG. A secondary motion reference sensor, usually an accelerometer, has been used in many types of research both to verify the accuracy of the method or as a guide to detecting the motion.

By the emergence of new devices for continuous vital sign monitoring, valuable information can be extracted from normal activities without interrupting the daily routines. These sensors are meant to be used in unconstrained normal life instead of limiting the users' activities [123]. The current sensors being used in the measurements of ballistocardiography are highly sensitive to motions, including the body or limb movements or other ambient motion artifacts such as floor vibration caused by walking [134]. Multiple studies showed the effectiveness of motion artifact detection and removal techniques on the ballistocardiographic data, including the works of

Friedrich, et al. [141] to reduce the limb movements, coughing or snoring artifacts to increase the accuracy of overnight beat-to-beat heart rate estimations. Table 6.1, in the next section, provides a comprehensive review of the current literature dealing with motion artifacts in multiple biosignals, including the BCG. The proposed techniques, the goal of each method (detection or reduction), and the data source are also provided for each article. Also, a column is dedicated in each row to highlight the use of a secondary reference sensor.

6.2.Related Work

There are two general approaches to deal with motion artifacts, the diagnosis (detection), and the accommodation (reduction) [146]. While an accommodative method tries to reduce the effect of noise, a diagnostic approach highlights (detects) the potential motion corrupted segments of the signal. Once detected, the system may remove these segments from future processing of the data. I have provided a review on the current leading methods to deal with the noise and motion artifacts in Table 6.1, which include some general categories of signal processing techniques such as linear filtering, adaptive filtering, wavelet denoising, blind source separation, and empirical mode decomposition (EMD) that have been used in reducing the noise content of the biosignals and reconstruction of noise-free signals [147].

Adaptive filters have generally been used for noise cancellation in a variety of signal sources [135]. They require a primary signal input and a reference noise input. Inan [134] used a seismic sensor as the reference signal to eliminate floor vibrations on ballistocardiogram signals acquired from the modified bathroom scale. In another study, they reported the use of foot-acquired electromyograms as the reference to cancel body movement on the modified weighing scale [3]. Similarly, Yang and Tavassolian [148] used a delayed version of the original seismocardiogram

(SCG) signal as the reference for the least mean squares (LSM) adaptive filter. However, a noise reference signal is not typically available for noninvasive in-home sensing systems.

Without having any *a priori* knowledge about the data, EMD decomposes the signal into a few components with well-defined modes [149]. EMD is shown to be more flexible than linear techniques in the reduction of noise, due to the dynamic assignment of signal and noise to different modes. EMD is used in [149] to improve the accuracy of heart rate estimations from unstable chair-based BCG records. However, the reconstructed signal provides incomplete dynamic features of the uncorrupted signal and causes the loss of detail in BCG components that are required for tracking health conditions.

In contrast, machine learning approaches for motion artifact detection mostly quantify the severity of the artifacts using some feature-based signal quality index (SQI) [148]. Some approaches quantify the SQI using waveform morphologies after segmentation. Their feature extraction is highly dependent on the accuracy of time-domain peak detection [146]. For instance, in Wijenayake and Park [150], a reference ECG signal is used to segment out BCG and PPG signals and create a cardiac template to be used in the reconstruction of the full-length signal. This reconstructed signal was then used to compute the signal to noise ratio and signal quality. Likewise, features such as y-axis variance, displacement of the center of mass, sensor mean value, mean diagonal energy of the load cells and mean percentage variance of each load cell, was extracted by the authors of [151] to feed a support vector machine (SVM) classifier to distinguish between different type of body movements.

Temporal features such as mean, variance, skewness, kurtosis, 75th percentile, and Shannon entropy are mostly extracted from consecutive cardiac cycles, after segmentation. Assuming that clean and corrupted segments form two separate groups, the statistical features may discriminate amplitude distributions between BCG segments. However, BCG morphology varies among

patients, which causes different levels of amplitude distortion. Therefore, it can be difficult to obtain high accuracy results from these algorithms in practice.

Table 6.1. Review of literature that deal with motion artifacts in different biosignals. *A column designates the use of a secondary reference sensor.*

Reference	Year	Target		Ref. Sensor	Technique	Data source			
		Detection	Reduction			ECG	PPG	BCG	SCG
Takla, et al. [123]	2006	✓	✓		Review	✓	✓		
Wiard, et al. [14]	2011	✓		✓	Thresholding			✓	
Alivar, et al. [152]		✓	✓		Thresholding, Auto-Regression			✓	
Hoog Antink, et al. [130]	2017	✓			Shape-Based SNR	✓	✓	✓	
Krishnan, et al. [153]	2010	✓	✓		Neyman–Pearson, FD-ICA		✓		
Dao, et al. [154]	2017	✓		✓	Time-Frequency Spectral Features		✓		
Młyńczak and Cybulski [143]	2017	✓		✓	Teager–Kaiser energy		✓		
Lee, et al. [129]	2012	✓			Empirical Mode Decomposition	✓			
Javaid, et al. [139]	2017	✓	✓	✓	Empirical Mode Decomposition				✓
Khan, et al. [140]	2016		✓	✓	Empirical Mode Decomposition		✓		
Barros, et al. [124]	1998		✓		Independent Component Analysis	✓			
Milanesi, et al. [126]	2006		✓	✓	Independent Component Analysis +Adaptive Filter (LMS+RLS)	✓			
Hamilton, et al. [125]	2000		✓	✓	Adaptive Filter (LMS)	✓			
Liu [127]	2011		✓	✓	Adaptive Filter (LMS)	✓			
Inan, et al. [134]	2010		✓	✓	Adaptive Filter (LMS)			✓	
Yang and Tavassolian [135]	2015		✓	✓	Adaptive Filter (NLMS)				✓
Shimazaki, et al. [136]	2014		✓	✓	Adaptive Filter (NLMS)		✓		
Seyedtabaii and Seyedtabaii [137]	2008		✓	✓	Adaptive Filter (Kalman)		✓		
Lee, et al. [138]	2010		✓	✓	Adaptive Filter (Kalman Smoother)		✓		
Lee, et al. [131]	2004		✓		Filter bank and the Matched Filter		✓		
Reddy, et al. [142]	2009		✓		Continuous Fourier Series Analysis		✓		
Friedrich, et al. [141]	2010		✓		Time-Frequency Distribution			✓	
Salehizadeh, et al. [144]	2014		✓		Feature Space (Clustering)		✓		
Petterson, et al. [145]	2007		✓		Feature Space (Data Averaging)		✓		
Lee and Zhang [132]	2003		✓		Wavelet		✓		
Raghuram, et al. [133]	2010		✓		Wavelet		✓		
Hashim, et al. [128]	2012		✓		Wavelet	✓			

Time-frequency techniques such as short-time Fourier transform (STFT), wavelet transform (WT), and Hilbert–Huang transform are also used in the analysis of non-stationary physiological signals such as BCG [155]. They transform the signal into different frequency bands and compute their power spectrum density. Various spectral features can be studied, including mean and median frequency, maximum to minimum drop in power density, and power spectrum deformation.

A linear time-frequency transform is used by Moukadem, et al. [155] to improve the heart rate estimations from the accelerometer BCG. A sequential detection algorithm is used in [152] to label successive BCG frames by comparing them to two thresholds. Dao, et al. [154] used the time-frequency spectrum first to detect the motion-artifact-corrupted data and next to discard the non-usable part.

As we do not have any reference signal for motions, adaptive filters are not an option. Here, the best options are either the wavelet decomposition that has been described and used by [128, 132, 133] or the empirical mode decomposition used by [139, 140]. The remainder of this chapter will provide detail information about these techniques and the results of my experiments in the application of these techniques, with the goal first enhancing the quality of the signals and then discarding the remaining portion of the signal that is highly contaminated with noise.

6.3. Motion Artifact Reduction

6.3.1. Method

Part of the work presented in this chapter specifically and this dissertation, in general, is related to different signal processing methods being applied on the biosignals of interest to acquire cleaner signals leading to more reliable time, frequency or time and frequency features. I will start with a brief definition of different transformation functions and encourage interested readers to refer to the book by Stark [156] as one of the most cited references in the literature.

I. Wavelet Decomposition

In general, transformation refers to the convolution of the input signal f(u) with an "analysis function" as represented in (1.1), where g(u) characterizes the chosen transform through different parameters, as described by [156]. Each transformation results in the decomposition of the input time-dependent function f(t) into a more compact representation. For example, the Fourier transform decomposes a signal into the weighted sum of multiple sinusoidal with circular frequency (ω) and is represented as $g_\omega(u) = e^{ju\omega}$ in equation 1.2.

$$f(t) : \int_{-\infty}^{+\infty} f(u)g(u)du \qquad (1.1)$$

$$f(\omega) : \int_{-\infty}^{+\infty} f(u)g_\omega(u)du \qquad (1.2)$$

Short-time Fourier transform (STFT) is the windowed version of the Fourier transform which is designed to provide localized information about the signal. The analysis function of STFT is as shown in (1.3)

$$g(\omega, t)(u) = e^{ju\omega}\omega(u - t) \qquad (1.3)$$

where w(u) is the shape of the window function (1.4)

$$f_\omega(\omega, t) = \int_{-\infty}^{+\infty} f(u)g_{(\omega,t)}(u)du \qquad (1.4)$$

The theoretical description of the wavelet transform is very similar to the Fourier transform, with an extended possibility of incorporating multiple scales in order to decompose the signal into several scales. In the Discrete wavelet transform (DWT), the coefficients are computed by the sequential application of a series of high-pass and low-pass filters on the input discrete-time signal [157]. This sequential process, also known as multi-resolution analysis, as represented in Figure 6.3, decomposes the signal through a step by step application of a filter bank of high-pass (HP) and low-pass (LP) filters**.** The output of the high-pass filter is addressed as the detail coefficient (D) of the input signal, and the output of the low-pass filter is called the approximation coefficients (A).

To increase the frequency resolution of the signal, the signal is down-sampled by a scale of 2 before being passed to the next filter. This process is repeated until a specified level has been reached [158].

The detail coefficients (D) are, in fact, the frequency-dependent properties of the signal. By repeatedly applying this process, the signal can be decomposed into lower resolution components. In the multi-resolution decomposition of a signal with length 2n, n level of resolutions can be retrieved [157]. The beauty of the transformation functions is they have an inverse function. More specifically for the case of discrete wavelet decomposition, we can always reconstruct the original signal from the wavelet coefficients by up-sampling the approximation coefficients and the detail coefficients then, respectively, pass them through a low-pass or high-pass filter and finally sum them at each decomposition level.

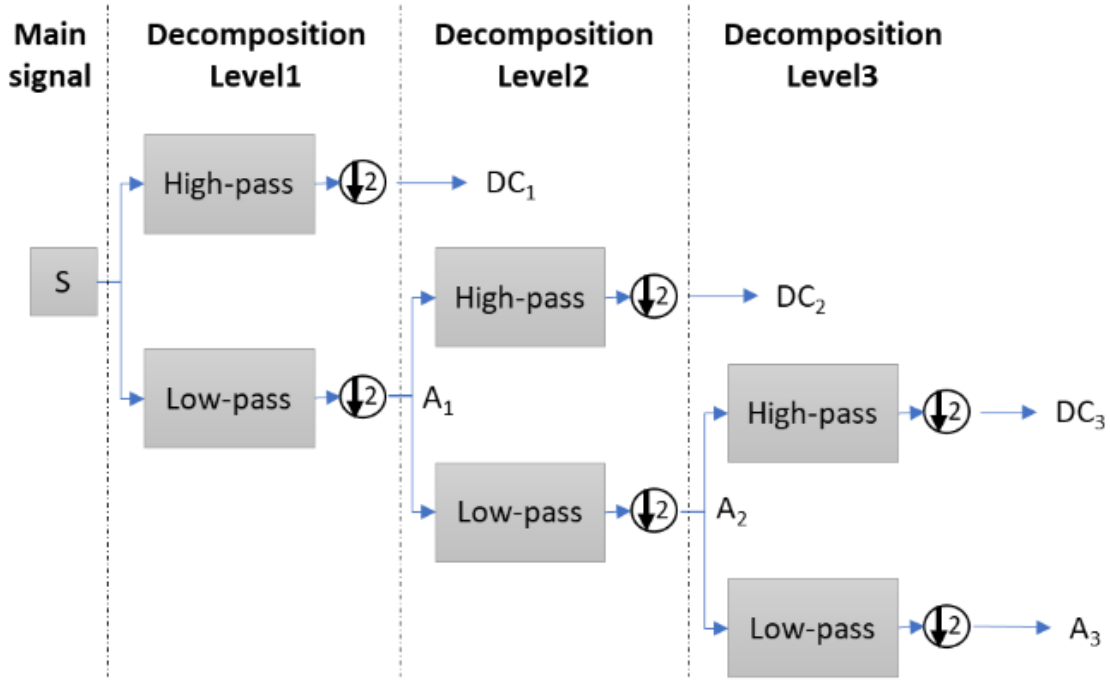

Figure 6.3. Representation of wavelet decomposition and its effect on BCG signals. The sequential process of wavelet decomposition, also known as multi-resolution analysis.

Wavelet transforms usually have been used for the denoising of non-stationary signals, as they provide a decomposition of the signal in the time-frequency domain [159]. Discarding some decomposition levels by thresholding some coefficients of the wavelet transform creates a smoother version of the input signal. This powerful threshold-based denoising method was introduced by Donoho [160]. Donoho's thresholding method for denoising has shown to be effective for a wide class of one-dimensional signals. The general denoising procedure involves three steps [159], that are described here and depicted in Figure 6.4:

1) **Decomposition:** First choose any wavelet with proper selection of level N. Then, compute the wavelet decomposition of the signals at level N.
2) **Thresholding:** Appropriate threshold is applied to the detailed coefficients prior to the Nth level of decomposition.
3) **Reconstruction:** Perform wavelet reconstruction using the original approximation coefficients of level N and the modified detailed coefficients of levels from 1 to N.

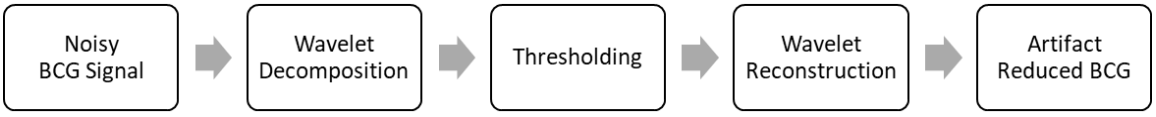

Figure 6.4. Workflow for motion artifact reduction using wavelet block processing.

II. Empirical Mode Decomposition

Empirical mode decomposition (EMD), has been widely used to filter nonlinear and nonstationary signals. EMD is much more flexible to the reduction of noise than linear techniques, and even than wavelets, as it can dynamically assign different modes to signals and noise. This technique decomposes a complex signal into some (almost) orthogonal components, where the Hilbert transform could provide their instantaneous frequencies. As described in [161], EMD empirically identifies the time lapse between the successive extrema, also known as the data's intrinsic physical time scales. Therefore, the extracted characteristic oscillatory modes are intrinsic

mode function (IMF), each of which satisfies the following properties. All IMFs should satisfy the following conditions:

1) Having the same number of minima and maxima. The number of zero crossings should also be the same or differing at most by one.
2) The mean value of the computed upper and lower envelopes should be zero, at any point.

For a given signal, the IMFs can be found via EMD by the following procedure, which is called the sifting procedure:

1) Identify all the extrema (maxima and minima) of the series X.
2) Generate the upper and lower envelope by applying the cubic spline interpolation among all the maxima and minima, respectively.
3) Average the two envelopes in a point by point manner to compute a local mean series m.
4) Subtract m from the data to obtain a candidate IMF $h = X - m$.
5) Check the properties of h:
    a. if h is not an IMF (i.e., it does not satisfy the previously defined properties), replace X with h and repeat the procedure from Step 1;
    b. if h is an IMF, evaluate the residue $r = X - h$.
6) Repeat the procedure from Steps 1 to 5 by sifting the residual signal.

At the end of the procedure, we have a residue r and a collection of n IMFs, named h_i ($i = 1, \dots, n$). The h_i are generated being sorted in descending order of frequency and therefore h1 is the one associated with the locally highest frequency. Moreover, the original X can be exactly reconstructed by a linear superposition:

$$X = \sum_{i=1}^{n} h_i + r$$

However, EMD suffers from a problem known as “mode mixing”, which is the presence of oscillations with different amplitudes in a mode, or the presence of very similar oscillations in different modes. To reduce the chance of mode mixing, Wu and Huang [162] have proposed an adaptive noise-assisted technique, named ensemble empirical mode decomposition (EEMD). EEMD is nothing more than averaging the results of the application of the original EMD on the random noise added to the original signal. The mode mixing problem is solved by the addition of white Gaussian noise, as the dyadic filter bank behavior of the EMD got used on the whole time-frequency space [163]. Considering the randomness of the noise, the hope is to cancel out the noise through the process while resolving the mode mixing. EEMD has the following procedure:

1) Add to the signal different realizations of the white Gaussian noise $x^i(n) = x(n) + w^i(n)$.
2) Compute the EMD on each noisy signal $x^i(n)$ and find the corresponding modes $IMF_k^i(n)$.
3) Average the IMFs of the same level, to reconstruct the modes for the overall EEMD:

$$IMF_k(n) = \frac{1}{W}\sum_{i=1}^{W} IMF_k^i(n)$$

where W represents the number of realizations of the white noise.

6.3.2. Experiments

I have used MATLAB’s wavelet toolbox to decompose each signal into its detail coefficients (D) and the approximation coefficients (A). For the first experiment, I have tried multiple different mother wavelets, including the Daubechies (dB), Symlets (Sym), Coiflets (coif) and Biorthogonal (bior) each one with different configurations. The first 9 detail coefficients resulted by the application of each wavelet on the same sample BCG signal is presented in Figure 6.5, to provide

a general sense about the effect of each wavelet on the signal. As a visual inspection of the denoised signals of different subjects, it seems that components at levels 6 through 8 are the best candidates to reduce the noise from the ballistocardiograph. Also, wavelets such as “bior1.3” and “Sym4” have undesirable effects on the BCG signals.

In the meantime, the approximation coefficients of the same configuration have been reported in Figure 6.6, where almost all wavelets could clearly extract the respiratory-like waveforms from the raw signal, very similar to the bandpass filtered signals.

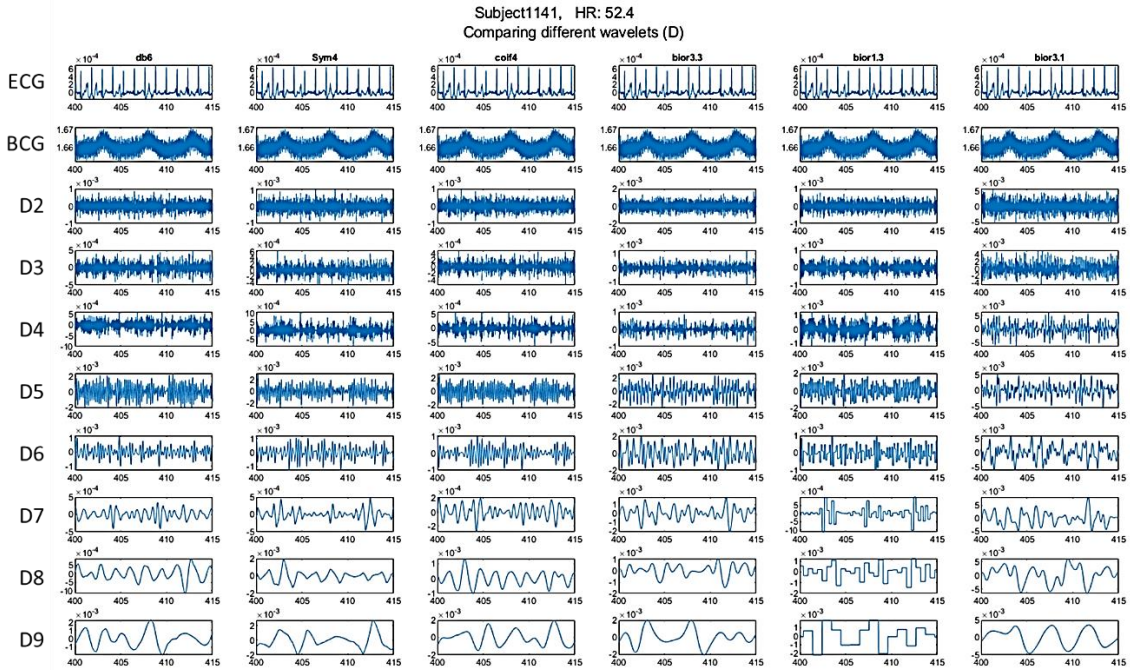

Figure 6.5. Example of applying different wavelet decompositions on raw BCG. Each column focuses on a specific mother wavelet. The top row is ECG and the second row is the raw BCG, followed by the detail coefficients (D2 to D9) of each wavelet transform on the same BCG signal.

This approach could simply change our viewpoints with respect to the extraction of the respiratory waveforms. The following code demonstrates the MATLAB implementation for wavelet decomposition:

Code sample I Wavelet decomposition

Goal: Extract the detail and approximation coefficients of the signal, used in denoising process.

Requires: Ni, Number of decompositions

WavletName, chosen from the list of available wavelets in MATLAB.

```
1: WavletName = 'bior3.3';                                  % Choose a wavelet.
2: [C,L] = wavedec(X,Ni, WavletName);                       % 1D wavelet decomposition.
3: for i_lev=1:15                                           % Process for 15 levels.
4:         D(:,i_lev) = wrcoef('d',C,L, WavletName,i_lev);  % Detail coeffs.
5:         A(:,i_lev) = wrcoef('a',C,L, WavletName,i_lev);  % Approximation coeffs.
6: end
```

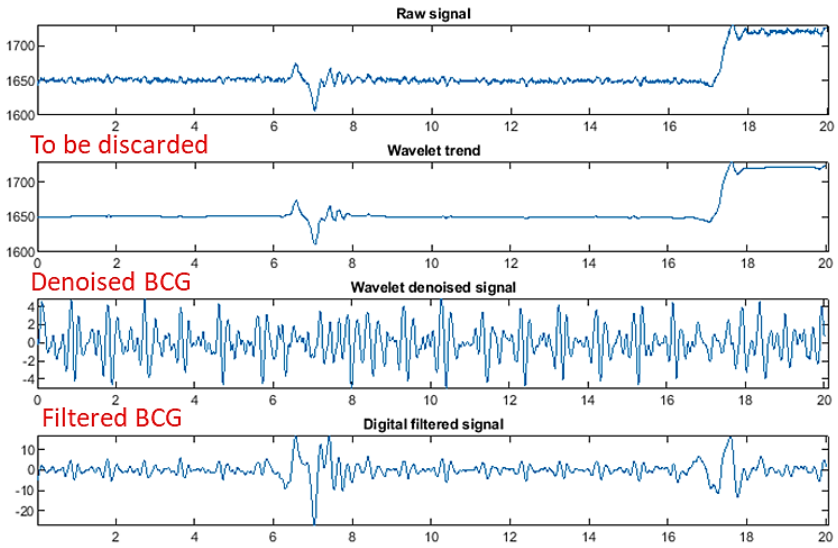

Figure 6.6. Wavelet thresholding used to reduce motion artifacts, by means of decomposing the signal into multiple detail coefficients, and then discarding some coefficients and summing up the rest of them. The 3rd row of this figure shows how wavelet thresholding can reduce the effect of motion artifacts, compared to the conventional bandpass filter, as shown in the last row.

After the wavelet decomposition, I have also tried the standard empirical mode decomposition (EMD) on the BCG signal of some random subjects. This was again to provide a visual inspection of the conditions and the differences of multiple IMFs. MATLAB's wavelet toolbox has a simple implementation of the EMD function which returns intrinsic mode functions (IMF) and the residual signals corresponding to the empirical mode decomposition of any input

signal X. EMD parameters such as the interpolation method, sifting stop criterion, decomposition stop criterion, and the boundary methods could be configured for different applications. I have used the following default settings for the EMD configuration.

Code sample II Empirical Mode Decomposition (EMD)

Goal: Decompose the signal into its IMFs used in the denoising process.

```
1:  [imf,residual,info] = emd(X,'Interpolation','pchip',          % Interpolation method
2:                             'SiftRelativeTolerance', 0.02,     % Tolerance of Sift
3:                             'SiftMaxIterations',100,           % Max num sift iterations
4:                             'MaxEnergyRatio',2);               % Max energy ratio
```

As described earlier, EMD suffers from the problem of mode mixing, and as a solution, the ensemble EMD (EEMD) has been introduced in the literature. I have implemented my own version of the EEMD, according to the literature and by means of the standard EMD function in MATLAB. As shown in the following code snippet, the process is very straight forward, which consists of generating different realizations of the normal Gaussian noise (using normrnd function) being added to the input signal. The resulting noisy signal will then be passed to the standard EMD function to create the corresponding IMFs (new_imf). The summation of all IMFs will be divided by the number of ensembles to create an average IMF set.

Code sample III Ensemble Empirical Mode Decomposition (EEMD)

Goal: Reduce the amount of mode mixing in the original EMD, using additive noise.

```
 1:noiseMU = 0;                                                          % Zero mean
 2:noiseSigma = 5*std(FilteredSignal);                                   % Relative STD
 3:imf_sum = zeros(sLen,MaxNumIMF);                                      % Initialization
 5:parfor i_ens = 1:numEns                                               % num iterations
 6:    noisySignal = inputSignal + normrnd(noiseMU, noiseSigma, sLen, 1); % Noise signal
 7:    imf_new = emd(noisySignal,'Interpolation','pchip',                % Standard EMD
 8:                  'SiftMaxIterations',10, 'MaxNumIMF', MaxNumIMF, 'Display',0);
 9:    imf_sum = imf_sum + imf_new;                                      % Sum of IMFs
10:End
11:imf_avg = imf_sum./numEns;                                           % Averaging
```

Figure 6.7 shows a sample BCG signal (on top) along with its 5 level decompositions through the normal EMD (left), ensemble EMD with 100 realizations of noise (middle), and the EEMD with 500 realizations of the noise (right). As the first few IMFs usually depict the high-frequency content of the signal, I show the 6th through the 10th IMFs. As theoretically expected, from left to right, each level of IMF shows a more stable form with less amount of mode mixing. Unfortunately, EEMD is a little slow compared to the standard EMD or the wavelet decomposition, due to the averaging process. Utilization of parallel computing could save time in large size analyzes.

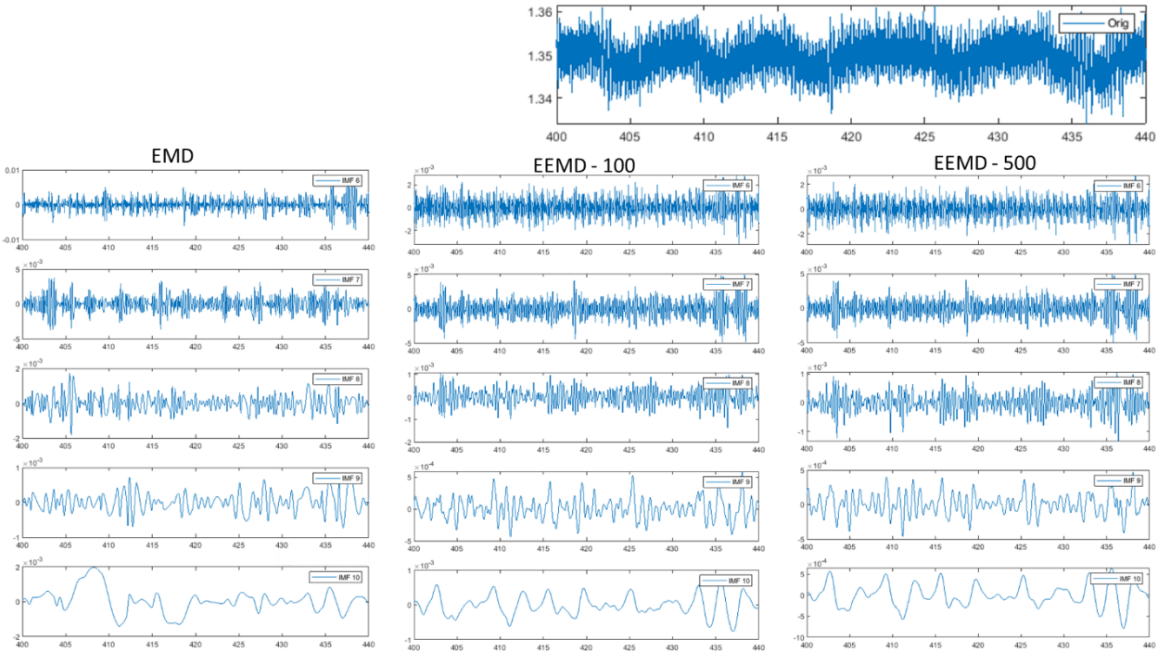

Figure 6.7. Comparing different implementations of the empirical mode decomposition. Sample BCG signal (on top) along with its 5 level decompositions through the normal EMD (left), ensemble EMD with 100 realizations of noise (middle), and the EEMD with 500 realizations of the noise (right).

I have also applied the EEMD to recover some small motion artifacts from the BCG recording. As depicted in Figure 6.8, the 6th IMF of the EEMD was able to recover from the small motion artifacts and provide a cleaner representation of the BCG signal compared to the conventional bandpass filter. Comparing the last two rows of the figure on the right, with the

bandpass filtered BCG and the 6th IMF from the EEMD, clearly shows the benefit of EEMD on denoising the signals recorded from an older resident of TigerPlace.

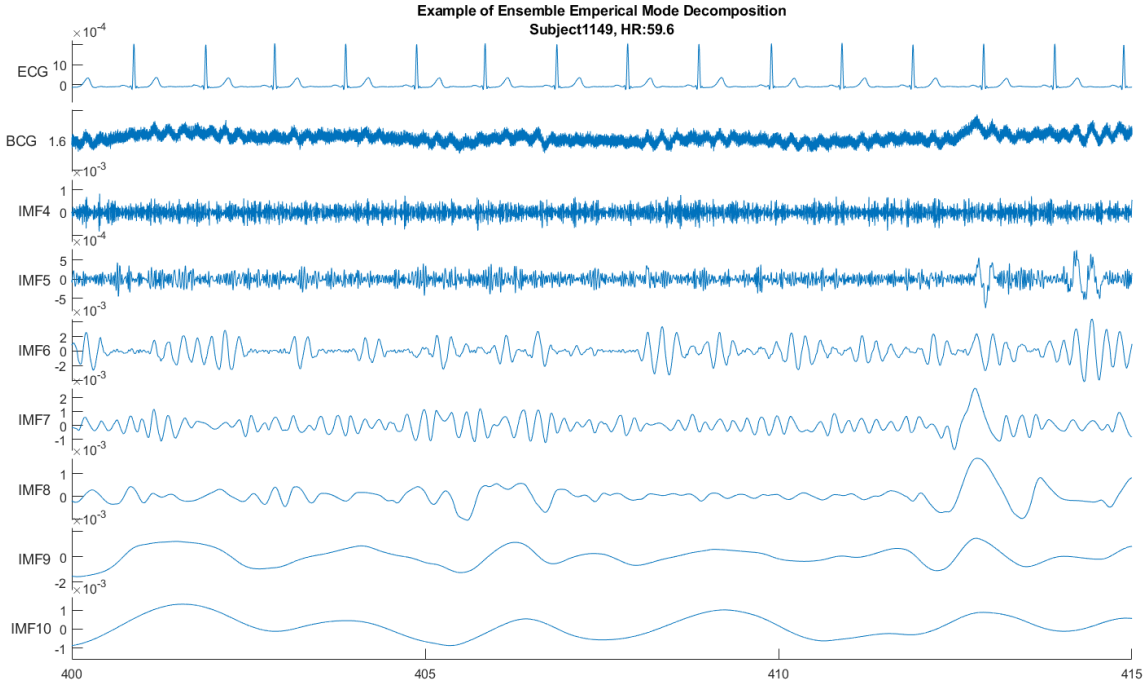

Figure 6.8. Example of how EEMD can reduce the noise contamination of BCG with the reference ECG, raw BCG, and IMFs 4 through 10 from the EEMD. As highlighted in the last row, IMF6 of the EEMD was able to recover BCG from the small motion artifacts, while the FIR bandpass filtered BCG shows considerably large distortions at that region.

After trying the above three methods on some random signals of different conditions, I chose a single best output from each method and plotted them along with the reference ECG signals and also the standard result of applying the bandpass filter on the BCG signal. Figure 6.9 shows the sample recordings of simultaneous ECG, finger sensor, and bandpass filtered BCG signal along with the 6th IMF of the standard EMD, 6th IMF of the EEMD, and finally on the last row the 9th detail coefficient of the db6 Daubechies wavelet.

The signal on the upper plot of Figure 6.9 is related to a young, healthy subject (HRV1046) who was relaxed for 10 minutes on supine position on the bed. While not having the cleanest

possible BCG waveform, still one can easily observe the cyclic variation of the BCG waveforms and estimate their locations from the bandpass filtered signal.

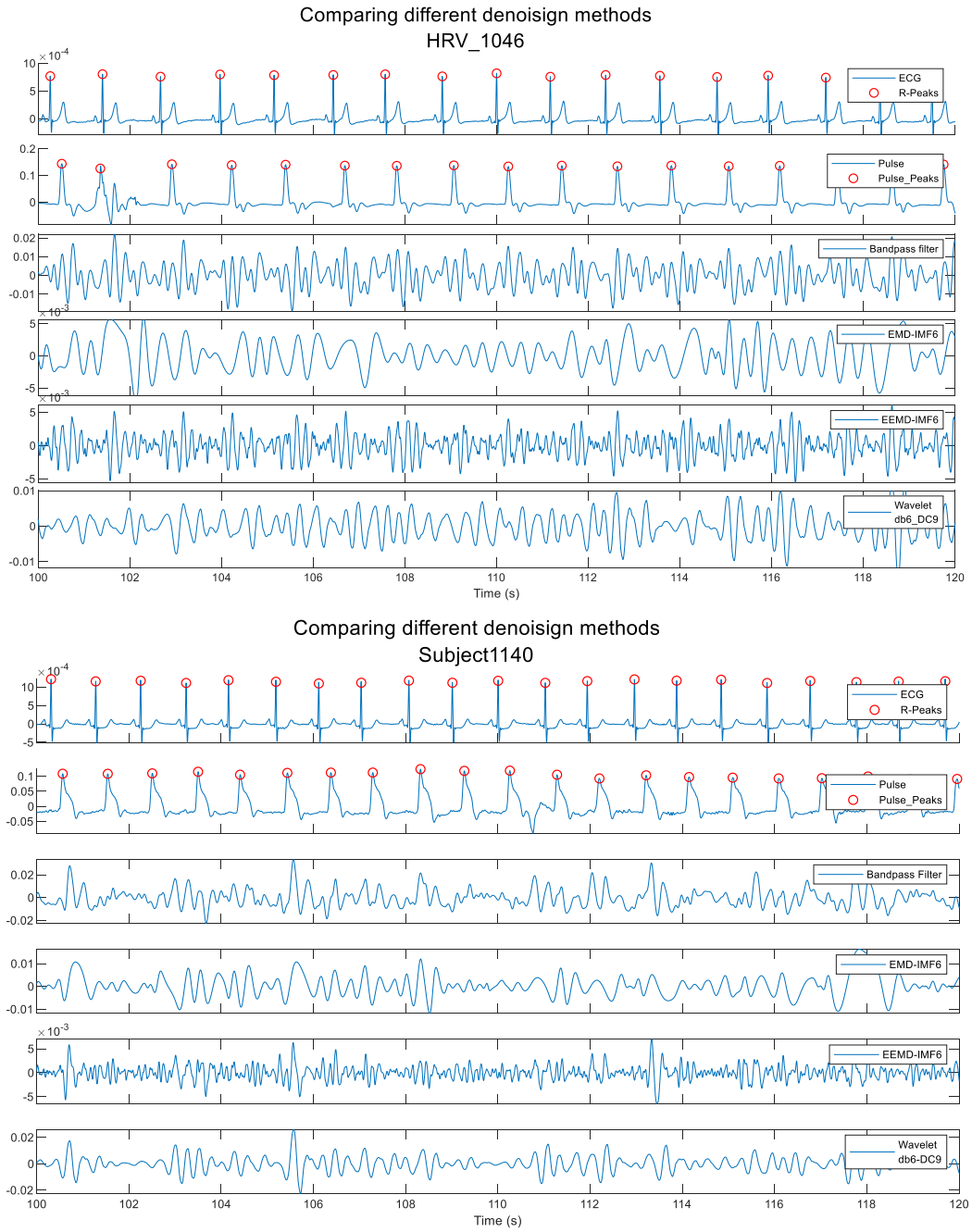

Figure 6.9. Comparing different denoising techniques between young and old subjects. ECG and its R-peaks, PPG and the bandpass filtered BCG, along with the EMD, EEMD and wavelet-based filters for a young, healthy subject (top) and an older subject with not clear BCG (bottom). For the younger subject, EEMD was more effective, and for the older subject the wavelet decomposition provides better results.

As shown in the 4th row of Figure 6.9, the standard EMD is affected by the mode mixing problem and contains multiple switches between different frequencies. Instead, the ensemble EMD was able to do a nice job in both discarding the remaining low-frequency content as well as some of the unnecessary high-frequency component. Therefore, in the 5th row, we can clearly segment every single beat of the BCG signal. Finally, in the 6th row, the application of the Daubechies wavelet decomposition is not that much satisfactory.

Conversely, the lower plot of the figure represents the signals acquired from a random older subject at TigerPlace (TP1140) with normal ECG but not a very clear BCG signal. The hope is to find at least one denoising technique to enhance the quality of the BCG signal for the purpose of beat detection. As shown in the 5th and 6th rows, while neither of the methods could completely clear the signal, the wavelet decomposition perhaps creates a better output for beat detection.

6.3.3. Results and conclusion

After reaching promising results in the application of both techniques (EEMD and wavelet) to enhance the quality of the BCG signal, I have studied the entire data set to provide a quantitative measure of the enhancement occurred after applying each method. I have used the synchronized ECG RR intervals as the ground truth for the instantaneous heart rate and applied both the original energy algorithm and my proposed enhanced energy algorithm to provide a beat to beat heart rate estimation from each channel of the hydraulic bed sensor. As discussed in Chapter 3, here, I have focused on evaluation of average heart rate estimations for epochs of 30 seconds long.

The data consist of the simultaneous ECG and BCG signals from the following datasets:

1) HRV: 60 young, healthy subjects, in the supine position with less motion.
2) POS : 60 young, healthy subjects (same as above), with successive change of posture.
3) TP : 51 volunteers from both older residents and younger workers of TigerPlace.
4) Sleep: 20 random patients from the Boone hospital sleep lab.

The process of analyzing the data from each subject consists of creating different denoised versions of the signal through the use of each of the previously described denoising techniques and then computing the beat to beat heart rate estimation from each one by applying both the original energy algorithm and the enhanced energy algorithm. For denoising, I have used the EMD (2^{nd} to 4^{th} IMFs), the EEMD (2^{nd} to 4^{th} IMFs), and from each of the four wavelet decompositions (db5, db6, bior3.1, bior3.2) I picked three detail coefficients (DC3, DC4, DC5). The beat to beat estimations then averaged for every epoch of 30 seconds and were compared to the average heart rates computed from the corresponding ECG signal. The entire process following these steps:

1) Load the signals from each of the four transducers
2) Apply different configurations of the described filtering techniques, including:
    a. A bandpass filter with 0.7-10 Hz as the reference. (4 channels)
    b. EMD and EEMD and storing the 2^{nd} to 4^{th} IMFs. (4 channels, 2 methods, 3 IMFs)
    c. Wavelet decomposition (db5, db6, bior3.1, bior3.2), (DC3, DC4, DC5)
3) Compute the beat to beat HR estimation of signals (Original and enhanced energy alg.).
4) Split the beat to beat heart rate estimations into epochs of 30 seconds.
5) Compute an average heart rate estimation for each segment.
6) Compute the error of each epoch compared to the ECG based estimations.

As the first goal, I have provided a comparative analysis of the potentials of application of denoising techniques on each of the original and enhanced energy algorithms. In Table 6.2, I showed the mean and standard deviation of the error in heart rate estimations, on the original (noisy) signal and each of its denoised versions. Regardless of the exact configuration of each technique (such as the wavelet type or IMF level), a general comparison provided on the best possible configuration of each method. In other words, for example for the dB wavelet, among all different wavelet configurations (db5, db6) and all choices for detail coefficients (DC3-DC5) and all choices to select the transducer (F1-F4), I have selected the lowest error in HR estimation (closest to the

reference HR). This will provide an "oracle" estimation of the lowest possible error of that general technique for each subject. Off course, automatic channel selection and the choice of decomposition level require further analysis.

As described, Table 6.2 provides an overall comparison of the best cases for each configuration. Here the lower error of each configuration was averaged over all subjects (in different groups), and the mean and standard deviation error in heart rate estimation of each group is provided in terms of beats per minute (bpm). Clearly, in all cases, the enhanced energy algorithm could provide a significant improvement in the estimation of heart rates. Also, it always has a smaller amount of deviation from the mean (STD), which shows it is a much more stable approach compared to the original energy algorithm.

Table 6.2. Effect of denoising on the original and enhanced beat detection algorithms*. This table shows the average error for each combination of the approaches in beat per minute (bpm).*

Estimation error by choosing the mean error of all four transducers (bpm)

Denoising Technique	Original Energy Alg.					Enhanced Energy Alg.					Overall Improvement	
	All	HRV	Pos	Sleep	TP	All	HRV	Pos	Sleep	TP	(bpm)	(%)
Without Denoising	17.8	16.7	18.6	15.6	19.1	11.3	11.4	11.1	10.1	12.0	6.5	36.5%
Wavelet Dec. bior33(DC3)	18.2	16.4	18.8	16.7	20.4	12.1	11.0	11.2	11.6	14.9	5.7	32.2%
Wavelet Dec. db5(DC5)	14.0	12.3	14.9	14.1	15.3	8.6	7.0	8.6	7.9	11.2	9.2	51.7%
EMD 2nd IMF	16.7	15.5	17.8	13.9	18.0	11.4	10.6	10.7	8.6	14.6	6.4	35.9%
EEMD 4th IMF	18.2	16.1	20.6	15.1	19.3	9.3	7.6	8.9	10.3	11.7	8.6	48.0%

* HRV, Pos, TP, and Sleep are the name of datasets used in the comparison.

Comparing different datasets also shows very interesting results, which mostly matches the expectation due to the data collection settings. As expected, the posture (POS) dataset, which contains large motion artifacts due to multiple changes of postures, usually has the highest average estimation error. In comparison, the HRV dataset of young, healthy subjects with minimal motion artifacts usually has the least amount of noise contamination and therefore, the smallest average error. The dataset of older TigerPlace residents (TP) with minimum movements is somewhere in between the previous two, as they have a smaller amount of motion artifact compared to the POS

dataset, but their BGC waveform is not as clean as the one for young, healthy subjects in the HRV dataset. Finally, the sleep lab data is always in the middle range as they were patients with sleep and breathing disorders, but perhaps not as bad as a very old TigerPlace resident, and with a smaller percentage of motion, artifacts compared to the POS dataset.

Regarding the comparison of the denoising techniques, my results show that application of EMD always improves the accuracy of HR estimation in either of the two energy algorithms. Also, the results of EEMD show some improvements in the estimation error of the enhanced energy algorithm. DB wavelet decomposition, even more, improves the estimation error of the enhanced energy algorithm while the Bior wavelet usually has the same accuracy as of the EEMD. The same improvements usually appear through the application of denoising techniques on the original energy algorithm (always with much higher error than the enhanced energy algorithm). But, surprisingly, EEMD was never better than the EMD on the original energy algorithm. This is despite the expected theoretical comparison of the EMD and EEMD and might be due to the higher level of uncertainty and randomness in the original energy algorithm.

In overall results, the dB wavelet decomposition always shows better accuracy in the estimation of heart rate using the enhanced energy algorithm. It also has the minimum standard deviation, which means the highest stability of the estimations. Its results are also comparable to the application of EMD for the original energy algorithm.

Despite the huge improvement in the accuracy of the heart rate estimates, still, large motion artifacts seem to produce errors in the estimations. Excluding the sleep dataset (which contains lots of unconstrained conditions), the POS dataset always has the highest error among the other two datasets, in each row and for both implementations of the energy algorithm. This opens up the importance of the next topic on the detection of motion artifacts and the cancellation of motion contaminated segments from the signal, before reporting the HR estimation.

6.4. Motion Artifact Detection

This section explores the use of machine learning methods for automatic identification of motion artifacts, i.e., variations in the time and frequency domain characteristics of ballistocardiography signals acquired from noninvasive in-home hydraulic bed sensors. Section 6.4.1 starts with the description of dataset and ground truth labeling, followed by the description of time-domain and time-frequency domain features of the BCG and their normalization. It finally describes the classification method that I propose to use on a fusion of time and frequency domain features extracted from multiple transducers for the detection task. Experiments and results of performance comparison for different classification algorithms are reported in 6.4.2, and finally, the conclusions are provided in 6.4.3.

6.4.1. Method

I. Dataset

The data used in this study were collected in two separate IRB-approved studies, with a total of 30 subjects being recruited. Four hydraulic transducers were placed under the mattress and a set of reference sensors (i.e., ECG, Chest band) placed on the body surface. The first dataset was collected from 25 young, healthy subjects in a controlled lab setting at MU. Subjects were asked to lie still on the bed for 10 minutes in a supine position, followed by changing posture to left, right and prone positions, consecutively, and staying still for 2 minutes at each posture.

The second dataset was collected at the Boone Hospital Sleep Center, under the standard polysomnography (PSG) conditions. IRB approved de-identified PSG data of 5 random patients were collected in synchrony with the hydraulic bed sensor signals placed under the mattress for an entire night for each subject. Random movements of the subjects during their PSG sleep study

provide great opportunity to approximate the uncontrolled settings, while some limitations are enforced by the PSG sensors.

II. Ground truth labeling

Many recent publications on motion artifact detection used human visual inspection by experts who were familiar with the signal, and their decisions are regarded as the gold standard in labeling motion-artifact-corrupted segments [154]. I have reviewed and manually annotated the collected signals three times each, with 2-4 days delay in-between, to reduce the possibility of biased labeling. During this process, each sample was annotated for being clean vs. noisy. The final label for each segment comes from the maximum severity assigned over the three review phases, as the goal here is to discard any possible noise.

III. Time Domain Features

Even small body movements on the bed are recorded by the bed-sensor transducers and could affect the quality of the signals (Figure 6.2). Abrupt jumps in the amplitude and DC level of transducers during posture changes are represented in Figure 6.10. Sequential detection algorithms can be used to analyze successive data frames of the BCG signal. This analysis requires the extraction of features from the time-domain representation of the BCG signal.

To compute the time-domain features, a sliding window of 30-second width with 50% overlap was used to move along the signal of each transducer. The standard deviation (STD), median absolute deviation (MAD), 75^{th} percentile, skewness, kurtosis, and Shannon entropy features from each window are computed and stored to build the feature set. Another very useful feature in our multi-channel hydraulic bed-sensor is the changes that appear in the DC value of the four transducers, after each posture change. Meanwhile, a novel fusion level feature computed by the MAD of the sum value of the four transducers at each time window is added, to make a total of 24 time-domain features.

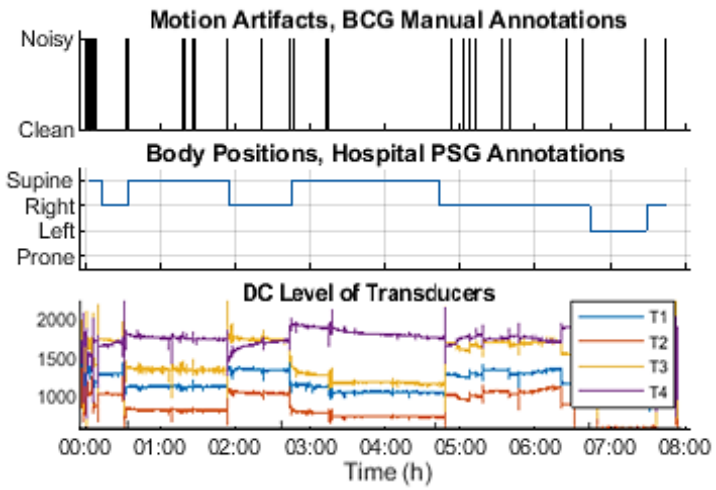

Figure 6.10. Example of overnight recording BCG, PSG and the motion annotations. Figure shows ballistocardiography signals (lower row) from our hydraulic bed sensor, along with the PSG annotations for sleep posture (middle row) and our expert's manual annotations for artifact regions, show good alignment between all sources. Significant variations in the DC level and amplitude of the transducers, are mainly correlated to the change in posture, or limb movements.

IV. Time-Frequency Features

The classical Fourier Transform does not deal with non-stationary physiological signals such as BCG. Time-Frequency domain analysis of the signals provides a joint platform to explore the varying spectral content of these signals [155]. Among all approaches available in the literature, I used the Short-Time Fourier Transform (STFT) to track the change in the frequency content of each signal in the time-frequency domain (Figure 6.11).

A 2D spectrogram of each channel created using a Hamming window of size 5 seconds with 80% overlap. Frequencies outside the range of 0.5-15 Hz are discarded. Again, another sliding window of length 60 seconds (12 samples here) with 90% overlap is run over the spectrogram to extract the features in the time-frequency domain of each channel. A total of 28 features including the minimum, maximum, mean and median of the power spectrum, the ratio of minimum to maximum frequency content, the ratio and variation of the maximum to minimum power density drop were extracted from the four transducers.

V. Normalizing the features

After extraction, all 53 features from both the time domain and time-frequency domain were resampled to the same timestamp and concatenated to build a single feature set. Each extracted feature was normalized separately between 0 to 1, over all subjects combined. Then two thresholds equal to the 20^{th} and the 70^{th} percentile value of each feature were used to discretize the feature values to 3 levels. These features were used for both visualization and classification purposes.

VI. Classification methods

All extracted features were set together in a columnar matrix with the last column containing the manually annotated class labels for each sample. MATLAB's implementation of support vector machines (SVM) and RUSBoost classifiers with 5-fold cross-validation were used to identify the motion artifact contaminated samples from the clean samples. A comparison of different classification settings is provided using different measures, i.e., the sensitivity, specificity, accuracy, and false-negative rate (Table 6.3).

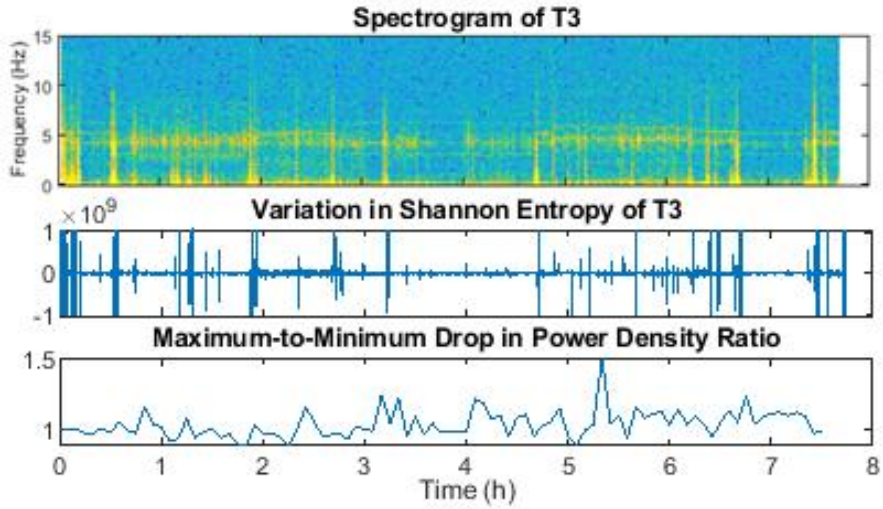

Figure 6.11. Sample spectrogram of transducer 3 during an overnight recording (Top row), along with the corresponding variation in the Shannon entropy and also Max2Min drop of the power density ratio. While the correlation of the first two is visually perceptible, the last feature peaks during the absence of the noise.

6.4.2. Experiments and Results

As suggested in the literature [154], support vector machines (SVM) with Gaussian kernels were initially selected for the binary classification of noisy vs. clean segments of the signal. We used standard MATLAB R2019a libraries, on a Windows PC with Intel Core i7 CPU of 3.7 GHz and 26 GB of RAM.

As listed in Table 6.3, it takes a long time (about 3 hours) to get the results using all 53 extracted features. Thus, a second experiment was conducted using the first 5 principal components estimated after passing the original features through principal component analysis (PCA). Analysis of the results shows that although the classification accuracy in both experiments is above 97%, they both have very low sensitivity (23% and 54% respectively) and very high values for the false-negative rate (77% and 45% respectively). This, in part, is due to the imbalanced distribution of the two classes. In other words, only 3% of the samples are labeled as noisy (5437), compared to the clean samples (181,958). As a test, a balanced dataset was made by simply replicating the samples in the smaller class (noisy) to get the same size as the larger class. A new round of experiments was performed on this balanced dataset both with and without the PCA. The balanced dataset significantly improved the sensitivity of the tasks to 99.4% and 98.7% respectively for the original features and the first 5 principal components.

I have also used the RUSBoost classification (with 30 learners of the type decision tree and a default learning rate of 0.1) as they are known to be fast (boosted) and also invariant to imbalanced datasets [164]. For the sake of comparability, I repeated all four of the previous SVM-based experiments, with the new approach. RUSBoost was orders of magnitude faster than SVM under similar configurations, especially on the unbalanced dataset where high accuracy results are achieved in less than a minute compared to hours of computation with the SVM, as reported in Table 6.3. Moreover, its sensitivity measure was much better than the SVM on the imbalanced

dataset. Meanwhile, synthetically increasing the number of samples in the noise class resulted in only a little higher sensitivity rate at the cost of more time and accuracy reduction (by about -2%).

Table 6.3. Noise classification using SVM vs. RUSBoost. *RUSBoost is much faster than SVM in the classification of clean vs. noisy segments and is almost invariant to imbalanced datasets.*

Method	**PCA**	**Accuracy (%)**	**Sensitivity (%)**	**Specificity (%)**	**FNR*(%)**	**Time *(S)***	**Balance**
SVM	No	97.3	23.0	99.5	77.0	10700	No
SVM	Yes	98.2	54.3	99.5	45.7	1200	No
SVM	No	99.2	99.4	98.9	0.6	8200	Yes
SVM	Yes	98.7	98.7	98.7	1.3	2300	Yes
RUSBoost	No	94.6	91.2	94.7	8.8	50	No
RUSBoost	Yes	94.2	91.0	94.3	9.0	50	No
RUSBoost	No	92.8	94.3	91.2	5.7	600	Yes
RUSBoost	Yes	92.1	92.6	91.7	7.4	600	Yes

** FNR: False Negative Rate*

6.4.3. Conclusion

Extracted features from successive data frames of each transducer were combined with features from the other channels. These features were then used as inputs for two machine-learning classifiers, namely the SVM and the RUSBoost, to identify those portions of the signal that are contaminated with noise. As the number of artifact contaminated samples are much smaller than the number of clean samples, the sensitivity of the results was low. To resolve the problem of imbalanced data, I tried two approaches, firstly, to make a balanced version of the dataset and secondly, to utilize algorithms such as RUSBoost which are invariant to data balance.

While the accuracy of all experiments tends to be higher than 92% (see Table 6.3), the sensitivity of SVM on the imbalanced dataset is as low as 23%. Our results show improved sensitivity rates after making the dataset balanced. Likewise, the RUSBoost algorithm handles imbalanced datasets at a much faster computation time but the cost of accuracy, compared to SVM. Overall the best results come from SVM with balanced dataset before the application of PCA. Meantime, RUSBoost classifies the data much faster, which might be of interest for future studies.

6.5. Channel Selection

6.5.1. Background

Digital processing of multi-channel signals has reached a wide application in the preparation and analysis of biosignals such as multi-lead ECG or EEG. Efficient channel selection approaches are needed to (i) reduce the computational cost and (ii) improve the quality of features and estimations, by selecting only the most relevant channels. It can also help in the selection of the best configuration at the design time, where multiple sensors are being placed at different locations with respect to the body and the goal is to find the best sensor configuration for a specific problem.

As described in Chapter 3, our BCG sensors usually consist of multiple channels, including the four transducers of the hydraulic bed sensor, or the three axes of accelerometers used in the chair sensor. While each of these channels provides some information about the cardiorespiratory activities, my observations confirmed that the estimated values of different parameters acquired from each channel might be different from the others. Motion artifacts also cause a different amount of distortion in each channel, usually due to the differences in the distance of body to the sensor or the relative direction of body and sensor. Therefore, channel selection not only improves the computational time by reducing the amount of data to process but also can improve the quality of features and estimations by means of rejecting the low-quality samples.

One data-driven approach to select the channel of the highest quality goes through the definition of signal quality indices (SQI) to be assigned to each channel in order to provide the means to sort the channels based on the quality of their signals. A rule-based assessment of the estimated heart rate values was used by Orphanidou, et al. [165] as the SQI to assess whether reliable heart rates (HRs) can be obtained from wearable ECG and PPG signals. A fuzzy logic representation of the waveforms and reasoning was also used by Zong, et al. [166] to assess the signal quality of the arterial blood pressure (ABP) in the intensive care unit (ICU).

Elgandi [167] has provided a complete list of different signal quality indexes for PPG signals. Some of these indices are in the time domain, and the rest are in the frequency domain, for example, the PerfusionSQI, which is the ratio of pulsatile blood flow to the static blood flow in the peripheral tissue. This index is reported as the gold standard in the assessment of signal quality in PPG signals. Other proposed indices such as Skewness, Kurtosis, or the entropy of the PPG beats were also discussed as carrying valuable signal quality information.

Frequency domain approaches for signal quality evaluation are also discussed in [167], including the relative power index, which is the ratio between the power of two different frequency bands of the signal. Pradhan, et al. [168] have used the median relative power variation between consecutive PPG beats, by means of the Welch periodogram in two different sub-frequency ranges. The first frequency range associated with "good signal" has chosen to be between 1-2.25 Hz (as most of the energy of PPG signal is concentrated in that range), while the entire frequency range was selected between 0-8 Hz. Then a "relative power index" computed as:

$$RelativePower = \frac{\int_1^{2.25} P(f)df}{\int_0^8 P(f)df}$$

Unfortunately, most of the SQI indices mentioned above are defined based on the properties of an individual cardiac cycle, and therefore need an accurate heartbeat detection as a prerequisite. In our case, we want to use a signal-level index for each BCG channel to enhance the quality of our beat detection algorithms.

In this section, I have relaxed some of these quality indices for not being limited to the individual cycles and applied them on a signal segment of 30 seconds as a single epoch. SQI values estimated from different BCG channels were compared in each epoch for the choice of the most reliable channel. Among them is the DC-based approach that was used in [13], and also the channel selection based on the variation of the estimated heart rates.

6.5.2. Method

This section contains the description of multiple signal quality indices (SQI) that I designed or adapted for the signal-level evaluation of the channels.

I. Signal to Noise Ratio:

Signal to Noise Ratio (SNR) is the first approach to evaluate the quality of the signal and can be used in the quality assessment of multiple channels. There are many different approaches to define the "signal" and "noise". In this work, I am using the standard Butterworth bandpass filter with cutoff frequencies between 0-10 Hz to define the signal, and the remainder of the input is selected as noise:

$$Signal_{ij} = BandpassFilter(S_{ij}, LF = 0.7, HF = 10, Fs)$$

$$Noise_{ij} = S_{ij} - Signal_{ij}$$

where S_{ij} is the ith epoch of the jth transducer, and Fs is the sample rate. Then the ratio between the variance of the signal to the variance of the noise creates the first SQI index as defined here:

$$SNR\_SQI_{ij} = \frac{variance(Signal_{ij})}{variance(Noise_{ij})}$$

II. Band Power Ratio:

In the same analogy as used by Elgendi [167],and Pradhan, et al. [168], I have split the frequency content of our sensor into two separate ranges, as the "good BCG frequency" containing frequencies from 4-15 Hz and the other "overall frequency content" including all frequencies from 0 to 60 Hz. The selection of 4-15 Hz frequency range was to emphasize the importance of higher frequencies of the BCG waveform, including the sharp J-peak, rather than low-frequency variations which mostly have overlaps with respiratory variations. Then the average power of each frequency

range computed using MATLAB's band power command, and their ratio was used as the SQI for each epoch, as represented bellow:

$$BPR\_SQI_{ij} = \left(\frac{bandpower(S_{ij}, Fs, [4,15])}{bandpower(S_{ij}, Fs, [0, min(60, (Fs/2)])}\right)$$

where S_{ij} is the i[th] epoch of the j[th] transducer, and Fs is the sample rate.

III. Heart Rate Deviation:

The variation in the estimated heart rate values is the other heuristic SQI that I am using here to compare the quality of different channels. The rationale behind this selection is based on the fact that in case the signal is contaminated by a high degree of noise, the chance of a missed detection (either more or less) is increased which therefore would increase the density of abnormally high or abnormally low HR estimations in that segment. I have computed the median absolute deviation (MAD) for an accurate estimate for the deviations in each channel.

$$MAD\_SQI_{ij} = mad(S_{ij})$$

IV. DC bias of each channel:

Especially for the case of our hydraulic bed sensor, the raw signals from each of the four transducers can have a different DC bias value, depending on the distribution of the weight on top of them. DC bias (offset) is usually undesirable, especially when causing the clipping on the target signal, for example, due to the change of posture or placement of the individual on the mattress. Therefore, usually by subtracting the mean amplitude of the signal in a moving manner, the DC offset is removed.

However, the DC bias can also contain useful information regarding the placement of the subject on the bed and how far they are away from the sensor. The historical thought was to assume the transducer with the highest DC being the closest one to the heart and therefore, the one which potentially could have more clear cardiac information. While we have been using this idea in different cases [13], it has never gone under a thorough test. Here I show the results of my investigation on this idea by treating the DC level of each transducer as an SQI and to choose the transducer with the highest DC bias. To compute the DC bias, I used the median of the signal in each epoch:

$$DC\_SQI_{ij} = median(S_{ij})$$

V. The oracle; the best choice of channels

In the imaginary world of the "best channel selection techniques", the error produced by the "best channel" should always be less than the rest of the channels. One way for reverse engineering of such an "oracle" technique is to use the actual errors computed for each channel compared to ECG-based ground truth as the "Oracle SQI". After finding the best possible choice between the available channels, I compared the number of times that both approaches match in choosing the same channel (Hit). The hit rate is defined as the ratio of the number of times the two outcomes match, to the total number of comparisons (epochs).

$$Hit\ Rate = \frac{Number\ of\ matches}{Total\ number\ of\ tests}$$

There are, of course, multiple important points to be considered in this approach, that I found in my experiments, including (i) the possibility of having multiple channels with the minimum error or the best (lowest or highest) SQI value, and (ii) also the fact that two, not exactly equal but very similar values, usually could be considered as "equal". To address all these considerations, I have relaxed the outcome of the channel selection to be as many channels as possible. I usually start with "the first best channel", and then incrementally add other channels as described here:

i) Find all transducers that have the same value as the best one (error or SQI).

ii) Accept a small tolerance in the estimated values (error or SQI)

Thereafter, I have a list of best channels produced by the oracle approach, and a list of channels by using each of the provided SQI indices for channel selection. A channel selection is considered acceptable if its output list of channels has at least one overlap with the oracle's list. I do not consider any penalty in case of missing of the oracle channels, as in my case, I need "the one" best channel to reduce the computational cost and improve the estimation error.

6.5.3. Experiments and Results

As the first experiment, I computed the heart rate estimation error of both the original energy algorithm and the enhanced algorithm, on the input signal after applying each of the previously described denoising techniques. To provide a better comparison, the average results of each dataset are also reported in separate columns. In the rightmost columns, the overall improvement of each combination (denoising x energy algorithm) is computed by comparing their estimation error to the error that traditionally the original energy algorithm produced without any denoising (cell (1,1)).

Table 6.4. Effect of denoising techniques on heart rate estimations. *Multiple denoising techniques were applied prior to the original and also the enhanced energy algorithm. The oracle approach is used to pick the best transducer. The overall improvement is computed based on the data from <u>all</u> datasets, compared to the original energy algorithm without any denoising.*

Estimation error by choosing <u>the best</u> transducer, using the oracle method (bpm)

Denoising Technique	Original Energy Alg.					Enhanced Energy Alg.					Overall Improvement	
	All	HRV	Pos	Sleep	TP	All	HRV	Pos	Sleep	TP	(bpm)	(%)
Without Denoising	**<u>16.4</u>**	**15.4**	**17.2**	**16.1**	**17.0**	**6.9**	**5.7**	**8.3**	**6.8**	**6.9**	**9.5**	**57.9%**
Wavelet Dec. bior33(DC3)	**16.5**	**14.3**	**17.1**	**17.9**	**18.1**	**7.3**	**4.4**	**8.8**	**8.6**	**8.9**	**9.1**	**55.6%**
Wavelet Dec. db5(DC5)	**12.9**	**11.3**	**13.4**	**14.7**	**13.8**	**5.0**	**3.1**	**6.2**	**5.5**	**6.1**	**<u>11.4</u>**	**<u>69.3%</u>**
EMD 2nd IMF	**14.9**	**13.6**	**16.1**	**13.9**	**15.5**	**7.5**	**6.8**	**8.3**	**6.1**	**8.1**	**8.9**	**54.3%**
EEMD 4th IMF	**17.0**	**15.1**	**19.1**	**17.1**	**17.0**	**5.4**	**3.0**	**6.6**	**8.5**	**6.1**	**11.0**	**66.9%**

I should emphasize the difference between the values of this table from previously shown Table 6.4, are only due to the application of the oracle method for channel selection, and is not reporting any SQI-based channel selection. This is to establish the superiority of the enhanced energy algorithm even in case of oracle channel selection, as in each row the lowest values are always related to the enhanced algorithm, regardless of the dataset or the denoising approach.

Meanwhile, most of the times the HRV dataset (young subjects with no movement) shows the minimum amount of error (as low as 3 bpm), which is consistent with our expectations, as it contains clean BCG signals from young, healthy volunteers in a controlled lab environment. On the other hand, the estimations from the three other datasets are usually at the same level. The "Pos" dataset has periods of large motion artifact due to the change of posture which perhaps is the cause of relatively higher errors (still improvements are obvious). The "TP" dataset contains the signals from the older subjects at TigerPlace. Not only some deformations appeared in their typical BCG waveform, but also three 30-second periods in the signal are contaminated by possible motion artifacts caused by the application of the automatic blood pressure cuff. Finally, in the sleep data, different random activities such as change of posture and use of oxygen masks may cause noisy segments in the signal. In fact, the results shown in this table for the sleep dataset, are higher than my initial expectations, considering the situation of the patients in the sleep lab.

As depicted by underscores in the last two columns, the wavelet decomposition using Daubechies wavelet provides the maximum overall improvement (reduction) in the HR estimation errors. The application of the enhanced energy algorithm on the denoised signal using the Daubechies wavelet could reduce the HR estimation error by almost 70%, compared to the overall estimation error of applying the original energy algorithm on the bandpass filtered signal (before denoising).

Secondly, I have also studied the effect of channel selection on the accuracy of the heart rate estimation. I compared multiple channel selection techniques based on the SQI indices that are

described earlier in this chapter, including the approaches based on the DC level, MAD of heart rate estimates, signal SNR, and finally the band power ratio. In this section, the analysis is done solely on the combination of the enhanced energy algorithm and the wavelet denoising, to see how well each SQI can match the channels selected by the oracle approach (hit).

Figure 6.12 shows the accuracy of each SQI in matching (hit%) the oracle selection on different datasets. As discussed earlier, despite the DC level approach, other SQI indices have acceptable performance in hitting the best transducer. Average hit percentage of 74% up to 78% on multiple datasets, could make a considerable improvement in accuracy of any future BCG analysis.

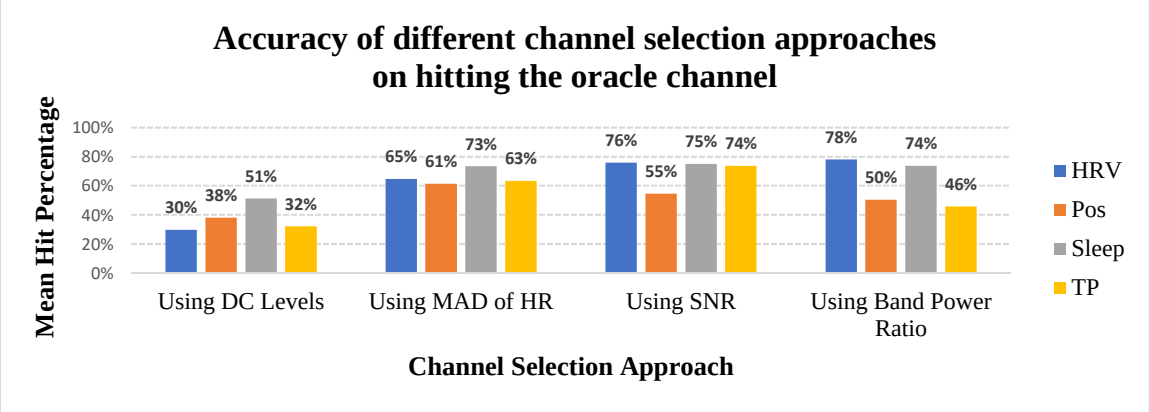

Figure 6.12. Comparing different channel selection approaches to the oracle approach. Results are shown in the percentage of times each SQI-based method hits the same channel as the oracle.

6.5.4. Conclusion

Among the investigated SQI indices, SNR shows the highest hit percentage on the combination of all datasets, with a minimum of 55% on the POS dataset. In fact, the POS and TP datasets have the lowest average percentage of hit among all channel selection approaches (HRV: 62%, POS: 51%, Sleep: 68%, and TP:53%), which is due to the existence of motion artifacts on all transducers. Despite the expectations, the Sleep dataset with 6-8 hours of over-night signals from the sleep lab patients shows a high hit rate. This could be due to the fact that in longer periods of

time, usually, the channel selection algorithms can compensate for random distortions in the signals by switching to another one.

On the other hand, while the band power ratio has very high hit rates on the HRV and Sleep datasets, it apparently was not successful on the TigerPlace data. This shows the existence of variation in the higher frequency contents of the BCG during the aging process. In other words, the selected frequency band (4-15 Hz) for the "good" BCG seems not as accurate for the older subjects.

As a summary, in this section, I have studied the effect of channel selection and denoising on the improvement of heart rate estimations. Even with the oracle channel selection, the enhanced energy algorithm always works much better than the original energy algorithm. Also, different SQI indices have been proposed for channel selection, and their results were compared against the channel selected by the oracle approach. Among all, the SNR and the MAD of HR have a higher hit rate with the oracle channel.

7. MORPHOLOGICAL ANALYSIS OF BCG

7.1.Background

The instantaneous beat by beat analysis of biological waveforms, such as the arterial pressure waves or the electrocardiogram waves, has been known as a definite approach in studying the cardiovascular system. But analyzing every single beat of a cardiovascular waveform might not be of interest to researchers as they usually are looking at the "average" value of parameters within a short period of time. This averaging is intended to cancel out the normal variations of the waveform caused by different sympathetic and parasympathetic activities. In this work, instead of extracting features from each beat and then smoothing the values, I will first construct an ensemble average (template) to represent the average morphology of the waveform in a time period.

For example, Szczepanski and Saeed [169] used templates to show changes in the schematic waveform of a single heartbeat in the ECG signal. This gave them the ability to analyze distortions, deformations, and delays that appear in normal ECG waveforms to produce an early warning system for ECG anomalies. In a similar way, Lilly [170] has reported a table with different templates created during the recovery period after the heart attack. As shown in Figure 7.1, their templates were showing completely different morphological properties during different time periods after the heart attack, which could be used as a reference to monitor the recovery process.

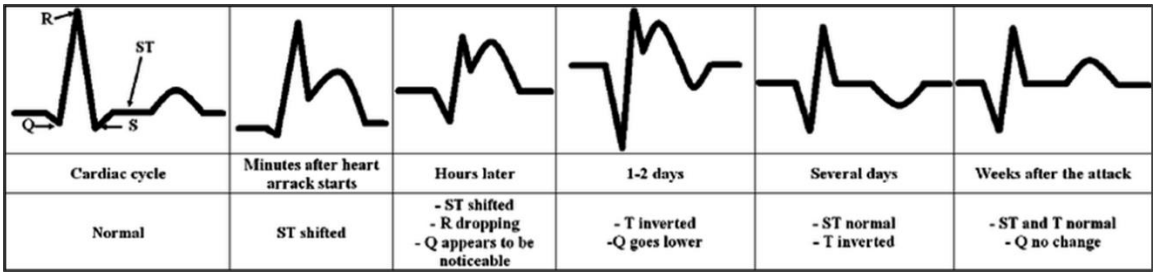

Cardiac cycle	Minutes after heart arrack starts	Hours later	1-2 days	Several days	Weeks after the attack
Normal	ST shifted	- ST shifted - R dropping - Q appears to be noticeable	- T inverted -Q goes lower	- ST normal - T inverted	- ST and T normal - Q no change

Figure 7.1. ECG waveform evolution shows pathological disturbances after heart attack in ST, T, and Q parts (basing on the knowledge acquired from [170],[169]). Any pathological change in any stage can automatically be described as an abnormal disturbance.

Similarly, the templates from the acceleration photoplethysmogram (i.e., the second derivative of the PPG, also known as APG) has previously been shown to correlate with the disorders such as atherosclerotic and arterial stiffness [171] (Figure 7.2).

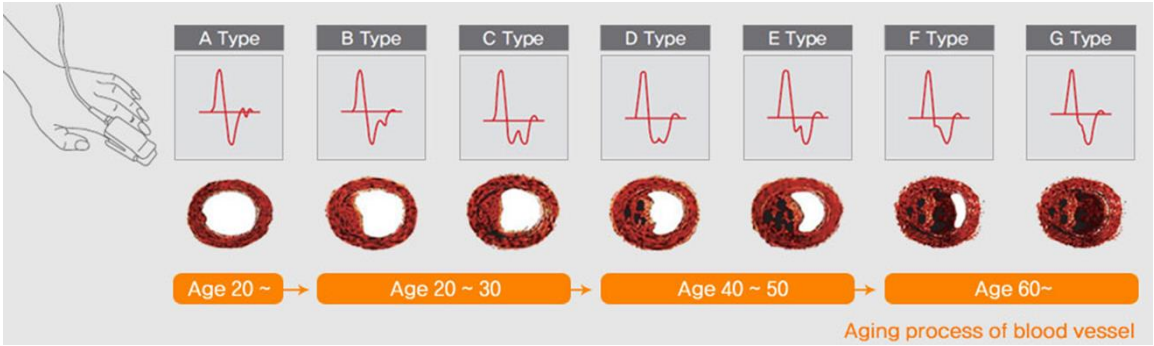

Figure 7.2. The morphological variation in APG templates during the process of aging is correlated to the stiffness of the blood vessels [171].

The morphological features of the APG templates were used by Elgendi [172] to create a cardiac age index, as shown in Figure 7.3. In this figure, sample APG waveforms are provided for different conditions. The waveform on the left (A) is related to the good circulation, whereas the amplitude of trough b is lower than that of peak c. The APG waveform on the right (G) is related to the bad circulation, where the amplitude of peak c is lower than that of trough b.

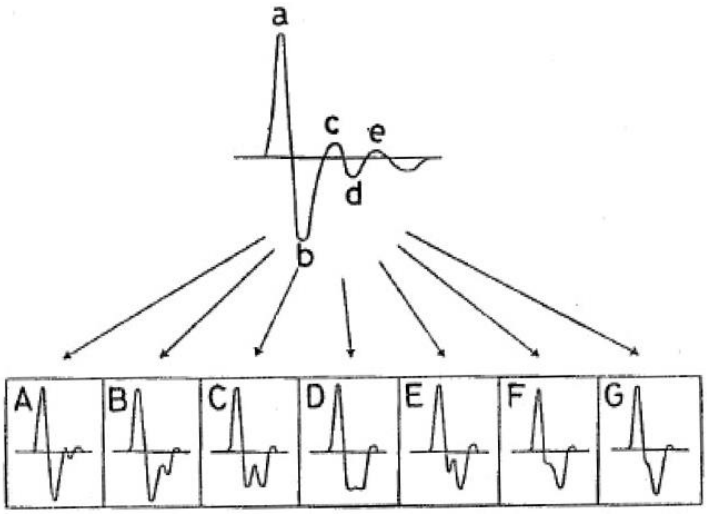

Figure 7.3. Variations in the morphology of APG signal as age increases, from left to right [172].

I have been searching for new methods for the early prediction of age-related disorders. Now that my proposed methods have the ability to reduce the noise from the signals, and also detect the individual heartbeat cycles of the BCG signal in different configurations, I can analyze and monitor the BCG templates for different reasons. In this chapter, I will first provide a detailed approach to create the templates from the BCG signals. Then, the possible effect of the mattress on the BCG morphology will be studied, on multiple mattresses and subjects of different age. Also, I will consider the well-known respiratory sinus arrhythmia, which correlates the heart rate to the point it appears in the respiratory cycles. This supports the future investigation of other respiratory-related variations in the BCG waveform.

7.2. Method

7.2.1. Preprocessing and Templates

Due to the natural variability of our heart rate, it is desirable to average the signals of multiple heartbeats in order to obtain a template that adequately represents the physiological signals of a given individual. Then, the template can be used for feature extraction or comparison. To this end, we will utilize the local R-peaks of the ECG signal as the reference for (i) heartbeat activities, and (ii) segmentation of the other signals, including BCG waveforms. Abnormal beats will be discarded if their amplitude is out of range or if their length is greater or less than acceptable thresholds for the regular heartbeat (e.g., 1.5 seconds (90 bpm) or less than 1 second (60 bpm)).

Two alternative segmentation strategies have been proposed in the literature to account for the variable length of segments due to the instantaneous variation of the heart rate. The first approach utilizes the entire cardiac cycle and reshapes (stretches or shrinks) all segments to the same length (calculated as the average heartbeat length during the time of data collection). This approach helps in later sample-by-sample averaging and all other matrix-based computations (such as dynamic time warping (DTW)). On the other hand, though, this averaging approach does not

retain the exact time-related morphological information of the waveforms. The second approach cuts (or zero-pads) all the segments at certain (method-dependent) distances before and after the reference point (usually the R-peak of the ECG). For example, Ashouri and Inan [173] used the minimum RR interval as a simple way to make all their signals of equal length, starting from the R-peak of ECG. While saving the timing information of the main waveform peaks, this method is vulnerable to potential miss-alignments of the smaller peaks that might cause unwanted variations in the computation of the final template. In this chapter, I compare both approaches and investigate potential differences in the templates that could be relevant for physiological BCG interpretation.

Other important issues in data processing are filtering and alignment. Due to the dynamic properties of vital signs, the fixed cut-off band-pass filters cannot completely separate and remove baseline variations associated with respiration. As a consequence, the baseline of each waveform might differ slightly from the others. I have proceeded by subtracting the mean of each waveform in order to make them zero-mean. Then I aligned all waveforms to the median one, based on their cross-correlation value. In order to eliminate motion artifacts, I have removed waveforms with the correlation below 0.4 and lag-time above 0.4 seconds. An additional step for outlier removal may be based on counting the number of peaks in each waveform and removing outliers, which may reduce the chance of having very low or very high-frequency variations, without necessarily knowing a priori the actual number of peaks.

7.2.2. Segmentation

The typical approach in creating morphological templates goes through the use of a secondary event as the reference for cardiac activity, like ECG R-peaks. I have also tried to always include multiple reference signals in our data collections, including ECG, PPG, and pulse sensor. This is critical not only because our current algorithms sometimes fail in accurately estimating the location of BCG J-peaks, but also because the ECG signal can provide a variety of extra information

about the cardiac activity of the subject. Moreover, the variations in the time intervals between electrical activities of the hearts (such as R-peak) to its mechanical activities (such as BCG J-Peak) known to be related to some hemodynamics variations.

In the first step, I have used an implementation of the famous Pan-Tompkins algorithm [112] to detect the ECG R-peaks. Figure 7.4 demonstrates how the Pan-Tompkins algorithm first transforms the input ECG signal (top row), to the clearer and more filtered version (bottom row) for the detection of ECG R-peaks. But the current implementation of the Pan-Tompkins algorithm is very slow and almost useless for sequences of as long as 6-7 hours related to the sleep lab data. So I decided to use another approach for ECG R-peak detection.

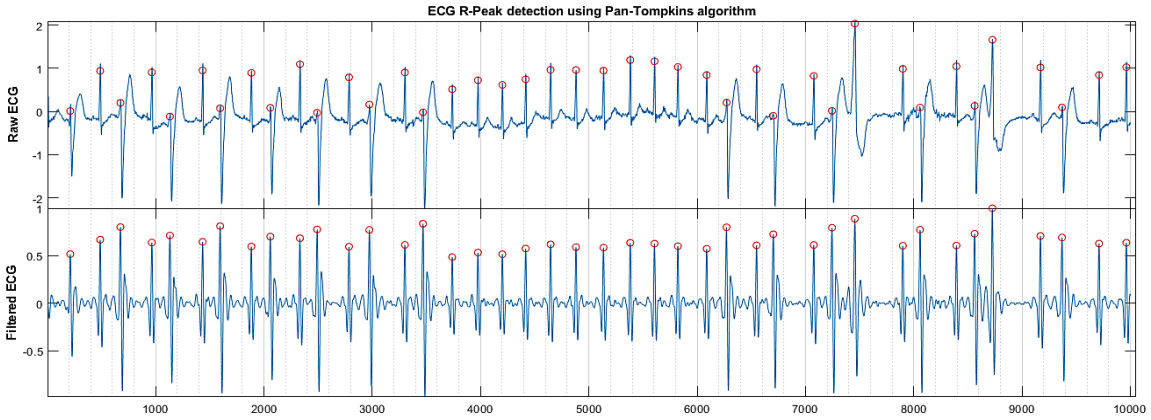

Figure 7.4. Running the Pan-Tompkins algorithm on a random and noisy ECG signal represents its great ability in detecting ECG R-peaks, with very high accuracy.

In order to reliably find the R-peaks, ECG signals were processed using the AD Instrument's LabChart, and filtered signals and the R-peak locations were exported to Matlab for further analysis. This was the most convenient and reliable approach, as we have used the same system (hardware and software) in our data collections in the lab. However, additional work was required to import the PSG signals from the sleep lab, as they were in EDF format. In order to import the PSG data from their original EDF format into Matlab, I first converted EDF files to CSV files, and then imported those CSV files to LabChart for peak detection.

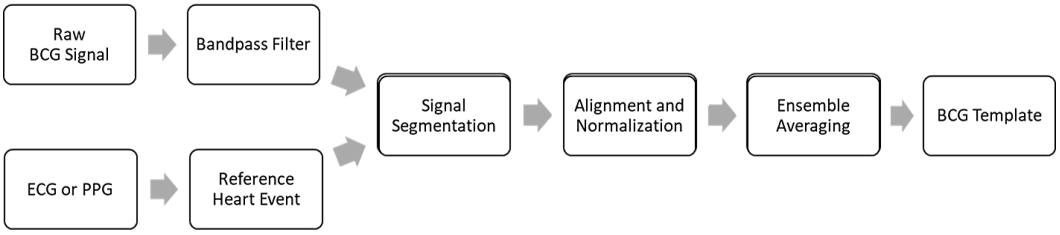

Figure 7.5. Ensemble averaging technique is used to create morphological templates. The figure shows a schematic overview of different steps required in creating a BCG template.

7.2.3. Ensemble average

Two general approaches have been taken in the literature to analyze BCG signals, including the linear and non-linear averaging techniques [53]. In the presence of a significant stimulus, the waveforms are averaged after being aligned with respect to a reference point, which is called the **synchronous averaging**. In the case of having an *a priori* reference waveform (i.e., the template), the **template-based** approach filters out non-similar waveforms from the signal, and averages the remaining similar ones. Finally, **non-linear averaging** techniques, such as the dynamic time warping (DTW) have been used to deal better with the quasi-periodic nature of biological signals, with morphological variation both in amplitude and in timing [53].

Usually, some bandpass filtering should be applied to the signals, before segmentation. I mostly used a bandpass Butterworth filter with frequency ranges between 0.7Hz to 10Hz. After finding the ECG R-peaks and segmentation, outlier sequences are detected and discarded based on amplitude, number of peaks, or their length. Then different averaging methods such as mean, median, medoid, and dynamic time warping were applied to the segments to create templates. Most of the times, a simple alignment procedure makes much more clear templates. Some normalizations on the length or amplitude of the waveforms might also be applied based on the experiment. Figure 7.6 shows an example of signals I collected from a young, healthy subject along with their average templates, and Figure 7.7 provides a visual comparison between the templates created from the ECG, SCG, Pulse and bed sensor signals and the ones reported in the literature in [66].

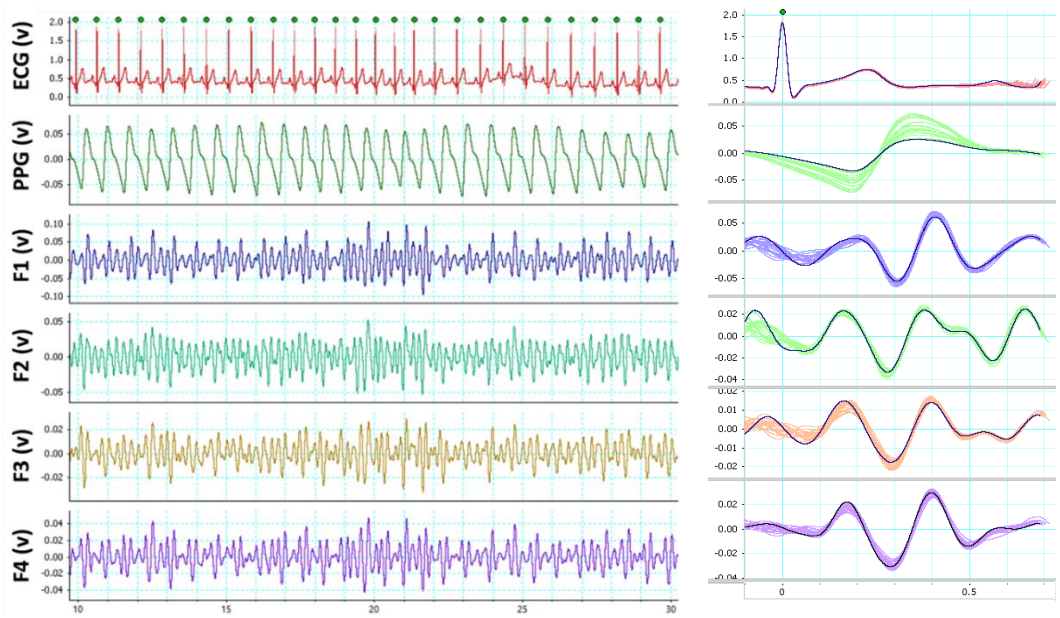

Figure 7.6. Example of the morphological templates creates from different channels. Left: Traces of ECG, PPG, and four BCG signals from a young, healthy subject. The ECG R-peaks are shown by green circles. Right: superimposed "beats" of each channel and their "average" waveform.

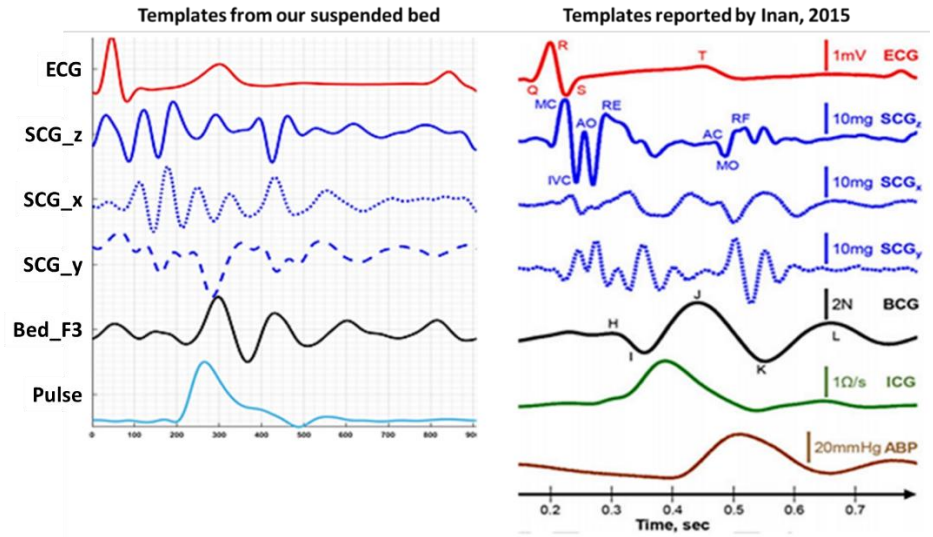

Figure 7.7. Comparing templates from our suspended bed to the ones in literature. Left, shows the templates that I created using the above-mentioned method, on ECG, SCG, BCG, and Pulse sensor. On right are the templates reported by [66]. Considering the difference in the sensing modality, and also the subject in these two experiments, the results are remarkably similar.

After creating these templates, I can track their variations over time, or between different groups to find more insights about the possible health conditions of the subjects in the study. Some of these variations are affected by respiratory activity. Section 7.3.2 will discuss the respiratory variations induced in the ballistocardiograms. The following section, on the other hand, focuses on the variation of BCG waveforms, as a result of a change in the blood pressure.

7.3. Experiments and results

7.3.1. Morphological variations caused by different mattresses

I. Introduction

Our hydraulic bed sensor, as described earlier, is designed to be placed underneath the mattress in the longitudinal direction aligned with the regular body placement. The mattress also works as a separate system to transfer the original ballistocardiographic movements of the body's center of mass, to the hydraulic transducers. An advantage of the mattress is that it transfers the signals to the transducers, even if the person is not directly above the sensor. It also provides some flexibility in the placement and direction of sensors, regardless of the exact placement of the person on the mattress.

Previous studies in our group [76] showed how the displacement of the transducers with respect to the body can change the BCG signal and, consequently, the quality of the heartbeat detections. However, the potential effect of different mattresses on the morphology of BCG waveforms is still under investigation. This section describes our experiments with different mattresses, to see if different mattresses cause significant variations in the acquired waveforms. This is important for longitudinal evaluations where subjects might decide to change their mattress or go to different sites for BCG measurements. Moreover, characterizing the effect of the mattress on the BCG waveform plays an important role in extending our current closed loop mathematical

modeling of the cardiovascular system [5]. Appropriate system identification is essential in the process of BCG standardization.

II. Experiments

Two male volunteers of almost the same height and weight and about 30 years difference in age were asked to lie still on different mattresses, while the bed sensor is placed under the mattress and the reference sensors (ECG, PPG) were connected to their bodies. The first subject ran each of the experiments two times, for the sake of consistent evaluation. Three completely different mattresses were chosen, including a twin and two queen size mattresses of about 7.5, 12 and 18 inches thickness, respectively. The second mattress was an air mattress in which different pressure settings (100%, 85%, 70%) were included in the measurements. During each trial, the subjects were asked to lie on the mattress in the supine position with the hydraulic transducers being placed under the mattress at the same location. The transducers and subjects' bodies were carefully aligned to reduce unwanted variations. Each trial took about 10 minutes long, and synchronous data were collected from the four transducers under the mattress and the reference sensors placed on the body, including a 3-lead ECG, PPG, Pulse pressure and the respiratory band.

Each signal was segmented using the ECG R-peaks as the reference, and segments were normalized in width and amplitude and aligned together using the cross-correlation. Putting the normalized and aligned segments in a matrix provides a 3D representation of the waveform amplitudes, and how stable it was over time. The normalized and aligned BCG cycles acquired from three trials of two subjects on three different mattresses are presented in Figure 7.8. For better visualization, two consecutive beats were segmented together to make the J-peaks recognizable. As expected, during each trial, the general morphology and timing of the normalized BCG peaks stayed stable. However, variations between subjects on the same mattress, or the same subject on different mattresses are of consideration in this section.

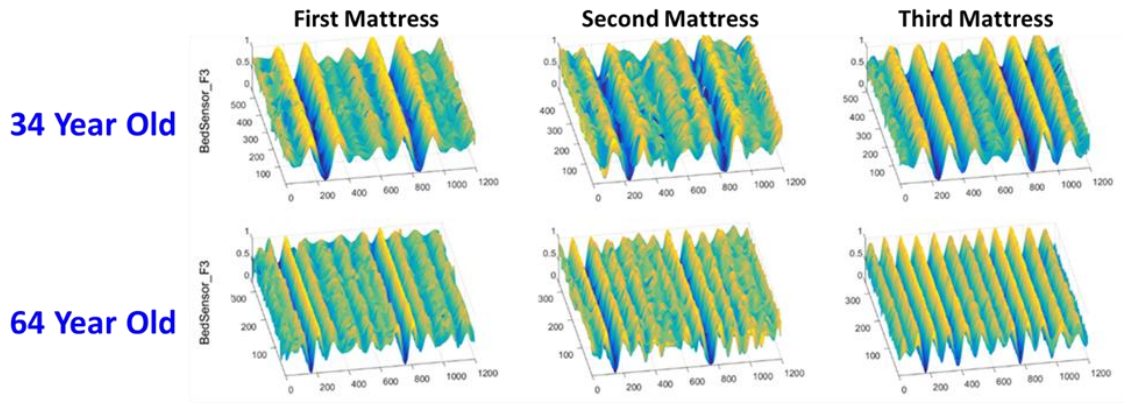

Figure 7.8. Normalized and aligned BCG cycles of two subjects on three mattresses. For better visualization, two consecutive beats were segmented together to make the J-peaks recognizable. As expected, during each trial, the general morphology and timing of the normalized BCG peaks remained stable. Variations between subjects on the same mattress, or the same subject on different mattresses are observed. The second column shows the results from the sleep number air mattress with the pressure set to 85% for both subjects.

III. Evaluation and conclusion

Comparing the two rows of Figure 7.8, personal differences of the BCG morphology are represented. The first subject, 30 years younger, has a relatively stronger J-peak and a smaller number of peaks, while the second subject has smaller peaks in the diastole. Multiple trials of the same subject with the similar settings show matching waveforms in general. Some small differences might appear between different trials, which are due to the subject's movements and physical activities between the two trial, which sets the heart rate variability outside the normal resting situation.

On the other hand, as it was expected, our observations confirm variations in the morphology of the BCG waveforms caused by changing the mattress. Going from left to right in each row of Figure 7.8, the effect of different mattresses is showed on a specific subject. To make the comparison a little easier, I have created the BCG templates for the first trial on the three mattresses,

as shown in Figure 7.9. The variations in the normalized BCG templates of the younger subject on three mattresses shows the thicker mattress (3rd mattress) has a kind of dampening effect on the BCG J-peak and caused more equally leveled peaks in one cycle, which, therefore, can cause difficulties in the beat detection. This is while the air mattress (2nd mattress), highlighted the J-peak and its significance with respect to the rest of the peaks, in a normalized template.

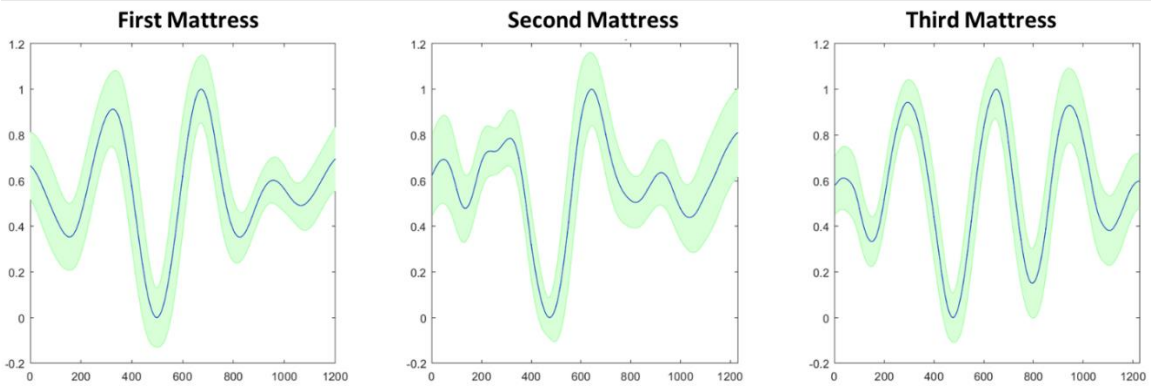

Figure 7.9. Variations in the BCG templates show the dampening effect of mattress. Comparing the normalized templates created from a young, healthy subject on each of the three mattresses shows the thicker mattress (3rd mattress) has more dampening effect on the BCG J-peak and causes more equally leveled peaks in one cycle, which may cause difficulties in the beat detection.

The final conclusion from these experiments, along with our on-site investigations is the apparent effect of the mattress on the amplitude of the waves in each BCG cycle. The air mattress is not capable to truly measure the smaller peaks such as the L, M, and N. At the same time, it makes the J-peak more distinguishable for the heartbeat algorithms such as the energy algorithm. The thicker mattresses dampened all the waves in a single cycle to a very similar level, a very similar case as for the subjects with stiffer arteries.

7.3.2. Morphological variations of the BCG during the respiratory cycles

Previous studies showed interactions between system hemodynamics and respiration [174]. Authors of [175] reported a 2% increase in heart rate during inspiration as well as other effects of phasic respiration such as 17% inspiratory decrease of left ventricular systolic volume (LVSV).

A study on PPG signals also showed a reduction in the peak amplitude during inspiration [176]. Significant changes in the morphology of the BCG signal were noted by Starr [111], which repeated in corresponding respiratory cycles. In this paper, we study several morphological features of the BCG waveform, to investigate their possible variations with respect to the respiration cycles, for better characterization of the BCG waveform, and non-invasive health monitoring and tracking.

The focus of this section is to provide a complete literature review on the source, possible effects, and potential predictive properties of the cardiorespiratory interactions. Based on this review, a couple of experiments will be done on our available data sets to detect an abnormal change of cardiac activity.

I. Background

Many time-varying physiological signals are the net results of two or more body functions while usually, obtaining "clean" signals of just one physiologic function at a time is desirable [177]. This requires the filtering and removal of unwanted components. Unfortunately, it is impossible to completely separate the noise from these signals by means of passive filtering, mostly as the frequency spectrums of the desired and undesired signals overlap. However, a suitable combination of the mixed-signal with another physiologic signal, that is correlated either to the wanted signal or to the unwanted signal can be used by "active" filtering, to do the separation [177].

Previous studies have shown interactions between system hemodynamics and respiration [174]. Some effects consist of periodic fluctuations in systolic blood pressure caused by respiration [178], reduced the diastolic filling time associated with a higher heart rate [179], and a decrease of left ventricular volume during inspiration [175]. A study on PPG signals also showed a reduction in the peak amplitude during inspiration [176]. Asking the subject to hold their breath provides a condition for recording a pure circulatory signal. However, this produces unphysiological

circulatory conditions as the lungs filling, and the intrathoracic pressure is getting fixed with altered venous return and pulmonary vascular resistances. What is desired is a displacement ballistocardiogram when all systems are functioning normally [177].

Ballistocardiograms are also subject to variations during each respiratory cycle. The respiratory and the circulatory forces are the two main components that cause the displacement of an ultra-low frequency BCG device. The circulatory component with the higher frequency is only about 20 percent of the amplitude of the respiratory component [177]. Dock [180] reported how the IJ wave is being affected by the respiration. As the subject inhales, the ballistic impact increases in size, to diminish again as he exhales; if the breath is held, this rhythmic variation disappears [111]. They also showed that if the glottis is kept open when the breath is held after a deep inspiration, the ballistic impact continues as normal; when held after a deep expiration, the impact remains small until respiration is resumed. It is shown that BCG signals contain more abnormal complexes at expiration while approaching normal patterns at full inspiration [23].

Respiratory-induced fluctuations in BCG are highly dynamic and not trivial to characterize. Due to the quasi-periodic nature of these signals and the overlapping frequencies of these two components, even advanced filtering methods [2, 14, 177] cannot provide the perfect separation. Figure 7.10 provides a trace of BCG records with its obvious variations during the respiratory cycle, even after filtering, both from our signals and also the one reported by Inan, et al. [2].

In the beginning, Starr and Wood [16] simply used the sum amplitudes of typical large and small complexes of the respiratory cycle ($I_{min} + J_{min} + I_{max} + J_{max}$), to define the amplitude of the records. Later, Bixby and Henderson [41] found it difficult to calibrate the ballistocardiography device in the presence of arching respiration, which in some cases made considerable changes in the magnitude. This is because, during breathing, the baseline is never straight unless the breath is held [41]. Asking the subjects to hold their breath during a recording,

causes the loss of the valuable information to be gained from the respiratory variations of the ballistocardiogram [34].

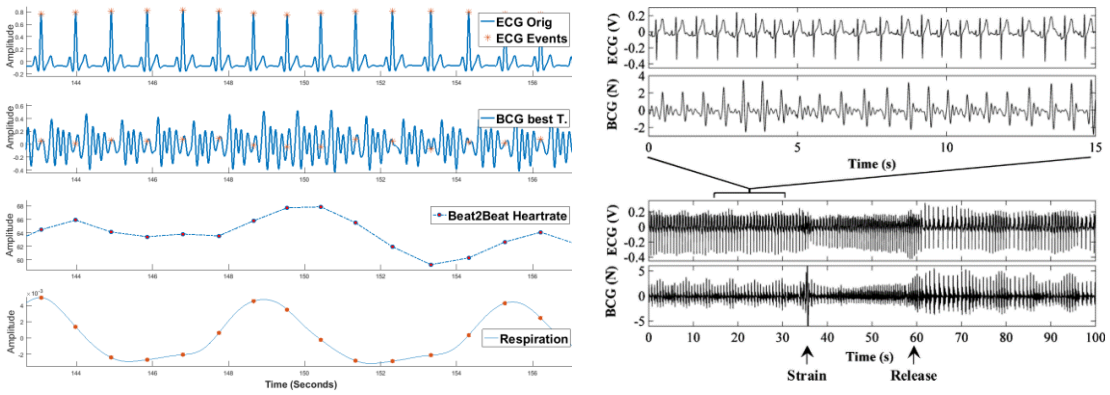

Figure 7.10. Respiratory related variation of the heart rate.(RSA) Left: Respiratory sinuous arrhythmia or the respiratory-related variations in the heart rate. This figure shows the ECG, BCG and the variation of Heartrate due to the respiration, from our hydraulic bed sensor. Right: ECG and BCG traces from a subject at rest (top) and during the Valsalva maneuver (bottom).

The respiratory variation of the heartbeat shape cannot be described with a simple model [181]. Tavakolian, et al. [182] found that the respiratory variation of the seismocardiogram is so significant that heartbeats corresponding to inspiration and expiration have to be treated separately when heartbeat shape averaging is performed for diagnostic purposes. Starr, et al. [39] first averaged the amplitude of all BCG waveforms and then compared it with the average amplitude of the highest and lowest complexes, in 50 ballistocardiography records. The latter estimation proved to be 4.2% different from the former, which should not be simply neglected.

In the current dissertation, instead of trying to filter out the respiratory variations of the ballistocardiograms, the goal is to investigate and extract useful information from the possible interrelation of BCG features with respect to the respiration cycles, for non-invasive health monitoring. One example of a similar utilization of respiratory information is the work of Tavakolian, et al. [182], wherein rather than removing the respiratory effect; it was utilized to enhance the diagnosis of cardiac malfunctions by ballistocardiogram.

II. Introduction

By definition, ballistocardiograms, are the sum of the force vectors in the head-toe direction of the body, exerted due to the blood flow in the cardiovascular system. In [111], Starr explored the relationship between the displacement of the heart's axis to the variation of BCG amplitudes during the respiration. He mentioned that the heart's axis is subject to a counter-clockwise rotation, as the cardiac apex moves to the left during the expiration and after the rise of the diaphragm. Any reasonable thought would conclude that this distraction of the heart's axis from the measurement direction is the cause of respiratory diminishes found in the recorded ballistic force. Instead, Starr found that a large portion of BCG comes from the movement of blood in the aorta, an organ whose position remains fixed during respiration, and concluded the change in the heart's direction should not be a primary factor.

Further studies by Starr's [111] supports a familiar physiological conception as follows; on inspiration, the filling, and so the output of the right heart, increases immediately, but the left heart's output does not increase until an interval of several seconds has elapsed. On expiration, the right heart output diminishes immediately, to be followed after an interval by a similar diminution of the left heart's output. It is also reported that the change in the right heart's output during the respiratory cycle is larger than that of the left. This phenomenon is known as the Starling's law of the heart, which states the weakening heart contracts best at that point in the respiratory cycle in which it is best filled [23]. Similarly, it is very common to see BCG signals where only the largest complex that appear during the respiratory cycle remains normal. Indeed, for patients in declining health, the percentage of abnormal BCG waveforms can be appropriately regarded as a guide to the severity of the myocardial impairment.

The respiratory variation in BCG has been proposed as a measure of abnormality universally present in patients with angina pectoris [31]. Respiratory weaving of the baseline is a prominent feature of all BCG signals made during normal breathing [41]. While this makes the baseline harder

to identify, it has certain advantages; the amplitude of the systolic complexes varies with their position in the respiratory cycle, as is well known. Any variation from the usual pattern can be detected in most ballistic signals by taking a simultaneous record of respiration.

There is a growing interest in studying the interaction between cardiovascular and cardiorespiratory systems [183]. Starr and Friedland [111] reported the sinus arrhythmia in young adults always happen in the expiration period. The arrhythmias coincident with a reduction in the ballistic impacts are due to changes in the cardiac filling. They are very similar to the heart's behavior before contracting.

The quasi-periodic BCG signal is characterized by considerable inter-beat variability in its morphology (both in duration and in amplitude), mainly related to the respiratory activity and mediated by the autonomic nervous system, thus affecting both preload and afterload by changes in intrathoracic pressure [53]. Studies have investigated the effect of respiratory sinus arrhythmia (RSA) on the cardiopulmonary coupling of the heart, blood pressure, and the coronary artery disease [177]. Zhang, et al. [183] studied the effect of regular and slow breathing on the blood pressure and cardiopulmonary coupling, by using the Stepwise-paced breathing (SPB) procedure (spontaneous breathing followed by paced breathing at 14, 12.5, 11, 9.5, 8 and 7 breaths per minute, 3 min each). They reported a significant reduction in blood pressure by the SPB procedure, SBP: From 122 to 114.2 mmHg, DBP: From 82.2 to 77.0 mmHg, and PTT: from 172.8 to 176.8 ms.

Despite common sense, the respiratory-related variation of BCG waveform is not only limited to the amplitude of its waves. about two-thirds of the respiratory cycle is related to the expiratory phase, as reported by Brown Jr, et al. [36] (Figure 7.11). In fact, multiple groups have studied the time variation of cardiac activities during the respiration. Van Leeuwen and Kuemmell [184] studied 25 subjects and reported 8 milliseconds modulation in the cardiac time intervals, due to the respiration. They have reported pre-ejection periods were longer in the transition from

inspiration to expiration, and shortest at mid-expiration. In contrast, the values for ejection time were lowest at the end of inspiration and highest around min-expiration.

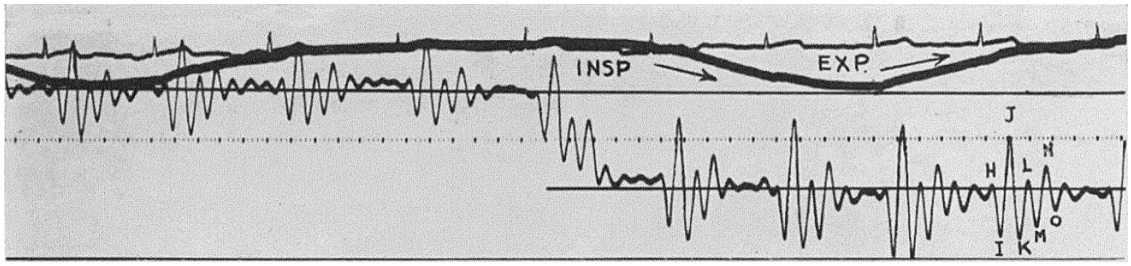

Figure 7.11. Expiratory phase covers about two-thirds of the respiratory cycle. (picture from [36])

III. Experiments

A group of 58 healthy volunteers (ages 18-50) were asked to lay in the supine posture on a bed. Ten minutes of continuous BCG signals were collected using four hydraulic sensors located under the mattress. The respiratory waveform was collected from the chest band. The ECG R-peaks were used for reference to segment heartbeats in the BCG signal. The best transducer was selected based on the highest DC-bias, to extract the BCG beats (Figure 7.12- Top). The BCG J-peaks were then mapped onto the respiratory signal to be assigned a label based on the respiratory phase. J-peaks with at least a 90% amplitude of the closet respiratory peak were labeled as Inhale Peaks (IP), and J-peaks with less than 10% of the amplitude of the closest respiratory valley were labeled as Exhale Peaks (EP). We used a moving range function (*movMax to movMin*) to estimate the upper and lower thresholds at each time. The rest of the heartbeats were labeled as Inhale Active (IA) or Exhale Active (EA) and were excluded from this study (Figure 7.12).

Common morphological features (amplitude and time location of BCG I, J and K peaks, and their differences, Amp_IJ and Amp_JK) were extracted from the BCG beats (Figure 7.12- Bottom). Then to evaluate the variation of the features between the two respiratory phases, I computed the average difference of each feature during IP and EP, from their global average. The average percentage of variation was computed for each feature, over all subjects. Thus, a positive value

over IP shows the percentage of increase in that feature during IP, compared to its average value over all four respiratory phases.

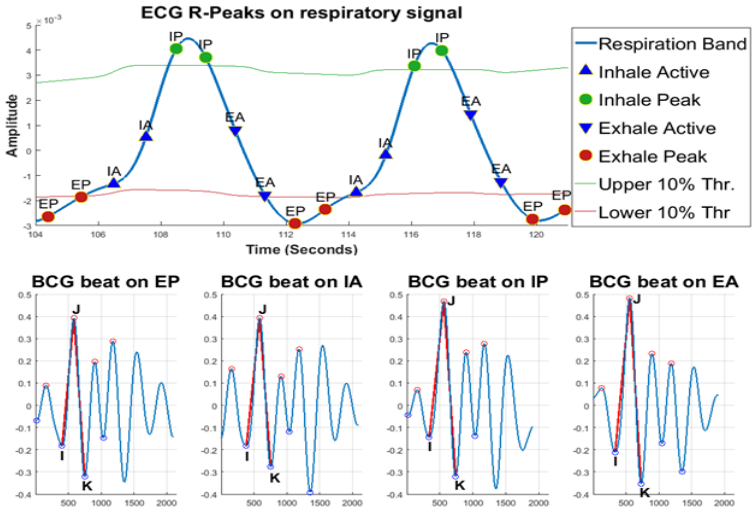

Figure 7.12. Heartbeats labeled with respect to the four respiratory phases. Upper and lower thresholds were computed using the moving range.

IV. Results

Figure 7.13 shows that despite the little variations in the time delay between I-J waves or J-K, during respiration, a higher variation happens in their ratio. While time delays of IJ and JK increase over IP respectively by 0.4% and 0.6%, their ratio decreases by 21.8% on IP. Also, while the amplitude of IJ wave decreases by 3.7%, and the amplitude of JK decreases by 4.7%, the ratio of these two numbers increases by 109.2%.

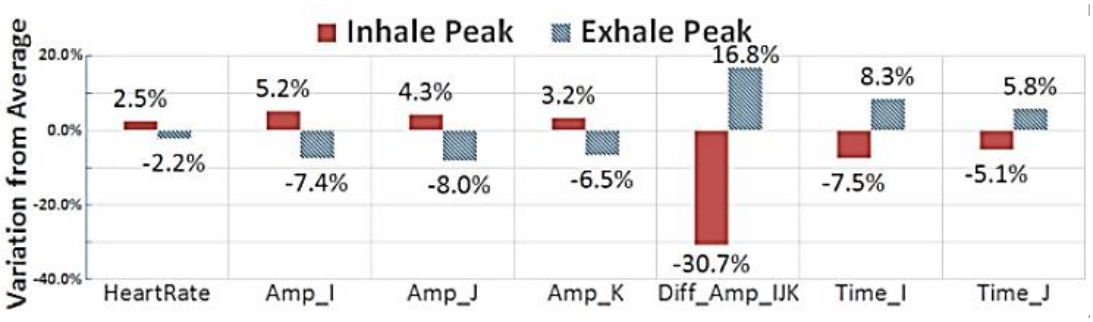

Figure 7.13. Respiratory-related variation of BCG features from their average values, compared between inhalation and exhalation.

V. Conclusion

Our results are in the same range as the ones previously reported in the literature. This represents a potential starting point for future work on “the application of hydraulic bed in prognostic studies”. Expanding one of the ideas provided in the literature review and using both respiratory and BCG information of the hydraulic bed sensor can help in early detection of conditions in the cardiorespiratory system.

7.4. Preliminary Studies for Future Work

In order to better understand our BCG sensors, I have tried multiple experiments. As the foundation for future research, I first tried to verify that our BCG signals from the suspended bed, are in fact, the same as the ones in the literature. In Section 7.4.1, I provide a visual comparison between the ensemble-averaged templates of the accelerometer signals to the ones of the reference. Then in Section 7.4.2, I investigate a transfer function to match the BCG signals from the hydraulic bed sensor to the ones recorded simultaneously by means of the suspended bed.

7.4.1. Characterizing the Suspended Bed

Despite the extensive work of Isaac Starr [185], the field of ballistocardiography still lacks standardization of devices and methods. Each device has slightly different mechanistic properties and therefore acquires a different amount of motion from the body. We also wanted to provide a model for our hydraulic bed sensor so that we could directly use the findings of other sensing modalities. As an effort in this direction, I have collected synchronous recordings of BCG on the suspended bed from the accelerometer (as the reference) and the hydraulic bed sensor. In order to consider the possible effect of motion on the hydraulic transducers, I have tried the same experiment both in the moving and the stationary state of the suspended bed. Then ECG R-peaks were used for segmentation and creation of ensemble averages.

As the first step, I tried to calibrate the signals acquired from the accelerometer to provide a quantitative comparison between our accelerometer-based BCG and the reference waveforms reported by Isaac Starr [87]. There he used "103 DYNES" as the scale for "Acceleration of BCG". Dyne is a unit of force that, acting on a mass of one gram, increases its velocity by one centimeter per second every second along the direction that it acts. ($1\,dyn = 1\,g \cdot cm/s^2 = 10^{-5}\,kg \cdot m/s^2 = 10^{-5}\,N$). For "Velocity of BCG", they used "102 g.cm/s"; for displacement they used g.cm. Even in other reference papers, Noordergraaf has used the same units and scales as presented in the book by [87].

Variations in the acceleration of the MU suspended bed were recorded in voltage using the 3-axis accelerometer (Kionix EVAL-KXR94-2283 [86]). This accelerometer has the sensitivity of 1000mV/g, according to the datasheet. Then to convert from g to the Dyns, I first converted values to Newtons, by multiplying by the weight of the system:

$$Weight = 78kg + 5kg;$$
$$F = m * g;$$
$$Newtons = Weight * (Volts * Sensitivity);$$

Then by definition, we convert Newtons to Dyns:

$$Dyns = Newtons * 10^5;$$

$$Dunes = Volts * (Sensitivity * Weight) * 10^5;$$

We also know that the Acceleration is the first derivative of velocity, and velocity is also defined as the first derivative of displacement:

$$Acceleration = \partial Velocity / \partial Time$$

$$Velocity = \partial Displacement / \partial Time$$

We should be able to go backward from acceleration to the displacement, by means of integrations:

$$Velocity = \int Acceleration\ \partial t$$

$$Displacement\ = \int Velocity\ \partial t$$

I have demonstrated in Figure 7.4, the acceleration ballistocardiogram (A-BCG), computed velocity ballistocardiogram (V-BCG), and the computed displacement ballistocardiogram (D-BCG) waveforms both from the book of Starr and Noordergraaf [87] and from our suspended bed. Obviously, by computing the first derivative of the displacement, we lost the "c" constant, and we cannot retrieve it back just by computing the integral of the velocity. The same thing happens while differentiating the velocity to acquire the displacement. This is the reason that the baseline of our displacement waveform, is not at the level of the baseline for Isaac Starr's. We need at least a single value for calibration.

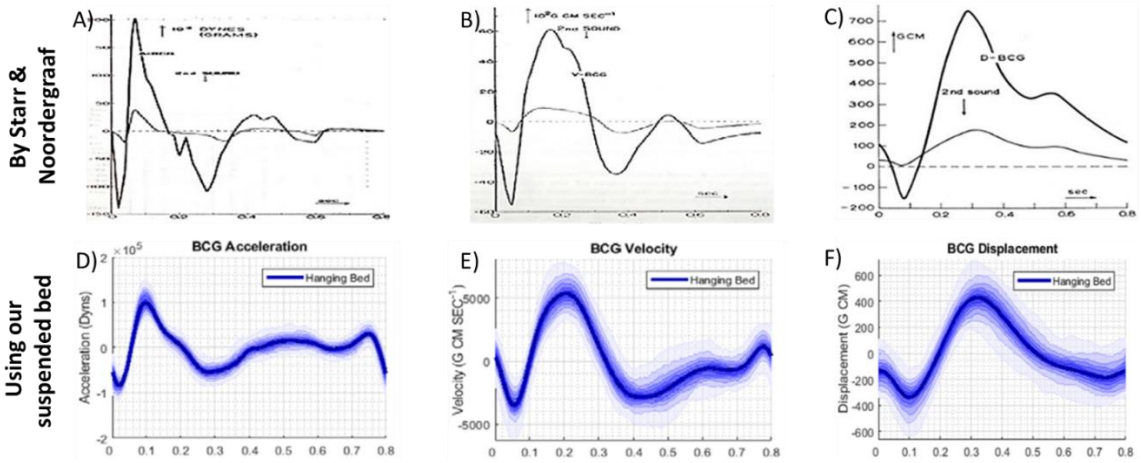

Figure 7.14. Obtaining Displacement-BCG and Velocity-BCG from Acceleration-BCG. The top row shows the waveforms from [87], the bottom row shows the MU suspended bed measurements on the same scale or computed through the integration of the Acceleration-BCG.

7.4.2. Characterizing the Hydraulic Bed Sensor

Some empirical investigations have been done previously by Rosales [76] to find the optimal dimensions, directions, and positions of the hydraulic transducers. However, no work was done to

study the exact physics behind the ballistic measurements, regarding the source of the change (acceleration, velocity, or displacement), and also its direction. Researchers in our team are currently working to mathematically describe how the displacement of transducers, relative to the body, may affect the BCG signal, or more importantly, which transducer most represents the actual status of the source ballistic waves.

To begin a characterization of the hydraulic bed sensor, here, I use the suspended bed as a reference for the measurements acquired from the hydraulic bed sensor. Experiments were run on the suspended bed, which was also equipped with the hydraulic transducers. Subjects were asked to lie on the bed in two conditions: first, while the bed was fixed stationary in place using external holders, and second, in the normal unconstrained suspension of the bed. As expected, the signals acquired from the hydraulic sensors when the bed was free to move, were poor. This probably is due to the fact that the movement of the bed frame and transducers affects the usual way of pressure measurement inside the transducers. Inversely, the accelerometer signals were not as clear when the bed motion was constrained.

Interestingly, as shown in Figure 7.15, the template of the hydraulic sensor (top) when the bed is stationary, looks very similar to the template created from the accelerometer in the Y (head-toe) direction on the moving bed, from the same subject.

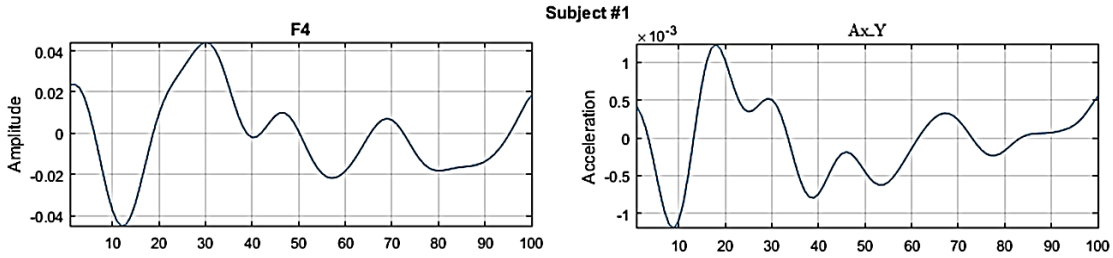

Figure 7.15. A visual comparison of accelerometer vs hydraulic bed template. The template of the hydraulic sensor (top) when the bed is stationary, looks very similar to the template created from the accelerometer in the Y (head-toe) direction on the moving bed, from the same subject.

Further investigations, as presented in Figure 7.16, shows the 1st derivative of the pressure sensor (second row) closely matches the acceleration of suspended bed (third row), on three different subjects. Also, the original templates from the hydraulic pressure sensor (first row) have a very similar shape as of the velocity of the suspended bed (fourth row).

Further data collections and investigations are required in order to find a mathematical relationship between the waveforms of these two modalities. Currently, we are working on a parallel research to use our previous mathematical model of the suspended bed [5] and extend it to the case of the hydraulic bed sensor. We should consider the fact that the suspended bed is a ULF device while the hydraulic bed sensor has some of the characteristics of the HF devices; therefore, the comparison should be carefully made between the waveforms of the same type.

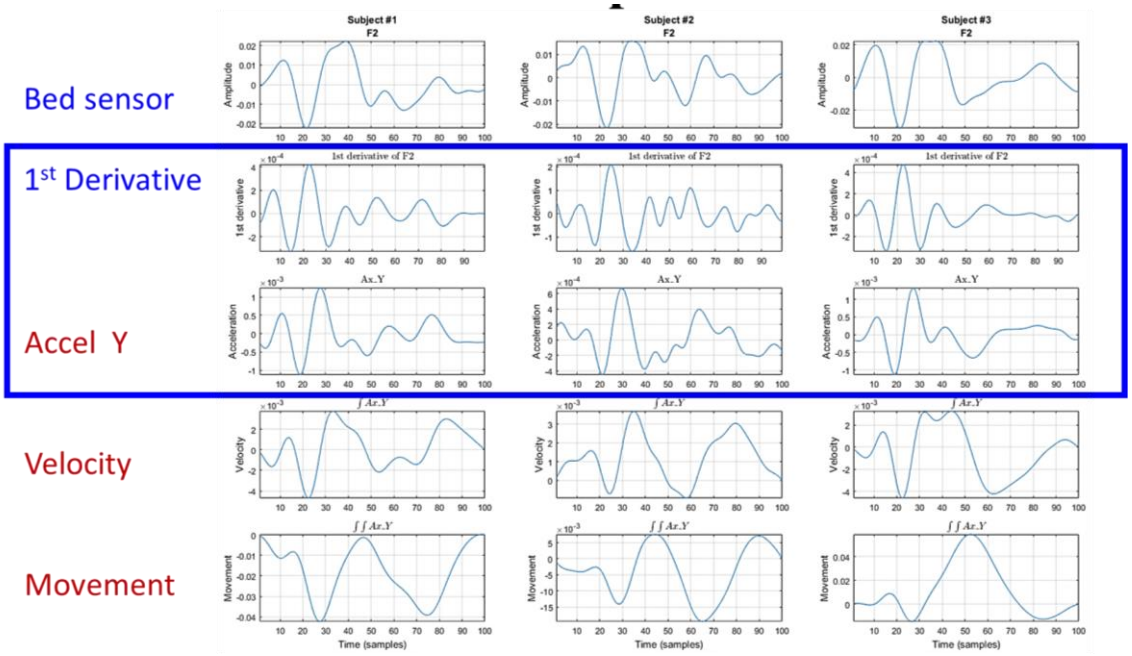

Figure 7.16. Similarity between the bed sensor and the Velocity-BCG. This figure compares the BCG waveform and its first derivative to the accelerometer signal and two of its integrals, over three subjects. The first row is the bed sensor; the second row is its first derivative, the third row is the accelerometer, the fourth row is the velocity (first integral of the accelerometer signal), and the last row is the displacement or movement (second integral of the accelerometer signal). Note the similarity of the second and the third rows; also, the first and the fourth rows as very similar.

8. CUFFLESS BLOOD PRESSURE MONITORING

8.1.Background

According to the American Heart Society [186], some of the most dangerous health concerns in the United States are related to cardiovascular diseases. The blood pressure of an individual appears to be a reliable indicator of health issues that could eventually lead to a cardiovascular-related illness [187]. Accurately estimating the blood pressure, either in the absolute or relative form can provide an early sign of cardiovascular conditions and used to prevent cardiovascular-related problems whenever the blood pressure exceeds the normal range, which is a challenging problem.

High blood pressure, termed "hypertension," is a condition that afflicts almost 1 billion people worldwide and is a leading cause of morbidity and mortality. More than 20% of Americans are hypertensive, and one-third of these Americans are not even aware they are hypertensive. Therefore, this disease is sometimes called the "silent killer." This disease is usually asymptomatic until the damaging effects of hypertension (such as stroke, myocardial infarction, renal dysfunction, visual problems, etc.) are observed. Hypertension is a major risk factor for coronary artery disease, myocardial infarction ("heart attacks") and stroke.

Blood pressure (BP) is the pressure exerted by circulating blood upon the walls of the blood vessels. It is expressed in terms of the systolic pressure over diastolic pressure in millimeters of mercury (mm Hg). Conventionally BP can be measured using a sphygmomanometer, which is a device composed of an inflatable rubber cuff wrapped around the arm. A measuring device indicates the cuff's pressure. A bulb inflates the cuff, and a valve releases pressure. As the heart beats, blood forced through the arteries causes a rise in pressure, called systolic pressure, followed by a decrease in pressure as the heart's ventricles prepare for another beat. This low pressure is called diastolic pressure.

By reviewing the history of blood pressure measurement [188, 189], arterial catheterization stands out in its ability to measure blood pressure directly from inside the artery. Invasive techniques and methods that require trained physicians or nurses provide a high precision measurement for critical hospital settings such as ICU. But there are other methods later proposed to reduce the invasiveness and expand the range of use of the device in the absence of physicians or nurses. These devices can be used in ambulatory and even home settings, using the hand-held automated oscillometric devices. These methods can also reduce the effect of white-coat hypertension (WCH), which is the elevation of blood pressure just due to the presence of the health care workers, particularly the physicians [189]. One factor that holds back the broader use of self-monitoring devices in clinical practice has been the lack of prognostic data. Two prospective studies have found that home blood pressure predicts morbid events better than conventional clinic measurements. There is an increasing body of evidence that home blood pressure may also predict target organ damage better than clinic pressure [189].

BP can also be estimated by combining information captured by the BCG and ECG [190] or BCG and Photoplethysmography (PPG) [191]. PPG is a technique that measures the change in skin blood volume using a small light probe that is placed on the surface of the skin. Different sites for measuring PPG include the ear, forehead, ankle, and finger; we will use a finger sensor for the PPG measurement. BCG has been used for unobtrusive estimation of blood pressure by combining information captured by BCG and ECG [190], [192] or BCG and Photoplethysmography (PPG) [191]. By developing algorithms that estimate changes in Blood Pressure, the hydraulic bed sensor can be used as an unobtrusive screening tool for monitoring the health status in senior housing or nursing care settings, allowing early detection of health changes [193]. In this context, Blood Pressure has an essential role for physicians.

8.1.1. Traditional Blood Pressure Measurement Methods

Arterial Catheterization: The most accurate but invasive approach to measure blood pressure is the use of an arterial catheter which is a thin, hollow tube that is placed into an artery (blood vessel) in the wrist, groin, or other location to measure blood pressure more accurately than is possible with a blood pressure cuff. This is often called an “art line” in the intensive care unit (ICU). There are risk factors involved in using the catheter, including the bleeding, pain, and discomfort of using it, possible infections, and blood clots on the tips of the catheters.

Sphygmomanometer: The auscultatory method has been the mainstay of clinical blood pressure measurement for over 100 years since it was first discovered. The Korotkoff’s blood pressure measurement technique is subject to limited accuracy but has continued without any substantial improvement. In this technique, first, by increasing the pressure inside the cuff, the arteries under the cuff are occluded. Then, by gradually decreasing the inflation of the cuff, the systolic peak of pressure can exceed the cuff pressure producing palpable pulsation. As cuff pressure is further diminished, the sounds increase in intensity and then suddenly become muffled at the level of diastolic pressure where the arteries remain open throughout the entire pulse wave [194].

The problems with sphygmomanometer appear especially for elderly patients who are more likely to have white-coat hypertension (WCH), isolated systolic hypertension. Also, in the case of arrhythmias, when the cardiac rhythm is very irregular, the cardiac output and blood pressure vary significantly from beat to beat. There is considerable interobserver and intra-observer error. Estimating blood pressure from Korotkoff sounds is a guess at best; there are no generally accepted guidelines. The blood pressure should be measured several times, and the average value used [189].

The Oscillometric Technique: This method, employed by most clinical-grade automated BP devices, analyzes pulse waves collected from the cuff during constricted blood flow. The oscillations of pressure in a sphygmomanometer cuff are recorded during gradual deflation, the point of maximal oscillation corresponds to the mean intra-arterial pressure. It yields valid

estimates of mean pressure but questionable estimates of systolic and diastolic pressures [195]. The main problem with the technique is that the amplitude of the oscillations depends on several factors other than blood pressure, most importantly, the stiffness of the arteries. Thus, in older people with stiff arteries and wide pulse pressures, the mean arterial pressure may be significantly underestimated.

The finger cuff method: This method is based on the principle of the "unloaded arterial wall", where in the arterial pulsation in a finger is detected by a photoplethysmography device under a pressure cuff. The output of the plethysmograph is used to drive a servo-loop, which rapidly changes the cuff pressure to keep the output constant so that the artery is held in a partially opened state. The oscillations of pressure in the cuff are measured and have been found to resemble the intra-arterial pressure wave in most subjects. This method gives an accurate estimate of the changes of systolic and diastolic pressure, although both may be underestimated (or overestimated in some subjects) when compared with brachial artery pressures; the cuff can be kept inflated for up to 2 hours. This method, in its present form, is not suitable for clinical use because of its cost, inconvenience, and relative inaccuracy for measuring absolute levels of blood pressure. Its most significant value is for research studies assessing short-term changes in blood pressure and its variability [189].

8.1.2. Cuff-less blood pressure estimation

A number of previous studies [191, 192, 196] used several sensor modalities to obtain the bio-signals for blood pressure estimation. The sensor modalities used, broadly speaking, can be categorized as wearable and non-wearable. Techniques based on the electrocardiogram (ECG) and photoplethysmogram (PPG) [197-200] signals require wearable sensors. Wearable techniques can give better results than non-wearable. However, an individual may feel uncomfortable wearing the sensors all the time and may not be able to use them at all. One of the nonwearable approaches uses

a standard weight scale equipped to measure both ballistocardiogram (BCG) and electrocardiogram (ECG)[190] for blood pressure estimation. The ability to thoroughly monitor blood pressure changes in an unobtrusive manner can have huge benefits with enormous health care implications.

In addition to the traditional methods, different approaches to estimate the blood pressure have been developed recently. One is the photoplethysmogram (PPG) that is capable of providing continuous blood pressure estimates [197-200] that are derived using the features extracted from the morphology of PPG. Yet another is the pulse transit time (PTT) [201-207], which is the time delay between the observations of ECG and PPG or two PPG devices from separate parts of the body to determine the relative blood pressure. The relative blood pressure from PTT can be mapped into the actual blood pressure when combined with other parameters. In papers such as [208], a connection between pulse pressure and PPG amplitude is reported. So other than episodic manual BP measurements, we use the PPG features to track the continuous estimation of pulse pressure.

Ballistocardiogram consists of two general categories of systolic and diastolic waves, which provides valuable information based on different mechanical properties of the cardiovascular system. The H, I, J, and K waves appear in systole followed by the diastolic waves of L, M, and N. Pinheiro, et al. [6] provided a complete review on the morphological variations of ballistocardiography (different BCG waves), as a result of cardiovascular complications, such as the decrease in the amplitude of the I and J waves caused by mitral stenosis, after malfunctioning of heart valves.

As reported by Kim, et al. [209], the J wave amplitude is related to the aortic pulse pressure by a scale factor related to the area of descending aortic cross-sectional. As the variation of this area is relatively small, the amplitude of the J wave can be used to estimate relative changes in the aortic pulse pressure. Meanwhile, the down-stroke amplitude of J-K have been shown to be correlated to the peripheral pulse pressure by a scale factor equal to the descending aortic cross-sectional [209]. This provides another predictor for the cardiovascular problems, by monitoring the

ratio of the amplitude of the J-K down-stroke to the amplitude of the J wave. Figure 8.1 contains a schematic presentation of BCG template along with the blood pressure waves and their annotations.

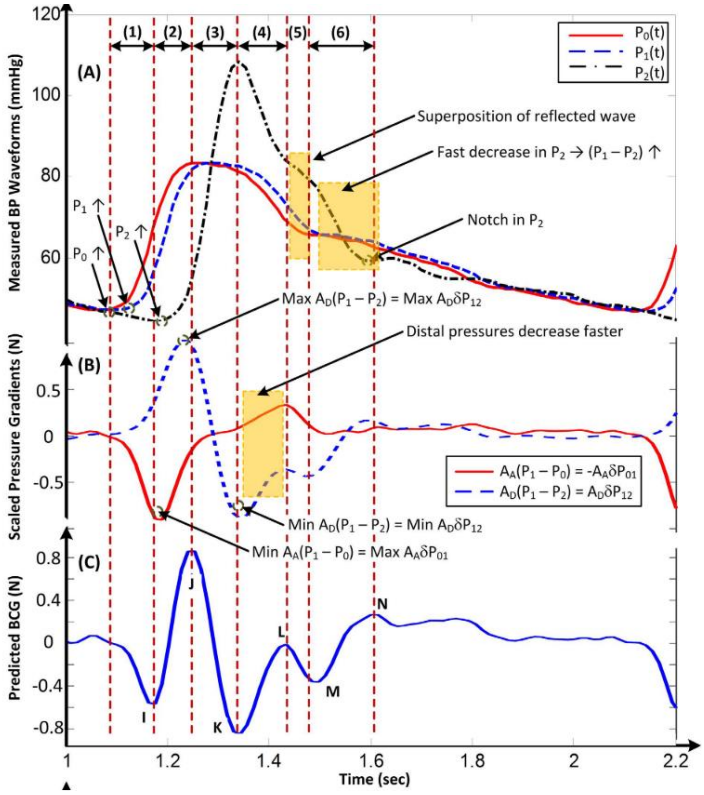

Figure 8.1. An example of a BCG waveform predicted via the mathematical model presented in [209]. (A) BP waveforms at the inlet of the aorta (P0), the apex of the aortic arch (P1) and outlet of the aorta (P2) measured from a human subject. (B) Scaled BP gradients in the ascending (AAδP01) and descending (ADδP12) aorta calculated from the measured BP waveforms and nominal values for the aortic cross-sectional areas. (C) BCG waveform predicted by taking the difference of the scaled BP gradients[209].

We proposed previously two new BCG features acquired non-invasively from the hydraulic bed sensor while the person lies on the bed [13]. Collecting BCG signals while the subject is in the supine position provides an ideal platform for non-invasive estimation of blood pressure. With the subject mostly flat in a similar position on the bed, body part elevations will not contribute to blood pressure change. Thus, blood pressure changes in this position are most likely related to some physiological variations.

Our hydraulic bed sensor system is capable of capturing the BCG signal of an individual lying on the mattress. The signal obtained from the bed sensor contains information about the heartbeat, respiration, and motion [210]. We previously have explored the potential of the bed sensor in monitoring the changes in the blood pressure [13]. Although it does not provide the absolute blood pressure, our studies showed the possibility of tracking the relative changes in the systolic blood pressure. The relative blood pressure differs from the actual by a scale factor and a constant offset only. The scale and offset parameters may be subject and sensor-specific but can be obtained through calibration for generating an actual blood pressure from the relative. The significance of tracking relative blood pressure with a sensor embedded in the bed is its ability in recognizing the blood pressure changes over time. As reported previously by our team [193, 211], tracking the changes in health parameters using in-home sensors provides a practical approach to facilitate the early detection of health status in older adults, which results in better health outcomes.

8.2. Method

Three features were extracted from the BCG signal of each transducer, in periods of time that matches the times of blood pressure measurement using the cuff. Two of these features have been introduced in our previous paper [13], and the other one is a newly proposed feature extracted from the morphology of the BCG signal. Extracted features from all transducers then go through different channel selection schemes and the correlation of the final outcome of each setting is compared against the reference blood pressure measurements.

8.2.1. Data

As lowering the systolic blood pressure is often the target of clinical treatments [212, 213], the focus of this work is on the monitoring of systolic blood pressure. I used a dataset consisting of 48 young, healthy subjects who were asked to do some exercise in order to increase their blood pressure before laying on the bed. These 48 subjects were selected from the entire dataset of 62

subjects, by discarding the records with motion artifacts. The hydraulic bed sensor signals, as well as ECG, PPG, and respiratory signals, were collected immediately after a 2-minute use of the stationary bike. An automatic blood pressure cuff was placed on the left arm of each subject (close to transducer 4); six to eleven blood pressure measurements were documented until the measurements stabilized, after exercise.

8.2.2. Feature extraction

We proposed in [13] two BCG related features for systolic blood pressure monitoring. The first is based on the strength of the BCG pulses in the bed sensor signal. An increasing trend in pulse strength indicates the heart is exerting larger force and hence an increase in blood pressure. The second feature is based on the shape of the BCG signal from cycle to cycle to indicate the variations in the morphology of BCG waveform due to the change of blood pressure.

Ballistocardiogram Pulse Strength (BPS):

The magnitude of the heartbeat signal captured by the hydraulic bed sensor is related to the stroke volume [87], which may provide indications about the blood pressure. First, I removed the low-frequency respiratory-related component, and the high-frequency noise artifacts by means of a passband from 0.7 Hz to 10 Hz. Then the short-term energy profile, E(n), was developed for each channel, by squaring the filtered data samples and applying an averaging filter (the impulse response was set equal to 1 for n = 0, 1,..., 29). The span of the filter is 30 samples, corresponding to an averaging window of 0.3 seconds. In other words,

$$E(n) = \sum_{i=0}^{29} x(n-i)^2$$

An example energy profile is shown in Figure 8.2(b). The feature for relative blood pressure is the local peak heights of the energy profile, and we shall call this local peak feature the Ballistocardiogram Pulse Strength (BPS).

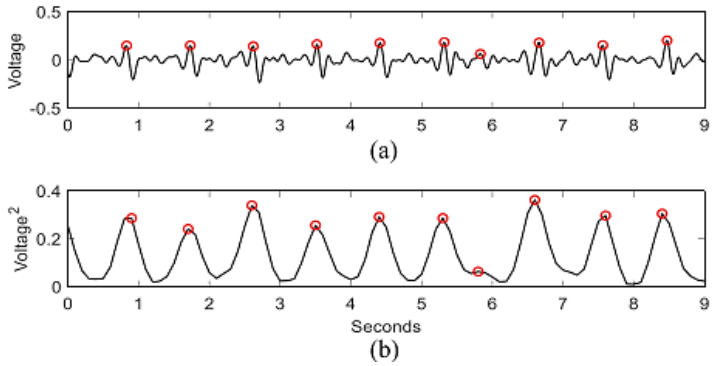

Figure 8.2. Peaks of the energy algorithm are used to estimate blood pressure. (a) Preprocessed data from the hydraulic bed sensor, and (b) its short-term energy profile.

Ballistocardiogram Pulse Deviation (BPD)

The shape of a BCG cycle is characterized by a number of peak properties [39]. Figure 8.3 shows a typical cycle obtained from the hydraulic bed sensor. The maximum amplitude value of the BCG beat in the first 300msec is located as the J-peak. The I-peak is detected as the minimum before the detected J-peak and after the first 70msec portion of the corresponding sample BCG. The K-peak is obtained by detecting the minimum after the J-peak of the sample mean BCG heartbeat in the 200msec interval.

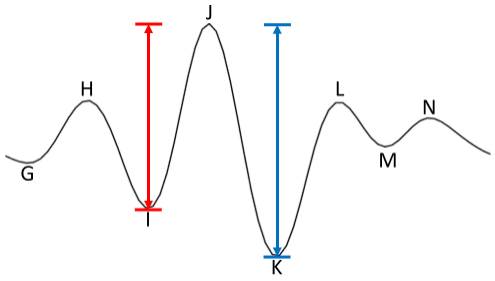

Figure 8.3. Illustration of morphological features extracted from the BCG waveform to estimate the relative blood pressure.

The first morphological feature to be discussed here is the difference in the amplitude of the two sides of the J-peak, as presented in the following formula by BPD:

$$BPD = Amplitude(JK) - Amplitude(IJ)$$

The IJK complex is the main part of the BCG signal. We notice that the difference between the JK-amplitude and IJ-amplitude is large immediately after exercise, and there is almost no difference when the subject returns to rest. BPD is in a sense the difference in the amplitude of the headward movement of the center of mass during the early systole (J-wave), and the footward reflection of it after reaching the aortic arch (the K-wave). This difference was hypothesized to be correlated to the difference between the two corresponding segments of the cardiovascular system.

Ballistocardiogram Pulse Integral (BPI)

The difference between JK-amplitude and IJ-amplitude, and also the IJ-amplitude or JK-amplitude provide direct information for monitoring the blood pressure. In the current work, in addition to the previous features, I am reporting the results of my study in the utilization of a new morphological feature. This feature depicts the total movement of the center of mass in an upward-backward cycle around the J-peak, as presented in the following formula:

$$BPI = Amplitude(JK) + Amplitude(IJ)$$

The BPI feature contains the two largest movements in the BCG waveform and is easy to measure. Small changes in the flow of the blood in each direction, causes a change in this feature.

Extracting features from the templates

In order to reduce the uncertainties that appear in the morphological features of the BCG waveform, mostly due to the respiratory variations, I have created an ensemble average (template) for each channel in a 10-second neighborhood around each measurement, as described in Section 7.2. The 10-second window is usually enough to contain a couple of respiratory cycles, and therefore, a good average of the respiratory effects.

Figure 8.4 shows the typical BCG pattern of five random subjects before and immediately after exercise when the heart rate, respiratory rate, and blood pressure of the subjects start at a high level and decline to normal after a while.

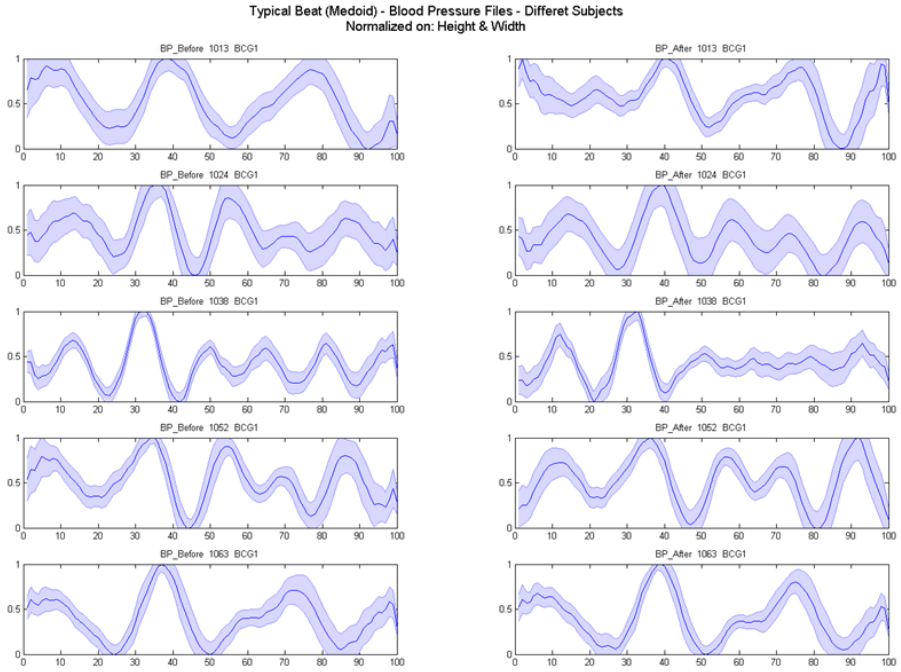

Figure 8.4. Effect of exercise on the typical BCG waveform. (Left) Before exercise, (Right) Immediately after exercise.

8.2.3. Channel selection:

We had used a simple approach for channel selection in [13], which was based on the DC level of the four transducers. The rationale was, as the transducers with higher DC values are usually the ones that are closer to the body's center of mass, they can better capture the cardiovascular information. But, as my experiments in Section 6.5 on signal quality and channel selection show, this is not the case for the estimation of heart rate. There, I showed that channel selection based on the DC level is usually not the best possible channel selection, which I referred to as the oracle approach.

In the current work, I have studied multiple channel selection techniques including the selections based on (i) the maximum DC bias, (ii) maximum SNR, (iii) maximum SQI, (iv) minimum, maximum and median of the measurement among all channels, and finally (vii) oracle

for blood pressure (maximum correlation). Here I provide a brief description of each of these channel selection approaches:

i) **Selection based on the maximum DC bias** is based on the computation of the DC bias (median) of each channel, once for the entire length of the data. Then the channel with the highest DC bias is selected for feature extraction and computing of the correlation to the reference.

ii) **Selection based on the maximum SNR** requires the computation of signal to noise ratio (SNR) for each channel and choosing the channel with the highest SNR. To compute the SNR, I have used the same approach as described in Section 6.5.

iii) **The oracle selection** is an after-fact process of choosing the channel with the highest correlation. Although the oracle approach for channel selection is not applicable to most of the real-world cases, it should provide an upper limit for the expectations from the improvements that a channel selection technique could provide.

iv) **Channel fusion** aggregates the measurements from the four transducers using simple statistics such as min, max, and median of all four values. This is an experiment to observe the possibility of simple statistical approaches compared to the more complex ones.

8.2.4. Computing the correlation

Over 6 to 10 minutes after active exercise, the blood pressure of a subject decreases gradually. To reduce the random variations, the BPS feature values are averaged over 5 seconds and BPD over 10 seconds. In average, the latter duration is longer since it has higher random variations. In acquiring the GT, the blood pressure cuff took about one minute to give a reading. The performance of the features was computed using the correlation of the two series of

measurements from the reference ground truth cuff, reference PTT, and our new proposed features. The correlation coefficient is obtained by using this formula:

$$\rho(x,y) = \frac{conv(x,y)}{\sigma_x \sigma_y}$$

When computing the correlation coefficients between a proposed feature and the GT, only the feature value at the beginning of 5 (for BPS) and 10 (for BPD, and BPI) seconds of each one minute in collecting the GT is used. Since we took the data right after the subject finished the exercise, the blood pressure decreased continuously. The beginning of 5 and 10 seconds in each one minute better corresponds with the time of the blood pressure cuff reading. Thus, the length of the two vectors in computing the correlation coefficient ranges from six to ten.

8.3.Experiments and Results

The first question to answer is whether there is a simple approach to selecting the best transducer. In other words, I wanted to investigate whether the position of the transducers with respect to the body makes any bias toward the quality of estimations from each one. To test this idea, I used the oracle approach (best possible selection) on all subjects in the BP dataset. Figure 8.5 left, shows a visualization of the channels being selected for each feature, using the oracle approach. I also have counted how many times each transducer got selected as the best channel for the energy features and also the J-peak feature, then computed the probability of being the best channel for each one, as presented in Figure 8.5 right. This figure provides a comparison between the channels that were selected for the J-peak morphological feature (BPI), vs. the ones selected for the energy feature.

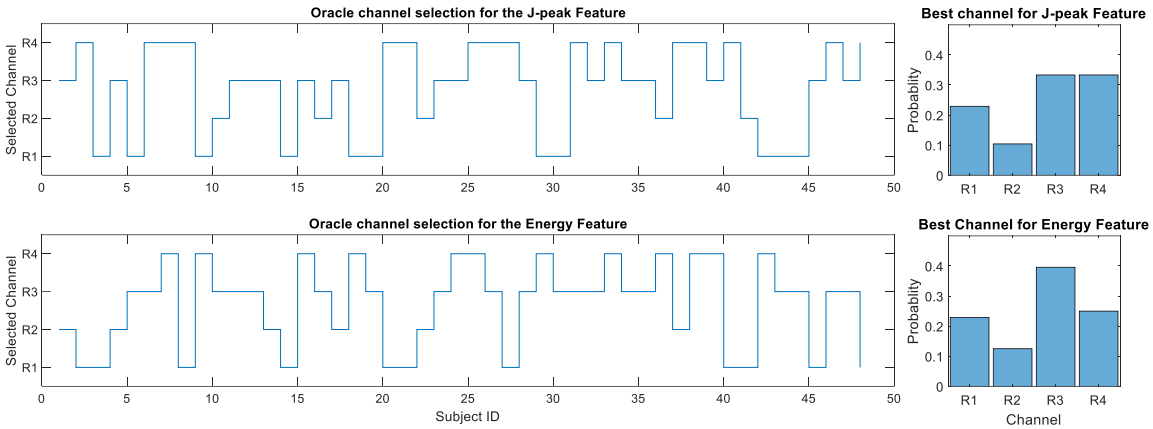

Figure 8.5. The highest correlated transducer differs between trials. This figure shows the comparison of channels with the highest correlation to the systolic blood pressure, for two features. Top row related to the BPD from the J-peak and the lower row is related to the BPS computed from the energy of the signal. On the right, the probability of selecting each channel as the most correlated channel is presented.

As depicted in Figure 8.5, the best choice of channel differs from one subject to the other, which is also different for different feature settings. Although the 3rd and 4th channels have the highest probability of being chosen as the most correlated ones, it is not only due to their distance from the heart. That is because the 2nd transducer sits closer to the body than the 1st one, but it has a lower probability of being selected as the best.

After studying the problem with pre-selection of one transducer based on their order, I have tried more objective channel selection approaches and compared their accuracies to the oracle approach. The average correlation of each channel selection is reported in Table 8.1 against the choice of the target feature. For example, the value 0.90 at the crossing of the first column and the first row, shows the correlation coefficient acquired by choosing the transducer with highest DC bias for the estimation of change in the blood pressure by means of the energy feature (BPS), and it matches the results reported in our previous paper [13].

Table 8.1. Effect of channel selection on the average correlation coefficient acquired from each of the three features.

Row Labels	Max DC	SNR	SQI	Min Val.	Median Val.	Max Val.	Oracle
BPS (Energy)	0.90	0.85	0.91	0.83	0.90	**0.94**	**0.95**
BPI (ij+jk)	0.90	0.85	0.89	0.83	0.90	**0.94**	**0.95**
BPD (ij-jk)	0.83	0.74	0.65	0.40	0.70	0.87	0.87

The highest correlations in this table are, of course, related to the oracle approach, in which the transducer with the highest correlation is selected. The selection based on the maximum DC bias is not the best approach for any of the features in the study, although it provides high correlations for two of the features, namely the energy of the wave and the summation of the two J-peak edges (BPI). These two features always provide higher correlations than the third feature (BPD, the difference between the IJ and JK edges of the J-peak).

Signal quality approaches such as SNR and SQI do not provide much improvement, while one of the aggregation approaches produces correlations almost as high as the oracle approach. Apparently, if at any point of measurement, we choose the maximum of the feature values from all four transducers, the overall measurement would have a very high correlation to the ground truth.

One should also consider the fact that this study has been done in the lab setting, and the subjects were asked to do some exercise and then come back to the bed. The measurements start from the first second that the subject stabilized on the bed, while they usually still have high respiratory rates and therefore the extra movement of the chest rib cage. This can cause artificially higher amplitudes for the signal and higher values for both features, at the beginning of the study. Therefore, choosing the maximum value among the four measurements results in the highest accuracy.

I also generated the scatter plots between the GT and the bed sensor blood pressure estimate to gain additional understanding. The bed sensor feature, either BPS or BPD, differs from the absolute blood pressure by a scale and an offset factor, that is

$$Actual\ Blood\ Pressure \approx scale \times Feature + offset$$

These two parameters are expected to be subject dependent and sensor unit specific. We obtain them separately for each subject by applying a least-squares fit of the bed sensor feature value to the GT blood pressure to generate the blood pressure estimate. Figure 8.6 depicts the scatter plot for the blood pressure estimate derived from the BPS feature. It clearly shows the results fit well to the 45-degree line, confirming a high correlation between the ground truth and the BPS feature.

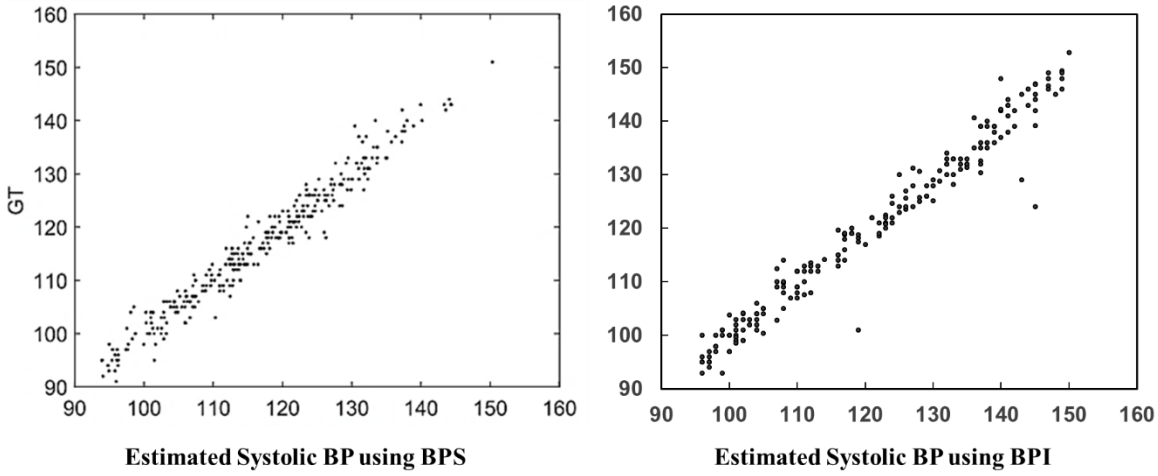

Figure 8.6. Scatter plot of blood pressure estimates derived from both features BPS and BPI vs. the ground truth GT.

The mean absolute error between GT and the blood pressure estimate is 1.8081 (mmHg) for BPS and 2.3350 (mmHg) for BPD, while that of PTT is 2.4221 (mmHg).

8.4. Conclusion

In this chapter, I proposed and compared the use of different channel selection techniques to improve the correlation of BCG related features to the reference blood pressure measurements, using the non-invasive hydraulic bed sensor. I have also introduced a new morphological feature, namely the summation of the two sides of the J-peak, which overall provides high correlations to the reference. This study has been done on the same dataset (48 young, healthy volunteers) as the one in our previous work [13] and I have shown how the new approach could improve the correlation coefficient of the features.

I have proposed use of the oracle approach as the golden reference to evaluate the quality of each channel selection scheme. On top of channel selection, I have also introduced for the first time, the combination of the measurements from the four transducers (fusion) to provide better performance.

This work opens the possibility of monitoring the relative systolic blood pressure continuously using our hydraulic bed sensor system. Future suggested work includes a longitudinal study of the TigerPlace residents with overnight data. By combining the proposed approach of this chapter on tracking the blood pressure, with other chapters of this dissertation including the channel selection, noise reduction and also sleep posture classification, researchers should be able to focus on the clear portions of the overnight data for feature extraction. We also can combine the blood pressure monitoring results with our previous studies in which health changes are tracked using non-obtrusive in-home sensors [193, 211].

8.5. Discussion

There are multiple points to discuss in this work and the previously published article, which might be helpful in future explorations and understanding of the physics of our hydraulic bed sensor. These include the design of an experiment to increase the blood pressure in the lab setting,

uncorrelated effects of the blood pressure cuff on the ballistic readings of the hydraulic bed sensor, channel selection and challenges with the older population.

To increase the blood pressure, we asked the subjects to use the stationary bike for about two minutes to increase their blood pressure, while making sure they will not hurt themselves by any means. This, of course, has some ambiguities in the description. For example, it is unclear how much increase in blood pressure or heart rate appeared right at the end of the exercise. Some subjects made a great effort on the bike and some apparently just used the most relaxed settings. Thus a significant discrepancy appears in the real amount of changes. Multiple other techniques have been proposed in the literature [214] to artificially change the blood pressure, including the respiratory maneuvers such as Valsalva, Müller's maneuver, or some muscle contractions such as hand grip or squatting. Knowing how each maneuver affects the cardiovascular system can help in predicting the corresponding changes in the morphology of the waveform.

Some of these exercises can change the venous return (VR) to the heart from the venous vascular. For example, lung expansion (inspiration), results in a substantial increase in the pressure gradient driving venous return from the peripheral circulation to the right atrium. Transient changes in venous return can occur in response to several factors including the rhythmical **contraction** of limb muscles during regular locomotory activity (walking, running, swimming), sympathetic activation of veins to decrease venous compliance, and the **respiratory activity,** which causes a decrease in right atrial pressure. For example, **squatting,** which decreases the distance between the legs to the heart, thus influences the blood return and increases the preload. **Handgrip** increases vascular resistance inside the arms and increases afterload and a slight increase in the preload. Respiratory Maneuvers, such as **Valsalva,** or the **Müller's maneuver** (inverse of Valsalva) affect the preload by changing the abdominal pressure [214].

Normal respiratory variations of the ballistocardiograms were also considered in the experiments. Respiratory sinus arrhythmia (RSA) is the automatic variation of heart rate during different phases of a respiratory cycle. As the BCG waves enlarge in amplitude during inspiration and cause an increased cardiac output, the systolic pressure and pulse pressure may simultaneously diminish, suggesting decreasing cardiac output. This apparent discrepancy is due to the fact that the ballistocardiogram records the sum of the impacts from the movement of blood coming from both sides of the heart while arterial blood pressure is affected by the output of the left heart [111].

Table 8.2, illustrates how different segmentations of the samples, according to the respiratory phase, could affect the overall correlation coefficient in blood pressure estimations using the BCG. Four respiratory phases including the Inhalation Peak (IP), Exhalation Active (EA), Exhalation Peak (EP), and the Inhalation Active (IA) were studied. Among all four, the expiration peak (EP), which is located at the end of exhaling period, has the biggest improvement. This is a potential strategy in establishing a general framework.

Table 8.2. Variations in the correlation coefficient during the respiratory cycle. *Focusing on certain phases of the respiratory cycle changes the accuracy of BP estimation. The best subjects are the 48 ones among the total 62 subjects without large motion artifacts in their recordings.*

		All	**IP**	**EP**	**IA**	**EA**
Best Subjects	**Energy**	0.93	0.96	0.97	0.93	0.93
	J-Peak	0.86	0.84	0.93	0.84	0.83
All Subjects	**Energy**	0.90	0.95	0.96	0.91	0.90
	J-Peak	0.83	0.85	0.92	0.81	0.83

Estimations on older subjects were the primary motivation of our work. Fundamental differences exist between the data of younger subjects compared to the ones collected from the older subjects. These differences include the natural differences between the morphology of the BCG signals acquired from older subjects compared to the younger ones, and also the fact that the

older subjects were not asked to do any exercise in our study (to reduce the risk factors of data collections). As expected, exercise causes a higher variation in the BCG waveforms acquired from the younger subjects, which was easier to capture using our features. To explore the real difference in the accuracy of estimations between different age groups, I repeated the entire study on each of the 3 data sets separately. Comparing four different features, on each of the three datasets (1. Young subjects before exercise, 2. Young subjects after exercise, 3. Old subjects before exercise) shows that none of these features achieves high accuracy estimations on older subjects. It also shows the morphological features are better than the energy algorithm for young-at-rest subjects.

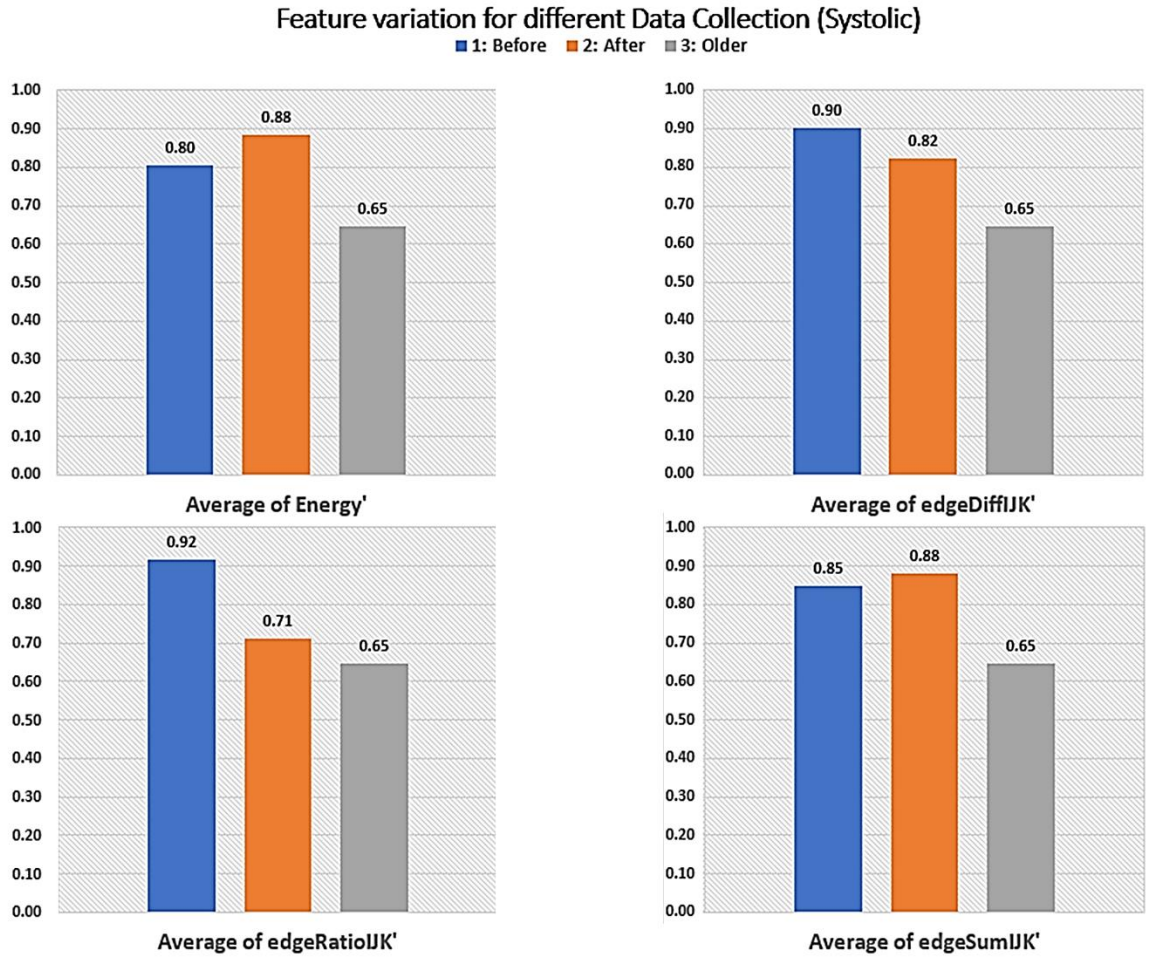

Figure 8.7. Comparing the correlation of four different features, on the three datasets (1. Young subjects at rest, 2. Young subjects after exercise, 3. Old subjects at rest). Correlation values show that none of these features achieves high accuracy estimations on older subjects. It also shows the morphological features are better than the energy algorithm for young-at-rest subjects.

A more detail comparison of the accuracy of each estimating feature on different age groups is provided in Figure 8.8. Clearly, the accuracy of all features declines as age increases. This should encourage us to do more data collections on older subjects, after the initial algorithm developments on young subjects.

Figure 8.8. The correlation of BP estimates using each feature decline by age group.

The effect of the blood pressure cuff on the acquired bed sensor signals at first looks very similar to the respiratory variation. More investigations showed a consistent change in the DC level of all four transducers caused by the inflation and deflation of the blood pressure cuff, which is not related to respiration or even the general reduction of blood pressure (Figure 8.9).

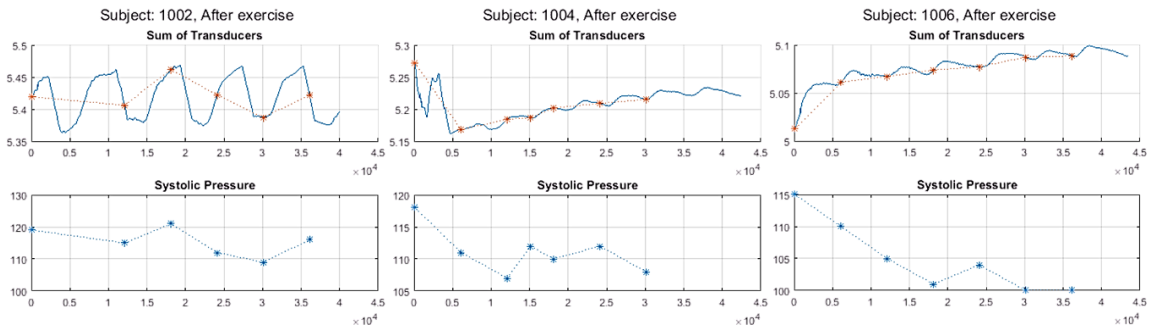

Figure 8.9. Variations in DC bias around the inflation of the blood pressure cuff. The figure shows the synchronized measurement of DC values (top) and blood pressure readings (bottom).

Some of the unwanted effects of the blood pressure cuff have already reported in the literature. Sheshadri, et al. [215] reported a transient rise of 0–10 mmHg in arterial blood pressure readings caused by the inflation of a blood pressure cuff. Also, Liu, et al. [216] reported a significant increase in the PTT measurement (ECG to PPG), within one minute after a four-minute cuff inflation and deflation process. All of these show a potential research area to study the causes and effects of these variations.

My investigation in Figure 8.10 shows the variations appeared right around the activation of blood pressure on all four transducers, while the subjects were at rest and before exercise. The reference manual blood pressure measurements (red dots) show the documented time of each manual blood pressure measurement. The interesting point in this figure is the opposite direction of the DC changes in transducer R4 vs. R1. R4 is the leftmost transducer as happens to be the closest to the left arm. As inflation starts, the DC level of R4 declines while the DC level of R1 increases at the same time.

This variation could be related to the decreased amount of blood circulation on the left side, as a result of cuff inflation, and increased circulation on the right side. An interesting study could explore the relation of these DC variations to the measured blood pressure of the subject at that time. So, for any future assessment of blood pressure using ballistocardiography, it is suggested to consider the DC variations caused by the inflation of the blood pressure cuff.

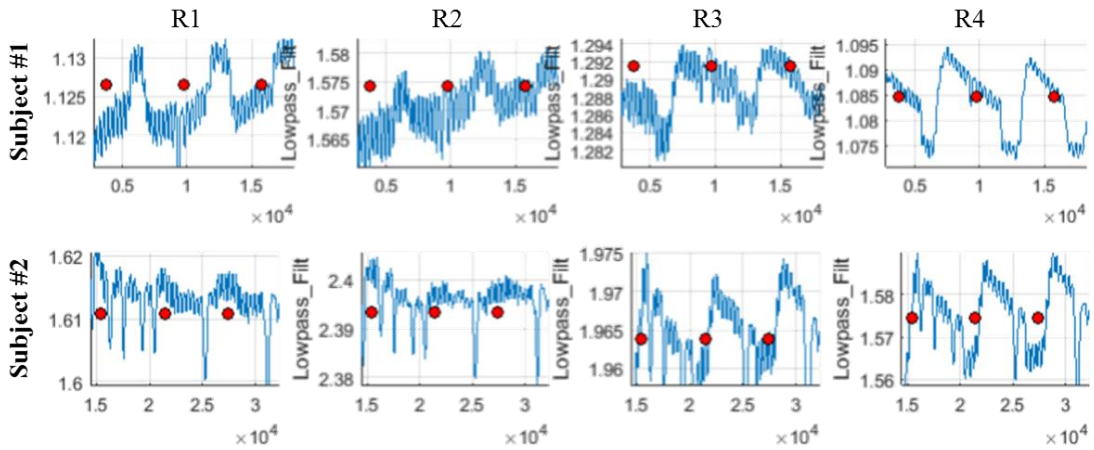

Figure 8.10. Inflation of blood pressure cuff causes a change in the DC bias of the four transducers. For both of the subjects represented in this figure, transducer R4 was the one closer to the left arm (heart), where the cuff was placed.

9. SLEEP STAGE CLASSIFICATION

9.1. Background

Normal human being spends almost one-third of their lives in sleep. During sleep, multiple mechanisms such as the sympathetic nervous system and cardiorespiratory system function differently, depending on the sleep stage. The quality of sleep is shown to have direct effects on the physiological and neurological abilities of individuals. Sleep disorders such as apnea or insomnia, and sleep distortions have been shown to be related to neurological and physiological diseases [217], and therefore can help physicians in the diagnosis of such diseases.

According to the American Academy of Sleep Medicine Manual (AASM, 2007) [218], a normal human sleep consists of multiple cycles of alternating between the two general sleep stages, namely the REM and non-REM, as well as some periods of wakefulness. Brain waves, muscle activities, and eye movements have different patterns in different sleep stages. REM stands for the rapid eye movement and is the restorative part of the sleep, which therefore is a clinically relevant parameter to monitor.

Recently we published a paper [219] on the classification of sleep stages using features extracted from the hydraulic bed sensor signals acquired from five regular patients in the Boone hospital's sleep center. These five subjects were chosen among a larger dataset, with lower Apnea-hypopnea index (AHI) and so that each one has all three main sleep stages during the night. Annotation for sleep stages and other events have been provided by a sleep-credentialled technician through de-identified PSG files. An example hypnogram from one of these subjects with multiple sleep cycles during the night is presented in Figure 9.1.

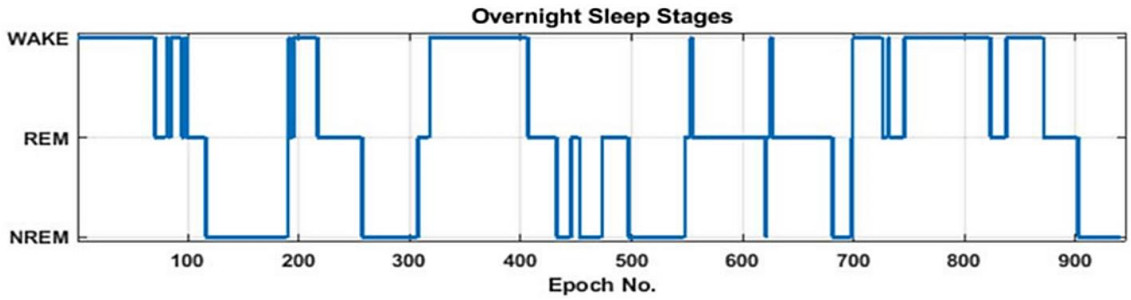

Figure 9.1. Example hypnogram with multiple sleep cycles during the night, acquired from the sleep lab annotations.

The original energy algorithm [11] was used to detect the individual heartbeats from the BCG signal, as described in Chapter 5. These detected locations were then used to compute the heartbeat intervals and heart rate variability (HRV). Nine features from the time domain and four frequency domain features were computed from the heartbeat intervals to build a set of thirteen HRV features. The heart-beat intervals and breath intervals were calculated from the filtered heart rate signal and the respiratory signal. Then, HRV features and RV features were extracted based on these intervals, respectively. The LFCC features were generated from the filtered heart rate signals.

In this section, I report the results of my experiments on the possibility of improving the sleep stage classification accuracy. I have used the enhanced energy algorithm for a better beat detection as my experiments in Chapter 5 show it improves the accuracy of beat to beat heart rate estimations. Also, based on the results reported in Section 6.5, here, I will show the effect of other channel selection approaches.

9.2.Experiments and results

I investigated multiple approaches to improve the accuracy of sleep stage classification, including the utilization of a different channel selection scheme or application of the enhanced

energy algorithm in extracting the beat to beat heart rates. I created three different feature datasets to represent different configuration settings including (i) the set of features extracted from the channel with the highest DC using the original energy algorithm, (ii) the feature set from the highest DC channel by means of the enhanced energy algorithm, and finally (iii) the features from the channel with minimum MAD of heartrate using the enhanced energy algorithm. For the channel selection using the MAD of heartrate, I first applied the enhanced energy algorithm on all channels and then used the estimations acquired from the channel with the minimum MAD in heart rate.

Table 9.1. Sleep classification accuracy and the area under the curve. *This table compares the classification accuracy (ACC) and the area under the curve (AUC) for the 3-classes of wake, REM, and non-REM on different configuration settings. The configurations consist of different subsets of the features, beat-detection algorithm, channel selection schemas, and four different classification methods.*

Feature Set	**Beat Detection**	**Channel Selection**	**Cubic SVM**		**KNN**		**Bagging**	
			Acc	**AUC**	**Acc**	**AUC**	**Acc**	**AUC**
All Features	Original Energy Alg.	DC Bias	84.5%	97.0%	73.8%	92.0%	80.3%	94.0%
	Enhanced Energy Alg.	DC Bias	85.3%	97.0%	73.1%	92.0%	79.6%	94.0%
	Enhanced Energy Alg.	MAD HR	85.5%	98.0%	73.4%	91.0%	81.0%	93.0%
HRV Features	Original Energy Alg.	DC Bias	55.4%	52.0%	57.4%	60.0%	56.3%	58.0%
	Enhanced Energy Alg.	DC Bias	57.5%	59.0%	57.5%	65.0%	55.4%	66.0%
	Enhanced Energy Alg.	MAD HR	49.4%	60.0%	60.3%	72.0%	57.4%	69.0%
Non-HRV Features	Original Energy Alg.	DC Bias	85.2%	97.0%	74.5%	93.0%	80.5%	93.0%
	Enhanced Energy Alg.	DC Bias	85.4%	97.0%	74.5%	93.0%	80.7%	93.0%
	Enhanced Energy Alg.	MAD HR	85.2%	97.0%	74.5%	93.0%	80.8%	94.0%

The upper three rows of Table 9.1 are related to the analysis of all features, and the middle three rows are related to the analysis using only the 13 HRV-related features, and finally, the last three rows are related to the non-HRV features. At first, I tried the new beat detection, and the new channel selection approaches on the entire features using 10-fold cross-validation for each of the three classification algorithms. Comparing the classification accuracies for the 3-class problem of WAKE, REM, and non-REM over different settings does not show a noticeable improvement in the accuracy or the area under the curve (AUC) for the REM class.

Then I decided to use only the 13 features that are related to HRV and are extracted from the beat to beat intervals. While expecting a lower accuracy than the combination of all features, studying only this subset of features would have a higher possibility in showing the effect of each setting on the total accuracy. But unfortunately, nothing more than a couple of percentages changed between these configurations. This is while the overall accuracy through the use of only HRV features has gone from about 85% in the original setting to as low as 55%, even for the energy algorithm and the DC bias approach for channel selection. This brings a question on how much the HRV features are important in the overall classification results because 55% works almost like a random variable.

To test this idea, I have also compared all the previous configurations against the non-HRV features, and as Table 9.1 shows the classification accuracy of each setting stays very close (or even a little higher) than the ones with all features being used. These experiments show that the HRV features are not playing an important positive role in the current classification problem, and therefore even an improvement in their extraction, might not have an effect on the outcome of the entire classification.

9.3. Conclusion

In this section, I have tried two ideas to improve the quality of sleep stage classifications that we previously reported in [219]. Two different channel selection schemas were used, including the traditional DC-based approach and the one based on the minimum deviation of the heart rate estimates, which shows improvement in the HR estimation as reported in Section 6.5. Also, the features extracted from the enhanced energy algorithm were compared to the features from the original beat detection algorithm.

Results show no considerable improvements in the accuracy of the sleep stage classifications. In fact, my further experiments with and without the HRV features show that the contribution of these features to the overall accuracy is minimal (either before or after the enhancements). In other words, by completely removing these features, the classification accuracy had even some small improvements. These results are not in agreement with what I presented in Section 6.5 on the improved quality of beat detection and heart rate estimations after the application of the enhanced energy algorithm on the selected channels.

Further studies of the relevance of these HRV features and also their implementation details are required to understand the source of the problem. Studying different denoising techniques is suggested for future work, as the hospital data consists of multiple sources for noise and artifacts, including vibrating devices such as the air mattress, CPAP, and BIPAP. It is also important to note the "patients" might have different syndromes, which changes their responses to the sleep stages. For example, although REM sleep in healthy subjects contains no movements, REM sleep behavior disorder (RBD) is common between patients with Parkinson's disease [220]. Studying the health condition of the patients, and the effect of abnormal REM sleep movements such as RBD could be another venue to explore.

10. CONCLUSION

10.1. Summary

The work described in this dissertation provides an accurate, robust, and real-time approach to detect cardiac cycles through the use of ballistocardiography with a particular focus on the longitudinal in-home data collections where a high degree of ambient noise diluted the signal quality. Reduction of the noise or detection and cancelation of the noisy regions enhances the potential of future BCG based research. Accurate localization of the fiducial points in the BCG can directly improve the accuracy in the estimation of HRV and sleep stage classification. Sleep posture classification, on the other hand, helps the researchers to focus on a specific posture for longitudinal studies. Creating physiologically, reliable templates from the BCG was also part of my work. It provides the foundation for morphological analysis of the BCG waveforms that appear due to different changes in the cardiovascular system, such as aging or the change in the blood pressure.

After providing the theoretical definition of BCG, some classical and modern BCG devices are mentioned in Chapter 2 including Starr's original suspended bed and the recent bathroom scale. I have also provided the standard categorization of BCG devices as the ultra-low frequency (ULF), low frequency (LF), and the high frequency (HF). Starr's free moving suspended bed is known to be ULF. We have made a replica of the Starr's suspended bed in our lab which uses a 3-axis accelerometer to record the ballistic movement of the subject's body. This device and our other BCG devices, including the hydraulic bed sensor and the chair sensor are described in Chapter 3.

Chapter 3, also provides the list of datasets that we collected for this study, including (i) the young, healthy subjects resting in supine position (HRV dataset), (ii) young, healthy subjects before and after exercise (BP dataset), (iii) young, healthy subjects shifting sleep postures (POS dataset), (iv) mostly older residents of TigerPlace in resting supine position (TP dataset), and finally overnight BCG and PSG dataset from sleep lab patients (Sleep Dataset).

In Chapter 4, I used the non-BCG components of the signals acquired from the four transducers of the hydraulic bed sensor to estimate sleep postures. By applying simple statistical functions on the DC levels of the four transducers, I was able to train neural networks for the classification of various sleep posture classes and have achieved average accuracies as high as 89% for separating the lateral (side) vs. the non-lateral postures. There, I also reported how the LOSO cross-validation has lower accuracies compared to the K-fold cross-validation. Having non-invasive tools for sleep posture classification helps researchers in extracting features only from the time periods that the subject is in a specific sleep posture. This would compensate partially the impact of sleep posture on the amplitude and shape of BCG waveforms.

Then by focusing on the BCG components of the signals, I was able to improve the accuracy of our previous beat detection algorithm by means of some enhancement steps, in Chapter 5. These steps include (i) the customization of the bandpass filter for better separation of the respiratory variations, (ii) reduce the remaining respiratory variations, by means of the signal envelopes, (iii) normalization of the BCG amplitude using the respiratory waveform, (iv) using the slope of the J-peak combined with its amplitude. My results show the average RMSE in beat to beat heart rate estimation, is higher for the original energy algorithm compares to the enhanced one. My results show on average, the RMSE of the enhanced energy algorithm is almost one-third of the original energy algorithm.

In Chapter 6, I have proposed and investigated different approaches to handle distortions and motion artifacts in the BCG signal. I first used different variations of the wavelet decomposition, and empirical mode decomposition to reduce the noise content of the signals. My results show the enhanced algorithm always has smaller errors in the beat to beat heart rate estimation. I also found the wavelet decomposition as the best denoising technique on each and all of our datasets. The combination of the wavelet denoising and the enhanced energy algorithm resulted in about 52% reduction of the beat to beat heart rate estimation.

Moreover, in Section 6.4, I proposed the use of SVM and RUSBoost on the combination of 53 features from all four transducers, and as reported in Table 6.3, the accuracy of detecting the noisy segments is as high as 99.2%. The data consist of 10-minute recordings from 25 young, healthy subjects during the change of postures, and also overnight signals from the sleep lab.

Then in Section 6.5, I have adapted some signal quality indices to evaluate the quality of different channels, including the (i) signal to noise ratio (SNR), (ii) band power ratio (BPR), (iii) heart rate deviation (MAD), (iv) the conventional DC-based selection, and finally (v) the oracle approach. The oracle approach is the manual process of choosing the best option after computing the performance of all possible selections. It can provide an upper limit on our expectations about the amount of improvements that we should expect after the utilization of channel selection techniques. In this section, the selected channels of each method are compared against the oracle, and if there was at least one match (hit) between these two sets, the selection reported as successful. My results show the conventional DC-based approach has the lowest hit rate, and the SNR usually outperforms the other methods on all datasets (HRV: 62%, POS: 51%, Sleep: 68%, and TP:53%).

After noise reduction and elimination of noisy sections, I proposed the use of ensemble averaging techniques to create morphological BCG templates. Morphological templates have been used in the literature to track the pathological disturbances in the ECG after heart attack, and also the age-related variations in the photoplethysmography signals. In Chapter 7, after describing the process of creating the morphological templates from our BCG signals, I provided evidence on different variations in the BCG template during the respiratory cycle, and also as the result of aging. I used the same approach and showed how well our suspended bed matches the ones described by Starr, and also provided some foundations for characterization of the waveforms from the hydraulic bed sensor.

These morphological templates were also used in Chapter 8 for non-invasive monitoring of the relative variations in blood pressure. I used different channel selection techniques on top of new

morphological features to improve the correlation in monitoring the blood pressure. Other than channel selection, aggregation (fusion) of the measurement from the four transducers proposed and compared against the oracle approach. My results show that choosing the maximum feature value among all four transducers always provides correlations as high as the oracle approach (best possible correlation). Also, the new morphological feature (BPI) shows correlations as high as the energy algorithm on the after-exercise data of the young subjects.

My further investigations in Table 8.2 show how the correlation changes with different stages of the respiratory cycle. Unfortunately, Figure 8.7 shows none of these features could achieve high accuracy estimations on older subjects. In fact, as reported in Figure 8.8, the correlation of the blood pressure estimations using each of the four features declines by age. This could be due to the age-related variations of the BCG morphology, or also the structural differences between the two datasets of younger and older subjects, as the latter one was not designed to change the blood pressure of the subjects.

In Chapter 9, I have studied the possibility of improving the sleep stage classification accuracy by introducing new channel selection techniques (MAD HR) and enhanced features, compared to our previously published paper. The newly proposed enhanced energy algorithm was used for feature extraction from the sleep lab data, specifically for the HRV-related features. Meanwhile, two new channel selection schemas were used to find the best transducer among the four. My experiments show no significant improvement in the accuracy of sleep stage classification after utilizing the new techniques. While further studies are required in this area, results show the current implementation of the HRV features does not have much contribution to the overall classification task. I showed that using only the HRV features produces about 55% classification accuracy, which is about the random decision making. Also, removing the 13 HRV features from the entire features does not reduce the overall accuracy of the classification.

10.2. Contributions

- Development of an enhanced algorithm for accurate beat detection in BCG
    - Fast, time domain, and robust against small motion artifacts.
- Investigating different approaches to evaluate and improve the quality of the BCG signal
    - Application of noise reduction techniques to minimize the effect of artifacts.
    - Designing a machine learning approach to detect and discard noisy segments.
    - Introducing the use of different signal quality indices to select the best transducer.
    - Relaxation of the SQI indices initially designed for beat-level, to the signal-level.
    - Innovative evaluation of the selection by defining the Oracle SQI and the Hit-Rate.
- Sleep posture classification from the four hydraulic bed sensors
    - Identifies consistent portions of sleep over multiple nights, which results in more consistent morphological templates in longitudinal studies
- Template-based analysis of the morphology of BCG waveforms
    - Designing the procedure to create physiologically reliable BCG templates.
    - Studying the variation of these templates during the respiratory cycle, or due to the change in cardiovascular parameters such as the change in blood pressure or aging.
- Preparation of the most extensive annotated datasets using the hydraulic bed sensor
    - I was engaged in 4 IRB approved data collections with more than 570 hours of BCG signal synchronized with other reference signals including but not limited to ECG and PPG.

10.3. Future Work

This dissertation consists of different experiments and approaches for a better understanding of the BCG devices and enhancing the quality of features being extracted from each device. While each chapter contains its own discussions and suggestions for future work, here I have provided some suggestions for future work.

In Section 2.3 on this dissertation, I have provided a list of different BCG devices and the standard categories that each one belongs to. As described, our suspended bed belongs to the category of ultra-low frequency devices, which have fewer waves included in them. Although our mathematical model was able to reproduce a matching BCG waveform to the ones we acquired from our suspended bed, they are still significantly different from the waveforms collected using the hydraulic bed. I suggest investigating a high-frequency device such as the ones I have introduced in Section 2.3, as the reference to characterize our hydraulic bed sensor.

In Chapter 4, I have reported the results of my experiments on finding the best configuration setting in the classification of sleep postures, using MU hydraulic bed sensor. This provides a foundation for future experiments using the deep NN structures to improve classification accuracy. Hierarchical classification is yet another powerful, relatively simple to implement and easily expandable method which can be explored in the future.

In Chapter 5, I have presented multiple steps in enhancing the overall accuracy of the energy-based algorithms for BCG beat detection. There I showed how different obstacles could be reduced by means of the enhanced energy algorithm and reported the improvements in the accuracy of predictions in multiple datasets. Here I did not study the gender-related differences in the BCG waveform. Future research should investigate the customization of these techniques for different gender and age groups.

I have previously reported [221] some of my observations on the age-related variations in the BCG waveforms. In addition, in Section 6.5.4 of this dissertation, I have discussed the low performance of the "band-power-ratio" SQI on the TigerPlace dataset (TP) and hypothesized the existence of some variations in the higher frequencies of the BCG during the aging process. By integrating these pieces together, I suggest designing a new BCG-based age index for non-invasive evaluation of cardiovascular health.

Directional BCG is another important topic for future researches that require careful design of experiments in the initial steps. In [111], Starr explored the relationship between the displacement of the heart's axis to the variation of BCG amplitudes during the respiration. He mentioned that the heart's axis is subject to a counter-clockwise rotation, as the cardiac apex moves to the left during the expiration and after the rise of the diaphragm. A reasonable conclusion is that this perturbation of the heart's axis from the measurement direction is the cause of respiratory effects found in the recorded ballistic force. Instead, Starr found that a large portion of BCG comes from the movement of blood in the aorta, an organ whose position remains fixed during respiration, and concluded the change in the heart's direction should not be a primary factor.

Chapter 8 contains some experiments on the non-invasive monitoring of the change in blood pressure through the use of our hydraulic bed sensor. Three features and multiple channel selection strategies were compared to the reference measurements using the correlation. Future suggested work includes a longitudinal study of the TigerPlace residents with overnight data. This is now possible by means of the techniques that I proposed in different chapters of this dissertation regarding the channel selection, noise reduction, and the creation of morphological templates. Also, focusing on a specific sleep posture and sleep stage would provide better consistency in the extracted features.

Also, as I described in Section 8.5, the enlargement of BCG waves during inspiration causes an increased cardiac output. At the same time, the systolic pressure and pulse pressure may

simultaneously diminish, suggesting decreasing cardiac output. This apparent discrepancy is due to the fact that the ballistocardiogram records the sum of the impacts from the movement of blood coming from both sides of the heart while arterial blood pressure is affected by the output of the left heart only [111]. My suggestion for the future work on the estimation of blood pressure is to take advantage of our mathematical model [5] to first investigate the components that are related to blood pressure and then take a fresh look at the measured BCG waveform.

Chapter 9 of this dissertation shows my studies on the application of channel selection and the new feature extraction based on the enhanced energy algorithm. One possible extension to this chapter is to investigate the noise reduction, noise detection techniques, and also other channel selection techniques. According to the results that I presented in Figure 6.12, the SNR-based channel selection may be a better option for the Sleep dataset. Also, based on the results presented in Table 6.2, signal denoising techniques such as the wavelet decomposition may provide considerable improvements in the accuracy of the heart rate estimation and therefore the overall contribution of the HRV features.

Another venue for future work is the application of the motion artifact detection technique that I developed in Section 6.4. In that section, I proposed the use of SVM and RUSBoost on the combination of 53 features from all four transducers, and as reported in Table 6.3, the accuracy of detecting the noisy segments is as high as 99.2%. The idea would be to use the model that I have already trained on the existing dataset and apply it to detect the noise on the rest of the Sleep dataset in order to detect and cancel the noisy segments. After this step, only segments with the minimum amount of noise should stay, and therefore, the accuracy of beat detection should be improved. This effort not only improves the accuracy of HRV features but also has the potential to improve the rest of the features that we use in the sleep stage classification, by discarding the noise.

APPENDICES

Appendix A. Details on the Datasets

In this section, a more detailed description is provided regarding the datasets that I used in this dissertation. All of the datasets are de-identified and IRB approved, and includes LabChart files and the exported data into Matlab. There are also txt or excel files included in the folders with data from the subjects' health questionnaire.

Each database was collected for a specific purpose, and therefore, acquired a name with respect to the initial goal; for example, the HRV database was designed and collected for an HRV study. For the sake of consistency with other documentation, I am using the same names for each dataset. An overview of these datasets is already provided in Table 3.1.

In all of these data collections, multiple standard reference sensors were also connected to the subjects including the 3-lead ECG, PPG, pulse figure sensor, and the respiratory chest band. All these sensors and the bed sensor channels were connected to the ADInstrument's PowerLab 16/35. The latest version of LabChart was used to manage, the data collection and signal preprocessing.

Each dataset is stored as a separate folder with all related files inside that folder. Our IT team has pushed a version of these files to our HTC storage at this address:

128.206.234.62:/storage/htc/eldercare/data/projectdata/bcgdatasets.

The first data collection covers multiple datasets that were collected from the same population but with different conditions and for different studies; 63 young, healthy volunteers were recruited with the age between 8 to 50, including 15 females and 47 males. These studies are namely the HRV, POS and the BP data collection; a short description of each is provided below. I have created a similar structure for all these datasets and have placed them in a common folder,

which is named "*HRV BedPosition BP data collection*". This folder contains the following subfolders:

- ***LabChart Recordings:*** there is a folder for each subject including the original LabChart ".adicht" files collected for each study (HRV, POS, BP), and an excel file for the blood pressure readings. The name of each channel recently added to these files for more clarification. It also has
- ***Additional Inf:*** has some excel files to provide age, gender, weight, height, BMI of each subject and a flag to show if they have any ectopic peaks.
- ***Matlab Exports:*** contains a Matlab file for each subject per study. These files were exported directly from the LabChart.
- ***MatlabTables:*** LabChart exports the data into Matlab in a very strange way; in this folder all those LabChart files into are converted to nice Matlab tables.
- ***StructsForPython***: converting Matlab structs to python is easier, so this folder has a Matlab struct for the python users.

I. The heart rate variability dataset (HRV):

This dataset was initially designed and collected to provide enough BCG data to develop a study on the heart rate variability (HRV). A population of 62 young, healthy volunteers were asked to come to our lab and lie still in the supine position on the bed, for 10 minutes. The files are stored in a folder named "*HRV BedPosition BP data collection*" which contains multiple datasets for different reasons from the same population.

II. The blood pressure dataset (BP):

This dataset was designed and collected to provide enough BCG data to develop a study on the estimation of change in blood pressure on the young subjects. A population of 62 young, healthy volunteers were asked to come to our lab and do the following steps:

a) Lie still in the supine position for 2 minutes. Their blood pressure was measured for 3 times.
b) Increase their blood pressure by using a stationary bike for 2 minutes with the intensity of their preference, while considering their safety.
c) Come back to the bed and lie on the bed until their blood pressure measurements become stable. Between 7 to 11 BP readings were recorded after the exercise.

III. The sleep posture dataset (Pos):

This dataset was designed and collected to provide enough BCG data to develop a study on the classification of sleep postures. A population of 62 young, healthy volunteers were asked to come to our lab and do the following steps:

a) Lay still in the middle of the bed and on the supine posture, for two minutes.
b) Turn to the left side and stay for two minutes.
c) Turn to the right side and stay for two minutes.
d) Turn on the stomach (prone) and stay for two minutes.

IV. The blood pressure dataset from the TigerPlace residents (TP):

This dataset was designed and collected to provide synchronous BCG and reference signals to study the estimation of blood pressure in older adults using the hydraulic bed sensor. While trying to collect the data from the older residents of TigerPlace, we had some younger volunteers from the staff who also joined this data collection. The overall population has an age range from

19 to 95 years with 34 females and 15 males. It took about 10 minutes for each subject and they were asked to lie still on their supine position, while 3 blood pressure readings were recorded at the beginning, in the middle and at the end of each data collection.

The files of this data collection are stored in a folder named "BCG - Blood Pressure – TigerPlace". Inside the subfolder "Original Data \AllSubjects" there is a single ".adicht" LabChart file for each subject. Each LabChart file is then exported to a Matlab folder and stored in subfolder named "Matlab". There are also two excel files in this project with data on each subject from the health questionnaires and also the health information of the subjects.

V. The Boone Sleep Lab dataset (Sleep):

In this dataset we collected overnight PSG data from 75 subjects along with our hydraulic bed sensor. The designated nurse pushed slightly on the chest of each subject, 3 times, to provide signal markers in both PSG and BCG for synchronization once at the beginning of night and once in the morning. Subjects were regular sleep lab patients and were aged between 31 to 86 years, including 27 females and 49 males.

The original EDF files from the sleep lab are stored in a folder named "Boone Hospital Sleep Study". The de-identified subjects are labeled by the date of their visits, and there is a folder for each subject. These folders contain many different files among which the ".txt" files are important as they include the annotations. The following folders are important:

- ***Natus Installation CD***: the installation material for the original sleep lab software named Natus.
- ***boone_Polysomnic_Data_EDF***: contains a single EDF file for each subject. In another folder I have converted them to Matlab.

- ***boone_Polysomnic_Data_Matlab***: contains the files created by exporting the EDF files as Matlab, and also some Matlab code used for this process.
- ***boone_bed_data\beddata\BedFiles_Original***: this folder contains all individual bed sensor files related to this dataset. In another folder I have concatenated them together to make a single Matlab file.
- ***Data Sets\Sleep Study\bcg_psg_sync_firstepoch***: this folder contains the Matlab files created after synchronization of the BCG and Bed sensor files together.
- ***PSG report:*** contains the word documentation of the PSG reports related to each subject. These reports include important information and statistics about the overnight experience.
- ***AlignSleepData:*** contains some Matlab codes to handle these EDF files and prepare them to be used in Matlab.
- ***no_break_psg_all:*** contains the files I created by importing the ECG signals to LabChart in order to create the reference for ECG R-peaks. It also has all channels resampled to 100Hz for simplicity of future computations. Also, for a subset of files the PSG_HR signals are also provided.

There are also multiple excel files in this folder, which contain statistics about the subjects, including the:

- ***Boone data info all.xlsx***: this file contains important information about the subjects such as age, gender, weight, height, BMI, and the total number of epochs in each condition including the apnea, REM, or different sleep stage.
- ***Readme_2_ExportChannelLabels.txt***: this file contains detailed information on the naming and sample rate of each channel in the PSG dataset.
- ***start time.xlsx***: contains the timing of the first epoch with respect to the BCG signal. This is done manually in our team by looking for the similar events on both signals.

Appendix B. Details on the Matlab Code Used in this Work

In this section, the details of Matlab code that I have used in this project are provided. I have created a separate folder for each project. Each folder works independently and may share some general codes with the others. Each folder is related to one project and has a few Matlab files (.m) that are designed for a specific task, and each file may contain multiple functions to handle the task. Folders, files, functions, and all variables have clear naming so the other researchers could easily work with them. More details of each part of the code are also provided as inline comments.

The general trend that I am following to write Matlab codes is to take advantage of Matlab Tables. In short, a Matlab table is a cell array (matrix of objects) with labels for each column. This is very important in codes and datasets to be shared between multiple researchers. Also, I have tried to take advantage of Matlab's parallel computing to increase the execution time. Especially the use of "parfor" instead of "for" which simply accelerated the execution by the number of CPU cores while having multiple input/output (I/O) file processes. In the current documentation, I have provided the following information for each "function":

Description: Brief description of each function and how it contributes to the entire project.

Input Arguments: Description of each argument, including datatype, and acceptable values.

Output Arguments: Description of each output parameter, including datatype.

List of Functions:

PROJECT I. ENHANCED ENERGY ALGORITHM

This folder contains all the required Matlab functions that I described in this dissertation in order to improve the time-domain estimation of heart rate through the enhancement of the energy algorithm. All files are pushed to the GitLab folder with the following address that is accessible to all students in our lab:

https://gitlab.missouri.edu/CERT-Students/studentProjects/bcgenhance/bcgenhance/tree/master/BCG_EnhancedEnergyAlg

This project includes the following functions:

FUNCTION 1. ENERGYALG_ORIG

[EngPk_Vals, EngPk_Locs, EnergyWave]=ME_EnergyAlg_Orig(inputSignal, Fs)

Description: This code is the "original" code that BoYu used for the energy algorithm paper. Here I just have some small code updates:

- Used my filtering code, to enforce zero-phase filtering using the filtfilt function, and then my bandpass implementation.
- Replaced the for-loop with the more efficient movsum, which will also generate the output in the same length (plus)
- Added a little extra smoothing, to make it like the original energy (for simplicity of the code)

Input arguments:

- *inputSignal:* The BCG signal that we want to compute its energy.
- *Fs:* Sample rate of the signal in Hz.

Output Parameters:

- *EngPk_Vals*: The value/amplitude of the energy waveform at its peaks.
- *EngPk_Locs*: The location/timing of the peaks of energy waveform.
- *EnergyWave*: The complete energy waveform/signal created here.

FUNCTION 2. ME_ENERGYALG_ENHANCED_SHORT

[EngPk_Locs] = ME_EnergyAlg_Enhanced_Short(inputSignal, Signal_FS)

Description: Simply trying to resolve the problems with the original energy algorithm as described in my dissertation. This function assumes the signal is in an acceptably short length. I use the following steps:

1. Filter the signal,
2. Compute its first derivative (related to the elder's deformation)
3. Smooth it by means of the movmean
4. Subtract the lower envelope to have all positive values
5. Compute the energy of this waveform
6. Smooth is in a step by step manner to get better results
7. Filter the energy for the range of 0.7-2.5Hz, which are the normal range of heart rate frequency.
8. Find the peaks of energy function in a two-step manner, to make it more precise.
9. Remove the outlier peaks using ME_RemoveOutlier_BeatLocations
10. Refine the location of J-peaks using the ME_FindClosestBCG_Peak
11. Remove the outlier locations ME_RemoveOutlier_BeatLocations

Input arguments:

- *inputSignal*: input BCG signal to compute its energy.
- *Signal_FS*: sample rate of the input signal.

Output arguments:

- *EngPk_Locs:* the enhanced location of the J-peaks using this function. These locations can be used to estimation the heart rate.

FUNCTION 3. ME_FINDCLOSESTBCG_PEAK

[closestBCG_Locs] = ME_FindClosestBCG_Peak(inputBCG, Ref_Locs, Fs)

Description: As mentioned in the dissertation, the J-peaks do not necessarily match the peaks of the energy algorithm. This function uses some ref_locs as the location of energy peaks and finds the closest J-peak to each of them. To resolve some of the exceptional cases, I first find the two closest peaks and then pick the one that has the highest amplitude. This function will provide a more realistic information about the location of J-peaks.

Input arguments:

- *inputBCG:* the input BCG signal.
- *Ref_Locs:* the reference locations which usually are the peaks of the energy waveform.
- *Fs:* the sample rate of the input signal.

Output arguments:

- *closestBCG_Locs:* the location of the closest J-peak to each of the input reference locations.

FUNCTION 4. ME_COMPUTE_B2BHR

[Interp_B2B_HR, Interp_Time] = ME_Compute_B2BHR(input_BeatLocs,input_Fs, output_Fs, output_DurInSeconds, filterOutliers)

Description: To provide a central function to compute the continuous HR estimates, from the estimated peak locations. I am doing an interpolation between the B2B HR estimates with the minimum amount of smoothing and correction, to stay close to the real estimations. If your goal is just the overall heart rate for a window of X minutes, do not hesitate to apply outlier removal and smoothing on top of this.

Input arguments:

- *input_BeatLocs:* the input locations of each cardiac cycle, like the J-peak locations.
- *input_Fs:* the sample rate of the input signal.
- *output_Fs:* it will interpolate the estimated HR values to any sample rate. Thus, you can easily compare the HR from different sources.
- *output_DurInSeconds:* In case you just need a subset of the data.
- *filterOutliers:* A Boolean flag to enable outlier cancellation.

Output arguments:

- Interp_B2B_HR: the interpolated HR values based on the *output_Fs* parameter.
- Interp_Time: the timing of the estimated HR locations.

FUNCTION 5. PHD_DEF_ENERGYALG_ENHANCED

[jLocs, jjHR, jjTimes] = PHD_DEF_EnergyAlg_Enhanced(inputSignal, Signal_FS, HR_FS)

Description: Enhancing the accuracy of beat detection using the energy idea. If the signal is longer than a certain threshold, it will cut the signal and estimate on each segment separately. The idea here is, due to the movement of the subject between transducers and also other artifacts, the quality

of the signal would change; thus, we cannot apply the same preparation on the entire signal, and it is better to do localized preparation.

Input arguments:

- inputSignal: Input BCG signal
- Signal_FS: the sample rate of the input signal
- HR_FS: the sample rate of the output heart rate.

Output arguments:

- jLocs: detected location of J-peaks
- jjHR: estimated HR based on the JJ-intervals
- jjTimes: the estimated JJ-intervals

PROJECT II. NOISE REDUCTION

This project focuses on the reduction of noise from the BCG signal. Two main techniques are used here, including the wavelet transform and empirical mode decomposition. Files are already pushed to the following path in our GitLab:

https://gitlab.missouri.edu/CERT-Students/studentProjects/bcgenhance/bcgenhance/tree/master/BCG_NoiseReduction

FUNCTION 6. MATLAB FILE NAMED: PHD_DEF_DENOISESIGNALS.M

Description: This file is the main code to load, process, and denoise the BCG signals. It will search for all files in a source folder and using a for loop goes through each of them to create a denoised version, and then saves that denoised file in the destination folder.

It contains the following functions:

FUNCTION 7. DENOISE_SINGLE_CHANNEL

[Den]=Denoise_Single_Channel(inputSignal, sourceFs, targetFs)

Description: takes an input BCG signal and denoise it using the following steps:

1. Downsample the signal, to reduce the complexity and improve the computational time.
2. Bandpass the signal to get the BCG components.
3. Apply different denoising techniques
    a. Empirical mode decomposition (EMD) on it.
    b. Ensemble empirical mode decomposition (EEMD) on it.
    c. Wavelet decomposition

Input parameters:

- *inputSignal*: the input BCG signal
- *sourceFs*: the sample rate of the input signal
- *targetFs*: the requested sample rate for the output denoised signal

Output parameters:

- *Den*: the denoised version of the input signal in the requested sample rate, in the Table format. In this table, each column has its label, which makes it easy to retrieve the following:
    - The input signal after downsampling, as the reference.
    - The bandpass filtered signal, as the reference.
    - IMFs number 2 to 4 from the EMD.
    - IMFs number 2 to 4 from the EEMD.
    - The detail coefficients of multiple wavelets.

FUNCTION 8. WAVELETDECOMPOSITION

[DC3, DC4, DC6] = WaveletDecomposition(inputSignal, WaveletName)

Description: will apply the wavelet decomposition using the specified mother wavelet.

Input parameters:

- *inputSignal*: the input BCG signal to be denoised
- *WaveletName*: the name of the mother wavelet, as defined by Matlab, could be one of the followings: db8, Sym8, coif5, bior3.5, bior3.9, haar.

Output arguments:

- *DC3, DC4, DC5:* are the 3 detail coefficients of the wavelet decomposition, as my experiments show the best value from these three.

PROJECT III. CHANNEL SELECTION

This project, as described in the dissertation, focuses on different approaches to find the best transducer. My selected approach goes through the use of Signal Quality Indices (SQIs) that I have the code for each one here. Also, here, I have provided the functions which use these SQI indices to make the actual channel selection. Files and codes of this project are pushed to our GitLab at: https://gitlab.missouri.edu/CERT-Students/studentProjects/bcgenhance/bcgenhance/tree/master/BCG_ChannelSelection

This project contains the following files and functions:

FUNCTION 9. PHD_DEF_UPDATE_NEWSQIS.M

Description: This file will compute the selected SQI values and append them to the current files if one exists. You can add more SQI indices here for your experiments.

FUNCTION 10. PHD_DEF_CHANNELSELECTION_VS_SQI.M

Description: This file is the main function of this project with loads all BCG files from a source folder and computes the "hit rate" of how well different channel selections match each other, using the following functions:

FUNCTION 11. HITORMISS

[HitPrc, MissPrc, Hit, Miss]=HitOrMiss(ErrorVector, SQIVector, sqiSortByMax, sqiVales)

Description: compares the SQI based channel selection to the oracle channel selection (the channel with the lowest error), by comparing the following methods:

1. Find the selected transducers based on Error (the oracle)
2. Find the selected transducers based on SQI

Then it computes the "hit rate" by counting the number of overlaps between these approaches.

Input arguments:

- *ErrorVector*: the estimation error of each channel as the reference.
- *SQIVector*: the SQI value computed for each channel.
- *sqiSortByMax*: the order of SQI, true corresponds to the ascending order.
- *sqiVales*: the range of the SQI measurements.

Output arguments:

- *HitPrc*: Percentage of overlap or Hit.
- *MissPrc*: Percentage of cases that no overlap exists.
- *Hit*: number of cases for the hit.
- *Miss*: number of cases for miss.

FUNCTION 12. SELECTTRANS_BY_MIN_ERROR

[selected_ch] = selectTrans_by_min_error(ErrorVector)

Description: find the transducer with the minimum error (oracle), with a 5% tolerance.

Input arguments:

- *ErrorVector*: the average error rate of each channel.

Output arguments:

- *Selected_ch*: is the selected transducers

FUNCTION 13. SELECTTRANS_BY_MIN_SQI

[selected_ch] = selectTrans_by_min_SQI(SQIVector, SQI_thr, sqiSortByMax, sqiRange)

Description: Uses the SQI value of each transducer to find the one with the best value. For some SQI indices, the best value is the lowest one, and for some, the best is the highest one. The sqiSortByMax input parameter defines this order. Here again, I am considering a tolerance in defining the best value.

Input arguments:

- *SQIVector*: a vector with the SQI values related to all channels.
- *SQI_thr*: not defined.
- *sqiSortByMax*: defines the sort order. If true, means SQI with maximum value is better.
- *sqiRange*: defines the maximum range for that SQI over all data.

Output arguments:

- *selected_ch*: the selected channel with the best SQI.

FUNCTION 14. PHD_DEF_SQI_SNR

[SNR] = PHD_DEF_SQI_SNR(inputSignal, Fs)

Description: computes the signal to noise ratio (SNR) of a signal based on my definition for signal (bandpass filter), and the noise (the rest of components). I used the ratio between the MAD of these two components as the measure of SNR.

ref: Optimal Signal Quality Index for Photoplethysmogram Signals, Mohamed Elgendi

Input arguments:

- *inputSignal*: the input BCG signal.
- *Fs*: the sample rate of the signal.

Output arguments:

- *SNR*: the computed SNR for that signal.

FUNCTION 15. PHD_DEF_SQI_NOISEINTENSITY_ISCHANGE

[intensity]=PHD_DEF_SQI_NoiseIntensity_ischange(selectedChannel)

Description: another SQI measure. I used Matlab's ischange function here and then computed the intensity of the noise as the ratio between the duration of the noisy part to the entire length of the signal.

Input arguments:

- *selectedChannel*: the input BCG signal of one channel

Output arguments:

- *intensity*: the noise intensity or density of the noise.

FUNCTION 16. PHD_DEF_SQI_NOISEINTENSITY_CUSUM

[intensity]=PHD_DEF_SQI_NoiseIntensity_Cusum(selectedChannel)

Description: another SQI measure. I used Matlab's cusum function here and then computed the intensity of the noise using a threshold of 100.

Input arguments:

- *selectedChannel*: the input BCG signal of one channel

Output arguments:

- *intensity*: the noise intensity or density of the noise.

FUNCTION 17. PHD_DEF_SQI_BANDPOWERRATIO

powerRatio = PHD_DEF_SQI_BandPowerRatio(inputSignal, Fs)

Description: uses Matlab's bandpower to estimate the frequency power of a signal inside a frequency range. To do that I defined two frequency ranges of MidPower and AllPower and computed their ration.

Input arguments:

- *inputSignal*: the input BCG signal of one channel.
- *Fs*: the sample rate of the signal.

Output arguments:

- *powerRatio*: the power ratio SQI.

PROJECT IV. TEMPLATE CREATION

In this project, I have included all codes that are needed to create templates from periodic signals such as BCG. The general idea is to use some reference point to cut the signal into segments and then create a morphological ensemble average from them. The code is pushed onto our GitLab repository at:

https://gitlab.missouri.edu/CERT-Students/studentProjects/bcgenhance/bcgenhance/tree/master/BCG_TemplateCreation

FUNCTION 18. PHD_DEF_CREATETEMPLATES_FORALL_ECG_RPEAK.M

This file contains the overall flow of creating BCG (or any signal) templates using some reference events. It will load all data files from the source folder. These files are suggested to be denoised but could be any filtered signal. It will create a template for each channel of those files using another function named PHD_DEF_CreateTemplates. Then will save the created templates inside the destination folder with the same name.

FUNCTION 19. PHD_DEF_INSPECTINGTEMPLATESVISUALLY.M

This file provides a visual inspection evaluation of ECG-Based Templates for each file. This can be helpful in demonstrating the effect of denoising on the templates. It will simply load a file of templates and plot them in a figure.

FUNCTION 20. PHD_DEF_CREATETEMPLATES

[theTemplate,SplittedBCG_Array] = PHD_DEF_CreateTemplates(inputSignal, refEvents)

Description: This function will create morphological templates from a signal by means of a reference event vector. The general process is as follows:

1. Use the reference events to cut the signal into small segments (of one cycle)
2. Normalize each segment in length and height (you can change these if you want)
3. Align all segments together using cross-correlation.
4. Compute the average of all segments to create a template.

Input parameters:

- *inputSignal*: the input BCG signal that should be filtered already.
- *refEvents*: the reference events such as ECG R-peaks.

Output arguments:

- theTemplate: the result template after going through all steps.
- SplittedBCG_Array: the segmented peace of the signal that is used in the creation of the template.

FUNCTION 21. PHD_DEF_SPLITESIGNALBYEVENT

[SplittedData] = PHD_DEF_SpliteSignalByEvent(InputSignal, events, numConcats, extraLength)

Description: To cut/split the inputSignal (i.e. BCG) into small segments based on the events (such as ECG_R_Locs).

Input arguments:

- *InputSignal*: the input BCG signal.
- *events*: the reference events such as the ECG R-peaks used to cut the signal.
- *numConcats*: if you want to create templates of two or more consecutive cycles.
- *extraLength*: if you want to include part of the next beat as well, for visualization.

Output arguments:

- *SplittedData*: a cell array containing all signal segments based on the provided events.

FUNCTION 22. PHD_DEF_ALIGNESIGNALS

[outputSignals,outputLags,corrVals,theMedoidIndex] = PHD_DEF_AligneSignals (signalsTobeAligned, minCorreleation, maxLagPercent, alignBy)

Description: will use the cross-validation to align multiple signal segments together. The user can define thresholds for the minimum correlation and maximum time lag computed between the

signals. If any signal happens to be outside of this threshold, it will be considered noisy and will be discarded.

Input arguments:

- *signalsTobeAligned*: the input segments to be aligned together.
- *minCorreleation*: the segments will be discarded if its correlation to the reference goes below this.
- *maxLagPercent*: the segments will be discarded if their time lag from reference goes above this.
- *alignBy*: used to create the reference template and could be Centroid or Median.

Output arguments:

- *outputSignals*: the remaining segments after alignment that pass the thresholds.
- *outputLags*: the time lag of each segment with respect to the reference template.
- *corrVals*: the correlation values of each segment with respect to the reference template.
- *theMedoidIndex*: the index of the medoid segment which used as the reference.

FUNCTION 23. PHD_DEF_SHIFTTOALIGN

[alignedSignal] = PHD_DEF_ShiftToAlign(currentToBeAlign, lagDiff)

Description: will shift the input segments by the amount provided in the lagDiff, to make them aligned.

Input arguments:

- *currentToBeAlign*: the cell array of segments to be shifted and aligned.
- *lagDiff*: the vector of lag values used for the shifting.

Output arguments:

- *alignedSignal*: the cell array of aligned segments.

FUNCTION 24. PHD_DEF_NORMALIZECELLARRAY

[normalizedSignal] = PHD_DEF_NormalizeCellArray(inputCellArray, normHeight, normWidth, strechWidth, cutWidth)

Description: To normalize elements of a cell array under different criteria, for example stretching the length or normalizing the height. This is sometimes very important in creating reasonable templates. I used the imresize to stretch the signals in length.

Input arguments:

- *inputCellArray*: a cell array of input segments which we want to normalize.
- *normHeight*: set true if you want the height of all to be normalized.
- *normWidth*: set true if you want all to have the same length.
- *strechWidth*: the length of each segment after stretching.
- *cutWidth*: if you just need a subsegment of each signal.

Output arguments:

- *normalizedSignal*: the array cell of normalized segments.

FUNCTION 25. PHD_DEF_AVERAGE_CENTROID

[theCentroid,theCentroidIndex] = PHD_DEF_Average_Centroid(matrix)

Description: This function is a combination of medoid and median it first finds the median of all signals, which is not necessarily a signal from the set then tries to find the closest signal to the median, and an actual representative. The process is as follows:

1. Filter outliers and Find the median of all signals.
2. Find the distance of all to the median
3. Remove outlier signals by means of their distance matrix.
4. Choose the signal with minimum distance to the median.

Input arguments:

- *matrix*: the matrix of input segments that are used in creating the template.

Output argument:

- *theCentroid*: the resulting signal which has the minimum distance to the median.
- *theCentroidIndex*: the index of the centroid among all segments.

FUNCTION 26. PHD_DEF_CELLARRAY2MATRIX

[theMatrix] = PHD_DEF_CellArray2Matrix(theCellArray,theAlignment,theWidth, withNaN)

Description: this function is designed to create a matrix from any cell array. The important point is in the cell array the length of elements might be different. This happens, for example, as a result of normal variation in the RR intervals. The general process is:

1. Find max array length of the cell(width).
2. Create the result matrix.
3. Fill the new matrix with the original data.
4. Will resample each sequence to get to the same length

Input arguments:

- *theCellArray*: the input cell array with elements (signal segments) of different length.
- *theAlignment*: could be one of 'LEFT', 'CENTER', 'RIGHT', or 'RESAMPLE'. The last one will resample each sequence to get to the same length.
- *theWidth*: could be 'MAX', 'MIN', or 'MEAN' of the length of all segments.

- *withNaN*: provides 3 different approaches to deal with the NaN values.

Output arguments:

- *theMatrix*: the output matrix of all elements with the same length.

REFERENCES

[1] E. J. Benjamin *et al.*, "Heart Disease and Stroke Statistics-2019 Update: A Report From the American Heart Association," *Circulation,* vol. 139, no. 10, pp. e56-e528, Mar 5 2019.

[2] O. T. Inan, M. Etemadi, R. M. Wiard, L. Giovangrandi, and G. T. Kovacs, "Robust ballistocardiogram acquisition for home monitoring," *Physiological Measurement,* vol. 30, no. 2, pp. 169-85, Feb 2009.

[3] O. T. Inan, G. T. Kovacs, and L. Giovangrandi, "Evaluating the lower-body electromyogram signal acquired from the feet as a noise reference for standing ballistocardiogram measurements," (in English), *IEEE Transactions on Information Technology in Biomedicine,* vol. 14, no. 5, pp. 1188-96, Sep 2010.

[4] E. Pinheiro, O. Postolache, and P. Girao, "Study on Ballistocardiogram Acquisition in a Moving Wheelchair with Embedded Sensors," (in English), *Metrology and Measurement Systems,* vol. 19, no. 4, pp. 739-750, 2012.

[5] G. Guidoboni *et al.*, "Cardiovascular function and ballistocardiogram: a relationship interpreted via mathematical modeling," *arXiv,* no. arXiv:.01044, 2018.

[6] E. Pinheiro, O. Postolache, and P. Girao, "Theory and developments in an unobtrusive cardiovascular system representation: ballistocardiography," *Open Biomedical Engineering Journal,* vol. 4, pp. 201-16, 2010.

[7] J. M. Perez-Macias, J. Viik, A. Varri, S. L. Himanen, and M. Tenhunen, "Spectral analysis of snoring events from an Emfit mattress," *Physiological Measurement,* vol. 37, no. 12, pp. 2130-2143, Dec 2016.

[8] C. Brüser, A. Kerekes, S. Winter, and S. Leonhardt, "Multi-channel optical sensor-array for measuring ballistocardiograms and respiratory activity in bed," in *Engineering in Medicine and Biology Society (EMBC), 2012 Annual International Conference of the IEEE*, 2012, pp. 5042-5045: IEEE.

[9] A. Akhbardeh *et al.*, "Towards a heart disease diagnosing system based on force sensitive chair's measurement, biorthogonal wavelets and neural networks," (in English), *Engineering Applications of Artificial Intelligence,* vol. 20, no. 4, pp. 493-502, Jun 2007.

[10] O. T. Inan, M. Etemadi, L. B. Giovangrandi, G. T. Kovacs, and R. M. Wiard, "Weighing scale and sensor systems and methods for monitoring heart function," 2015.

[11] K. Lydon *et al.*, "Robust heartbeat detection from in-home ballistocardiogram signals of older adults using a bed sensor," in *Engineering in Medicine and Biology Society (EMBC), 2015 37th Annual International Conference of the IEEE*, 2015, pp. 7175-7179: IEEE.

[12] M. Enayati, M. Skubic, J. M. Keller, M. Popescu, and N. Z. Farahani, "Sleep Posture Classification Using Bed Sensor Data and Neural Networks," in *Engineering in Medicine and Biology Society (EMBC), 2018 40th Annual International Conference of the IEEE*, 2018: IEEE.

[13] B. Y. Su *et al.*, "Monitoring the Relative Blood Pressure Using a Hydraulic Bed Sensor System," *IEEE Transactions on Biomedical Engineering*, 2018.

[14] R. M. Wiard, O. T. Inan, B. Argyres, M. Etemadi, G. T. Kovacs, and L. Giovangrandi, "Automatic detection of motion artifacts in the ballistocardiogram measured on a modified bathroom scale," *Medical & Biological Engineering & Computing*, vol. 49, no. 2, pp. 213-20, Feb 2011.

[15] H. W. March, "Three-plane ballistocardiography: the effect of age on the longitudinal, lateral, and dorsoventral ballistocardiograms," *Circulation*, vol. 12, no. 5, pp. 869-82, Nov 1955.

[16] I. Starr and F. C. Wood, "Twenty-year studies with the ballistocardiograph," *Circulation*, vol. 23, no. 5, pp. 714-732, 1961.

[17] J. Earisman, "Passive Biometric Authentication via Head Mounted Display using Ballistocardiography," Ph.D. Major Qualifying Project, Worcester Polytechnic Institute, 2017.

[18] J. W. Gordon, "Certain Molar Movements of the Human Body produced by the Circulation of the Blood," *Journal of Anatomy and Physiology*, vol. 11, no. Pt 3, pp. 533-6, Apr 1877.

[19] S. W. Moss, "Alonzo Thrasher Keyt," *Clinical Cardiology*, vol. 29, no. 10, pp. 471-3, Oct 2006.

[20] Y. Henderson, "The mass-movements of the circulation as shown by a recoil curve," *American Journal of Physiology-Legacy Content*, vol. 14, no. 3, pp. 287-298, 1905.

[21] G. Angenheister and E. Lau, "Seismographische Aufnahmen der Herztätigkeit," *Naturwissenschaften*, vol. 16, no. 25, pp. 513-515, 1928.

[22] E. Abramson, "Die Rückstoßkurve des Herzens (Kardiodynamogramm) 1," *Skandinavisches Archiv Für Physiologie*, vol. 66, no. 2, pp. 191-224, 1933.

[23] I. Starr, "Essay on the ballistocardiogram," *Journal of the American Medical Association (JAMA)*, vol. 155, no. 16, pp. 1413-25, Aug 14 1954.

[24] I. Starr, "Prognostic Value of Ballistocardiograms. Studies on Evaluation of the Doctor's Experience," *Journal of the American Medical Association (JAMA)*, vol. 187, no. 7, pp. 511-7, Feb 15 1964.

[25] J. Alametsä and J. Viik, "Twelve Years Follow-up of Ballistocardiography," in *Joint Conference of the European Medical and Biological Engineering Conference (EMBEC) and the Nordic-Baltic Conference on Biomedical Engineering and Medical Physics (NBC)*, Tampere, Finland, 2017, pp. 1117-1120, Singapore: Springer.

[26] T. N. Lynn and S. Wolf, "The prognostic significance of the ballistocardiogram in ischemic heart disease," *American Heart Journal*, vol. 88, no. 3, pp. 277-80, Sep 1974.

[27] Y. V. Erina, "The Significance of the Time Interrelationships in Ballistocardiographic Analysis," JOINT PUBLICATIONS RESEARCH SERVICE ARLINGTON VA1960.

[28] W. R. Scarborough *et al.*, "A ballistocardiographic study of 369 apparently normal persons; an analysis of normal and borderline ballistocardiograms," *American Heart Journal,* vol. 45, no. 2, pp. 161-89, Feb 1953.

[29] W. B. Abrams and H. D. Edger, "A Ballistocardiographic study of healthy young adult males," *Circulation,* vol. 8, no. 5, pp. 738-43, Nov 1953.

[30] L. Brotmacher, "The normal ballistocardiogram," *British Heart Journal,* vol. 18, no. 2, pp. 145-52, Apr 1956.

[31] R. J. Jones, "The Nickerson ballistocardiogram in arteriosclerotic heart disease with and without congestive failure," *Circulation,* vol. 6, no. 3, pp. 389-401, 1952.

[32] C. B. Henderson, "Ballistocardiograms after cigarette smoking in health and in coronary heart disease," *British Heart Journal,* vol. 15, no. 3, pp. 278-86, Jul 1953.

[33] M. Moser, L. Pordy, K. Chesky, R. C. Taymor, and A. M. Master, "The ballistocardiogram in myocardial infarction: a study of one hundred cases," *Circulation,* vol. 6, no. 3, pp. 402-7, Sep 1952.

[34] H. Mandelbaum and R. A. Mandelbaum, "Studies utilizing the portable electromagnetic ballistocardiograph. I. Abnormal HIJK patterns in hypertensive and coronary artery heart disease," *Circulation,* vol. 3, no. 5, pp. 663-73, May 1951.

[35] L. Pordy, R. C. Taymor, M. Moser, K. Chesky, and A. M. Master, "Clinical evaluation of the ballistocardiogram. I. Normal subjects," *American Heart Journal,* vol. 42, no. 3, pp. 321-7, Sep 1951.

[36] H. R. Brown Jr, M. J. Hoffman, and V. de Lalla Jr, "Ballistocardiographic findings in patients with symptoms of angina pectoris," *Circulation,* vol. 1, no. 1, pp. 132-140, 1950.

[37] I. Starr *et al.*, "First report of the committee on ballistocardiographic terminology," *Circulation,* vol. 7, no. 6, pp. 929-931, 1953.

[38] I. Starr, "The place of the ballistocardiogram in a Newtonian cardiology; and the new light it sheds on certain old clinical problems," *Proceedings of the Royal Society of Medicine,* vol. 60, no. 12, pp. 1297-306, Dec 1967.

[39] I. Starr, A. Rawson, H. Schroeder, and N. Joseph, "Studies on the estimation of cardiac ouptut in man, and of abnormalities in cardiac function, from the heart's recoil and the blood's impacts; the ballistocardiogram," *American Journal of Physiology-Legacy Content,* vol. 127, no. 1, pp. 1-28, 1939.

[40] I. Starr and H. A. Schroeder, "Ballistocardiogram. II. Normal standards, abnormalities commonly found in diseases of the heart and circulation, and their significance," *The Journal of clinical investigation,* vol. 19, no. 3, pp. 437-450, 1940.

[41] E. W. Bixby and C. B. Henderson, "A method of securing the direct body ballistocardiogram by means of a microscope, giving a record readily calibrated," *Circulation,* vol. 8, no. 4, pp. 579-84, Oct 1953.

[42] N. Kohden. (1953, 03/04/2019). *MB-1 Ballistocardiograph*. Available: https://www.nihonkohden.com/company/history/1950s.html

[43] H. C. Burger, A. Noordergraaf, and A. M. Verhagen, "Physical basis of the low-frequency ballistocardiograph," *American Heart Journal,* vol. 46, no. 1, pp. 71-83, Jul 1953.

[44] K. Tavakolian, "Characterization and analysis of seismocardiogram for estimation of hemodynamic parameters," Ph.D. Dissertation, Engineering Science Department, Applied Science: School of Engineering Science, 2010.

[45] B. Ngai, K. Tavakolian, A. Akhbardeh, A. P. Blaber, B. Kaminska, and A. Noordergraaf, "Comparative analysis of seismocardiogram waves with the ultra-low frequency ballistocardiogram," in *Engineering in Medicine and Biology Society, 2009. EMBC 2009. Annual International Conference of the IEEE*, 2009, pp. 2851-2854: IEEE.

[46] J. L. Nickerson and H. J. Curtis, "The design of the ballistocardiograph," *American Journal of Physiology-Legacy Content,* vol. 142, no. 1, pp. 1-11, 1944.

[47] W. R. Scarborough and S. A. Talbot, "Proposals for ballistocardiographic nomenclature and conventions: revised and extended report of Committee on Ballistocardiographic Terminology," *Circulation,* vol. 14, no. 3, pp. 435-50, Sep 1956.

[48] W. Dock and F. Taubman, "Some technics for recording the ballistocardiogram directly from the body," *The American Journal of Medicine,* vol. 7, no. 6, pp. 751-755, 1949.

[49] S. R. Arbeit and N. Lindner, "A new full-frequency range calibrated ballistocardiograph. I: Recording the body ballistics in displacement, velocity, and accelleration," *American Heart Journal,* vol. 45, no. 1, pp. 52-59, 1953.

[50] R. P. Walker, T. J. Reeves, K. Willis, L. Christianson, J. R. Pierce, and D. Kahn, "The effect of surface and recording technique on the direct ballistocardiogram," *American Heart Journal,* vol. 46, no. 2, pp. 166-79, Aug 1953.

[51] J. Alametsa, J. Viik, J. Alakare, A. Varri, and A. Palomaki, "Ballistocardiography in sitting and horizontal positions," *Physiological Measurement,* vol. 29, no. 9, pp. 1071-87, Sep 2008.

[52] K. Tavakolian, A. Akhbardeh, and B. Kaminska, "An Objective Approach towards Assessment of the Physiological Age of Heart," in *AAAI Fall Symposium: AI in Eldercare: New Solutions to Old Problems*, 2008, pp. 131-133.

[53] A. Martin-Yebra *et al.*, "Evaluation of respiratory- and postural-induced changes on the ballistocardiogram signal by time warping averaging," (in English), *Physiological Measurement,* vol. 38, no. 7, pp. 1426-1440, Jun 27 2017.

[54] J. Alihanka, K. Vaahtoranta, and I. Saarikivi, "A new method for long-term monitoring of the ballistocardiogram, heart rate, and respiration," *The Journal of Physiology*, vol. 240, no. 5, pp. R384-92, May 1981.

[55] O. Postolache, P. S. Girao, G. Postolache, and M. Pereira, "Vital signs monitoring system based on emfi sensors and wavelet analysis," in *Instrumentation and Measurement Technology Conference Proceedings, 2007. IMTC 2007. IEEE*, 2007, pp. 1-4: IEEE.

[56] J. Lekkala and M. Paajanen, "EMFi-New electret material for sensors and actuators," in *Electrets, 1999. ISE 10. Proceedings. 10th International Symposium on*, 1999, pp. 743-746: IEEE.

[57] M. Paajanen, J. Lekkala, and H. Valimaki, "Electromechanical modeling and properties of the electret film EMFI," (in English), *IEEE Transactions on Dielectrics and Electrical Insulation*, vol. 8, no. 4, pp. 629-636, Aug 2001.

[58] C. Bruser, K. Stadlthanner, S. de Waele, and S. Leonhardt, "Adaptive beat-to-beat heart rate estimation in ballistocardiograms," *IEEE Transactions on Information Technology in Biomedicine*, vol. 15, no. 5, pp. 778-86, Sep 2011.

[59] G. S. Chung, J. S. Lee, S. H. Hwang, Y. K. Lim, D.-U. Jeong, and K. S. Park, "Wakefulness estimation only using ballistocardiogram: Nonintrusive method for sleep monitoring," in *Engineering in Medicine and Biology Society (EMBC), 2010 Annual International Conference of the IEEE*, 2010, pp. 2459-2462: IEEE.

[60] W. K. Lee, H. Yoon, C. Han, K. M. Joo, and K. S. Park, "Physiological Signal Monitoring Bed for Infants Based on Load-Cell Sensors," *Sensors (Basel)*, vol. 16, no. 3, p. 409, Mar 19 2016.

[61] M. Nagura, Y. Mitsukura, T. Kishimoto, and M. Mimura, "A practical BCG measuring system with bed sensors and algorithm for heartbeat detection," in *Advanced Motion Control (AMC), 2018 IEEE 15th International Workshop on*, 2018, pp. 317-321: IEEE.

[62] M. Etemadi, O. T. Inan, R. M. Wiard, G. T. Kovacs, and L. Giovangrandi, "Non-invasive assessment of cardiac contractility on a weighing scale," in *Engineering in Medicine and Biology Society, 2009. EMBC 2009. Annual International Conference of the IEEE*, 2009, pp. 6773-6776: IEEE.

[63] O. T. Inan, D. Park, G. T. Kovacs, and L. Giovangrandi, "Multi-signal electromechanical cardiovascular monitoring on a modified home bathroom scale," in *2011 Annual International Conference of the IEEE Engineering in Medicine and Biology Society*, 2011, pp. 2472-2475: IEEE.

[64] (2019, 03/04/2019). *Murata SCA61T inclinometer, Murata Manufacturing Co., Ltd.* Available: http://www.murata.com/products/sensor/inclinometer/sca61t

[65] (2019, 03/04/2019). *Contactless Bed Sensor, Accelerometers, Sensors*. Available: http://www.murata.com/products/sensor/accel/sca10h_11h

[66] O. T. Inan *et al.*, "Ballistocardiography and seismocardiography: a review of recent advances," *IEEE Journal of Biomedical and Health Informatics*, vol. 19, no. 4, pp. 1414-27, Jul 2015.

[67] P.-F. Migeotte *et al.*, "Three dimensional ballisto-and seismo-cardiography: HIJ wave amplitudes are poorly correlated to maximal systolic force vector," in *2012 Annual International Conference of the IEEE Engineering in Medicine and Biology Society*, 2012, pp. 5046-5049: IEEE.

[68] M. Di Rienzo *et al.*, "A wearable system for the seismocardiogram assessment in daily life conditions," in *Engineering in Medicine and Biology Society, EMBC, 2011 Annual International Conference of the IEEE*, 2011, pp. 4263-4266: IEEE.

[69] Z. Chen, J. T. Teo, S. H. Ng, and X. Yang, "Portable fiber optic ballistocardiogram sensor for home use," in *Optical Fibers and Sensors for Medical Diagnostics and Treatment Applications XII*, 2012, vol. 8218, p. 82180X: International Society for Optics and Photonics.

[70] D. C. Mack, J. T. Patrie, P. M. Suratt, R. A. Felder, and M. A. Alwan, "Development and preliminary validation of heart rate and breathing rate detection using a passive, ballistocardiography-based sleep monitoring system," (in English), *IEEE Transactions on Information Technology in Biomedicine*, vol. 13, no. 1, pp. 111-20, Jan 2009.

[71] K. Watanabe, T. Watanabe, H. Watanabe, H. Ando, T. Ishikawa, and K. Kobayashi, "Noninvasive measurement of heartbeat, respiration, snoring and body movements of a subject in bed via a pneumatic method," *IEEE Transactions on Biomedical Engineering*, vol. 52, no. 12, pp. 2100-7, Dec 2005.

[72] X. Zhu *et al.*, "Real-time monitoring of respiration rhythm and pulse rate during sleep," *IEEE Transactions on Biomedical Engineering*, vol. 53, no. 12 Pt 1, pp. 2553-63, Dec 2006.

[73] R. Rate, "Emfit Sensor Technology," *Journal of Medical Systems*, vol. 31, pp. 69-77, 2007.

[74] B. E. Westerhof, J. Gisolf, W. J. Stok, K. H. Wesseling, and J. M. Karemaker, "Time-domain cross-correlation baroreflex sensitivity: performance on the EUROBAVAR data set," *Journal of Hypertension*, vol. 22, no. 7, pp. 1371-80, Jul 2004.

[75] D. Heise, Licet Rosales, Mary Sheahen, Bo-Yu Su, and Marjorie Skubic., "Non-invasive measurement of heartbeat with a hydraulic bed sensor Progress, challenges, and opportunities," in *Instrumentation and Measurement Technology Conference (I2MTC)*, Minneapolis, MN, USA, 2013.

[76] L. Rosales, "Short-term heart rate variability as a general indicator of health estimated by ballistocardiography using a hydraulic bed sensor in elder care," Ph.D., University of Missouri--Columbia, 2016.

[77] U. R. Acharya *et al.*, "Application of empirical mode decomposition (EMD) for automated identification of congestive heart failure using heart rate signals," (in English), *Neural Computing & Applications*, vol. 28, no. 10, pp. 3073-3094, Oct 2017.

[78] A. Ullal, "Non-invasive monitoring of vital signs using recliner chair and respiratory pattern analysis," Masters, Electrical and Computer Engineering, University of Missouri--Columbia, 2018.

[79] R. Kumar, A. Bayliff, D. De, A. Evans, S. K. Das, and M. Makos, "Care-chair: sedentary activities and behavior assessment with smart sensing on chair backrest," in *2016 IEEE International Conference on Smart Computing (SMARTCOMP)*, 2016, pp. 1-8: IEEE.

[80] B. W. Lee and H. Shin, "Feasibility Study of Sitting Posture Monitoring Based on Piezoresistive Conductive Film-Based Flexible Force Sensor," (in English), *IEEE Sensors Journal*, vol. 16, no. 1, pp. 15-16, Jan 2016.

[81] J. Meyer, B. Arnrich, J. Schumm, and G. Troster, "Design and Modeling of a Textile Pressure Sensor for Sitting Posture Classification," (in English), *IEEE Sensors Journal*, vol. 10, no. 8, pp. 1391-1398, Aug 2010.

[82] H. Z. Tan, L. A. Slivovsky, and A. Pentland, "A sensing chair using pressure distribution sensors," (in English), *IEEE/ASME TRANSACTIONS ON MECHATRONICS*, vol. 6, no. 3, pp. 261-268, Sep 2001.

[83] S. Junnila, A. Akhbardeh, A. Varri, and T. Koivistoinen, "An EMFi-film sensor based ballistocardiographic chair: performance and cycle extraction method," in *IEEE Workshop on Signal Processing Systems Design and Implementation, 2005.*, 2005, pp. 373-377: IEEE.

[84] H. J. Baek, G. S. Chung, K. K. Kim, and K. S. Park, "A smart health monitoring chair for nonintrusive measurement of biological signals," *IEEE Transactions on Information Technology in Biomedicine*, vol. 16, no. 1, pp. 150-8, Jan 2012.

[85] T. Fu and A. Macleod, "Intellichair: An approach for activity detection and prediction via posture analysis," in *2014 International Conference on Intelligent Environments*, 2014, pp. 211-213: IEEE.

[86] KionixInc. (4/9/2019). *Evaluation board for KXR94-2283*. Available: https://www.digikey.com/product-detail/en/kionix-inc/EVAL-KXR94-2283/1191-1031-ND/3137343

[87] I. Starr and A. Noordergraaf, *Ballistocardiography in cardiovascular research: Physical aspects of the circulation in health and disease*. Lippincott, 1967.

[88] J. Ramos-Castro *et al.*, "Heart rate variability analysis using a seismocardiogram signal," in *2012 annual international conference of the IEEE engineering in medicine and biology society*, 2012, pp. 5642-5645: IEEE.

[89] K.-H. Seo, C. Oh, and J.-J. Lee, "User pose estimation using sensor distribution bed," in *Industrial Electronics Society, 2004. IECON 2004. 30th Annual Conference of IEEE*, 2004, vol. 1, pp. 598-602: IEEE.

[90] R. S. Leung, M. E. Bowman, J. D. Parker, G. E. Newton, and T. D. Bradley, "Avoidance of the left lateral decubitus position during sleep in patients with heart failure: relationship to cardiac size and function," *Journal of the American College of Cardiology*, vol. 41, no. 2, pp. 227-30, Jan 15 2003.

[91] P. Jiang and R. Zhu, "Dual tri-axis accelerometers for monitoring physiological parameters of human body in sleep," in *IEEE SENSORS, 2016* 2016, pp. 1-3: IEEE.

[92] M. Jackson, A. Collins, D. Berlowitz, M. Howard, F. O'Donoghue, and M. Barnes, "Efficacy of sleep position modification to treat positional obstructive sleep apnea," *Sleep Med*, vol. 16, no. 4, pp. 545-52, Apr 2015.

[93] M. B. Pouyan, J. Birjandtalab, M. Heydarzadeh, M. Nourani, and S. Ostadabbas, "A pressure map dataset for posture and subject analytics," in *Biomedical & Health Informatics (BHI), 2017 IEEE EMBS International Conference on*, 2017, pp. 65-68: IEEE.

[94] G. W. Pien and R. J. Schwab, "Sleep disorders during pregnancy," *Sleep*, vol. 27, no. 7, pp. 1405-17, Nov 1 2004.

[95] N. Mohsin, X. Liu, and S. Payandeh, "Signal processing techniques for natural sleep posture estimation using depth data," in *Information Technology, Electronics and Mobile Communication Conference (IEMCON), 2016 IEEE 7th Annual*, 2016, pp. 1-8: IEEE.

[96] S. Boughorbel, F. Bruekers, and K. de Groot, "Pressure-Sensor System for Sleeping-Posture Classification," *Measuring Behavior*, p. 358, 2012.

[97] Q. Sun, E. Gonzalez, and Y. Sun, "On bed posture recognition with pressure sensor array system," in *SENSORS, 2016 IEEE*, 2016, pp. 1-3: IEEE.

[98] H. J. Lee, S. H. Hwang, S. M. Lee, Y. G. Lim, and K. S. Park, "Estimation of body postures on bed using unconstrained ECG measurements," (in English), *IEEE Journal of Biomedical and Health Informatics*, vol. 17, no. 6, pp. 985-93, Nov 2013.

[99] S. Rus, T. Grosse-Puppendahl, and A. Kuijper, "Recognition of bed postures using mutual capacitance sensing," in *European Conference on Ambient Intelligence*, 2014, pp. 51-66: Springer.

[100] C.-C. Hsia, Y.-W. Hung, Y.-H. Chiu, and C.-H. Kang, "Bayesian classification for bed posture detection based on kurtosis and skewness estimation," in *e-health Networking, Applications and Services, 2008. HealthCom 2008. 10th International Conference on*, 2008, pp. 165-168: IEEE.

[101] W. Viriyavit, V. Sornlertlamvanich, W. Kongprawechnon, P. Pongpaibool, and T. Isshiki, "Neural network based bed posture classification enhanced by Bayesian approach," in *2017 8th International Conference of Information and Communication Technology for Embedded Systems (IC-ICTES)*, 2017, pp. 1-5: IEEE.

[102] S. Liu and S. Ostadabbas, "A Vision-Based System for In-Bed Posture Tracking," in *Proceedings of the IEEE Conference on Computer Vision and Pattern Recognition*, 2017, pp. 1373-1382.

[103] P. Jeng and L.-C. Wang, "An accurate, low-cost, easy-to-use sleep posture monitoring system," in *Applied System Innovation (ICASI), 2017 International Conference on*, 2017, pp. 903-905: IEEE.

[104] I. Safonov, I. Gartseev, M. Pikhletsky, O. Tishutin, and M. J. A. Bailey, "An approach for model assissment for activity recognition," *Pattern Recognition and Image Analysis*, vol. 25, no. 2, pp. 263-269, 2015.

[105] L. Rosales, M. Skubic, D. Heise, M. J. Devaney, and M. Schaumburg, "Heartbeat detection from a hydraulic bed sensor using a clustering approach," in *Engineering in Medicine and Biology Society (EMBC), 2012 Annual International Conference of the IEEE*, 2012, pp. 2383-2387: IEEE.

[106] B. Y. Su, K. C. Ho, M. Skubic, and L. Rosales, "Pulse rate estimation using hydraulic bed sensor," in *Engineering in Medicine and Biology Society (EMBC), 2012 Annual International Conference of the IEEE*, 2012, pp. 2587-2590.

[107] J. R. Braunstein, *The ballistocardiogram; a dynamic record of the heart beat* (no. 143). Thomas, 1953.

[108] M. Enayati, B. Y. Su, L. Despins, M. Skubic, J. M. Keller, and M. Popescu, "Investigating the Interaction between Ballistocardiogram and Respiratory Phases," in *2017 IEEE International Conference on Biomedical and Health Informatics Feb. 16-19, 2017, Orlando, Florida, USA*, 2017.

[109] P. Vermeire and J. Butler, "Effect of respiration on pulmonary capillary blood flow in man," *Circulation Research,* vol. 22, no. 2, pp. 299-308, Feb 1968.

[110] A. Otis, H. Rahn, M. Brontman, L. Mullins, and W. Fenn, "Ballistocardiographic study of changes in cardiac output due to respiration," *The Journal of clinical investigation,* vol. 25, no. 3, pp. 413-421, 1946.

[111] I. Starr and C. K. Friedland, "On the cause of the respiratory variation of the ballistocardiogram, with a note on sinus arrhythmia," *Journal of Clinical Investigation,* vol. 25, no. 1, p. 53, 1946.

[112] J. Pan and W. J. Tompkins, "A real-time QRS detection algorithm," *IEEE Transactions on Biomedical Engineering,* vol. 32, no. 3, pp. 230-6, Mar 1985.

[113] H. Bazett, "An analysis of the time-relations of electrocardiograms," *Annals of Noninvasive Electrocardiology,* vol. 2, no. 2, pp. 177-194, 1997.

[114] H. Sedghamiz. (2014, 08/05/2019). *Matlab implementation of Pan Tompkins ECG QRS detector*. Available: URL https://fr.mathworks.com/matlabcentral/fileexchange/45840-complete-pan-tompkins-implementationecg-qrs-detector

[115] I. Starr, "Normal standards for amplitude of ballistocardiograms calibrated by force," *Circulation,* vol. 11, no. 6, pp. 914-26, Jun 1955.

[116] I. Starr, "Progress towards a physiological cardiology: a second essay on the ballistocardiogram," *Annals of Internal Medicine,* vol. 63, no. 6, pp. 1079-105, Dec 1965.

[117] H. L. Taylor and H. C. Walker, "A comparison of factors affecting the high-frequency (Starr) and the low-frequency, critically damped (Nickerson) ballistocardiographs with special reference to age and body dimension," *American Heart Journal,* vol. 53, no. 3, pp. 326-33, Mar 1957.

[118] E. Vogt, D. MacQuarrie, and J. P. Neary, "Using ballistocardiography to measure cardiac performance: a brief review of its history and future significance," (in English), *Clinical Physiology and Functional Imaging,* vol. 32, no. 6, pp. 415-20, Nov 2012.

[119] B. M. Baker, "Ballistocardiography: predictor of coronary heart disease," *Circulation,* vol. 37, no. 1, pp. 1-3, Jan 1968.

[120] M. Manley, "Ballistocardiography: Promise and Practice," in *Perspectives in Biomedical Engineering*: Springer, 1973, pp. 255-259.

[121] W. H. Rosenblatt, "Ballistocardiography: concepts of its applicability in the office practice of cardiology," *Diseases of the chest,* vol. 32, no. 4, pp. 400-12, Oct 1957.

[122] W. R. Scarborough, R. E. Mason, F. W. Davis, Jr., M. L. Singewald, B. M. Baker, Jr., and S. A. Lore, "A ballistocardiographic and electrocardiographic study of 328 patients with coronary artery disease; comparison with results from similar study of apparently normal persons," *American Heart Journal,* vol. 44, no. 5, pp. 645-70, Nov 1952.

[123] G. Takla, J. H. Petre, D. J. Doyle, M. Horibe, and B. Gopakumaran, "The problem of artifacts in patient monitor data during surgery: a clinical and methodological review," *Anesthesia & Analgesia,* vol. 103, no. 5, pp. 1196-204, Nov 2006.

[124] A. K. Barros, A. Mansour, and N. Ohnishi, "Removing artifacts from electrocardiographic signals using independent components analysis," (in English), *Neurocomputing,* vol. 22, no. 1-3, pp. 173-186, Nov 1998.

[125] P. Hamilton, M. Curley, R. Aimi, and C. Sae-Hau, "Comparison of methods for adaptive removal of motion artifact," in *Computers in Cardiology 2000*, 2000, pp. 383-386: IEEE.

[126] M. Milanesi *et al.*, "Multichannel techniques for motion artifacts removal from electrocardiographic signals," in *Engineering in Medicine and Biology Society, 2006. EMBS'06. 28th Annual International Conference of the IEEE,* 2006, pp. 3391-3394: IEEE.

[127] S. H. Liu, "Motion Artifact Reduction in Electrocardiogram Using Adaptive Filter," (in English), *Journal of Medical and Biological Engineering,* vol. 31, no. 1, pp. 67-72, 2011.

[128] F. R. Hashim, L. Petropoulakis, J. Soraghan, and S. I. Safie, "Wavelet based motion artifact removal for ECG signals," in *Biomedical Engineering and Sciences (IECBES), 2012 IEEE EMBS Conference on*, 2012, pp. 339-342: IEEE.

[129] J. Lee, D. D. McManus, S. Merchant, and K. H. Chon, "Automatic motion and noise artifact detection in Holter ECG data using empirical mode decomposition and statistical approaches," (in English), *IEEE Transactions on Biomedical Engineering,* vol. 59, no. 6, pp. 1499-506, Jun 2012.

[130] C. Hoog Antink, F. Schulz, S. Leonhardt, and M. Walter, "Motion Artifact Quantification and Sensor Fusion for Unobtrusive Health Monitoring," *Sensors (Basel),* vol. 18, no. 1, p. 38, Dec 25 2017.

[131] J. Lee, W. Jung, I. Kang, Y. Kim, and G. Lee, "Design of filter to reject motion artifact of pulse oximetry," (in English), *Computer Standards & Interfaces,* vol. 26, no. 3, pp. 241-249, May 2004.

[132] C. Lee and Y. T. Zhang, "Reduction of motion artifacts from photoplethysmographic recordings using a wavelet denoising approach," in *Biomedical Engineering, 2003. IEEE EMBS Asian-Pacific Conference on*, 2003, pp. 194-195: IEEE.

[133] M. Raghuram, K. V. Madhav, E. H. Krishna, and K. A. Reddy, "Evaluation of wavelets for reduction of motion artifacts in photoplethysmographic signals," in *Information Sciences Signal Processing and their Applications (ISSPA), 2010 10th International Conference on*, 2010, pp. 460-463: IEEE.

[134] O. T. Inan, M. Etemadi, B. Widrow, and G. T. Kovacs, "Adaptive cancellation of floor vibrations in standing ballistocardiogram measurements using a seismic sensor as a noise reference," (in English), *IEEE Transactions on Biomedical Engineering,* vol. 57, no. 3, pp. 722-7, Mar 2010.

[135] C. Yang and N. Tavassolian, "Motion Artifact Cancellation of Seismocardiographic Recording from Moving Subjects," *Sensors,* vol. 13625, no. R1, p. 1, 2015.

[136] T. Shimazaki, S. Hara, H. Okuhata, H. Nakamura, and T. Kawabata, "Cancellation of motion artifact induced by exercise for PPG-based heart rate sensing," in *Engineering in Medicine and Biology Society (EMBC), 2014 36th Annual International Conference of the IEEE*, 2014, pp. 3216-3219: IEEE.

[137] S. Seyedtabaii and L. Seyedtabaii, "Kalman Filter Based Adaptive Reduction of Motion Artifact from Photoplethysmographic Signal," (in English), *Proceedings of World Academy of Science, Engineering and Technology,* vol. 27, pp. 173-+, 2008.

[138] B. Lee, J. Han, H. J. Baek, J. H. Shin, K. S. Park, and W. J. Yi, "Improved elimination of motion artifacts from a photoplethysmographic signal using a Kalman smoother with simultaneous accelerometry," (in English), *Physiological Measurement,* vol. 31, no. 12, pp. 1585-603, Dec 2010.

[139] A. Q. Javaid *et al.*, "Quantifying and Reducing Motion Artifacts in Wearable Seismocardiogram Measurements During Walking to Assess Left Ventricular Health," *IEEE Transactions on Biomedical Engineering,* vol. 64, no. 6, pp. 1277-1286, Jun 2017.

[140] E. Khan, F. Al Hossain, S. Z. Uddin, S. K. Alam, and M. K. Hasan, "A Robust Heart Rate Monitoring Scheme Using Photoplethysmographic Signals Corrupted by Intense Motion Artifacts," (in English), *IEEE Transactions on Biomedical Engineering,* vol. 63, no. 3, pp. 550-62, Mar 2016.

[141] D. Friedrich, X. L. Aubert, H. Führ, and A. Brauers, "Heart rate estimation on a beat-to-beat basis via ballistocardiography-a hybrid approach," in *Engineering in Medicine and Biology Society (EMBC), 2010 Annual International Conference of the IEEE*, 2010, pp. 4048-4051: IEEE.

[142] K. A. Reddy, B. George, and V. J. Kumar, "Use of Fourier Series Analysis for Motion Artifact Reduction and Data Compression of Photoplethysmographic Signals," (in English), *IEEE Transactions on Instrumentation and Measurement,* vol. 58, no. 5, pp. 1706-1711, May 2009.

[143] M. Młyńczak and G. Cybulski, "Motion artifact detection in respiratory signals based on Teager energy operator and accelerometer signals," in *Joint Conference of the European Medical and Biological Engineering Conference (EMBEC) and the Nordic-Baltic Conference on Biomedical Engineering and Medical Physics (NBC), EMBEC & NBC 2017*, Tampere, Finland, 2017, pp. 45-48: Springer.

[144] S. M. Salehizadeh *et al.*, "Photoplethysmograph signal reconstruction based on a novel motion artifact detection-reduction approach. Part II: Motion and noise artifact removal," *Annals of Biomedical Engineering,* vol. 42, no. 11, pp. 2251-63, Nov 2014.

[145] M. T. Petterson, V. L. Begnoche, and J. M. Graybeal, "The effect of motion on pulse oximetry and its clinical significance," *Anesthesia & Analgesia*, vol. 105, no. 6 Suppl, pp. S78-84, Dec 2007.

[146] V. J. Hodge and J. Austin, "A survey of outlier detection methodologies," (in English), *Artificial Intelligence Review*, vol. 22, no. 2, pp. 85-126, Oct 2004.

[147] P. Chetlur Adithya, R. Sankar, W. A. Moreno, and S. Hart, "Trends in fetal monitoring through phonocardiography: Challenges and future directions," (in English), *Biomedical Signal Processing and Control*, vol. 33, pp. 289-305, Mar 2017.

[148] C. Yang and N. Tavassolian, "Motion noise cancellation in seismocardiogram of ambulant subjects with dual sensors," in *Engineering in Medicine and Biology Society (EMBC), 2016 IEEE 38th Annual International Conference of the*, 2016, pp. 5881-5884: IEEE.

[149] E. C. Pinheiro, O. A. Postolache, and P. S. Girão, "Online heart rate estimation in unstable ballistocardiographic records," in *Engineering in Medicine and Biology Society (EMBC), 2010 Annual International Conference of the IEEE*, 2010, pp. 939-942: IEEE.

[150] U. Wijenayake and S. Y. Park, "Real-Time External Respiratory Motion Measuring Technique Using an RGB-D Camera and Principal Component Analysis," (in English), *Sensors (Basel)*, vol. 17, no. 8, p. 1840, Aug 9 2017.

[151] A. Sivanantham, "Measurement of heartbeat, respiration and movements detection using Smart Bed," in *Intelligent Computational Systems (RAICS), 2015 IEEE Recent Advances in*, 2015, pp. 105-109: IEEE.

[152] A. Alivar *et al.*, "Motion Artifact Detection and Reduction in Bed-Based Ballistocardiogram," (in English), *IEEE Access*, vol. 7, pp. 13693-13703, 2019 2019.

[153] R. Krishnan, B. B. Natarajan, and S. Warren, "Two-stage approach for detection and reduction of motion artifacts in photoplethysmographic data," *IEEE Transactions on Biomedical Engineering*, vol. 57, no. 8, pp. 1867-76, Aug 2010.

[154] D. Dao *et al.*, "A Robust Motion Artifact Detection Algorithm for Accurate Detection of Heart Rates From Photoplethysmographic Signals Using Time-Frequency Spectral Features," *IEEE Journal of Biomedical and Health Informatics*, vol. 21, no. 5, pp. 1242-1253, Sep 2017.

[155] A. Moukadem, A. Finnaoui, H. E. Gassara, D. Adolphe, L. Schacher, and A. Dieterlen, "Time-Frequency Domain for BCG Analysis," in *2018 International Conference on Computer and Applications (ICCA)*, 2018, pp. 226-230: IEEE.

[156] H.-G. Stark, *Wavelets and signal processing: an application-based introduction*. Springer Science & Business Media, 2005.

[157] O. Yildirim, "A novel wavelet sequence based on deep bidirectional LSTM network model for ECG signal classification," *Computers in Biology and Medicine*, vol. 96, pp. 189-202, May 1 2018.

[158] D. Cvetkovic, E. D. Ubeyli, and I. Cosic, "Wavelet transform feature extraction from human PPG, ECG, and EEG signal responses to ELF PEMF exposures: A pilot study," (in English), *Digital Signal Processing,* vol. 18, no. 5, pp. 861-874, Sep 2008.

[159] M. Alfaouri and K. Daqrouq, "ECG signal denoising by wavelet transform thresholding," *American Journal of Applied Sciences,* vol. 5, no. 3, pp. 276-281, 2008.

[160] D. L. Donoho, "De-Noising by Soft-Thresholding," (in English), *IEEE Transactions on Information Theory,* vol. 41, no. 3, pp. 613-627, May 1995.

[161] R. Balocchi *et al.*, "Deriving the respiratory sinus arrhythmia from the heartbeat time series using empirical mode decomposition," (in English), *Chaos Solitons & Fractals,* vol. 20, no. 1, pp. 171-177, Apr 2004.

[162] Z. Wu and N. E. Huang, "Ensemble empirical mode decomposition: a noise-assisted data analysis method," *Advances in adaptive data analysis,* vol. 1, no. 01, pp. 1-41, 2009.

[163] M. E. Torres, M. A. Colominas, G. Schlotthauer, and P. Flandrin, "A complete ensemble empirical mode decomposition with adaptive noise," in *2011 IEEE international conference on acoustics, speech and signal processing (ICASSP)*, 2011, pp. 4144-4147: IEEE.

[164] M. Galar, A. Fernandez, E. Barrenechea, H. Bustince, and F. Herrera, "A Review on Ensembles for the Class Imbalance Problem: Bagging-, Boosting-, and Hybrid-Based Approaches," (in English), *IEEE Transactions on Systems Man and Cybernetics Part C-Applications and Reviews,* vol. 42, no. 4, pp. 463-484, Jul 2012.

[165] C. Orphanidou, T. Bonnici, P. Charlton, D. Clifton, D. Vallance, and L. Tarassenko, "Signal-quality indices for the electrocardiogram and photoplethysmogram: derivation and applications to wireless monitoring," *IEEE Journal of Biomedical and Health Informatics,* vol. 19, no. 3, pp. 832-8, May 2015.

[166] W. Zong, G. Moody, and R. Mark, "Reduction of false arterial blood pressure alarms using signal quality assessement and relationships between the electrocardiogram and arterial blood pressure," *Medical and Biological Engineering and Computing,* vol. 42, no. 5, pp. 698-706, 2004.

[167] M. Elgendi, "Optimal Signal Quality Index for Photoplethysmogram Signals," *Bioengineering (Basel),* vol. 3, no. 4, p. 21, Sep 22 2016.

[168] N. Pradhan, S. Rajan, and A. Adler, "Evaluation of the signal quality of wrist-based photoplethysmography," *Physiological Measurement,* vol. 40, no. 6, p. 065008, Jul 1 2019.

[169] A. Szczepanski and K. Saeed, "A mobile device system for early warning of ECG anomalies," *Sensors (Basel),* vol. 14, no. 6, pp. 11031-44, Jun 20 2014.

[170] L. S. Lilly, *Pathophysiology of heart disease: a collaborative project of medical students and faculty*. Lippincott Williams & Wilkins, 2012.

[171] K. S. Hong, K. T. Park, and J. M. Ahn, "Aging Index using Photoplethysmography for a Healthcare Device: Comparison with Brachial-Ankle Pulse Wave Velocity," (in English), *Healthcare Informatics Research,* vol. 21, no. 1, pp. 30-4, Jan 2015.

[172] M. Elgendi, "On the analysis of fingertip photoplethysmogram signals," *Curr Cardiol Rev*, vol. 8, no. 1, pp. 14-25, Feb 2012.

[173] H. Ashouri and O. T. Inan, "Improving the accuracy of proximal timing detection from ballistocardiogram signals using a high bandwidth force plate," in *Biomedical and Health Informatics (BHI), 2016 IEEE-EMBS International Conference on*, 2016, pp. 553-556: IEEE.

[174] F. Feihl and A. F. Broccard, "Interactions between respiration and systemic hemodynamics. Part I: basic concepts," (in English), *Journal of Intensive Care Medicine,* vol. 35, no. 1, pp. 45-54, Jan 2009.

[175] B.-H. Kim, Y. Ishida, Y. Tsuneoka, and N. Matsubara, "Effectsof Spontaneous Respirationon Right and Left VentricularFunction: Evaluation by Respiratoryand ECG Gated Radionucide Ventriculography," *Journal of Nuclear Medicine,* vol. 28, no. 173â, p. 177, 1987.

[176] A. Johansson and P. A. Oberg, "Estimation of respiratory volumes from the photoplethysmographic signal. Part I: Experimental results," *Medical & Biological Engineering & Computing,* vol. 37, no. 1, pp. 42-7, Jan 1999.

[177] D. A. Winter, M. A. Lodge, and W. T. Josenhans, "The elimination of respiratory signals from the ultralow-frequency ballistocardiogram," *American Heart Journal,* vol. 71, no. 5, pp. 666-70, May 1966.

[178] P. D. Larsen, Y. C. Tzeng, P. Y. Sin, and D. C. Galletly, "Respiratory sinus arrhythmia in conscious humans during spontaneous respiration," *Respir Physiol Neurobiol,* vol. 174, no. 1-2, pp. 111-8, Nov 30 2010.

[179] K. Toska and M. Eriksen, "Respiration-synchronous fluctuations in stroke volume, heart rate and arterial pressure in humans," *The Journal of Physiology,* vol. 472, pp. 501-12, Dec 1993.

[180] W. Dock, "The Extravascular Basis for Respiratory Variation in the BallistocardiogramWith Notes on the Effects of Constrictive Pericarditis, Atrial Septal Defect, and the Valsalva Maneuver," *Annals of internal medicine,* vol. 57, no. 3, pp. 398-405, 1962.

[181] J. Paalasmaa, "A respiratory latent variable model for mechanically measured heartbeats," *Physiological Measurement,* vol. 31, no. 10, pp. 1331-44, Oct 2010.

[182] K. Tavakolian, A. Vaseghi, and B. Kaminska, "Improvement of ballistocardiogram processing by inclusion of respiration information," *Physiological Measurement,* vol. 29, no. 7, pp. 771-81, Jul 2008.

[183] Z. Zhang, B. Wang, H. Wu, X. Chai, W. Wang, and C. K. Peng, "Effects of slow and regular breathing exercise on cardiopulmonary coupling and blood pressure," *Medical & Biological Engineering & Computing,* vol. 55, no. 2, pp. 327-341, Feb 2017.

[184] P. Van Leeuwen and H. C. Kuemmell, "Respiratory modulation of cardiac time intervals," *British Heart Journal,* vol. 58, no. 2, pp. 129-35, Aug 1987.

[185] I. Starr, O. Horwitz, R. Mayock, and E. Krumbhaar, "Standardization of the ballistocardiogram by simulation of the heart's function at necropsy; with a clinical method for the estimation of cardiac strength and normal standards for it," *Circulation,* vol. 1, no. 5, pp. 1073-1096, 1950.

[186] P. A. Heidenreich *et al.*, "Forecasting the future of cardiovascular disease in the United States: a policy statement from the American Heart Association," *Circulation,* vol. 123, no. 8, pp. 933-44, Mar 1 2011.

[187] S. S. Lim *et al.*, "A comparative risk assessment of burden of disease and injury attributable to 67 risk factors and risk factor clusters in 21 regions, 1990-2010: a systematic analysis for the Global Burden of Disease Study 2010," *Lancet,* vol. 380, no. 9859, pp. 2224-60, Dec 15 2012.

[188] J. Booth, "A short history of blood pressure measurement," *Proceedings of the Royal Society of Medicine* vol. 70, no. 11, pp. 793-9, Nov 1977.

[189] T. G. Pickering *et al.*, "Recommendations for blood pressure measurement in humans and experimental animals: part 1: blood pressure measurement in humans: a statement for professionals from the Subcommittee of Professional and Public Education of the American Heart Association Council on High Blood Pressure Research," *Circulation,* vol. 111, no. 5, pp. 697-716, 2005.

[190] J. H. Shin and K. S. Park, "HRV analysis and blood pressure monitoring on weighing scale using BCG," in *2012 Annual International Conference of the IEEE Engineering in Medicine and Biology Society*, 2012, pp. 3789-3792: IEEE.

[191] Z. Chen, X. Yang, J. T. Teo, and S. H. Ng, "Noninvasive monitoring of blood pressure using optical ballistocardiography and photoplethysmograph approaches," in *Engineering in Medicine and Biology Society (EMBC), 2013 35th Annual International Conference of the IEEE*, 2013, pp. 2425-2428: IEEE.

[192] J. H. Shin, K. M. Lee, and K. S. Park, "Non-constrained monitoring of systolic blood pressure on a weighing scale," *Physiological Measurement,* vol. 30, no. 7, pp. 679-93, Jul 2009.

[193] M. J. Rantz *et al.*, "A New Paradigm of Technology-Enabled 'Vital Signs' for Early Detection of Health Change for Older Adults," (in English), *Gerontology,* vol. 61, no. 3, pp. 281-90, 2015.

[194] H. E. Lim, C. G. Park, S. H. Shin, J. C. Ahn, H. S. Seo, and D. J. Oh, "Aortic pulse wave velocity as an independent marker of coronary artery disease," (in English), *Blood Pressure,* vol. 13, no. 6, pp. 369-375, 2009.

[195] C. F. Babbs, "Oscillometric measurement of systolic and diastolic blood pressures validated in a physiologic mathematical model," *BioMedical Engineering OnLine,* vol. 11, no. 1, p. 56, Aug 22 2012.

[196] E. Pinheiro, O. Postolache, and P. Girao, "Pulse arrival time and ballistocardiogram application to blood pressure variability estimation," in *Medical Measurements and Applications, 2009. MeMeA 2009. IEEE International Workshop on*, 2009, pp. 132-136: IEEE.

[197] S. C. Huang, P. H. Hung, C. H. Hong, and H. M. Wang, "A New Image Blood Pressure Sensor Based on PPG, RRT, BPTT, and Harmonic Balancing," (in English), *IEEE Sensors Journal,* vol. 14, no. 10, pp. 3685-3692, Oct 2014.

[198] X. C. He, R. A. Goubran, and X. P. P. Liu, "Secondary Peak Detection of PPG Signal for Continuous Cuffless Arterial Blood Pressure Measurement," (in English), *IEEE Transactions on Instrumentation and Measurement,* vol. 63, no. 6, pp. 1431-1439, Jun 2014.

[199] P. A. Shaltis, A. Reisner, and H. H. Asada, "Wearable, cuff-less PPG-based blood pressure monitor with novel height sensor," in *2006 International Conference of the IEEE Engineering in Medicine and Biology Society*, 2006, pp. 908-911: IEEE.

[200] A. Gaurav, M. Maheedhar, V. N. Tiwari, and R. Narayanan, "Cuff-less PPG based continuous blood pressure monitoring—A smartphone based approach," in *2016 38th Annual International Conference of the IEEE Engineering in Medicine and Biology Society (EMBC)*, 2016, pp. 607-610: IEEE.

[201] P. A. Obrist, K. C. Light, J. A. McCubbin, J. S. Hutcheson, J. L. Hoffer, and Instrumentation, "Pulse transit time: Relationship to blood pressure," *Behavior Research Methods,* vol. 10, no. 5, pp. 623-626, 1978.

[202] T. M. Seeberg *et al.*, "A Novel Method for Continuous, Noninvasive, Cuff-Less Measurement of Blood Pressure: Evaluation in Patients With Nonalcoholic Fatty Liver Disease," *IEEE Transactions on Biomedical Engineering,* vol. 64, no. 7, pp. 1469-1478, Jul 2017.

[203] M. Gao, H. M. Cheng, S. H. Sung, C. H. Chen, N. B. Olivier, and R. Mukkamala, "Estimation of Pulse Transit Time as a Function of Blood Pressure Using a Nonlinear Arterial Tube-Load Model," (in English), *IEEE Transactions on Biomedical Engineering,* vol. 64, no. 7, pp. 1524-1534, Jul 2017.

[204] M. Kachuee, M. M. Kiani, H. Mohammadzade, and M. Shabany, "Cuffless Blood Pressure Estimation Algorithms for Continuous Health-Care Monitoring," *IEEE Transactions on Biomedical Engineering,* vol. 64, no. 4, pp. 859-869, Apr 2017.

[205] D. Buxi, J. M. Redout, and M. R. Yuce, "Blood Pressure Estimation Using Pulse Transit Time From Bioimpedance and Continuous Wave Radar," (in English), *IEEE Transactions on Biomedical Engineering,* vol. 64, no. 4, pp. 917-927, Apr 2017.

[206] M. Forouzanfar, S. Ahmad, I. Batkin, H. R. Dajani, V. Z. Groza, and M. Bolic, "Coefficient-free blood pressure estimation based on pulse transit time-cuff pressure dependence," *IEEE Transactions on Biomedical Engineering,* vol. 60, no. 7, pp. 1814-24, Jul 2013.

[207] S. Ahmad *et al.*, "Electrocardiogram-assisted blood pressure estimation," *IEEE Transactions on Biomedical Engineering,* vol. 59, no. 3, pp. 608-18, Mar 2012.

[208] W. J. Kim, J. W. Kim, Y. J. Moon, S. H. Kim, G. S. Hwang, and W. J. Shin, "The photoplethysmographic amplitude to pulse pressure ratio can track sudden changes in vascular compliance and resistance during liver graft reperfusion: A beat-to-beat analysis," (in English), *Medicine (Baltimore),* vol. 96, no. 22, p. e7045, Jun 2017.

[209] C. S. Kim *et al.*, "Ballistocardiogram: Mechanism and Potential for Unobtrusive Cardiovascular Health Monitoring," *Scientific Reports*, vol. 6, p. 31297, Aug 9 2016.

[210] L. Rosales, B. Y. Su, M. Skubic, and K. C. Ho, "Heart rate monitoring using hydraulic bed sensor ballistocardiogram," (in English), *Journal of Ambient Intelligence and Smart Environments*, vol. 9, no. 2, pp. 193-207, 2017.

[211] M. Skubic, R. D. Guevara, and M. Rantz, "Automated Health Alerts Using In-Home Sensor Data for Embedded Health Assessment," (in English), *IEEE Journal of Translational Engineering in Health and Medicine*, vol. 3, p. 2700111, 2015.

[212] T. E. Strandberg and K. Pitkala, "What is the most important component of blood pressure: systolic, diastolic or pulse pressure?," (in English), *Current Opinion in Nephrology and Hypertension*, vol. 12, no. 3, pp. 293-7, May 2003.

[213] L. F. Buckley, D. L. Dixon, G. F. t. Wohlford, D. S. Wijesinghe, W. L. Baker, and B. W. Van Tassell, "Intensive Versus Standard Blood Pressure Control in SPRINT-Eligible Participants of ACCORD-BP," *Diabetes Care*, vol. 40, no. 12, pp. 1733-1738, Dec 2017.

[214] Y. Imai *et al.*, "Factors that affect blood pressure variability - A community-based study in Ohasama, Japan," (in English), *American Journal of Hypertension*, vol. 10, no. 11, pp. 1281-1289, Nov 1997.

[215] V. Sheshadri, A. K. Tiwari, M. Nagappa, and L. Venkatraghavan, "Accuracy in Blood Pressure Monitoring: The Effect of Noninvasive Blood Pressure Cuff Inflation on Intra-arterial Blood Pressure Values," *Anesthesia, Essays and Researches*, vol. 11, no. 1, pp. 169-173, Jan-Mar 2017.

[216] J. Liu, Y. Li, X.-R. Ding, W.-X. Dai, and Y.-T. Zhang, "Effects of cuff inflation and deflation on pulse transit time measured from ECG and multi-wavelength PPG," in *2015 37th Annual International Conference of the IEEE Engineering in Medicine and Biology Society (EMBC)*, 2015, pp. 5973-5976: IEEE.

[217] R. Yi, "Sleep stage classification using hydraulic bed sensor," MS, 2018.

[218] R. B. Berry *et al.*, "Rules for scoring respiratory events in sleep: update of the 2007 AASM Manual for the Scoring of Sleep and Associated Events. Deliberations of the Sleep Apnea Definitions Task Force of the American Academy of Sleep Medicine," *Journal of Clinical Sleep Medicine*, vol. 8, no. 5, pp. 597-619, Oct 15 2012.

[219] R. Yi, M. Enayati, J. M. Keller, M. Popescu, and M. Skubic, "Non-Invasive In-Home Sleep Stage Classification Using a Ballistocardiography Bed Sensor," in *IEEE EMBS International Conference on Biomedical & Health Informatics (BHI)*, Chicago, IL, USA, 2019: IEEE.

[220] V. C. De Cock *et al.*, "Restoration of normal motor control in Parkinson's disease during REM sleep," *Brain*, vol. 130, no. Pt 2, pp. 450-6, Feb 2007.

[221] M. Enayati, B.-Y. Su, L. Despins, and M. Skubic, "Investigating the Interaction between Ballistocardiogram and Cardiac Age," in *European Medical and Biological Engineering Conference EMBEC*, Tempre, Finland, 2017.

VITA

Moein Enayati received the Bachelor of Science Degree in Computer Science and the Master of Science Degree in Industrial Engineering, both from Tehran Polytechnic. He was a graduate research assistant in the Center for Eldercare and Rehabilitation Technology, in the EECS department at the University of Missouri – Columbia. He has worked on multiple interdisciplinary studies on the application of machine learning and signal processing techniques in early detection of changes in the cardiovascular health conditions. The results of his works are published in multiple IEEE journals and EMBC conference proceedings. His research interests include machine learning, computational intelligence and data-driven models for the analysis of health relate time-series.